

**The Silicate, Sulfide, and Platinum - Group
Petrology and Mineralogy
of the Kawene Intrusion, Quetico Subprovince**

by Julie Selway ©

**A thesis submitted in partial fulfillment of the
requirements for the degree of
Master of Science**

**Supervisor : Dr. R. H. Mitchell
Lakehead University
Thunder Bay, Ontario
Canada**

November 1993

ProQuest Number: 10611873

All rights reserved

INFORMATION TO ALL USERS

The quality of this reproduction is dependent upon the quality of the copy submitted.

In the unlikely event that the author did not send a complete manuscript and there are missing pages, these will be noted. Also, if material had to be removed, a note will indicate the deletion.



ProQuest 10611873

Published by ProQuest LLC (2017). Copyright of the Dissertation is held by the Author.

All rights reserved.

This work is protected against unauthorized copying under Title 17, United States Code
Microform Edition © ProQuest LLC.

ProQuest LLC.
789 East Eisenhower Parkway
P.O. Box 1346
Ann Arbor, MI 48106 - 1346



National Library
of Canada

Acquisitions and
Bibliographic Services Branch

395 Wellington Street
Ottawa, Ontario
K1A 0N4

Bibliothèque nationale
du Canada

Direction des acquisitions et
des services bibliographiques

395, rue Wellington
Ottawa (Ontario)
K1A 0N4

Your file *Votre référence*

Our file *Notre référence*

The author has granted an irrevocable non-exclusive licence allowing the National Library of Canada to reproduce, loan, distribute or sell copies of his/her thesis by any means and in any form or format, making this thesis available to interested persons.

L'auteur a accordé une licence irrévocable et non exclusive permettant à la Bibliothèque nationale du Canada de reproduire, prêter, distribuer ou vendre des copies de sa thèse de quelque manière et sous quelque forme que ce soit pour mettre des exemplaires de cette thèse à la disposition des personnes intéressées.

The author retains ownership of the copyright in his/her thesis. Neither the thesis nor substantial extracts from it may be printed or otherwise reproduced without his/her permission.

L'auteur conserve la propriété du droit d'auteur qui protège sa thèse. Ni la thèse ni des extraits substantiels de celle-ci ne doivent être imprimés ou autrement reproduits sans son autorisation.

ISBN 0-315-86173-8

Canada

**The Silicate, Sulfide, and Platinum - Group
Petrology and Mineralogy
of the Kawene Intrusion, Quetico Subprovince**

Abstract

The Kawene Intrusion is an ultramafic, layered, metamorphosed Cu- Ni- PGE- bearing intrusion located 29 km east of Atikokan within the Quetico Subprovince of northwestern Ontario. The Kawene Intrusion is emplaced primarily in metasedimentary turbiditic wacke. The intrusion is composed of hornblende wehrlite in the center, with hornblende clinopyroxenite, clinopyroxene hornblendite, and hornblende melagabbro at the margin. The intrusion has been metamorphosed to upper greenschist - to - lower amphibolite metamorphic grade.

The mineralized area is composed of alternating layers of hornblende clinopyroxenite and clinopyroxene hornblendite intruded by tonalite veins, and sulfide veinlets. The sulfide veinlets and the disseminated sulfides consist mainly of chalcopyrite, pyrrhotite, and pentlandite. The other sulfides found in these ultramafic rocks in decreasing order of abundance are : galena, violarite, and sphalerite. The Platinum - Group Minerals (PGM) are spatially associated with the sulfides.

A total of 1078 Platinum Group Minerals (PGM), Bi telluride and Bi sulfide grains were found in 42 polished thin sections from the mineralized area of the Kawene Intrusion. The most common PGM are : PdBiTe (michenerite), PdBi₂ (floodite), Pd₂Bi₅ (unnamed), PtAs₂

(sperrylite), and native Bi. The compositional groups of the PGM in descending order of abundance are :

1. Pd - Bi compounds, michenerite, Pd-Bi-Te-Sb compounds
2. native Bi, Bi - S compounds, Bi - Te compounds, Bi-Te-Se-S compounds
3. sperrylite, (Ag,Ni)S, hessite, stutzite, Co-bearing hollingworthite, electrum, altaite.

The PGM range in size from 1 - 25 μm , and in habit from euhedral - to - subhedral.

The most abundant Platinum Group Mineral parageneses are enclosed within sulfides, and at sulfide - silicate boundaries. The other PGM parageneses are enclosed within silicates (usually clinopyroxenes), and at silicate - silicate boundaries.

The Platinum Group Minerals, Bi - S compounds, and Bi - Te compounds may cluster together. The most common PGM found in clusters are Pd - Bi compounds, michenerite, Bi - S compounds, and Bi - Te compounds which reflects their abundance in the intrusion.

Many of the PGM grains are intergrowths of two or more PGM which indicates simultaneous crystallization. In the Kawene Intrusion, the Pd - Bi - Te - Sb compositional group, Bi - Te - Se - S compositional group, electrum, Se-bearing galena, sperrylite, and Co-bearing hollingworthite crystallized at the same time (assemblage 1). Hessite, stutzite, altaite, Se-bearing galena, Bi_3Te_2 , pilsenite, and Pt - Sb compounds crystallized at the same time (assemblage 2), but not contemporaneously with the minerals in assemblage 1.

The Platinum - Group Minerals in the mineralized area in the Kawene Intrusion crystallized from a late magmatic, hydrothermal fluid. PGM assemblage 1 crystallized first between 489 - 254 °C and $f_{Te_2} \approx f_{S_2}$. PGM assemblage 2 crystallized later between 145 - 120 °C and $f_{Te_2} > f_{S_2}$ from the same, yet more evolved hydrothermal fluid. The O_2 fugacity is low during the deposition of the PGM, as the f_{O_2} is less than $10^{-33.5}$ bars at 300 °C (Figure 10.4). The presence of abundant pyrrhotite and rare magnetite is further evidence of a reducing environment.

Metamorphism has had no effect upon the PGM assemblages, although silicates have been altered to secondary amphibole, chlorite, and calcite. Metamorphic, hydrothermal fluid precipitated sphalerite and altered pentlandite to violarite.

Acknowledgements

I would like to thank Dr. Mitchell, my supervisor, for his advice and guidance. He proofread many versions of this thesis, and offered suggestions for improvement.

I would also like to thank Al MacKenzie from the Instrumentation Laboratories at Lakehead University who taught me how to use the scanning electron microscope, answered countless questions, and solved many technical problems. Mike Johns developed the scanning electron microscope pictures for this thesis.

I would also like to thank Dr. Platt who acted as my co-supervisor while Dr. Mitchell was away. Dr. Kissin told me how to stain pyrrhotite and chalcopyrite, and proofread my sulfide mineralogy and petrology chapter. Dr. Kehlenbeck examined the metamorphic textures found in my polished thin sections.

I would also like to thank Jian Xiong who provided emotional support during stressful times, listened to many stories about my thesis, and offered many tidbits of advice. Jian drafted all of the paragenesis diagrams on the computer for this thesis.

I would also like to thank my family and friends who continued to support me and did not forget about me even though I was living far from Nova Scotia.

Table of Contents

	Page
Abstract	i
Acknowledgements	iv
List of Figures	x
List of Tables	xiii
Chapter 1 : Introduction	
1.1. General Statement	1
1.2. Regional Geology	4
1.2.1. Superior Province	4
1.2.2. Quetico Subprovince	4
1.2.3. Crooked Pine Lake	6
1.3. Quetico Intrusions	8
1.3.1. Quetico Intrusions	8
1.3.2. Kawene Intrusion Previous Studies	10
1.4. Objectives	11
Chapter 2 : Analytical Methods	
2.1. Instrumentation	12
2.2. Energy Dispersive Analysis	12
2.3. Backscattered Electrons	14
2.4. Standards	15
2.5. Quantitative Analysis	16
2.5.1. ZAF Correction Procedure	16
2.5.2. SQ and MicroQ	17
2.6. Calibration of SQ Correction Factors	19
2.7. Accuracy and Precision	23

2.8. Method for Analyzing the Platinum - Group Element Minerals	23
2.9. Analytical Difficulties	24
Chapter 3 : Silicate Petrology of the Mineralized Area	
3.1. Introduction	32
3.2. Clinoproxenites and Hornblendites	33
3.2.1. Petrographic Descriptions	33
3.2.2. Paragenesis	51
3.3. Tonalite Veins	54
3.3.1. Petrographic Descriptions	54
3.3.2. Paragenesis	58
3.4. Metamorphic Textures	59
3.5. Petrogenesis of Mineralized Area	60
3.5.1. Petrography	60
3.5.2. Lithographic Column	61
3.5.3. Crystallization Sequence of the Intrusion	63
Chapter 4 : Silicate Mineralogy	
4.1. Clinopyroxene	64
4.2. Amphibole	64
4.3. Biotite	68
4.4. Chlorite	71
4.5. Feldspar	73
4.6. Summary	73
Chapter 5 : Sulfide Mineralogy and Petrology	
5.1. Introduction	75

5.2. Sulfides in the Ultramafic Rocks	77
5.2.1. Pyrrhotite	77
5.2.2. Pyrrhotite Paragenesis	78
5.2.3. Chalcopyrite Paragenesis	86
5.2.4. Pentlandite Paragenesis	92
5.2.5. Violarite Paragenesis	97
5.2.6. Galena Paragenesis	102
5.2.7. Sphalerite Paragenesis	103
5.2.8. Paragenesis of the Sulfides in the Ultramafic Rocks	104
Chapter 6 : Platinum - Group Minerals	
Pd - Bi - Te - Sb Compositional Group	
6.1. Introduction	106
6.2. Pd - Bi Compounds	113
6.3. Michenerite	123
6.4. Pd - Bi - Te - Sb Compounds	130
Chapter 7 : Bi - Te - Se - S Compositional Group	
7.1. Native Bi	141
7.2. Bi - S Compounds	141
7.3. Bi - Te Compounds	146
7.4. Bi - Te - Se - S Compounds	154
Chapter 8 : Miscellaneous Platinum - Group Minerals	
8.1. Sperrylite	164
8.2. (Ag,Ni)S	172
8.3. Ag - Te Compounds	172
8.4. Hollingworthite - Cobaltite	175

8.5. Electrum	183
8.6. Altaite	186
Chapter 9 : Platinum - Group Minerals Intergrowths and Clusters	
9.1. Intergrowths	189
9.1.1. Intergrowths	189
9.1.2. Intergrowths within the Pd - Bi - Te Compositional Group	190
9.1.3. Intergrowths between Pd - Bi - Te and Bi - S Compositional Groups	192
9.1.4. Intergrowths between Native Bi and Bi - S Compounds	195
9.1.5. Intergrowths with Sperrylite	195
9.1.6. Intergrowths with Stutzite and Hessite	195
9.2. Platinum - Group Mineral Assemblage	203
9.3. Platinum - Group Mineral Clusters	204
Chapter 10 : Discussion	
10.1. Temperature of Formation of Platinum - Group Minerals	210
10.2. Te_2 , S_2 , and O_2 Fugacities	212
10.3. Hydrothermal Origin of Platinum - Group Minerals	216
10.4. Hydrothermal Genesis	222
Chapter 11 : Conclusions	
11.1. General Statement	225
11.2. Silicate Petrology	226

11.3. Sulfide Petrology	227
11.4. Platinum - Group Minerals	227
11.5. Hydrothermal Origin	230
11.6. Petrogenesis of the Mineralized Area of the Kawene Intrusion	231
References	235
Appendix 1 : The polished thin sections in which each Platinum - Group Mineral is found.	253
Appendix 2 : Compositions of Platinum - Group Minerals $\geq 5 \mu\text{m}$.	256

List of Figures

	Page
Chapter 1	
1.1 Geology of the Kawene Intrusion	2
1.2 Mineralized Area of the Kawene Intrusion	3
1.3 Regional Geology of Study Area	7
Chapter 2	
2.1 Variation in peak width and resolution as a function of x-ray energy	13
2.2 Absorption of X-rays due to the thickness of the sample and takeoff angle.	18
2.3 SEM / EDS spectrum of Se-bearing galena	18
2.4 Absorption of x-rays by tilting sample	26
2.5 SEM / EDS spectrum showing Pb, Bi and S peak overlaps	26
2.6 Simulated spectra showing Pb, Bi, and S peak overlaps	27
2.7 SEM / EDS spectrum showing Pt and Ir peak overlaps	28
2.8 SEM / EDS spectrum showing Rh and Pd peak overlaps	28
Chapter 3	
3.1 Prismatic hornblende and biotite aligned parallel to tonalite vein.	34
3.2 Oikocrystic amphiboles	36
3.3 Twinned clinopyroxene	40
3.4 Altered clinopyroxene	42
3.5 Granoblastic clinopyroxene grains	44
3.6 Biotite cluster	47
3.7 Granoblastic quartz and plagioclase and aligned biotite (tonalite).	55
3.8 Plagioclase phenocryst (tonalite).	57
3.9 Drill core column from K87-1.	62
Chapter 4	
4.1 Classification of calcic amphiboles, $(Na + K) < 0.50$.	66
4.2 Classification of calcic amphiboles, $(Na + K) > 0.50$.	67
4.3 Classification of biotites	70
Chapter 5	
5.1 Hexagonal and monoclinic pyrrhotite	79
5.2 Hexagonal and monoclinic pyrrhotite, and pentlandite	79
5.3 Pentlandite veinlet intruding pyrrhotite	82
5.4 Granular pyrrhotite and chalcopyrite	82
5.5 Interstitial monoclinic pyrrhotite and pentlandite	84
5.6 Euhedral hornblende enclosed in monoclinic pyrrhotite	84
5.7 Untarnished and weakly tarnished chalcopyrite	88
5.8 Twinned chalcopyrite	88
5.9 Interstitial chalcopyrite and sphalerite	90
5.10 Pentlandite "eye" enclosed in monoclinic pyrrhotite	90
5.11, 5.12 Pentlandite "eye", chalcopyrite, pyrrhotite	94
5.13 Pentlandite flames exsolved from monoclinic pyrrhotite	96
5.14 Pentlandite altering violarite	98
5.15 Pentlandite altering to violarite	100

Chapter 6

6.1 PGM partially enclosed in sulfides	109
6.2 PGM enclosed in silicates	109
6.3 PGM parallel to grain boundaries	110
6.4 PGM attached to a fine grained sulfide enclosed within a silicate	110
6.5 PGM euhedral to sulfide, and subhedral - anhedral to silicate	111
6.6 PGM at silicate triple junctions	112
6.7 Froodite cluster	115
6.8 Pd - Bi - Te ternary diagram	118
6.9 SEM / EDS spectrum of a) Pd ₂ Bi ₅ and b) michenerite	119
6.10 Bi : Pd histogram	121
6.11 38 μm michenerite grain and 25 μm sobolevskite - stibiopalladinite (ss) enclosed within monoclinic pyrrhotite	125
6.12 Michenerite cluster	126
6.13 SEM / EDS spectrum of sobolevskite - stibiopalladinite (ss)	132
6.14 PdBi - PdSb - PdTe ternary diagram	135
6.15 Pd - Bi - Sb ternary diagram	136
6.16 Intergrowth of Sb-bearing michenerite and sobolevskite - stibiopalladinite - michenerite (ss)	137

Chapter 7

7.1 Bi ₂ S ₃ grains in contact with pyrrhotite, pentlandite, diopside	144
7.2 SEM / EDS spectrum of a) Bi ₂ S ₃ and b) Bi ₃ Te ₂	145
7.3 20 μm Bi ₄ (S,Te,Se) ₃ - Bi ₃ (Te,S,Se) ₂ grain at augite - chalcopyrite boundary	156
7.4 SEM / EDS spectrum of Bi ₄ (S,Te,Se) ₃	158
7.5 S vs. Bi graph for Bi - Te - Se - S compounds	159
7.6 S - Te - Se ternary diagram	160
7.7 Se vs. Bi graph for Bi - Te - Se - S compounds	161
7.8 Bi ₂ S ₃ - Bi ₂ Te ₃ - Bi ₂ Se ₃ ternary diagram	162

Chapter 8

8.1 150 μm sperrylite enclosed in monoclinic pyrrhotite	165
8.2 SEM / EDS spectrum of a) sperrylite and b) hessite	167
8.3 (Ag,Ni)S cluster enclosed in violarite	170
8.4 Rh - Pt - Ir ternary diagram	179
8.5 Rh - Pt - Co ternary diagram	180
8.6 SEM / EDS spectrum of electrum	184

Chapter 9

9.1 Intergrowths in Pd - Bi - Sb - Te compositional group	191
9.2 Intergrowths between Pd - Bi - Te and Bi - S compositional group	193
9.3 Intergrowth between PdBi, BiS, and Au	194
9.4 Intergrowths between Bi - Te - Se - S compositional group and Se-bearing galena	196

9.5 Intergrowths with sperrylite	198
9.6a Intergrowth with sperrylite	199
9.6b Intergrowth with hessite	200
9.7 Intergrowths with hessite and stutzite	201
9.8 Intergrowth of altaite, hessite, stutzite, and Pt - Sb compound	202
9.9 Cluster of 73 grains from Pd - Bi - Te - Sb compositional group and Bi - S compounds	205

Chapter 10

10.1a Log f_{Te_2} vs. log f_{S_2} graph at 300 °C	213
10.1b Log f_{Te_2} vs. log f_{S_2} graph at 200 °C	213
10.2a Log f_{Te_2} vs. log f_{S_2} graph at 100 °C	214
10.2b Log f_{Te_2} vs. log f_{O_2} graph at 300 °C	214

List of Tables

	Page
Chapter 2	
2.1 Comparison of the precision of MicroQ and SQ	20
2.2 SEM SQ correction factors	21
2.3 Accuracy and precision of SQ EDS analyses	22
Chapter 4	
4.1 Representative compositions of amphibole	65
4.2 Representative compositions of biotite	69
4.3 Representative compositions of chlorite	72
4.4 Representative compositions of feldspar	74
Chapter 5	
5.1 Representative compositions of sulfides	87
5.2 Maximum thermal stabilities of sulfide minerals	104
Chapter 6	
6.1 Platinum - Group Minerals and Bi compounds found in the mineralized area of the Kawene Intrusion	107
6.2 Platinum - Group Minerals and Bi compounds compositionally grouped	108
6.3 Representative compositions of Pd - Bi compounds	117
6.4 Representative compositions of Te-, S-, and Au-bearing Pd - Bi compounds	117
6.5 Comparative sobolevskite and froodite compositions	122
6.6 Representative compositions of michenerite	128
6.7 Representative compositions of Sb-bearing michenerite	128
6.8 Comparative michenerite compositions	129

6.9 Representative compositions of Pd - Bi - Te - Sb compounds	133
6.10 Comparative Pd - Bi - Te - Sb compositions	139

Chapter 7

7.1 Representative compositions of Bi - S compounds	143
7.2 Comparative Bi ₂ S ₃ compositions	143
7.3 Representative compositions of Bi - Te compounds	150
7.4 Representative compositions of Se- and Pd-bearing Bi - Te compounds	150
7.5 Comparative Bi - Te compositions	153
7.6 Representative compositions of Bi - Te - Se - S compounds	157

Chapter 8

8.1 Representative compositions of sperrylite	168
8.2 Comparative sperrylite compositions	168
8.3 Representative compositions of (Ag,Ni)S	171
8.4 Representative compositions of Ag - Te compounds	171
8.5 Comparative Ag - Te compounds	174
8.6 Representative compositions of Rh - Co sulfarsenide	178
8.7 Comparative hollingworthite and cobaltite compositions	182
8.8 Representative compositions of electrum	185
8.9 Comparative electrum compositions	185
8.10 Representative compositions of altaite	187
8.11 Comparative altaite compositions	187

Chapter 10

10.1 Maximum thermal stabilities of Platinum - Group Minerals	211
10.2 Temperature of formation of other hydrothermal deposits	221

Chapter 1

Introduction

1.1. General Statement

The Kawene Intrusion is an ultramafic, layered, metamorphosed Cu- Ni- PGE- bearing intrusion located 29 km east of Atikokan within the Quetico Subprovince of northwestern Ontario. The Kawene Intrusion is emplaced primarily in metasedimentary turbiditic wacke. Metasedimentary migmatite is found along its northern margin. The intrusion is composed of hornblende wehrlite in the center, with hornblende clinopyroxenite, clinopyroxene hornblendite, and hornblende melagabbro at the margin (Figure 1.1). The intrusion is modally layered with gradational contacts between the alternating clinopyroxenite and hornblendite layers. The intrusion has been metamorphosed to upper greenschist - to - lower amphibolite metamorphic grade (Pirie and Mackasey, 1978). This indicates P-T conditions of 2.5 - 3.2 Kb and 450 - 525 °C (MacTavish, 1992).

The mineralized area of the Kawene Intrusion, located along the northeastern margin, is 90 m long, 30 m wide, and 17 m thick (Figure 1.2). The mineralized area is composed of alternating layers of hornblende clinopyroxenite and clinopyroxene hornblendite intruded by tonalite veins, and sulfide veinlets. The sulfide veinlets and the disseminated sulfides consist mainly of chalcopyrite, pyrrhotite, and pentlandite. The Platinum - Group Minerals (PGM) are spatially associated with the sulfides.

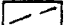
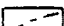
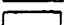
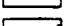
Legend

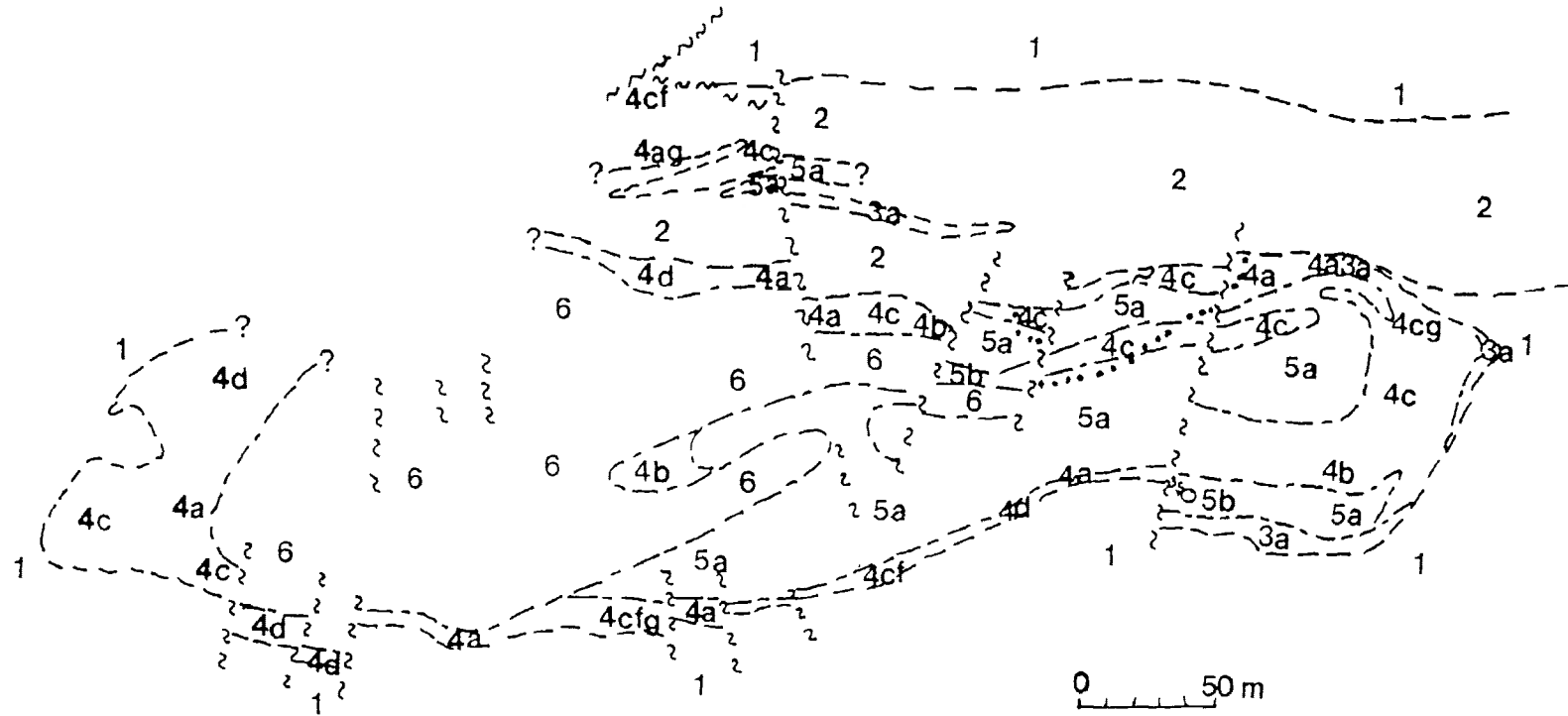
- 6 Hornblende Wehrlite
- 5a Hornblende Clinopyroxenite
- 5b Olivine-hornblende Clinopyroxenite
- 5c Biotitic Clinopyroxenite
- 4a Hornblendite
- 4b Olivine-clinopyroxene Hornblendite
- 4c Clinopyroxene Hornblendite

- 4d Feldspathic Hornblendite
- 4e Porphyritic Hornblendite
- 4f Biotitic Hornblendite
- 4g Appinitic Hornblendite
- 3a Hornblende Melagabbro
- 3b Biotitic Melagabbro
- 3c Appinitic Melagabbro

- 2 Metasedimentary Migmatite
- 1 Turbiditic Wacke

Symbols

-  Assumed contact
-  Gradational contact
-  Fault / Shearing
-  Mineralization Limit

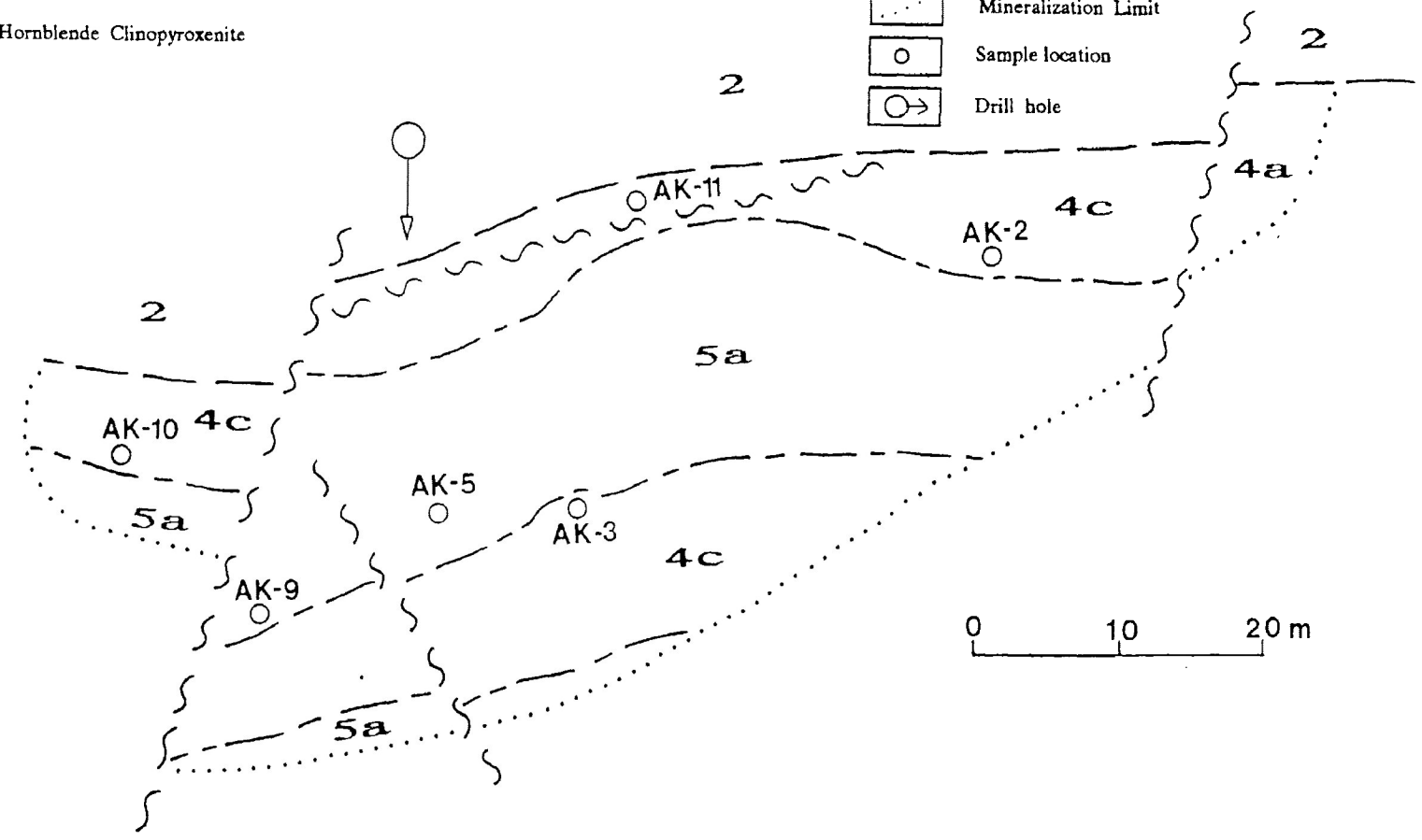


GEOLOGY OF THE KAWENE INTRUSION

Figure 1.1 : (MacTavish, 1992)

- Legend**
- 2 Metasedimentary Migmatite
 - 4a Hornblendite
 - 4c Clinopyroxene Hornblendite
 - 5a Hornblende Clinopyroxenite

- Symbols**
- Assumed contact
 - Gradational contact
 - Fault / Shearing
 - Mineralization Limit
 - Sample location
 - Drill hole



Geology of the Mineralization Area of the Kawene Intrusion

Figure 1.2 : (MacTavish, 1992)

1.2. Regional Geology

1.2.1. Superior Province

The Superior province of the Precambrian Canadian Shield is one of the world's largest Archean cratons with an area of 23% of the Earth's exposed Archean crust (Thurston, 1991; Card, 1990). The rocks in the Superior province were formed during the Middle and Late Archean, and stabilized 2.65 Ga ago (Card, 1990; Percival, 1989). The Superior province can be subdivided into volcano - plutonic ("granite - greenstone"), metasedimentary, plutonic, and high grade gneiss subprovinces on the basis of lithology, structure, metamorphism, geophysical and metallogenetic characteristic, and ages of rock units and tectonic events (Card, 1990). The subprovinces are generally east - west linear belts (Williams, 1991). The southern part of the Superior province consists of alternating volcano - plutonic (e.g. Wabigoon and Wawa) and metasedimentary subprovinces (e.g. Quetico) (Card, 1990; Percival, 1989).

1.2.2. Quetico Subprovince

The metasedimentary Quetico subprovince is 10 - 100 km wide and 1200 km long (Card, 1990; Percival, 1989). It is bounded by the Wabigoon subprovince to the north and the Wawa subprovince to the south (Williams, 1991). The Quetico subprovince consists mostly of metasedimentary turbiditic wacke (Williams, 1991; Card, 1990; Percival, 1989). The metasediments were rapidly deposited in deep water as unchanneled, distal turbiditic fans (Williams, 1991;

Card, 1990). The Quetico subprovince also contains metasedimentary siltstone, mudstone, and rare conglomerates. The igneous rocks found in the Quetico subprovince include :

1. I-type - hornblendites, diorites, syenites, and tonalite,
2. S-type - peraluminous granites, biotite and muscovite leucogranites, pegmatites
3. migmatite, granodiorite, gabbro, and rare ultramafic bodies (MacTavish, 1992; Williams, 1991; Card, 1990; Percival, 1989).

The Quetico subprovince has an east - west linear structural trend (Percival, 1989). The steep Quetico fault forms the boundary between the Quetico and Wabigoon subprovinces east of Lake Nipigon for about 200 km (Williams, 1991; Card, 1990; Percival, 1989). The easterly trending, steeply dipping, transcurrent Quetico fault is a regional - scale dextral shear and fault zone with a 120 km offset (MacTavish, 1992; Williams, 1991; Percival, 1989). The Quetico Fault zone ranges in width from 10 - 300 m, but locally attains widths of over 1 km (MacTavish, 1992).

All of the rocks in the Quetico subprovince were regionally metamorphosed (Williams, 1991). The metamorphic grade in the subprovince varies from low grade (greenschist) in the marginal rocks, to amphibolite, and to high grade (granulite) in the central migmatite - intrusive granite zone (Williams, 1991; Card, 1990; Percival, 1989). The lowest metamorphic grades are usually found along the northern boundary with the Wabigoon subprovince (Williams, 1991). The metamorphic pressure varies from 2.5 kb in the east to 6 kb in the western granulites (Card, 1990; Percival,

1989). The estimated metamorphic conditions are 500°C and 2.5 kb for the western marginal rocks (Card, 1990). Card (1990) suggested that the heat for the high temperature, low pressure metamorphism was supplied by rising anatectic granitic magmas in the central parts of the subprovince.

Detrital zircons from the metasedimentary rocks range in age from 3.0 - 2.7 Ga (Williams, 1991; Card, 1990). The major plutonism occurred 2.67 - 2.65 Ga ago (Percival, 1989). Rb-Sr and K-Ar geochronology reveal that the metamorphism and subsequent cooling of the Quetico subprovince occurred at 2.6 - 2.4 Ga (Williams, 1991).

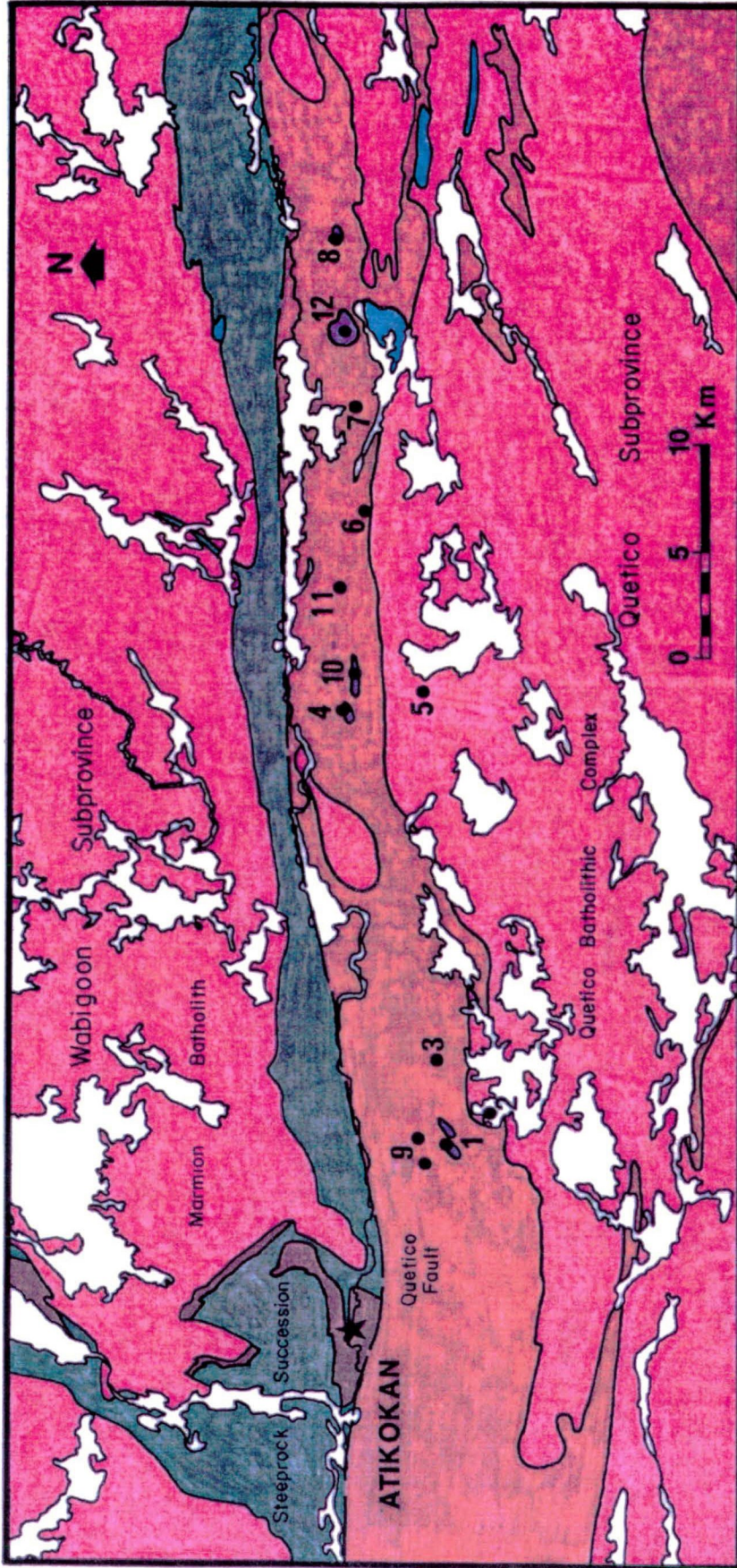
The Quetico subprovince may represent a fore - arc accretionary prism (Williams, 1991; Card, 1990; Percival, 1989). The metasediments were deposited in a submarine fan as abyssal turbidites, accreted onto the Wabigoon arc, and later compressed by docking of the Wawa arc (Williams, 1991; Card, 1990; Percival, 1989).

1.2.3. Crooked Pine Lake

The Crooked Pine Lake area (study area) straddles parts of the Wabigoon (north) and Quetico (south) subprovinces separated by the Quetico fault (Figure 1.3) (Pirie, 1978). North of the Quetico fault lies an east trending belt of mafic metavolcanics, and intermediate to felsic plutonic rocks of the Marmion batholith (Pirie, 1978). The Quetico fault forms a narrow, highly deformed, and mylonitized zone along the north shore of Crooked Pine Lake

Figure 1.3 : (MacTavish, 1992)

Regional Geology of Study Area



Legend

- Felsic to Intermediate Intrusive Rocks (Quetico)
- Quetico Intrusions
- Clastic Metasedimentary Rocks
- Mafic Metavolcanic Rocks
- Steeprock Group
- Felsic to Intermediate Intrusive Rocks (Marmion)

Quetico Intrusions

- | | |
|--------------------|-----------------------|
| 1) Plateau Lake | 7) Mud Lake |
| 2) Bergman | 8) Chief Peter Lake |
| 3) Fire Lake Dykes | 9) Plateau Lake Dykes |
| 4) Kawene | 10) Kawene Lake |
| 5) Eva Lake | 11) Heward Lake |
| 6) Abiwin | 12) North Elbow Lake |

(Pirie, 1978). South of this fault is a 6 km wide belt of metamorphosed turbidites (MacTavish, 1992). The metamorphic grade within the metasedimentary belt ranges from lower greenschist to amphibolite (MacTavish, 1992). South of the metasediments is the Quetico batholithic complex which is composed of felsic to intermediate granitoid rocks and migmatites (MacTavish, 1992).

1.3. Quetico Intrusions

1.3.1. Quetico Intrusions

Cu- Ni- PGE- bearing, ultramafic Quetico intrusions intrude the metasedimentary belt of the Quetico subprovince (MacTavish, 1992). The Quetico intrusions range in size from 3 - 5 m thick dykes to small, elliptical stocks 3.3 km long and up to 1.8 km wide (MacTavish, 1992). The Quetico intrusions contain hornblende wehrlite or hornblende clinopyroxenite in the core with clinopyroxene hornblendite, hornblendite, feldspathic hornblendite, hornblende gabbro, and rare hornblende diorite, in various proportions, forming gradational discontinuous envelopes (MacTavish, 1992; Pirie, 1978). The Quetico intrusions contain minor pyrrhotite - chalcopyrite - PGM mineralization (MacTavish, 1992). The grain size within the Quetico intrusions ranges from fine- to very coarse-grained, to locally pegmatitic (MacTavish, 1992).

The Quetico intrusions are characterized by hornblende-rich lithologies (MacTavish, 1992). Large, interstitial poikilitic amphibole grains occur within all ultramafic rock types. Coarse-

to very coarse-grained, locally pegmatitic diorite and gabbro contain skeletal, prismatic to acicular hornblende grains often cored with plagioclase and quartz (MacTavish, 1992).

MacTavish (1992) concluded that the Quetico intrusions resemble appinite suite bodies rather than Alaskan - type complexes. The Quetico and appinite intrusions have a similar average size of 0.3 km² and 0.5 km² respectively. Appinite suites and Quetico intrusions are identical in lithologies and textural features. Appinites contain feldspathic hornblende, hornblende, and hornblende peridotite which are sometimes divided into pyroxene-rich and pyroxene-poor varieties. The absence of dunites, chromite, and the rare magnetite in the Quetico intrusions is another feature in common with the appinites. The Quetico and appinite magmas were initially very rich in MgO and CaO. During crystallization, the magma underwent a rapid decrease in MgO (due to fractionation of olivine), a slight decrease in CaO, and constant FeO (during crystallization of clinopyroxene and hornblende). During the final stages of crystallization, the magma was enriched in K₂O which resulted in crystallization of biotite. Plots of SiO₂ vs. Al₂O₃ and of Al₂O₃ vs. TiO₂ in clinopyroxenes in the Quetico intrusions indicate a sub-alkaline affinity and a similarity with appinites.

The Quetico intrusions crystallized from a sub-alkaline, possibly calc-alkaline, olivine basalt liquid at relatively high P_{H₂O} (MacTavish, 1992). The intrusions must have crystallized under relatively high P_{H₂O} in order for hornblende to be stable over such

a wide range of magmatic conditions.

1.3.2. Kawene Intrusion Previous Studies

This thesis is a continuation of MacTavish's (1992) M.Sc. study. Field studies by MacTavish (1992) revealed that there is a sharp, undulatory, weakly chilled contact between the intrusion and the surrounding turbiditic, metasedimentary rocks which is commonly offset by faulting. The 2 - 10 m thick contact aureole exhibits little or no schistosity, or preserved sedimentary structures. A readily observable chilled margin and the absence of a significant contact metamorphic aureole suggests that the intrusion was probably emplaced into an already hot, dry country rock. The heat of the intrusion may have caused some partial melting of the overlying sediments producing a narrow migmatite zone along the north margin of the intrusion.

Two periods of deformation followed the formation of the Kawene intrusion (MacTavish, 1992). The first period of deformation is east - west shearing parallel to the long axis of the intrusion, and the regional schistosity. The second period of deformation is cross-cut faulting dominately NNE - SSW and rarely NW - SE. Vertical to oblique movement along these faults resulted in offsets of 2 - 15 m.

The Cu-Ni-PGE mineralized zones within many of the Quetico intrusions are in contact with the surrounding clastic metasedimentary country rocks (MacTavish, 1992). The mineralized zone in the Kawene Intrusion occurs along the contact with the

metasedimentary migmatite.

Geochemical data from MacTavish (1992) revealed that copper is the most abundant base metal within the mineralized zones of the Quetico intrusions as Cu : Cu + Ni ratios are generally greater than 0.6. There is a positive correlation between (Cu, Ni) and (Pt, Pd) in the Kawene Intrusion. The average Pt : Pd ratio for the Kawene Intrusion is 0.96 with a range of 0.11 - 2.41 (MacTavish, 1992). There is a positive relationship between Pt and Pd i.e. as the Pt content increases, so does the Pd content. The Pd : Ir ratio for the Kawene Intrusion is 145 which suggests that it is a more evolved melt than other primary PGE deposits (MacTavish, 1992). The Cl-chondrite normalized PGE + Au plot for the Kawene Intrusion shows a positive slope with Pd > Au > Pt > Rh >> Ir > Ru > Os, and a similar shape to the Rathbun Lake hydrothermal PGE deposit (MacTavish, 1992).

1.4. Objectives

The objectives of this thesis are :

1. To describe the petrology and mineralogy of the silicates.
2. To describe the petrology and mineralogy of the sulfides.
3. To use scanning electron microscopy (SEM) - energy dispersive spectrometry (EDS) to identify and describe the paragenesis of the Platinum - Group Minerals, Tellurides, and Bismuthides present.
4. To estimate the temperature of formation, the sulfur and tellurium fugacities, and to determine the origin of the PGM.
5. To determine the petrogenesis of the mineralized area.

Chapter 2

Analytical Methods

2.1. Instrumentation

The Platinum - Group Minerals (PGM) were found using backscattered electron (BSE) imagery, and were identified using energy dispersion X-ray spectrometry (EDS) using a Hitachi 570 scanning electron microscope (SEM) at Lakehead University. The operating conditions were : accelerating voltage 20 kV, working distance 28 mm, dead time 20 - 30 %, beam current approximately 0.38 nA, spot size $\pm 0.2 \mu\text{m}$, takeoff angle 18° , and counting time 100 s.

2.2. Energy Dispersive Analysis

Energy dispersive analysis is a method for collecting and counting X-rays leaving an electron irradiated specimen (Morgan, 1985).

The major advantage of EDS is : it can perform rapid (100 s) multi-element analysis over the energy range 1 - 20 KeV (Potts and Tindle, 1991; Morgan, 1985; Goldstein et al., 1981).

The disadvantage of EDS is its poor energy resolution which causes peaks to broaden with increasing energy which reduces the peak heights and decreases peak to background ratios (Morgan, 1985; Goldstein et al., 1981) (Figure 2.1). This also results in several peak overlaps in EDS analyses (Morgan, 1985).

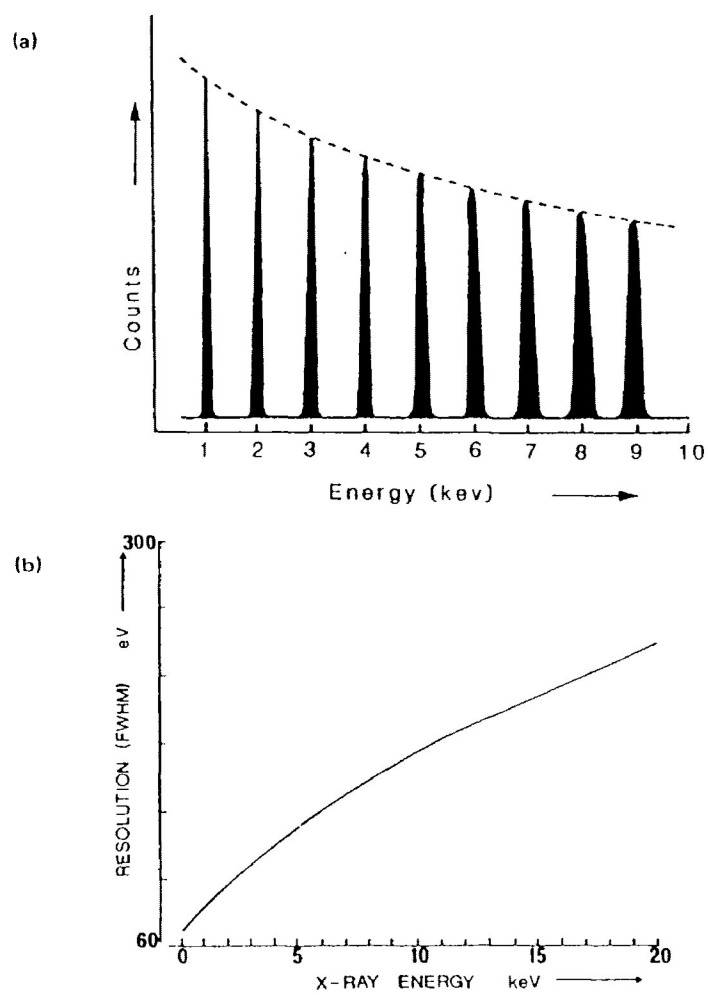


Figure 2.1 : Variation of peak width (a) and resolution (b) as a function of x-ray energy (after Morgan, 1985, p.26).

2.3. Backscattered Electrons

Backscattered electrons (BSE) are incident electrons which are elastically scattered through a large angle (Morgan, 1985). Incident electrons from the electron beam interact with the specimen's atomic nuclei, and are elastically scattered back through the specimen's surface. (Morgan, 1985; Wells, 1974; Fitzgerald, 1973). As the interaction with the atomic nuclei is elastic, negligible energy is lost from the electrons (Wells, 1974; Fitzgerald, 1973). Therefore, the BSE have high energies (> 50 eV) which are approximately equal to the electron beam accelerating potential (Morgan, 1985; Wells, 1974; Fitzgerald, 1973). The efficiency, or yield, of BSE increases with average atomic number of the specimen because the higher the average atomic number, the higher the energy of the electrons (Morgan, 1985; Fitzgerald, 1973). The lower atomic numbers (e.g. Na) have lower energy, and therefore can not always pass through the Be window of the BSE detector.

BSE are used for qualitative and quantitative compositional analyses (Morgan, 1985). The BSE images on the CRT screen are average atomic number maps (Wells, 1974). BSE images are particularly useful in investigating Platinum - Group Minerals (PGM) in a silicate - sulfide matrix as the PGM have high average Z , and therefore stand out as bright white grains in the grey silicate - sulfide matrix.

2.4. Standards

The PGM and sulfide standards used in this study were synthesized at Purdue University from pure elements in stoichiometric proportions by the sealed silica tube method by R. Loucks. The synthetic standards were :

<u>sulfides</u>	<u>tellurides</u>	<u>arsenides</u>	<u>electrum</u>
Ag ₂ S acanthite	Ag ₂ Te hessite	Ag ₃ AsS ₃ proustite	Ag ₃ Au ₂
AgBiS ₂ matildite	PdTe ₂ merenskyite		Ag ₂ Au ₃
Ag ₄ SeS aguilarite	PdBiTe michenerite		
Cu ₅ FeS ₄ bornite	PdSbTe testibiopalladite		
(Zn,Mn)S Mn-sphalerite			
(Zn,Fe)S sphalerite			

Three natural minerals from the Two Duck Lake PGE deposit (Watkinson and Dahl, 1987) were also used as standards :

Pd_{1.6}NiAs_{1.5} unnamed; PtAs₂ sperrylite; RhAsS hollingworthite. The Pd_{1.6}NiAs_{1.5} and PtAs₂ were analyzed at Lakehead University by MicroQ (see below) by the method of Mulja (1989).

The hollingworthite was analyzed by SEM / EDS at Lakehead University using the Tracor Northern analysis package MicroQ. A total of 17 analyses with totals of 100 ± 1.5 wt% were used to obtain the average composition for each element. These average compositions are used in calibrations of SQ correction factors (see below).

The silicate standards used in this study were well

characterized, homogeneous, natural minerals previously analyzed by wave length dispersive electron microprobe analysis.

orthoclase	$(K, Na)AlSi_3O_8$
kaersutite	$Ca_2(Na, K)(Mg, Fe)_4Ti[Si_6Al_2O_{22}](O, OH)_2$
augite	$Ca(Mg, Fe, Ti, Al)(Si, Al)_2O_6$
apatite	$Ca_5(PO_4)_3(F, Cl, OH)$
sylvite	KCl

2.5. Quantitative Analysis

2.5.1. ZAF Correction Procedure

The X-ray spectra were processed using the Tracor Northern computer program SQ (see below) with the ZAF correction procedure. The atomic number (Z) factor corrects for two effects both dependent on the average atomic number of the target : electron backscattering and electron retardation (Morgan, 1985; Goldstein et al., 1981). The Z factor accounts for the beam electrons backscattered from the surface of the bulk sample (Morgan, 1985). The fraction of the energy lost from the electrons to backscattering will not be the same in the sample and in the standard (Wells, 1974). The Z factor also accounts for the matrix stopping power which is how many characteristic X-rays are likely to be generated before the incident electrons decay to zero energy within the sample (Morgan, 1985). The stopping power decreases with atomic number (Wells, 1974). If this effect is not corrected for, analyses of heavy elements in a light element matrix generally yields values which are too low, and analyses of light elements in

a heavy matrix usually yields values which are too high (Goldstein et al., 1981).

The absorption (A) factor corrects for X-rays absorbed by the sample (Morgan, 1985). The lower the takeoff angle, the longer the distance that the X-rays must travel through the sample to reach the detector (Figure 2.2).

The fluorescence (F) factor corrects for primary x-rays which produce secondary X-rays or secondary fluorescence (Morgan, 1985). If the characteristic X-ray energy E for element i is greater than the ionization energy E_c of element j , $E_i > E_{cj}$, then element i will lose some of its characteristic X-rays to element j , and element j will have more X-rays generated than normal. In thin samples, the fluorescence correction is negligible or small because of the low probability of primary X-rays interacting with the sample (Morgan, 1985).

2.5.2. SQ and MicroQ

There are two computer programs devised by Tracor Northern to process EDS spectra : SQ and MicroQ. SQ is a standardless method of analysis based on multiple least squares fitting of the sample spectrum to the reference spectra as described by McMillan et al.(1985). The fitting technique assumes that each peak has a definite shape and location (Morgan, 1985). For SQ, the dead time, which is proportional to the beam current, is set at 20 - 30%DT. Therefore, the beam current has a broad range for SQ. The dead time is the time when the EDS system is not recording the incoming

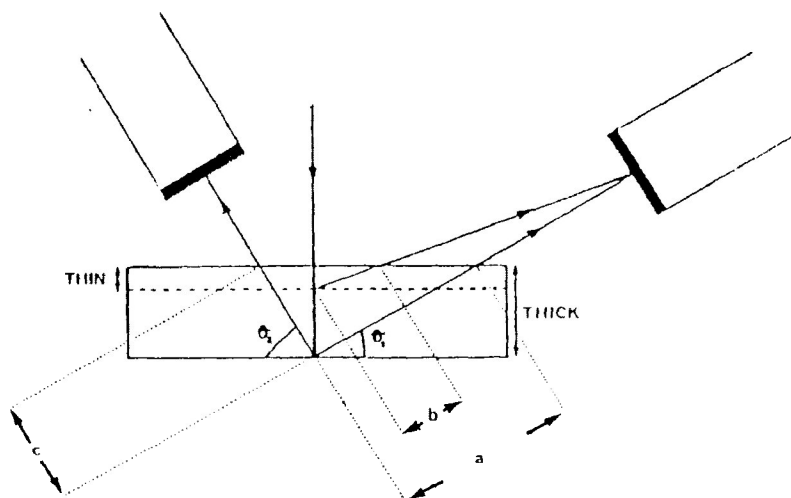


Figure 2.2 : Absorption distances are greater for thick specimens (a) compared with thin specimens (b). An increase in the takeoff angle from θ_1 to θ_2 reduces the absorption pathway from (a) to (c) (after Morgan, 1985, p.16).

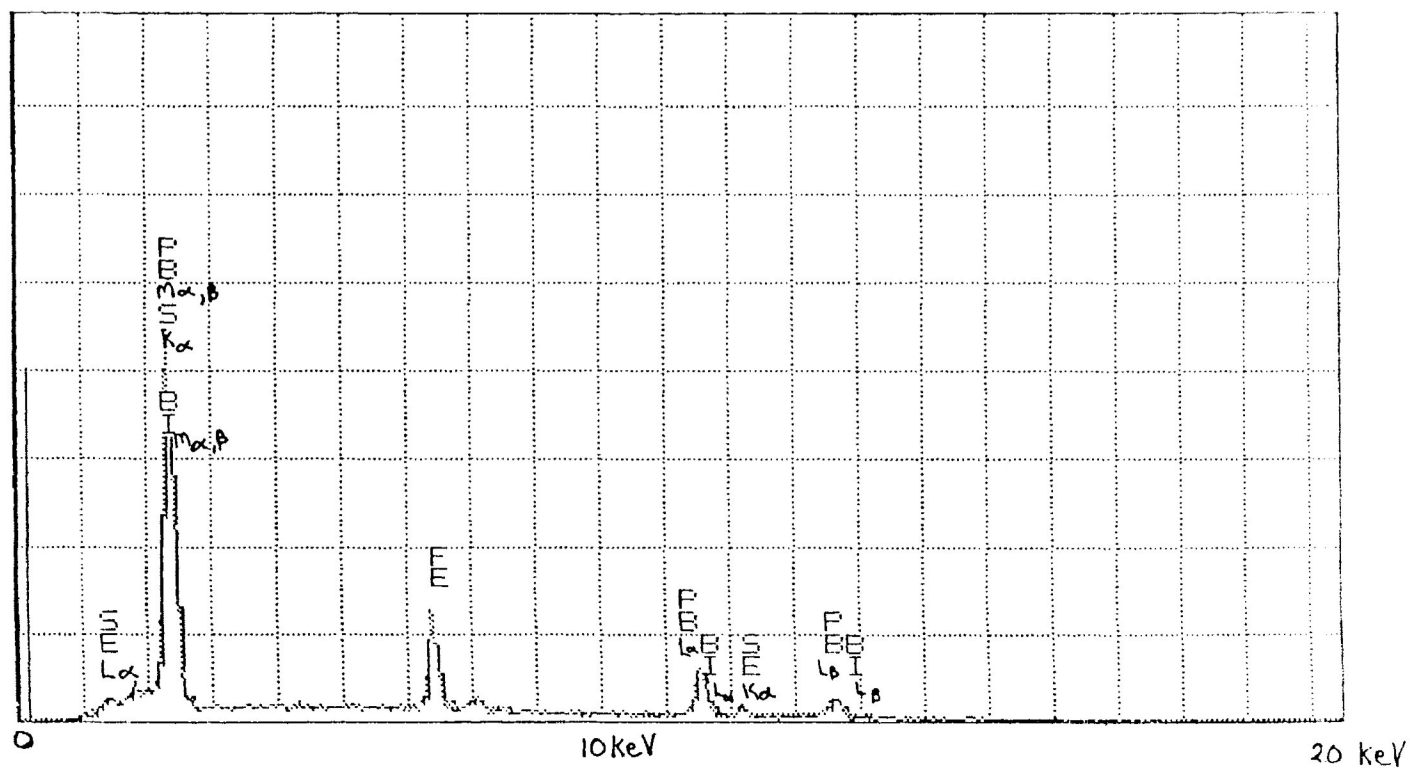


Figure 2.3 : An SEM / EDS spectrum of Se - bearing galena from drill core 13D-1.

photons (Morgan, 1985).

For MicroQ, the standards are analyzed and their spectra saved in a reference library. These spectra and count rates are compared with those in the spectrum for the sample. For MicroQ, the beam current is measured by a picoammeter at 0.38 nA before and after analysis. Therefore, the beam current has a narrower range for MicroQ than SQ.

The precision of SQ and MicroQ were compared by analyses of Pd₂Bi₅. Table 2.1 demonstrates that for heavy elements the precision of SQ is equal to MicroQ. Because the agreement between the two methods is excellent for PGM analyses, and SQ is less time consuming to use than MicroQ, SQ was used for this thesis.

2.6. Calibration of SQ Correction Factors

The SQ correction factors adjust quantitative analyses for instrumental drift within the SEM. The standards were analyzed once a month. The compositions obtained by the EDS SQ method were compared with the standard compositions. Then the correction factors were adjusted so that the SQ and the standard wt% compositions were approximately equal (within ± 0.50 wt%). Over a year, the correction factors vary due to instrumental drift caused by the age of the filament at the time of analysis, and a residue coating forming on the Be window of the detector (Table 2.2).

Table 2.1 : The comparison of the precision of MicroQ and SQ by the analyses of one grain of Pd₂Bi₅ from drill core sample 13B-1.

R% is the relative standard deviation and is defined as :

$$R\% = (2\sigma / \text{average}) * 100.$$

MicroQ			SQ		
analysis	Pd	Bi	analysis	Pd	Bi
7	26.98	73.02	3	27.77	72.23
2	27.33	72.67	4	27.97	72.03
3	27.72	72.28	5	28.27	71.73
12	27.78	72.22	6	28.31	71.69
10	27.92	72.08	2	29.25	70.75
6	28.27	71.73			
4	28.48	71.52			
13	28.61	71.39			
8,9	28.63	71.37			
11	28.68	71.32			
14	28.88	71.12			
15	28.98	71.02			
1	29.09	70.91			
average	28.26	71.81	average	28.31	71.88
1 σ	± 0.66	± 0.64	1 σ	± 0.57	± 0.55
2 σ	± 1.32	± 1.27	2 σ	± 1.14	± 1.11
R%	± 4.67	± 1.77	R%	± 4.01	± 1.54

Table 2.2 : SEM SQ correction factors. Note Oct. 12, 1992 the detector was cleaned.

		1991		1992										average	STD	Elements		
Elements		Oct.24	Nov.21	Jan.7	Feb.7	Mar.6	May 2	Jun.5	Jul.6	Aug.10	Sept.11	Oct.19	Nov.16					
Sulfides	Bi	1.18	1.13	1.13	1.30	1.20	1.22	1.25	1.16	1.25	1.26	1.20	1.17	1.20	0.05	Bi	Sulfides	
	Ag	2.00	1.80	1.90	2.10	1.90	1.90	1.95	1.92	2.00	2.05	2.10	1.95	1.96	0.09	Ag		
	S	1.40	1.40	1.40	1.40	1.40	1.40	1.40	1.40	1.40	1.40	1.40	1.40	1.40	0.00	S		
	Se	3.10	3.00	2.35	3.10	2.85	3.50	3.64	4.00	4.70	4.70	3.00	3.25	3.43	0.72	Se		
	Cu	1.25	1.25	1.40	1.30	1.23	1.20	1.16	1.01	1.07	1.07	1.10	1.15	1.18	0.11	Cu		
	Fe	1.38	1.38	1.45	1.45	1.30	1.30	1.24	1.08	1.15	1.15	1.20	1.30	1.28	0.12	Fe		
	Mn	1.40	1.40	1.60	1.50	1.35	1.37	1.37	1.15	1.15	1.20	1.25	1.45	1.35	0.14	Mn		
	Zn	1.20	1.20	1.20	1.25	1.20	1.17	1.08	0.93	1.01	1.01	1.03	1.15	1.12	0.10	Zn		
Tellurides	Pd	1.20	1.15	1.15	1.15	1.30	1.20	1.23	1.30	1.25	1.20	1.25	1.20	1.22	0.05	Pd	Tellurides	
	Te	0.95	0.95	0.95	0.95	0.95	0.95	0.95	0.95	0.95	0.95	0.95	0.95	0.95	0.00	Te		
	Bi	0.85	0.79	0.83	0.88	0.97	0.93	0.98	0.97	0.96	0.95	0.85	0.85	0.90	0.07	Bi		
	Sb	0.93	0.90	0.91	0.94	1.18	0.95	0.95	1.12	0.96	0.97	0.99	0.95	0.98	0.08	Sb		
	Ag	1.25	1.16	1.20	1.20	1.12	1.17	1.13	1.20	1.25	1.20	1.10	1.15	1.18	0.05	Ag		
Arsenides	Pd	1.75	1.62	1.25	1.60	1.53	1.46	1.55	1.35	1.50	1.50	1.65	1.65	1.53	0.14	Pd	Arsenides	
	Ag	2.10	2.00	2.10	1.90	1.90	1.90	1.85	1.82	1.80	1.80	1.98	1.95	1.93	0.10	Ag		
	S	1.40	1.40	1.40	1.40	1.40	1.40	1.40	1.40	1.40	1.40	1.40	1.40	1.40	0.00	S		
	As	3.30	3.30	2.60	2.70	3.20	3.20	3.37	3.40	3.68	3.68	3.00	3.00	3.20	0.34	As		
	Ni	1.20	1.18	1.35	1.15	1.05	1.07	1.00	0.85	0.90	0.90	1.13	1.13	1.08	0.15	Ni		
	Pt,Os,Ir	1.20	1.30	1.25	1.15	1.23	1.17	1.10	1.06	1.10	1.05	1.27	1.23	1.18	0.08	Pt,Os,Ir		
	Rh,Ru	1.95	1.90	2.00	1.80	1.80	1.85	1.85	1.60	1.74	1.60	2.15	2.00	1.85	0.16	Rh,Ru		
Metal	Ag	2.00	2.00	2.20	2.10	2.15	2.05	1.90	2.13	1.95	1.90	2.30	2.20	2.07	0.13	Ag	Metal	
	Au	1.00	1.07	1.07	1.07	1.07	1.07	1.07	1.07	1.07	1.07	1.07	1.07	1.06	0.02	Au		
Silicates		Jan.23, Feb.20, Mar.27 1993																
	Si	0.93																
	Ti	0.78																
	Al	1.04																
	Fe	0.68																
	Mg	1.38																
	Ca	0.78																
	Na	2.00																
	K	0.92																
	P	0.90																
Cl	0.92																	

Table 2.3 : Accuracy and precision of SQ EDS analyses of the PdBiTe standard (atomic %).
 Note that the filament burned out after analysis 20, so analysis 21 is with a new filament.

analysis	Pd	Bi	Te	Bi/Pd
ideal	33.33	33.33	33.33	
1	33.04	33.61	33.35	1.02
2	33.15	33.25	33.60	1.00
3	32.71	33.35	33.95	1.02
4	32.56	33.56	33.89	1.03
5	32.48	33.40	34.12	1.03
6	33.42	33.10	33.47	0.99
7	32.24	34.29	33.47	1.06
8	33.92	31.83	34.25	0.94
9	32.38	33.13	34.50	1.02
10	33.22	33.01	33.77	0.99
11	32.56	33.33	34.11	1.02
12	32.69	33.21	34.10	1.02
13	33.32	32.54	34.14	0.98
14	32.96	32.89	34.16	1.00
15	32.71	33.64	33.65	1.03
16	32.88	33.73	33.38	1.03
17	32.48	33.60	33.92	1.03
18	33.68	32.79	33.54	0.97
19	34.08	33.36	32.56	0.98
20	34.31	33.56	32.12	0.98
21	31.83	33.45	34.72	1.05
22	32.92	33.24	33.84	1.01
23	33.41	33.71	32.88	1.01
24	34.02	33.32	32.65	0.98
25	34.44	32.63	32.93	0.95
26	32.84	34.39	32.76	1.05
27	33.06	33.09	33.85	1.00
28	32.86	33.22	33.92	1.01
29	33.50	33.75	32.75	1.01
30	33.05	33.03	33.91	1.00
31	31.53	32.74	35.74	1.04
32	32.02	34.05	33.92	1.06
33	34.78	32.74	32.49	0.94
34	32.71	33.77	33.52	1.03
35	34.00	32.85	33.15	0.97
	Pd	Bi	Te	Bi/Pd
average	33.08	33.29	33.63	1.01
STD	+0.74	+0.51	+0.72	+0.03
2*STD	+1.48	+1.02	+1.44	+0.06
accuracy	-0.25	-0.04	0.30	0.01

2.7. Accuracy and Precision

The michenerite (PdBiTe) standard was analyzed for atomic % values 5 times a day for a total of 7 days over a 2 week period. The filament burned out and was replaced in the middle of the 2 week period. Therefore, these analyses account for the instrumental changes as a filament ages. The analyses are found in Table 2.3. Over the 2 week period, the SQ EDS analyses maintained good accuracy and precision. This validates the reliability of the SQ EDS analyses.

2.8. Method for Analyzing the Platinum - Group Element Minerals

The method for analyzing the PGM is as follows :

- a) A quick and simple map of each polished thin section is used as an orientation guide.
- b) The scanning speed on the SEM CRT (cathode ray tube) screen is set at one half rather than rapid because this gives a sharper focused image. The focus is adjusted at 3 500 x magnification, since most of the grains are < 4 μm in size. The backscattered electron (BSE) image on the monochrome SEM CRT screen is different shades of grey. The contrast is adjusted so that the silicates appear as dark grey, the sulfides as pale grey, and the PGM as bright white grains. The brightness of the mineral on the CRT screen reflects its average atomic number (Z). Platinum - Group Elements have high average Z and appear as bright white grains.
- c) A polished thin section is then scanned using a raster pattern to cover the entire polished thin section at 21.8 magnification.

Only PGM $> 10 \mu\text{m}$ can be seen at this magnification. After this scan has been completed, another scan at 200 magnification is used to find PGM $> 1 \mu\text{m}$.

d) When a grain of high average Z is found, it is qualitatively analyzed to determine if it is a PGM or galena. Galena is the other common high average Z mineral. It is impossible to distinguish between a PGM and galena by the BSE image. As Pb M_β and Bi M_α peaks overlap, the Pb $L_{\alpha,\beta}$ and Bi $L_{\alpha,\beta}$ peaks are used to distinguish between these two elements. A 10 s analysis over the energy range 1 - 20 KeV will reveal the Pb $L_{\alpha,\beta}$ and Bi $L_{\alpha,\beta}$ peaks. The problem is illustrated by figure 2.3 which shows Pb $M_{\alpha,\beta}$, and Pb $L_{\alpha,\beta}$ peaks and no Bi peaks. It also shows Se L_α and Se K_α peaks. Se substitutes for S in galena $\text{Pb}(\text{S},\text{Se})$. The S K_β peak is hidden under the Pb $L_{\beta 1}$ peak. Therefore, this grain is galena.

e) A sketch of the paragenesis of the PGM is then drawn to show its habit. Its shape (ie. anhedral, subhedral, euhedral) is noted, and its maximum diameter measured.

f) The magnification is increased so that the PGM fills most of the CRT screen to accurately place the beam spot, and reduce influence from the matrix. The PGM is then analyzed for 100 s using SQ.

2.9. Analytical Difficulties

There are several difficulties encountered in analyzing PGM:

a) The biggest problem concerns the small grain size of the PGM. Most of the PGM found were $\leq 2 \mu\text{m}$ in diameter. Another related

problem is grains that are too thin. Consequently, the elements in the surrounding minerals are excited by the overlap of the electron beam (Stone et al., 1992). These elements have to be subtracted from the quantitative analysis, and the remaining elements are renormalized to 100 at% and wt% (Stone et al., 1992). If the surrounding mineral is a sulfide and the PGM contains S, then the S from the sulfide has to be subtracted from the analysis according to the proportion of S found in the sulfide (Harney and Merkle, 1990). The remaining S belongs in the PGM. Stone et al. (1992) found the recalculated compositions in most cases approximate nominal stoichiometries which validates these correction procedures. Stone et al. (1992) also found that the WDS and EDS recalculated compositions for a submicrometric grain of chalcopyrite gave the similar results. A Fortran program was written to perform these calculations for analyses undertaken in this thesis.

b) The low takeoff angle of 18° for the Hitachi 570 EDS system affects the analysis. If the grain is wedge - shaped, tilted, or the whole polished thin section is tilted, the X-rays produced have a longer distance to travel and therefore, can be absorbed by the sample (Figure 2.4). This will produce an incorrect quantitative analysis.

c) The poor energy resolution of 150 eV at Mn K_α for the EDS system results in spectral peak overlap (Goldstein et al., 1981; Morgan, 1985). Peak overlap can hide smaller peaks that may be easily missed. The most common spectral overlaps are (S K_β , Bi M_α ,

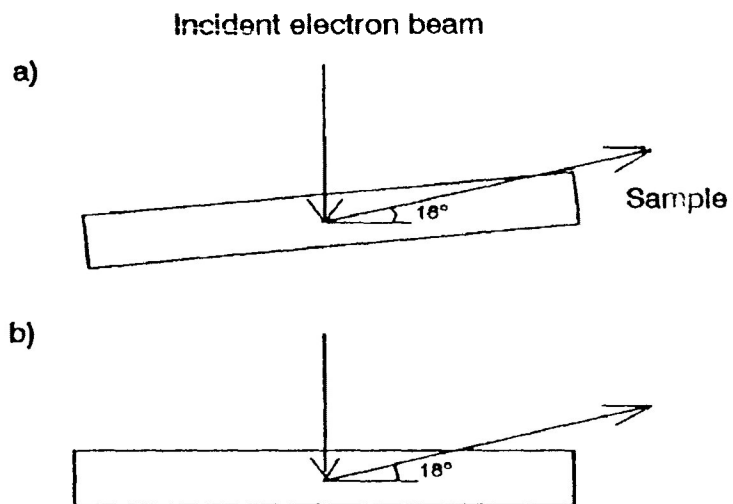


Figure 2.4 : More x-rays are absorbed by a tilted sample than by a horizontal sample. a) tilted sample and b) horizontal sample. takeoff angle = 18° .

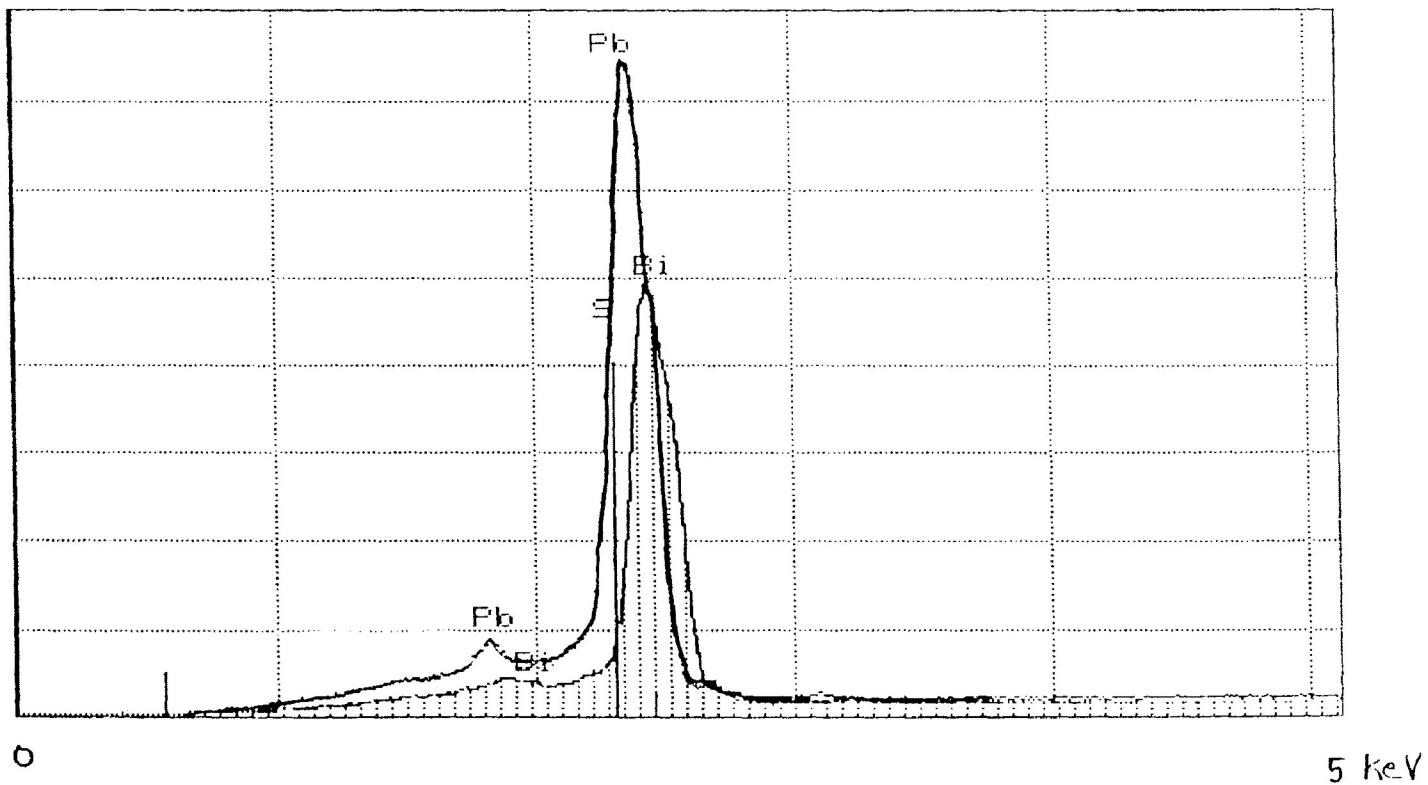


Figure 2.5 : SEM / EDS spectral peak overlap of Pb $M_{\alpha, \beta}$, Bi M_{α} , and S $K_{\alpha, \beta}$.

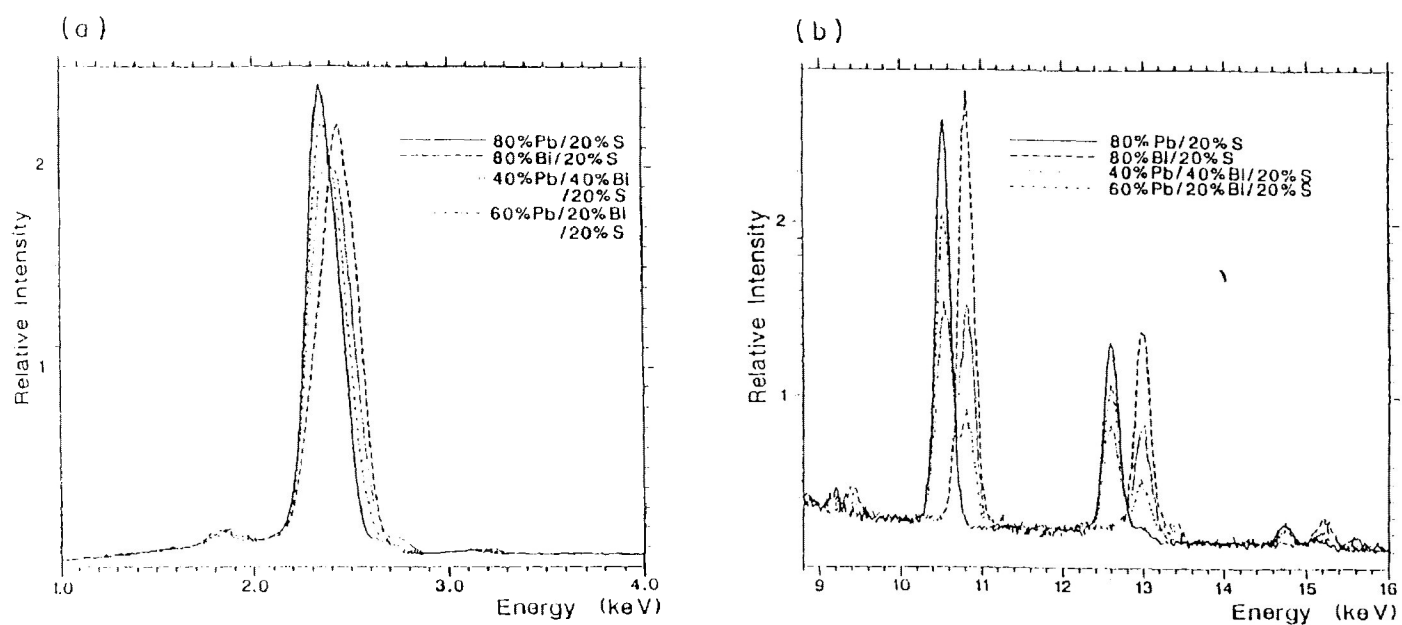


Figure 2.6 : Simulated spectra demonstrating the overlap interference between :
 a) the Bi M, Pb M, and S K lines and
 b) the Bi L and Pb L lines.
 Spectra correspond to apparent Bi contents of 80, 40, 20, 0 %, the balance corresponding to Pb and a fixed 20% contribution from S (pyrite) (after Potts and Tindle, 1991, p.127).

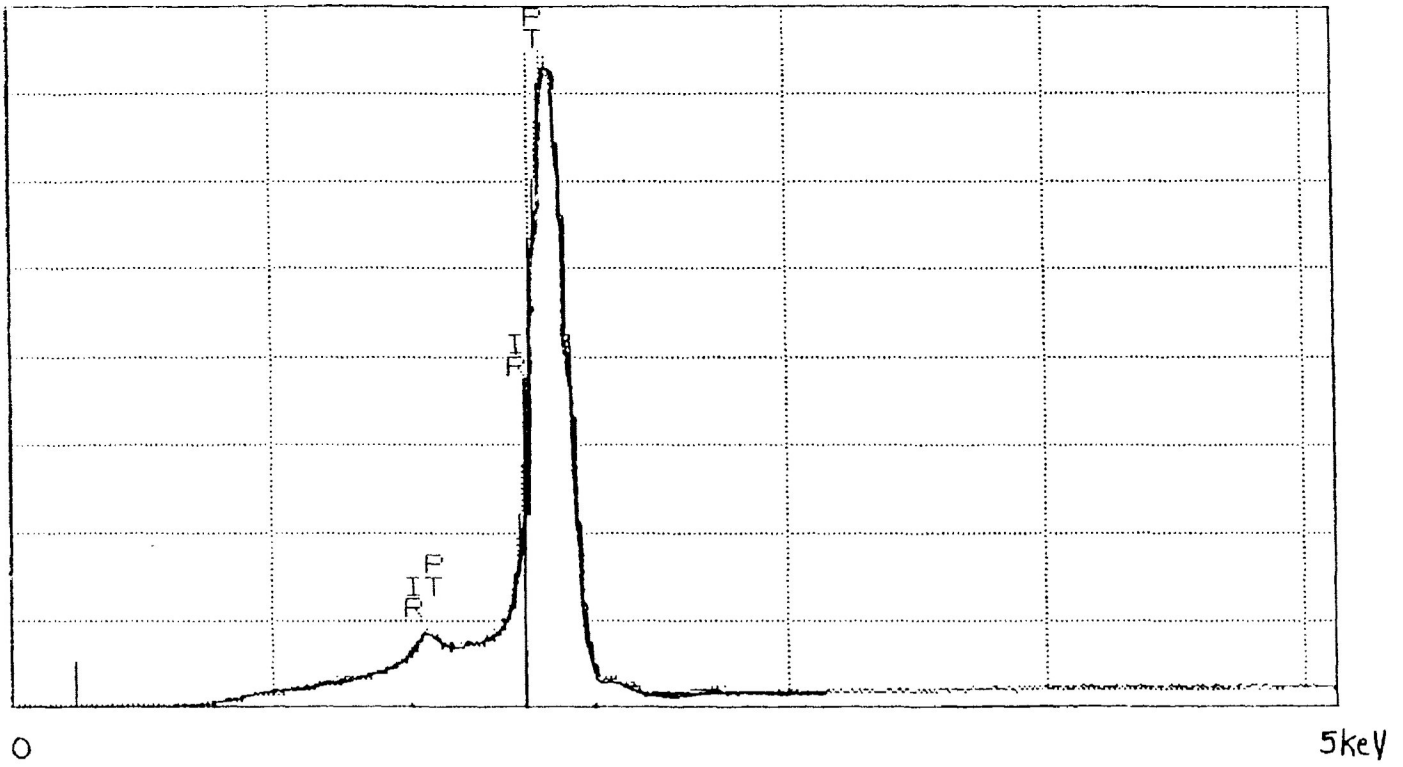


Figure 2.7 : SEM / EDS spectral peak overlap of Pt M_0 and Ir M_0 .

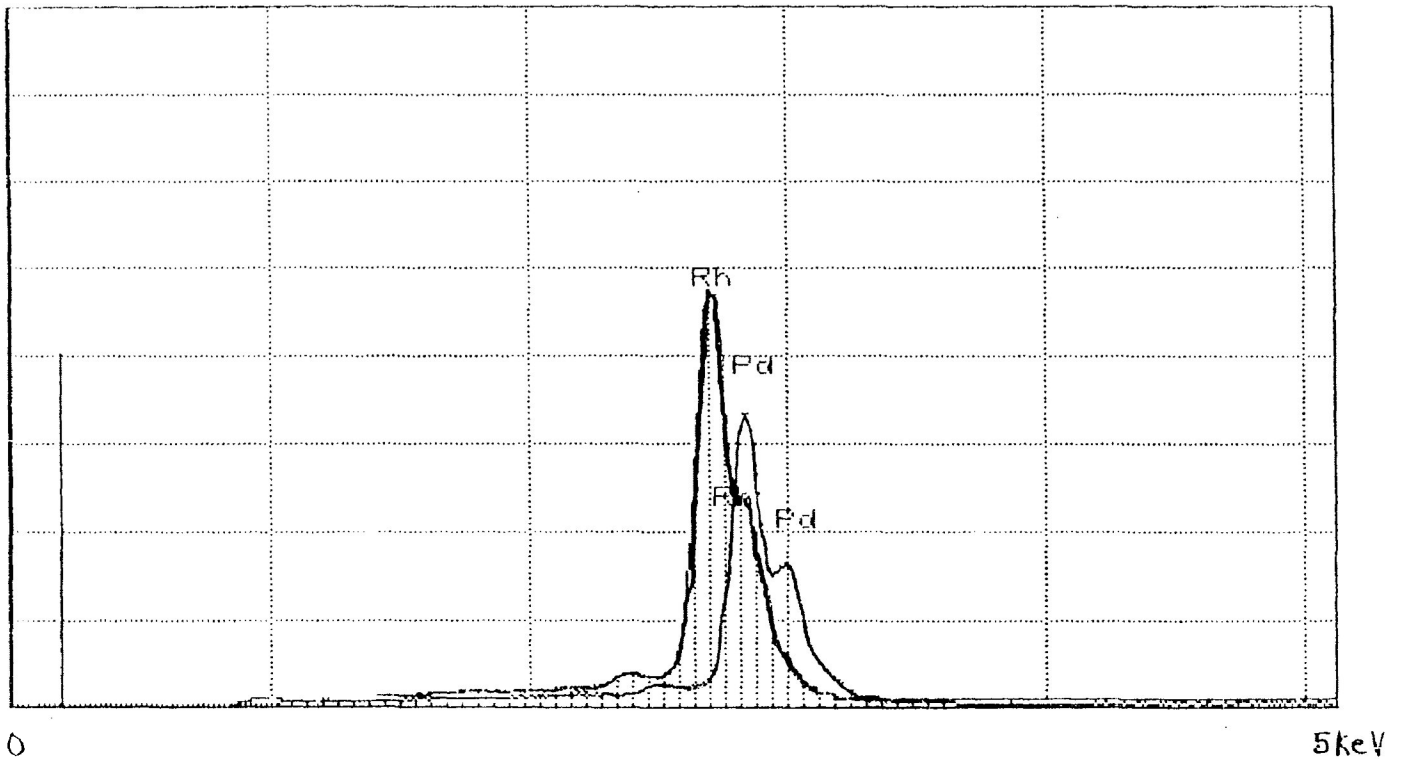


Figure 2.8 : SEM / EDS spectral peak overlap of Rh L_0 and Pd $L_{0,1}$.

and Pb M_β) and (S K_α and Pb M_α) (Figure 2.5, 2.6) (Potts and Tindle, 1991; Miller, 1981). Other peak overlaps are (Pt M_α and Ir M_α), (Rh $L_{\beta 1}$ and Pd L_α), (Rh $L_{\beta 2}$ and Pd $L_{\beta 1}$), (Ag L_α and Pd L_α), (Fe K_β and Co K_α), (Mg K_α and As L_α), (Ca K_α , Sb L_α , and Te L_α) and (Ca K_β , Sb $L_{\beta 1}$, and Te $L_{\beta 1}$) (Figure 2.7, 2.8). Harney and Merkle (1990) also noted the Te - Sb peak overlaps. The elements with M peaks usually have L peaks which can be seen by analyzing over the energy range 1 - 20 KeV. These L peaks do not overlap (Figure 2.3).

Another way to find hidden peaks is to subtract the peaks of the known elements from the spectrum. This is known as peak stripping or deconvolution. The spectrum deconvolution procedure incorporates least squares fitting of the prerecorded library spectra to the sample spectra (Potts and Tindle, 1991). The advantage of this procedure is that a specific shape for an X-ray photopeak (e.g. Gaussian) is not assumed, and the application can use K, L, and M X-ray lines (Potts and Tindle, 1991). The disadvantage of the least squares deconvolution procedure is the relatively high fitting error (chi-squared) associated with the deconvolution calculation which may reduce detection limits (Potts and Tindle, 1991). Miller (1981) found a detection limit of 0.1% S in a 50 - 60% Bi matrix with an analytical accuracy of ± 0.2 wt%. Potts and Tindle (1991) found a detection limit of 2.2% for Bi L and 1.5% for Bi M lines for compositions with $< 2.5\%$ Bi in a Pb - S matrix. They concluded that in cases of severe overlap, the numeric data from the spectrum deconvolution program is a more reliable indicator of the presence of an element than a visual

examination of the original spectrum (Potts and Tindle, 1991).

d) A spectrum is processed for quantitative analysis by subtracting one elemental peak from the spectrum at a time until all of the peaks have been removed. The chi-squared is the measure of the residual counts left after spectrum processing. An acceptable chi-squared for an analysis is < 3.0 . The chi-squared for most of the analyses in this thesis is < 1.5 . A high chi-squared commonly indicates (an) element(s) in the spectrum is not included in the quantitative analysis or poor peak resolution. To find the missing element, increase the peak to background ratio of the spectrum to see the smaller peaks. The missing element may also be hidden in a peak overlap, so subtract the known peaks to find it. A 10 s analysis over the energy range 1 - 20 KeV may also reveal the missing element.

The major cause of a high chi-squared is a poor fitting of the library peaks with the observed peaks which is influenced by the poor resolution of EDS (Potts and Tindle, 1991). This is commonly the case with sperrylite and electrum where Pt $M_{\alpha,\beta}$ and Pt $L_{\alpha,\beta}$, and Au $M_{\alpha,\beta}$ and Au $L_{\alpha,\beta}$ peaks can not be fitted very well.

A high chi-squared may also result from instrumental problems. Small fragments of ice can "dance" in the cryostat during boiling of the liquid nitrogen (Goldstein et al., 1981). This vibration can be transmitted to the EDS detector and reduces the resolution by as much as 30 eV (Goldstein et al., 1981). Residual oil and water vapour can condense on the Be window (Goldstein et al., 1981). This causes increased X-ray absorption and loss of

sensitivity at low X-ray energies (Goldstein et al., 1981).

e) Sometimes the SEM EDS has serious instrumental drift, especially just before a filament is about to burn out. This makes getting a good analysis of a grain $\leq 2 \mu\text{m}$ difficult since the beam spot drifts off the PGM grain. The beam size is assumed to be constant for a given current. To improve the quality of the analysis, analyze the grain for segments of time (e.g. 20 s) which are added to the previous analysis until the total of 100 s is reached. This allows the beam spot to be put back on the PGM grain every 20 s. A preferable option is to change the filament.

Chapter 3

The Silicate Petrography of the Mineralized Area

3.1. Introduction

The mineralized area of the Kawene Intrusion contains two rock types : clinopyroxenite and hornblendite. More detailed names can be given to these ultramafic rocks by adding the mineral qualifiers hornblende and/or biotite to the clinopyroxenites, and clinopyroxene and/or biotite to the hornblendites. The mineralogy and petrology of the clinopyroxenites and hornblendites are identical except for variable amounts of clinopyroxene, hornblende, and biotite. The clinopyroxenites contain 45 - 82 vol% clinopyroxene, 1 - 20 vol% hornblende, and 0 - 20 vol% biotite. The hornblendites contain 50 - 90 vol% hornblende, 2 - 20 vol% clinopyroxene, and 0 - 10 vol% biotite.

The primary minerals in these ultramafic rocks are : clinopyroxene, hornblende, biotite, calcite, and sulfides. The accessory minerals are : apatite, plagioclase, K-feldspar, rutile, and rare zircon, and sphene. Alteration of clinopyroxene and hornblende to actinolite is common in these rocks. Clinopyroxene and hornblende also alter to secondary biotite, secondary calcite, and chlorite. Feldspar alters to saussurite.

The mineralized area is cut by tonalite veins containing the primary minerals : 20 - 50 vol% quartz, 15 - 48 vol% plagioclase, 1 - 40 vol% hornblende, and 2 - 25 vol% biotite. The accessory minerals are apatite, sphene, opaques, and rare microcline. The

plagioclase alters to saussurite, sericite, secondary calcite, epidote, and minor muscovite. Drill core sample #12, hornblende tonalite, is cut by a veinlet consisting of quartz, plagioclase, and secondary calcite.

The ultramafic rocks are also cut by pyrrhotite - chalcopyrite veins, and veinlets containing calcite, biotite, opaques, rutile, chlorite, and minor epidote.

The minerals in the mineralized area are fine grained (< 1 mm) except for the actinolite oikocrysts which range from medium to coarse grained (2 - 4 mm).

3.2. Clinopyroxenites and Hornblendites

3.2.1. Petrographic Descriptions

As the petrology of the clinopyroxenites and hornblendites is identical, the minerals will be described just once.

Primary Minerals

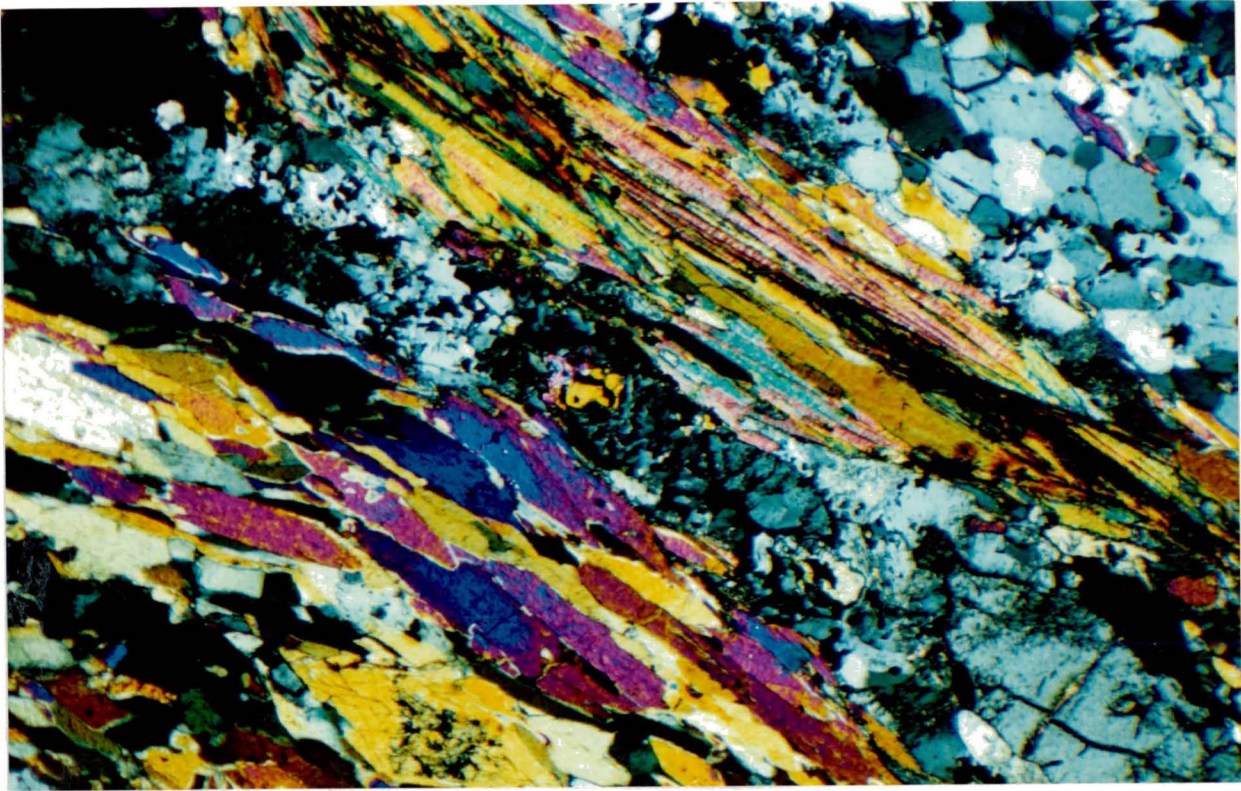
Amphiboles

There are four different habits of amphiboles in the ultramafic rocks : prismatic, columnar, anhedral, and oikocrystic.

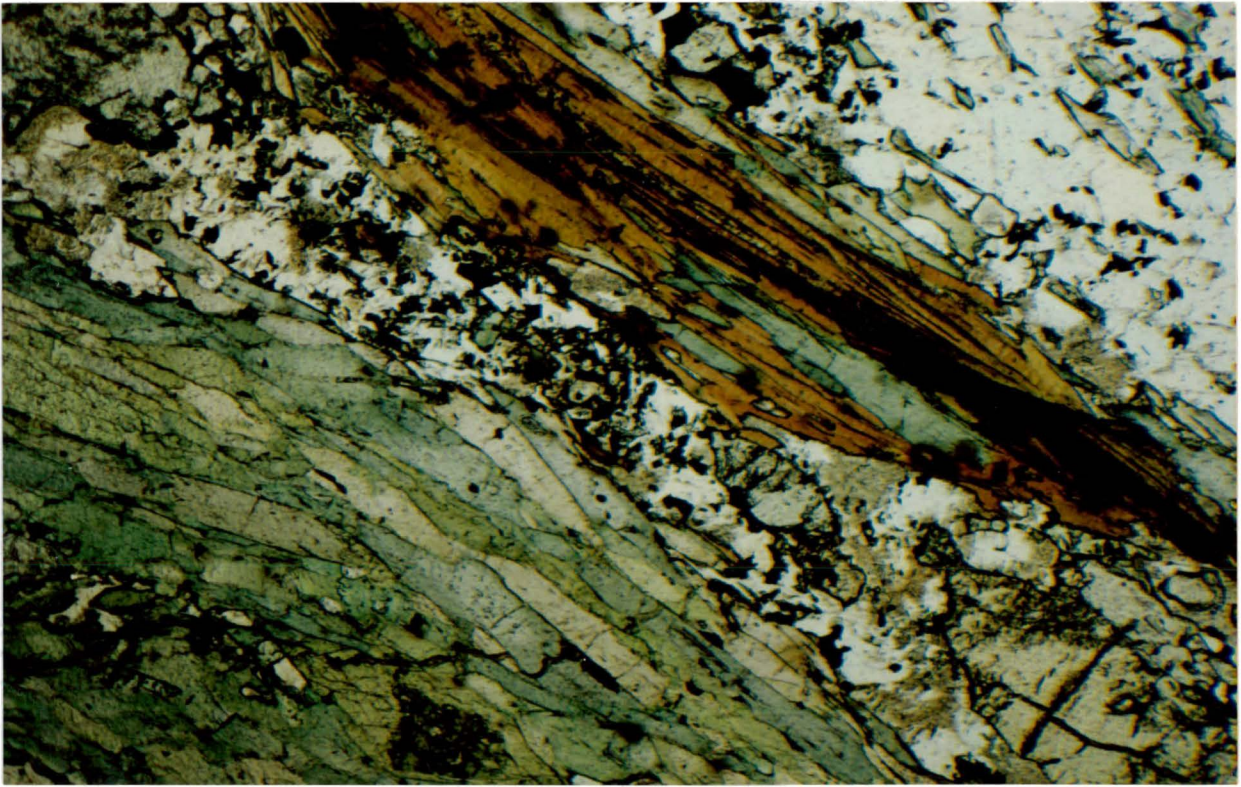
The prismatic, unaltered hornblendes are euhedral - to - subhedral, and are fine grained. They show simple and herringbone twinning, and are pleochroic yellow - to - green, colorless - to - pale green, or pale green - to - green in color. Prismatic hornblendes contain apatite, sphene, and opaque inclusions. Euhedral prismatic hornblendes are enclosed in sulfides. They are

Figure 3.1 : Prismatic hornblende and biotite from hornblendite aligned parallel to tonalite vein from drill core 15B-1.
a) crossed nicols b) plane polarized light.

a



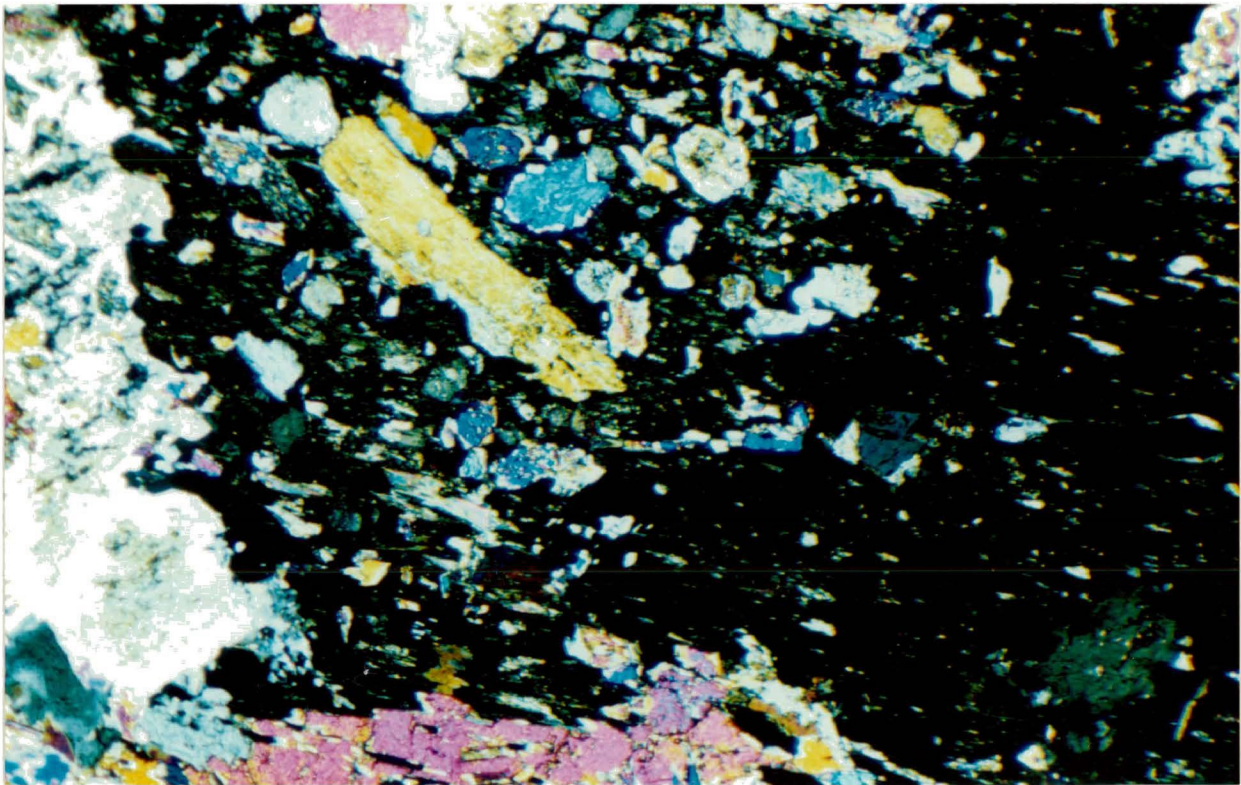
b



0 1 mm

A horizontal scale bar is located below the micrographs. It consists of a solid black line with short vertical tick marks at each end. The number '0' is positioned at the left end, and '1 mm' is positioned at the right end.

Figure 3.2 : Oikocrystic amphiboles (in extinction) with clinopyroxene inclusions from drill core 17A-2. crossed nicols.



0 1 mm

aligned parallel to the tonalite veins and the sulfide veinlets (Figure 3.1a,b).

The subhedral, fine grained, columnar amphiboles are hornblendes altering to actinolite. The columnar amphiboles show simple twinning, and are pleochroic pale green - to - colorless. They contain clinopyroxene, primary biotite, and sulfide inclusions, and they are rarely enclosed in sulfides.

Anhedral actinolite is the most common alteration product. Actinolite often shows strong cleavage. It is colorless or shows green - to - dark green pleochroism. The actinolites are commonly zoned : brown core - orange - red - purple - blue rim birefringence. Another common texture is grains with subhedral clinopyroxene or hornblende rims and anhedral actinolite cores. Actinolite contains inclusions of clinopyroxene and opaques, and is enclosed in clinopyroxene and hornblende grains. Actinolite alters to secondary biotite and chlorite along cleavage planes, and is replaced by secondary calcite.

Oikocrysts are large crystals of one mineral (actinolite) which enclose numerous, randomly distributed smaller crystals of another mineral (clinopyroxene) (MacKenzie et al., 1982). Actinolite oikocrysts are subhedral - to - anhedral and are medium - to - coarse grained. They contain inclusions of apatite, clinopyroxene, primary biotite, feldspar, and sulfides (Figure 3.2). The actinolite oikocrysts are primary since they contain inclusions of sulfides. Subhedral - to - anhedral clinopyroxene is the most common inclusion. There are tremolitic - hornblende

coronas around many of the inclusions. Actinolite oikocrysts alter to chlorite, secondary biotite, and secondary calcite.

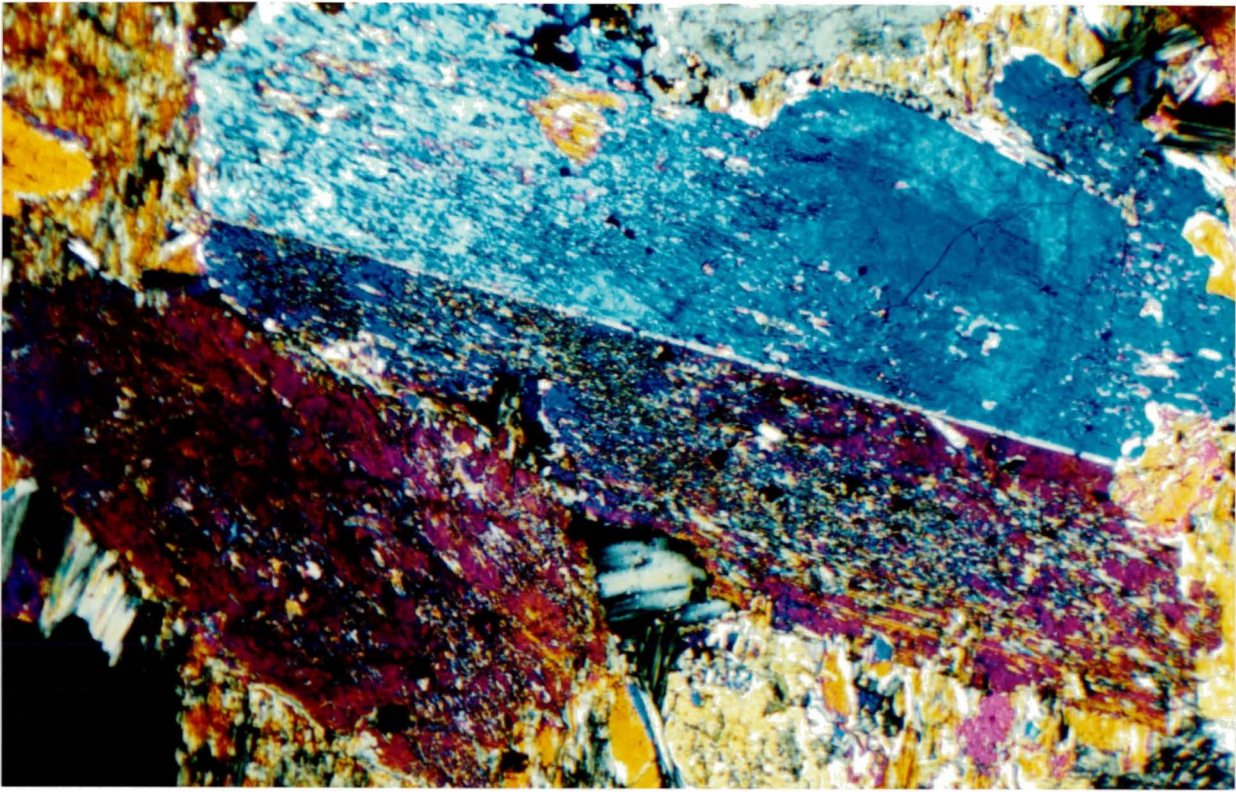
Three amphibole habits may result from an evolving magma during crystallization from fine grained, euhedral prismatic hornblende, to subhedral columnar hornblende, to coarse grained, anhedral actinolite oikocrysts. As the amphiboles increase in size, they lose their euhedral shape and their primary twinning. The actinolite oikocrysts and anhedral actinolite are untwined whereas the prismatic and columnar hornblendes show simple twinning. As the amphibole oikocrysts increase in size, they engulf other primary silicates. Anhedral actinolite is an alteration product of clinopyroxene and hornblende.

Clinopyroxenes

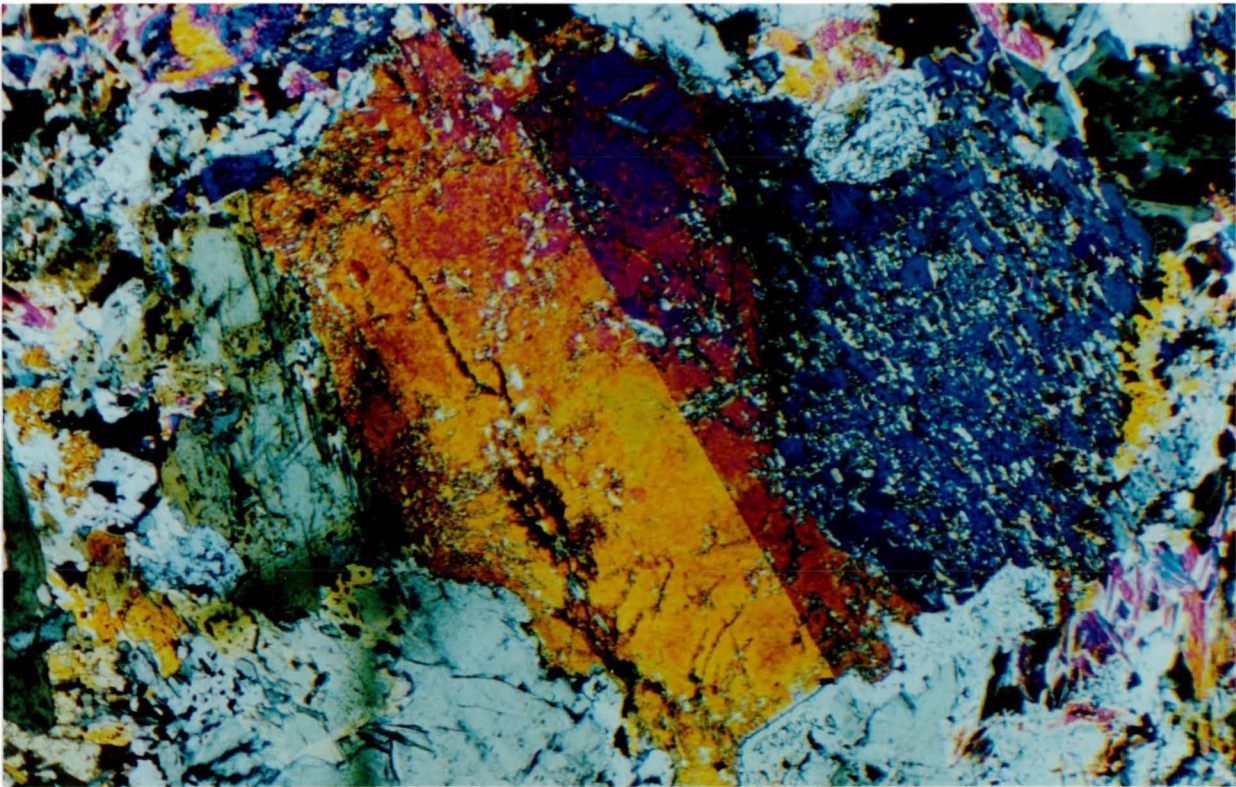
The clinopyroxenes, according to the microprobe analysis found in MacTavish (1992) using the classification system of Morimoto (1989), are diopside ($\text{CaMgSi}_2\text{O}_6$) and Ca-rich augite. The clinopyroxenes commonly show simple and herringbone twinning, and rarely show polysynthetic twinning (Figure 3.3). They are usually anhedral - to - subhedral due to uraltization and alteration to actinolite (Figure 3.4). Uralitization is the alteration of pyroxenes to secondary fibrous, greenish - blue amphiboles which are commonly considered to be actinolitic in composition (Deer et al., 1992). Uralitization begins along the rims and cleavages of pyroxene crystals (Deer et al., 1992). Uralite is derived from a reaction between residual water - enriched magmatic fluids and

Figure 3.3 : a) Clinopyroxene showing herringbone and polysynthetic twinning from drill core 27B-1. Clinopyroxene is weakly uralitized. Note interstitial chlorite (bottom center). crossed nicols.
b) Weakly uralitized clinopyroxene showing simple twinning next to (blue grain to the right) a more strongly uralitized clinopyroxene grain from drill core 22. crossed nicols.

a



b



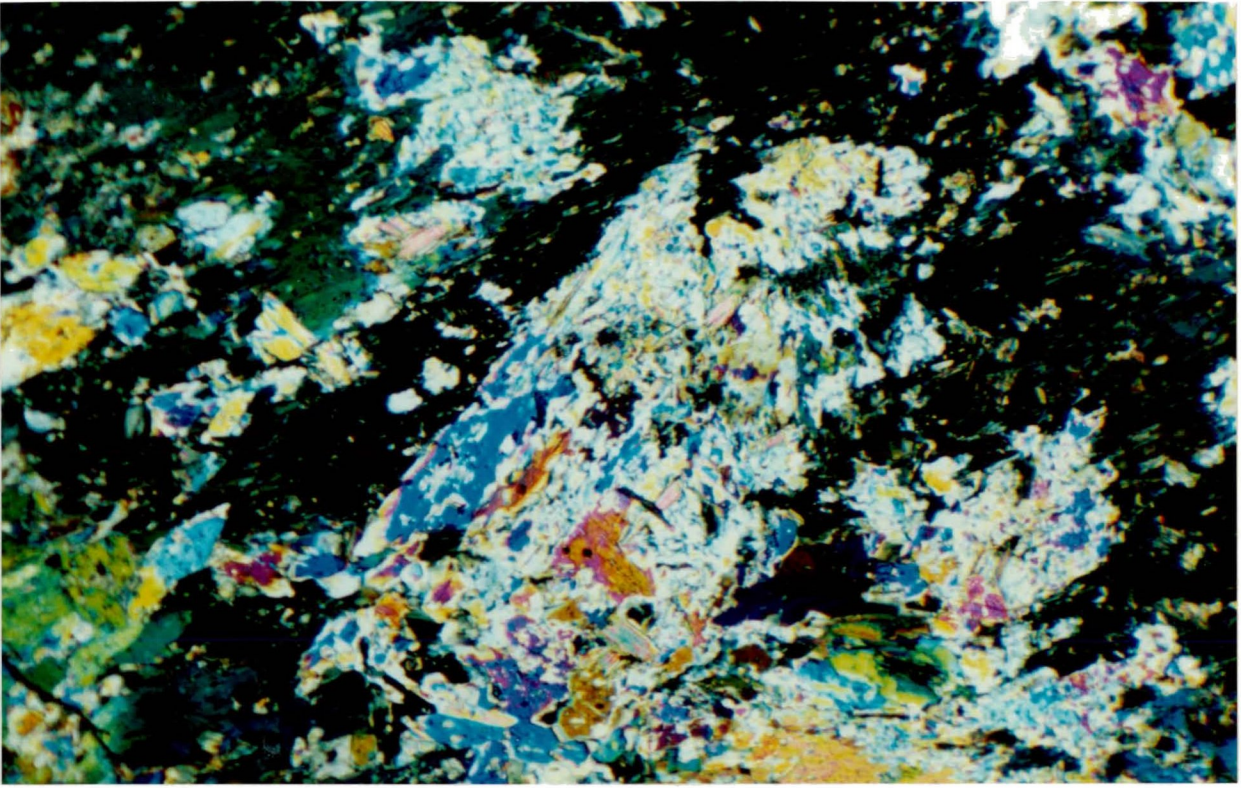
0 1 mm



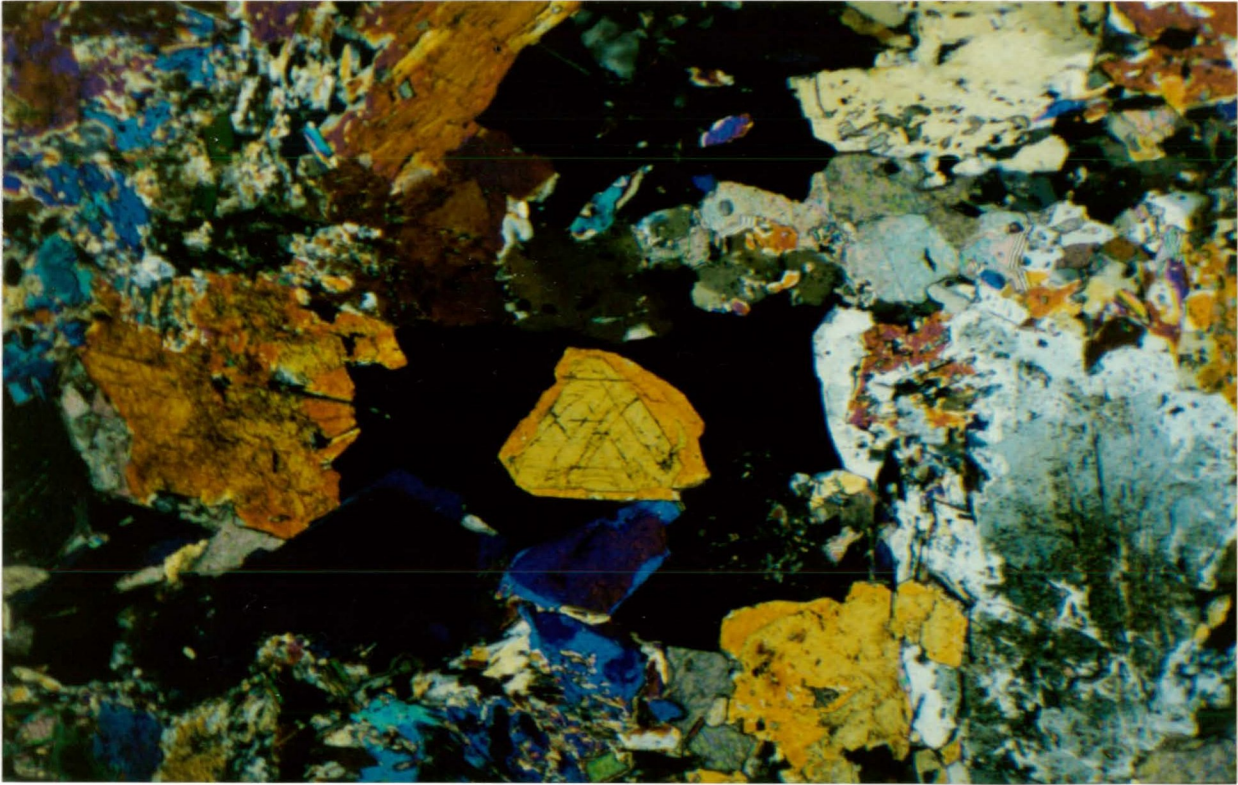
Figure 3.4 : a) Clinopyroxene (in extinction) altering to uralite and secondary biotite in the core from drill core 13D-1. crossed nicols.

b) Clinopyroxene (orange, blue) altering to actinolite (yellow, purple) in the core (center) from drill core 13D-1. Sulfide grains (opaque) are interstitial to the clinopyroxene and calcite grains. crossed nicols.

a



b

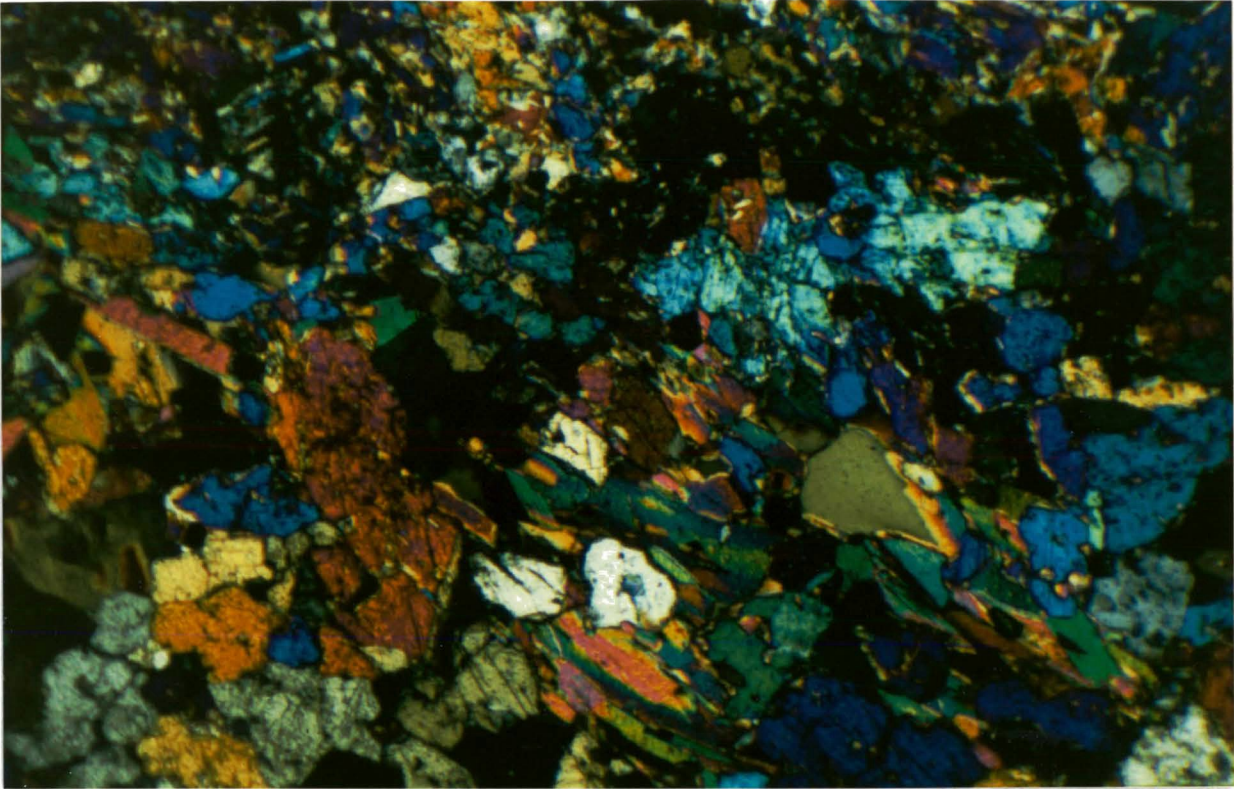


0 1 mm

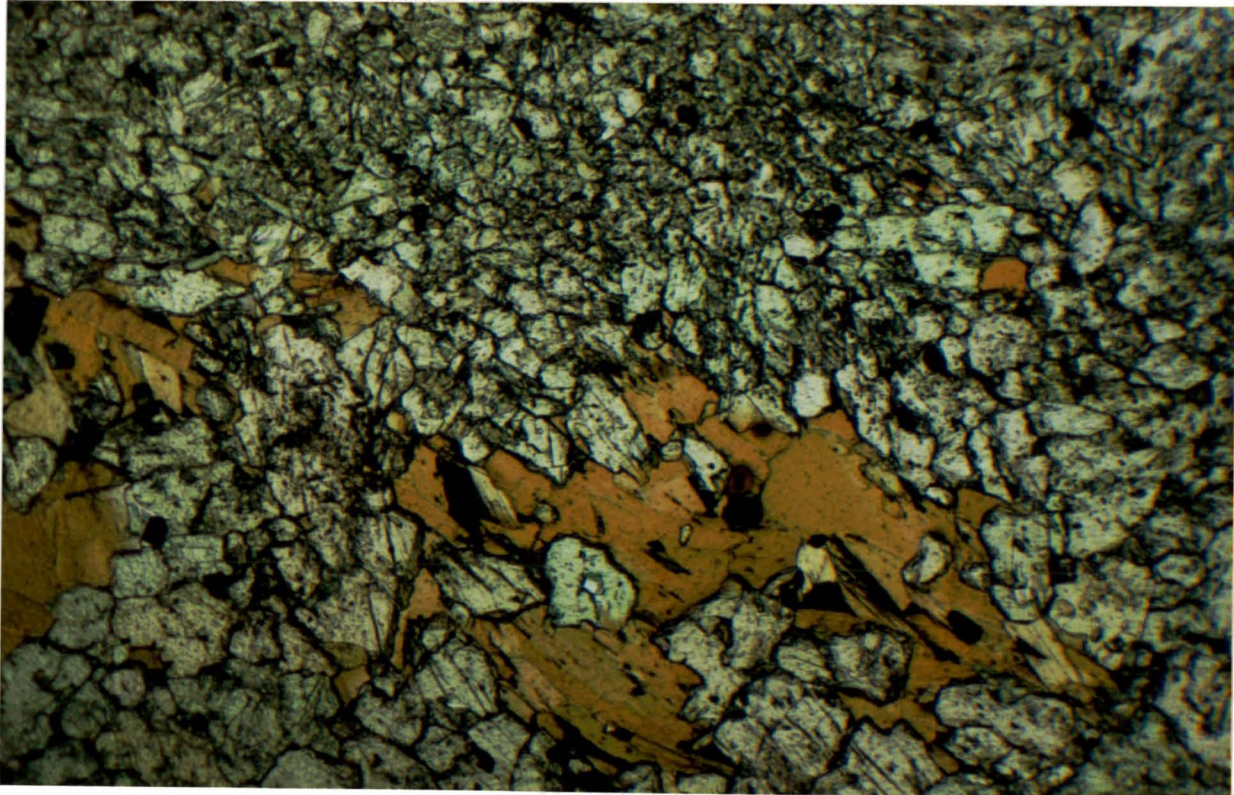
A horizontal scale bar with vertical end caps, indicating a length of 1 millimeter.

Figure 3.5 : Cluster of granoblastic clinopyroxene grains and interstitial biotite grains from drill core 24.
a) crossed nicols b) plane polarized light.

a



b



0 1 mm

A horizontal scale bar with vertical end caps. The number '0' is positioned at the left end, and '1 mm' is positioned at the right end. The bar itself is a thin black line.

earlier crystallized pyroxenes, or derived from regional, contact, or metasomatic metamorphism (Deer et al., 1992).

Clusters of equidimensional clinopyroxene grains with polygonal grain boundaries form a granoblastic mosaic texture (Figure 3.5). Granoblasts are granular - shaped crystalloblasts formed by "in situ" recrystallization of the pre-existing grains (Augustithis, 1990).

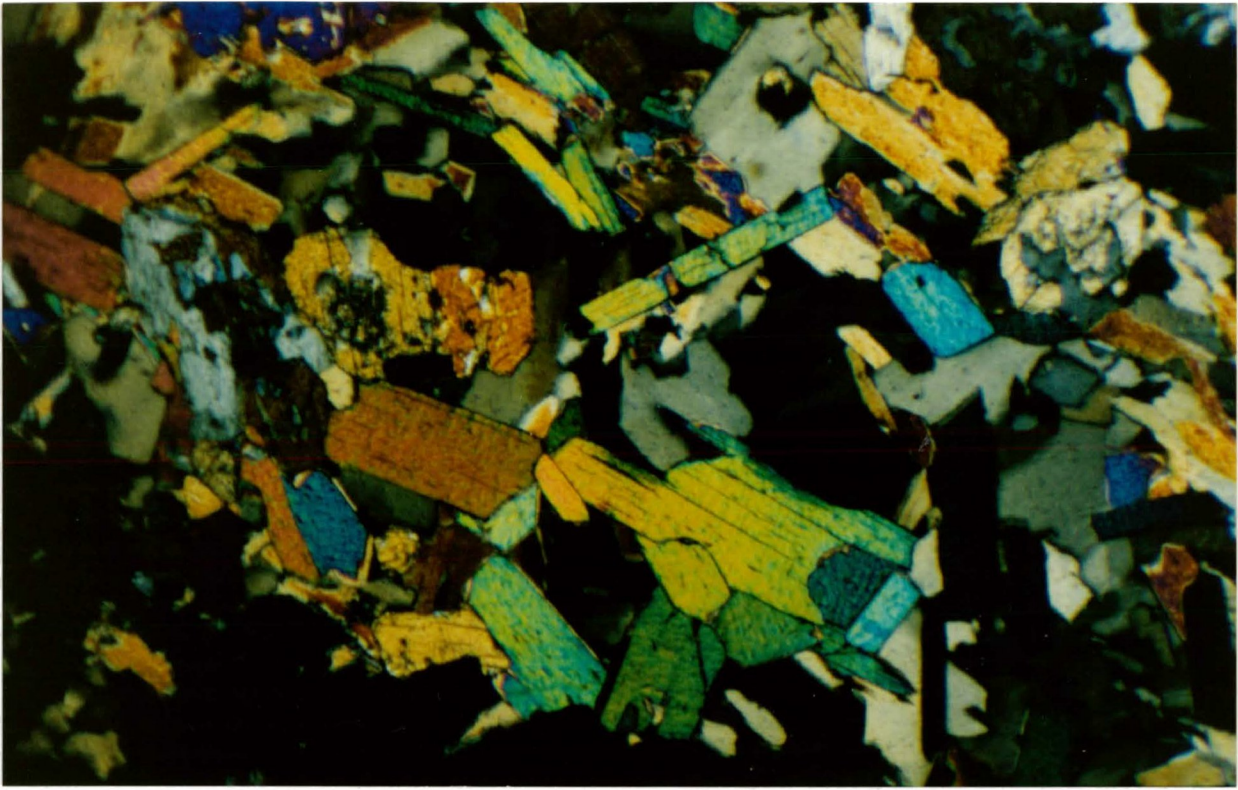
The clinopyroxenes are euhedral when in contact with sulfides. The clinopyroxenes contain inclusions of primary biotite, calcite, sulfides, actinolite, and minor plagioclase and K-feldspar. They are enclosed in sulfides and actinolite, and they are associated with biotite, hornblende, sulfides, and sphene.

Both primary and secondary biotites (see below) are found in these ultramafic rocks. The primary biotites are subhedral - to - euhedral and are commonly found in clusters (Figure 3.6). Whereas, secondary biotites are anhedral alteration products. The primary biotites contain pleochroic halos, and dendritic opaque inclusions. The primary biotite also contains inclusions of apatite, zircon, clinopyroxene, sphene, and sulfides. They are enclosed in columnar hornblende, primary calcite, and sulfides. They are also interstitial to clinopyroxene.

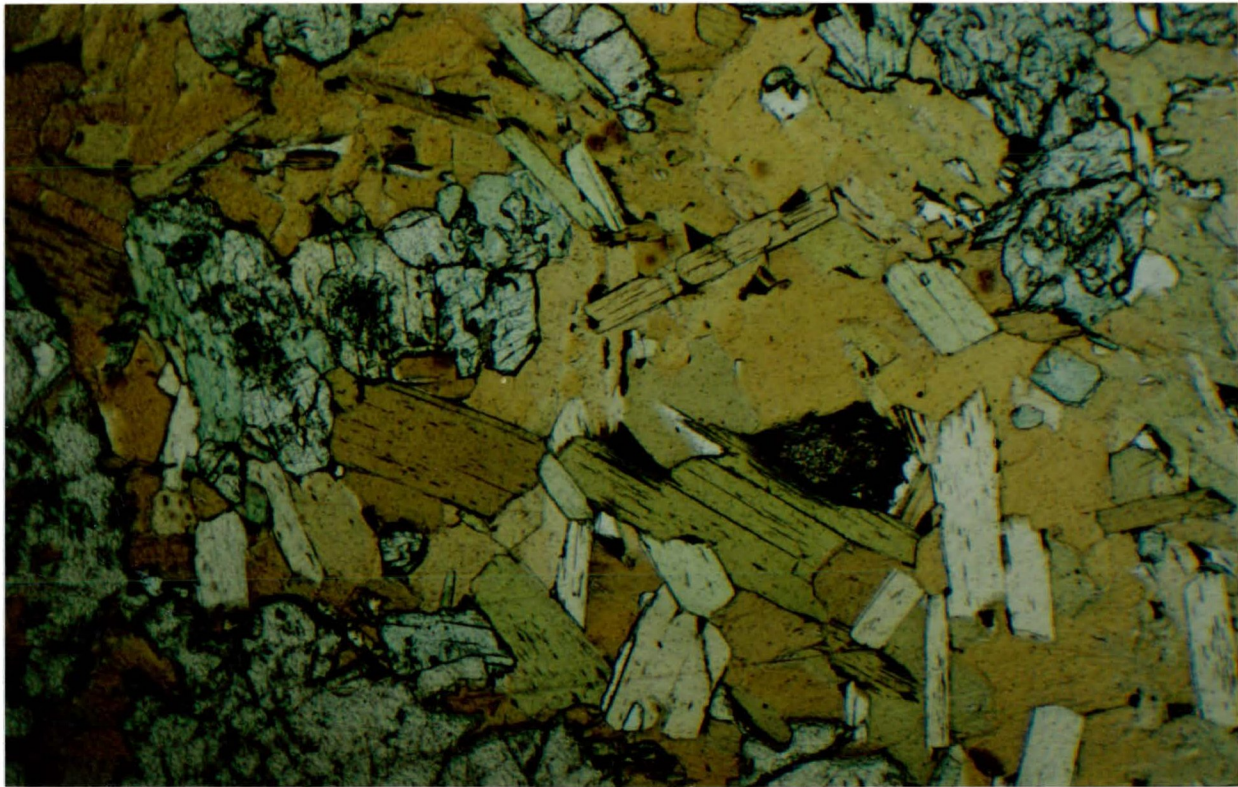
Both primary and secondary calcite (see below) are found in these ultramafic rocks. The primary calcite is subhedral - to - euhedral, shows polysynthetic twinning, and is rarely found in clusters. It is interstitial to clinopyroxene, prismatic

Figure 3.6 : A biotite cluster and granoblastic clinopyroxene grains from drill core 24.
a) crossed nicols b) plane polarized light

a



b



0 1 mm

A horizontal scale bar is located below the micrographs. It consists of a solid line with vertical tick marks at each end. The left end is labeled '0' and the right end is labeled '1 mm'.

hornblende, and feldspar. The primary calcite contains inclusions of clinopyroxene and euhedral primary biotite, and is enclosed in sulfides.

The most common sulfides are : chalcopyrite, pyrrhotite, and pentlandite. Some of the other sulfides are : galena, violarite $(\text{Fe,Ni})_3\text{S}_4$, and sphalerite. The sulfides are anhedral, and are interstitial to clinopyroxene, prismatic hornblende, columnar hornblende, primary calcite, and rare actinolite. The sulfides contain inclusions of euhedral clinopyroxene, prismatic hornblende, primary biotite, columnar hornblende, and primary calcite. The sulfides also contain minor inclusions of sphene, plagioclase, K-feldspar, and acicular chlorite.

Accessory Minerals

Apatite is euhedral and is enclosed in clinopyroxene, biotite, prismatic hornblende, feldspar, sulfides, and actinolite. Sphene is anhedral - to - euhedral, and rarely shows polysynthetic twinning. Sphene is enclosed in prismatic hornblende, biotite, sulfides, and actinolite. Where it is enclosed in sulfides, it is euhedral. Sphene is in contact with clinopyroxene, prismatic hornblende, primary biotite, columnar hornblende, feldspar, primary calcite, and sulfides.

Feldspar is anhedral - to - subhedral, and rarely euhedral. It shows weak albite twinning, and rarely Carlsbad twinning. The feldspar is plagioclase and K-feldspar (MacTavish, 1992). Feldspar contains inclusions of apatite, clinopyroxene, and biotite. It also

has inclusions of sulfides along its rim. Feldspar is enclosed in actinolite oikocrysts, and it only occurs in rocks with > 10 vol% hornblende.

Euhedral zircon is zoned, enclosed in biotite, and clinopyroxene. Zircon is only found in drill core sample #15, a biotite clinopyroxenite.

Secondary Minerals

The secondary biotites are anhedral, and are alteration products of clinopyroxene, hornblende, and actinolite. Secondary biotite is enclosed in actinolite, parallel to cleavage. It is associated with clinopyroxene, hornblende, actinolite, secondary calcite, chlorite, and rutile. Anhedral, secondary calcite is enclosed in actinolite parallel to cleavage. It is also enclosed in clinopyroxene and feldspar. Secondary calcite contains minor inclusions of euhedral sulfides.

Chlorite is another anhedral secondary mineral. Where it is enclosed in sulfides, it is acicular subhedral. In this habit, chlorite may have crystallized from residual water - rich fluids trapped in pore spaces with the immiscible sulfide melt. Chlorite is intergrown with biotite, and is enclosed in prismatic hornblende, biotite and columnar hornblende. Chlorite is also enclosed in actinolite and clinopyroxene parallel to cleavage.

Epidote is anhedral - to - subhedral, and is an alteration product of feldspar. Rutile is subhedral and is usually found in veinlets along clinopyroxene grain boundaries. Rutile is enclosed

in hornblende and actinolite, and is associated with biotite, actinolite, and opaques.

3.2.2. Paragenesis

The order of crystallization of the minerals in these ultramafic rocks was determined by examining their petrographic relationships with each other. The order of crystallization is :

Primary Minerals

1. apatite, zircon
2. clinopyroxene
3. sphene
4. prismatic hornblende
5. primary biotite
6. columnar hornblende, feldspar
7. actinolite oikocrysts
8. primary calcite
9. sulfides

Secondary Minerals

10. anhedral actinolite
11. chlorite, secondary biotite, secondary calcite, epidote
12. rutile

There is petrographic evidence for this order of crystallization. Apatite is enclosed in clinopyroxene, prismatic

hornblende, primary biotite, feldspar, and sulfides. Zircon is enclosed in clinopyroxene and primary biotite. Clinopyroxene contains inclusions of primary biotite and feldspar. Clinopyroxene is in contact with prismatic hornblende, primary biotite, columnar hornblende, sulfides, and minor sphene. Sphene is enclosed in prismatic hornblende, primary biotite, and sulfides. Prismatic hornblende contains apatite, sphene, and sulfide inclusions, and is enclosed in sulfides. Primary biotite is interstitial to clinopyroxene and prismatic hornblende. Primary biotite contains inclusions of apatite, zircon, clinopyroxene, and sphene, and is enclosed in columnar hornblende, feldspar, primary calcite, and sulfides. Columnar hornblende contains clinopyroxene, primary biotite, and sulfide inclusions, and is enclosed in sulfides. Feldspar contains inclusions of apatite, clinopyroxene, and primary biotite. Feldspar is enclosed in actinolite oikocrysts, and it only occurs in rocks with > 10 vol% hornblende. Feldspar and prismatic hornblende have euhedral boundaries. Actinolite oikocrysts contain clinopyroxene, primary biotite, feldspar, sulfide and rare apatite inclusions. Actinolite oikocrysts alter to chlorite, secondary biotite, and secondary calcite along cleavage planes. Primary calcite is interstitial to clinopyroxene, prismatic hornblende, and feldspar, and contains inclusions of clinopyroxene and euhedral primary biotite. Primary calcite has euhedral boundaries with clinopyroxene and sulfides, and commonly occurs between clinopyroxene and sulfide grains.

The sulfides are interstitial to euhedral primary silicates.

The sulfides contain inclusions of euhedral clinopyroxene, prismatic hornblende, primary biotite, columnar hornblende, and primary calcite, and rare apatite, sphene, and feldspar.

Anhedral actinolite is an alteration product of and is enclosed in clinopyroxene and hornblende. Anhedral actinolite alters to chlorite, secondary biotite, and secondary calcite along cleavage planes. Chlorite is an alteration product of clinopyroxene, prismatic hornblende, primary biotite, columnar hornblende, and actinolite. It is enclosed in clinopyroxene, and actinolite parallel to cleavage, and is intergrown with primary biotite. Secondary biotite is an alteration product of and is enclosed in clinopyroxene, biotite, and hornblende. Secondary calcite is an alteration product of and is enclosed in clinopyroxene and feldspar. Epidote is an alteration product of feldspar. Rutile is found in veinlets along clinopyroxene grain boundaries and cutting through hornblende and actinolite.

Watkinson and Irvine (1964) thought the order of crystallization for the Quetico intrusions was : olivine, olivine plus clinopyroxene, clinopyroxene plus hornblende, hornblende, hornblende plus plagioclase, and sphene. MacTavish (1992) interpreted a similar order of crystallization : olivine, olivine plus clinopyroxene, clinopyroxene, clinopyroxene plus hornblende, hornblende, and hornblende plus plagioclase. The order of crystallization for the Kawene Intrusion is similar, except for sphene which is placed before hornblende because it is enclosed in prismatic hornblende.

3.3. Tonalite Veins

3.3.1. Petrographic Descriptions

The petrographic descriptions of the mafic minerals in the tonalite is the similar to that of the ultramafic rocks. The major difference between the ultramafics and tonalite is, of course, the dominance of quartz and plagioclase in the tonalite.

Primary Minerals

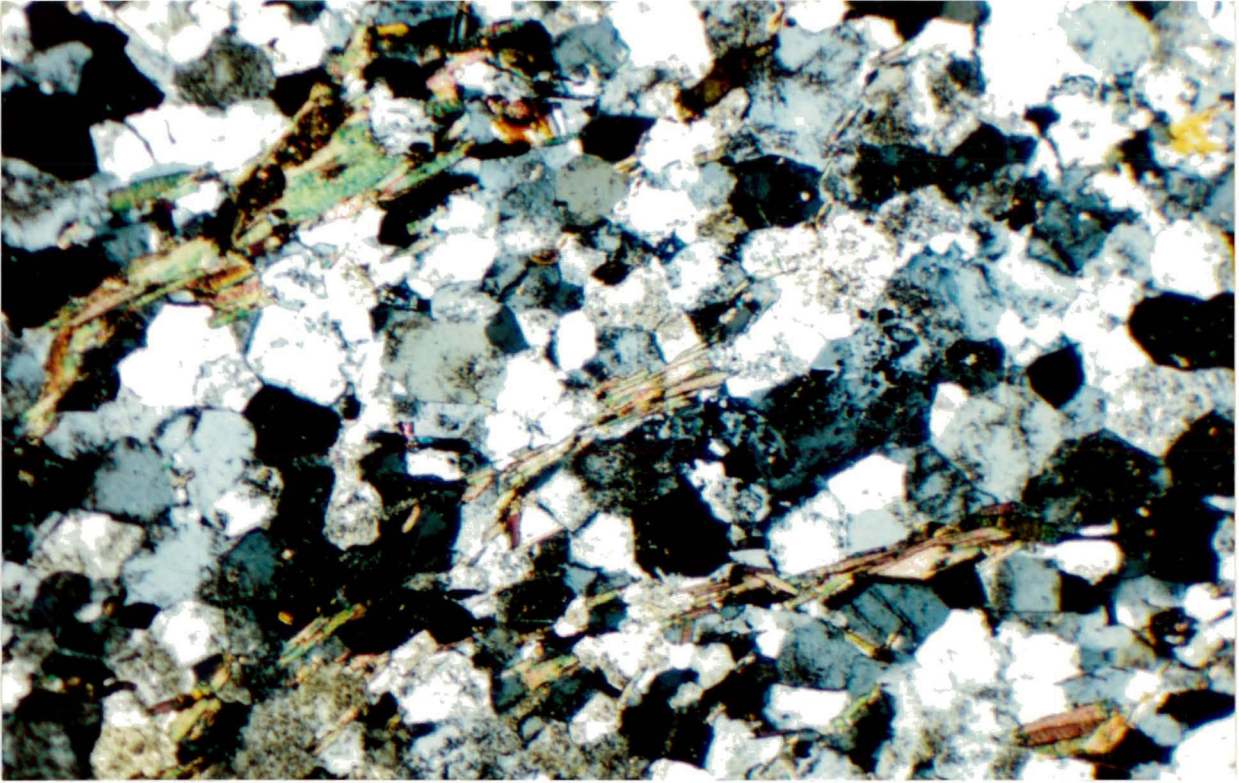
The quartz ranges in habit from anhedral - to - euhedral, and has apatite inclusions. In drill core sample #12, fractured quartz is found in oval pods surrounded by hornblende and saussuritized plagioclase. In drill core sample #18, the quartz and plagioclase have polygonal triple junctions, and form the metamorphic texture known as granoblastic mosaic (Figure 3.7).

Plagioclase is anhedral - to - subhedral tabular. It shows albite, Carlsbad, and rarely pericline twinning. Using the Michel-Levy method, the plagioclase in drill core sample #12 was determined to be oligoclase (An_{14}). Some of the plagioclase grains show zonation and undulose extinction. Plagioclase contains inclusions of apatite, primary biotite, hornblende, epidote, and secondary calcite. Plagioclase alters to saussurite, sericite, calcite, epidote, and rare muscovite. In the porphyritic biotite hornblende tonalite, drill core sample #14, the phenocrysts are plagioclase (Figure 3.8).

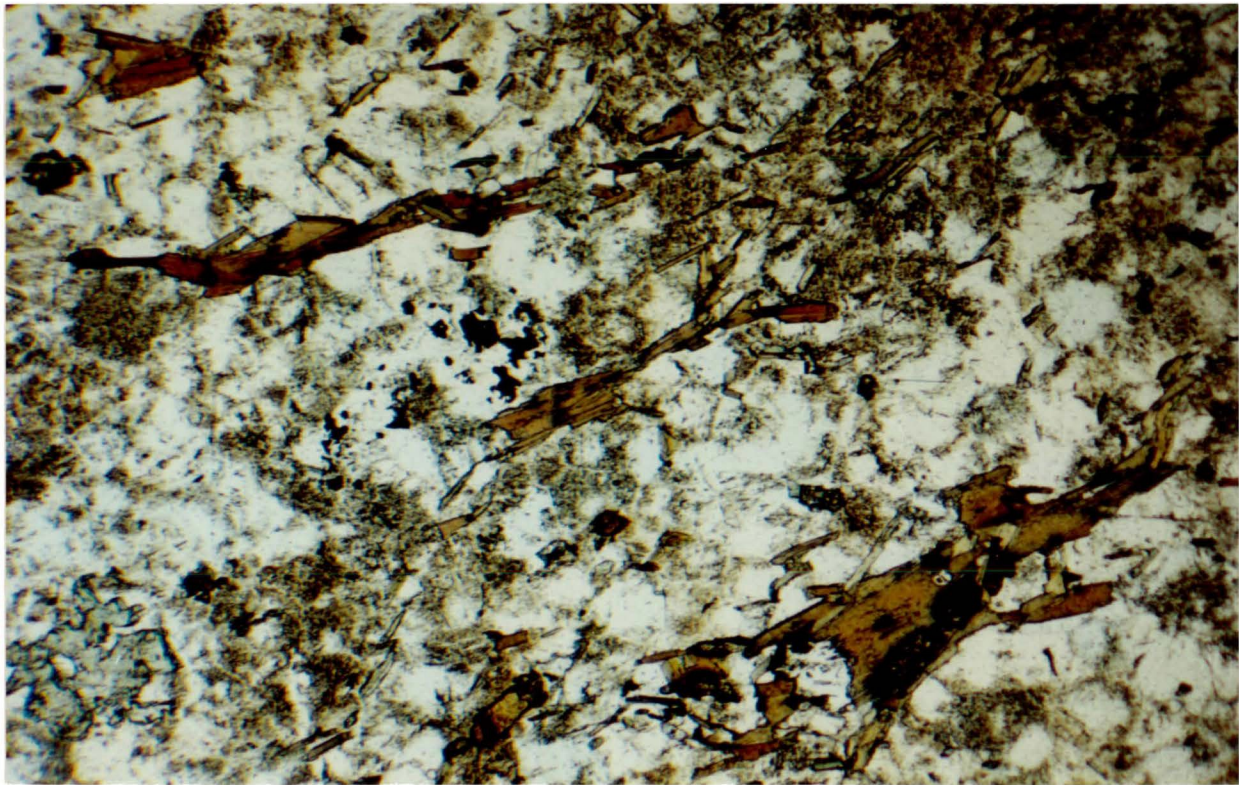
Hornblende is anhedral - to - euhedral and shows simple twinning. Hornblende has yellow - to - green, pale green - to -

Figure 3.7 : Granoblastic quartz and plagioclase, and aligned biotite from drill core 18 (tonalite). Plagioclase is altering to saussurite.
a) crossed nicols b) plane polarized light.

a



b



0 1 mm

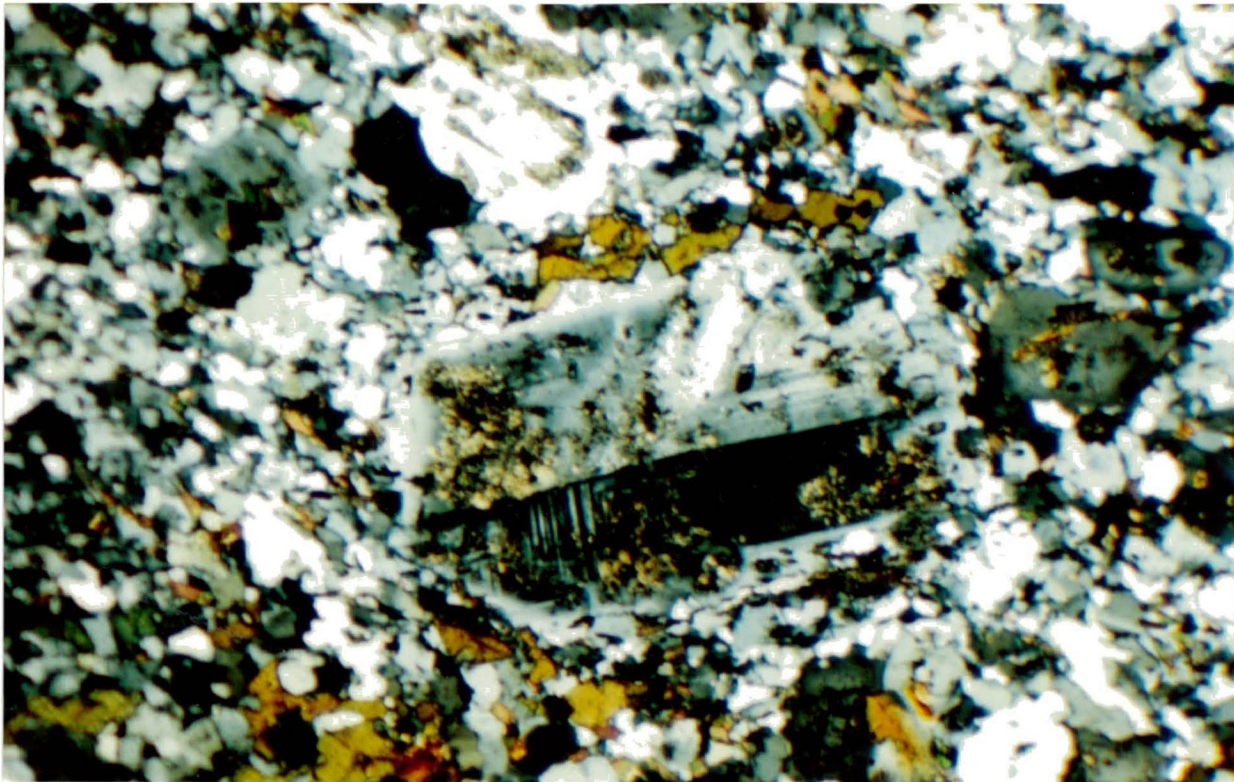


Figure 3.8 : Plagioclase phenocryst showing Carlsbad and albite twinning and altering to saussurite. Groundmass consists of quartz, biotite, and hornblende from drill core 14 (tonalite). crossed nicols.

green, and colorless - to - pale green pleochroism. Hornblende contains inclusions of apatite and sphene. Primary biotite is subhedral - to - euhedral and is associated with hornblende. Hornblende and primary biotite are aligned within the tonalite vein, and in the intruded ultramafic rocks parallel to the vein (Figure 3.7, 3.1).

Accessory Minerals

Euhedral apatite is enclosed in quartz, plagioclase, and hornblende. Sphene is subhedral - to - euhedral, and is associated with hornblende, and rare sulfides, plagioclase, calcite, biotite, and quartz. Anhedral microcline shows microcline twinning. The sulfides are anhedral - to - euhedral.

Secondary Minerals

Anhedral epidote is enclosed in plagioclase or associated with sulfides. Anhedral muscovite is also enclosed in plagioclase. Anhedral secondary calcite is interstitial to and enclosed within plagioclase.

3.3.2. Paragenesis

The petrographically determined order of crystallization is :

Primary Minerals

1. apatite, sphene
2. hornblende, primary biotite
3. plagioclase, quartz

Secondary Minerals

4. epidote, secondary calcite, muscovite

Apatite is enclosed in hornblende, plagioclase, and quartz. Hornblende contains inclusions of apatite and sphene. Biotite is associated with and has euhedral boundaries with hornblende. Plagioclase contains inclusions of apatite, hornblende, and biotite. Quartz and plagioclase have euhedral grain boundaries with each other.

Plagioclase alters to and has inclusions of epidote, secondary calcite, and muscovite.

3.4. Metamorphic Textures

The mineralized area has been metamorphosed to upper greenschist - to - lower amphibolite metamorphic grade (Pirie and Mackasey, 1978). Several metamorphic textures can be seen in the petrography of the ultramafic rocks and the tonalite veins.

The mineralized area has undergone deuteric, hydrothermal alteration. Clinopyroxene and hornblende altering to actinolite, secondary biotite, and chlorite is the dominate texture in the ultramafic rocks. Some of the clinopyroxenes have actinolite cores (Figure 3.4b). Some of the clinopyroxenes are altering to secondary fibrous amphiboles known as uralite (Figure 3.4a).

As the evolving amphiboles crystallize fine grained, euhedral, prismatic hornblende; subhedral, columnar hornblende; and medium - to - coarse grained actinolite oikocrysts, they increase in size

and lose their euhedral habit. The actinolite oikocrysts engulfed primary minerals as they grew (Figure 3.2). Some of the inclusions in the oikocrysts are surrounded by coronas.

The preferred orientation of minerals in the mineralized area indicate that the area has undergone low energy, ductile stress (Best, 1982). Within the hornblendites, prismatic hornblendes are aligned parallel to tonalite veins and sulfide veinlets (Figure 3.1). Within the tonalite veins, hornblende and primary biotite are aligned parallel to the ultramafic - tonalite contact (Figure 3.7b). Another indicator of ductile stress is the plagioclase in the tonalite veins shows undulose extinction.

Some of the primary minerals have been recrystallized during deformation by high energy, thermodynamic ductile stress (Best, 1982). The clinopyroxenes in the ultramafic rocks, and the quartz and plagioclase in the tonalite veins show a granoblastic mosaic texture (Figure 3.5, 3.7a). The minerals within this texture are equidimensional grains with straight boundaries and 120° triple junctions.

3.5. Petrogenesis of Mineralized Area

3.5.1. Petrography

The primary minerals of the clinopyroxenites and hornblendites crystallized first. Then the interstitial primary calcite crystallized. Next the interstitial sulfides crystallized filling in the spaces between the primary minerals and even engulfing some of them. MacTavish (1992) agreed that the sulfides are

interstitial.

The clinopyroxene was uralitized, and the primary minerals altered to secondary minerals. Since primary sulfides and secondary minerals crystallize at similar low temperatures, these minerals may have formed at approximately the same time. This would explain why euhedral chlorite can be found enclosed in sulfides.

Finally veinlets containing rutile, biotite, calcite, chlorite, sulfides, and minor epidote intrude clinopyroxenites and hornblendites. Sulfide veinlets and tonalite veins also cut through the ultramafic rocks. The tonalite veins are not cut by silicate or sulfide veinlets. Hornblende and biotite in the intruded ultramafic rocks are aligned parallel to the tonalite veins, but not to the sulfide veinlets. Therefore, the tonalite veins intruded the ultramafic rocks after the sulfide veinlets.

As both the ultramafic rocks and the tonalite veins have been affected by metamorphism, the metamorphic event must have occurred after the cooling of the ultramafic rocks and the tonalite veins.

3.5.2. Lithographic Column

Since the petrographic characteristics of the clinopyroxenites and hornblendites are identical, these ultramafic rocks were derived from the same magma chamber. A lithographic column of drill hole K87-1 shows the relationships between the rock types (Figure 3.9). There is a noticeable alternation of clinopyroxenite and hornblendite. Tonalite veins cut between several of the

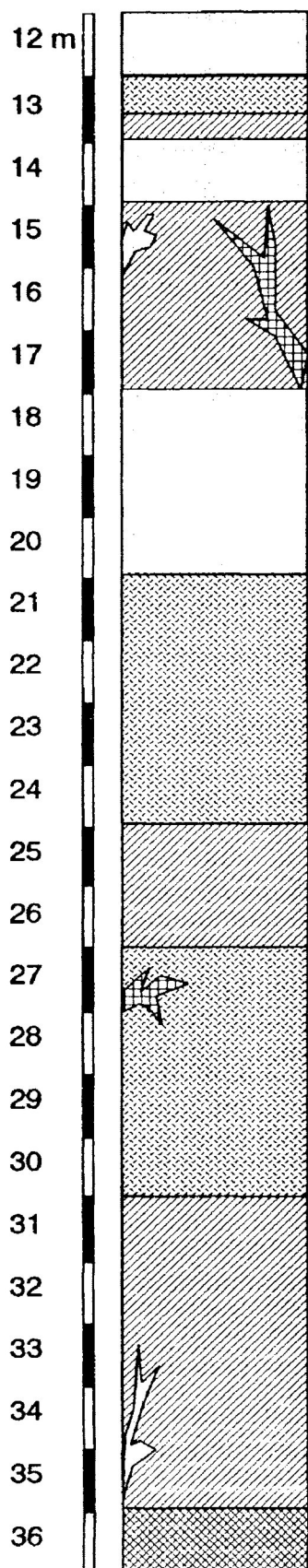

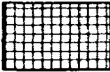
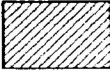
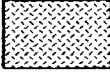
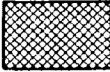


Figure 3.9 : Lithographic column of drill hole K87-1.

Legend

-  Tonalite vein
-  Sulfide veinlet
-  Clinopyroxene Hornblendite
-  Hornblende Clinopyroxenite
-  Wehrlite

clinopyroxenite and hornblendite layers. The distribution of ultramafic units resembles that of layered intrusions. The wehrlite represents the unmineralized core of the Kawene Intrusion. Clinopyroxene crystallized before hornblende. Therefore, the magma could have crystallized clinopyroxenite until the magma was depleted in clinopyroxene and enriched in hornblende. Then the magma crystallized hornblendite until it was depleted in hornblende and enriched in clinopyroxene. This cycle continued until the magma was consumed.

3.5.3. Crystallization Sequence of the Intrusion

The map of the Kawene intrusion can be used to examine the relationships between the lithological units (Figure 1.1). The center of the intrusion is hornblende wehrlite. This would have crystallized first since olivine usually crystallizes before clinopyroxene. Next to crystallize is the hornblende clinopyroxenite. Along the outer edge of the intrusion is hornblendite which would crystallize next, since clinopyroxene crystallizes before hornblende. The last to crystallize is hornblende melagabbro which is along the outer rim of the eastern part of the intrusion.

Chapter 4

Silicate Mineralogy

4.1. Clinopyroxene

The clinopyroxene in the Kawene Intrusion was classified according to Morimoto (1989). In the hornblende clinopyroxenite, the clinopyroxene is diopside (CaMgSiO_6) and Ca-rich augite [$(\text{Ca}, \text{Mg}, \text{Fe})_2\text{Si}_2\text{O}_6$] $\text{Wo}_{44.0-48.8}\text{En}_{45.8-49.0}\text{Fs}_{5.4-7.9}$, and in the clinopyroxene hornblendite, the clinopyroxene is diopside $\text{Wo}_{49.3-50.0}\text{En}_{40.9-44.6}\text{Fs}_{5.4-9.3}$ (see MacTavish, 1992, Figure 4.5). The clinopyroxene in the hornblendite is more Ca-rich and more Mg-poor than the clinopyroxene in the clinopyroxenite.

4.2. Amphibole

Oikocrystic and prismatic calcic amphiboles from hornblendites, and calcic amphiboles from tonalite veins were analyzed and classified according to Leake (1978) (Figure 4.1, 4.2). Representative compositions of the amphiboles from the Kawene Intrusion are given in Table 4.1. Most of the oikocrystic amphiboles from the hornblendites are magnesio - hornblende, actinolitic - hornblende, and edenite. Rare oikocrystic amphiboles are tremolitic - hornblende, edenitic - hornblende, and actinolite.

Most of the prismatic amphiboles from hornblendites are actinolitic - hornblende and edenite, and rare prismatic amphiboles are magnesio - hornblende and actinolite. The amphibole oikocrysts are more Mg-rich and Fe-poor than the prismatic amphiboles (Figure

Table 4.1 : Representative compositions of amphibole from the Kawene Intrusion oxides recalculated to ideal amphibole composition total (97%).

sample analysis	AK-11A			16B-1		15B-1		17D-1	12-1	
	1	2	3	4	5	6	7	8	9	10
SiO ₂	49.77	51.68	54.83	53.24	47.39	48.57	50.83	47.09	49.05	53.53
TiO ₂	0.38	0.35	0.00	0.00	0.67	0.46	0.00	0.46	0.32	0.13
Al ₂ O ₃	7.81	5.47	2.56	3.70	8.87	5.70	4.19	7.53	6.82	4.65
Cr ₂ O ₃	0.00	0.00	0.00	0.32	0.00	0.21	0.60	0.35	0.87	0.16
FeO(tot)	10.12	8.79	7.41	6.04	8.47	13.07	13.90	12.87	12.38	10.97
MnO	0.00	0.00	0.27	0.19	0.19	0.38	0.00	0.00	0.37	0.00
MgO	15.75	17.45	19.07	19.90	16.58	14.50	14.32	13.92	14.03	16.00
CaO	12.51	12.77	12.69	12.23	12.04	12.44	12.85	12.70	11.16	11.30
Na ₂ O	0.00	0.00	0.00	1.10	2.04	1.00	0.00	1.37	1.42	0.00
K ₂ O	0.65	0.50	0.18	0.28	0.74	0.68	0.31	0.72	0.59	0.26
Total	97.00	97.00	97.00	97.00	97.00	97.00	97.00	97.00	97.00	97.00

Structural formulae based on 23 oxygens and 13 cations

Si	7.09	7.32	7.69	7.46	6.82	7.12	7.41	6.95	7.12	7.54
Ti	0.04	0.04			0.07	0.05		0.05	0.04	0.01
Al	1.31	0.91	0.42	0.61	1.51	0.99	0.72	1.31	1.17	0.77
Cr				0.04		0.03	0.07	0.04	0.10	0.02
Fe ³⁺	0.48	0.40	0.35	0.40	0.29	0.33	0.33	0.11	0.45	0.64
Fe ²⁺	0.73	0.64	0.52	0.31	0.73	1.28	1.37	1.48	1.05	0.66
Mn			0.03	0.02	0.02	0.05			0.05	
Mg	3.35	3.69	3.99	4.16	3.56	3.17	3.11	3.06	3.03	3.36
Ca	1.91	1.94	1.91	1.84	1.86	1.96	2.01	2.01	1.73	1.71
Na				0.30	0.57	0.28		0.39	0.40	
K	0.12	0.09	0.03	0.05	0.14	0.13	0.06	0.14	0.11	0.05
Total	15.03	15.03	14.94	15.19	15.56	15.37	15.06	15.54	15.24	14.75
Mg/(Mg+Fe ²⁺)	0.82	0.85	0.89	0.93	0.83	0.71	0.69	0.67	0.74	0.84

1 - 8. from hornblendite

1. core of oikocrystic grain (magnesio - hornblende)
2. oikocrystic grain (actinolitic - hornblende)
3. rim of oikocrystic grain (actinolite)
4. halo around oikocrystic grain (tremolitic - hornblende)
5. oikocrystic grain (edenite)
6. prismatic grain (magnesio - hornblende)
7. prismatic grain (actinolitic - hornblende)
8. prismatic grain (edenite)

9. magnesio - hornblende from tonalite vein
10. actinolite from tonalite vein

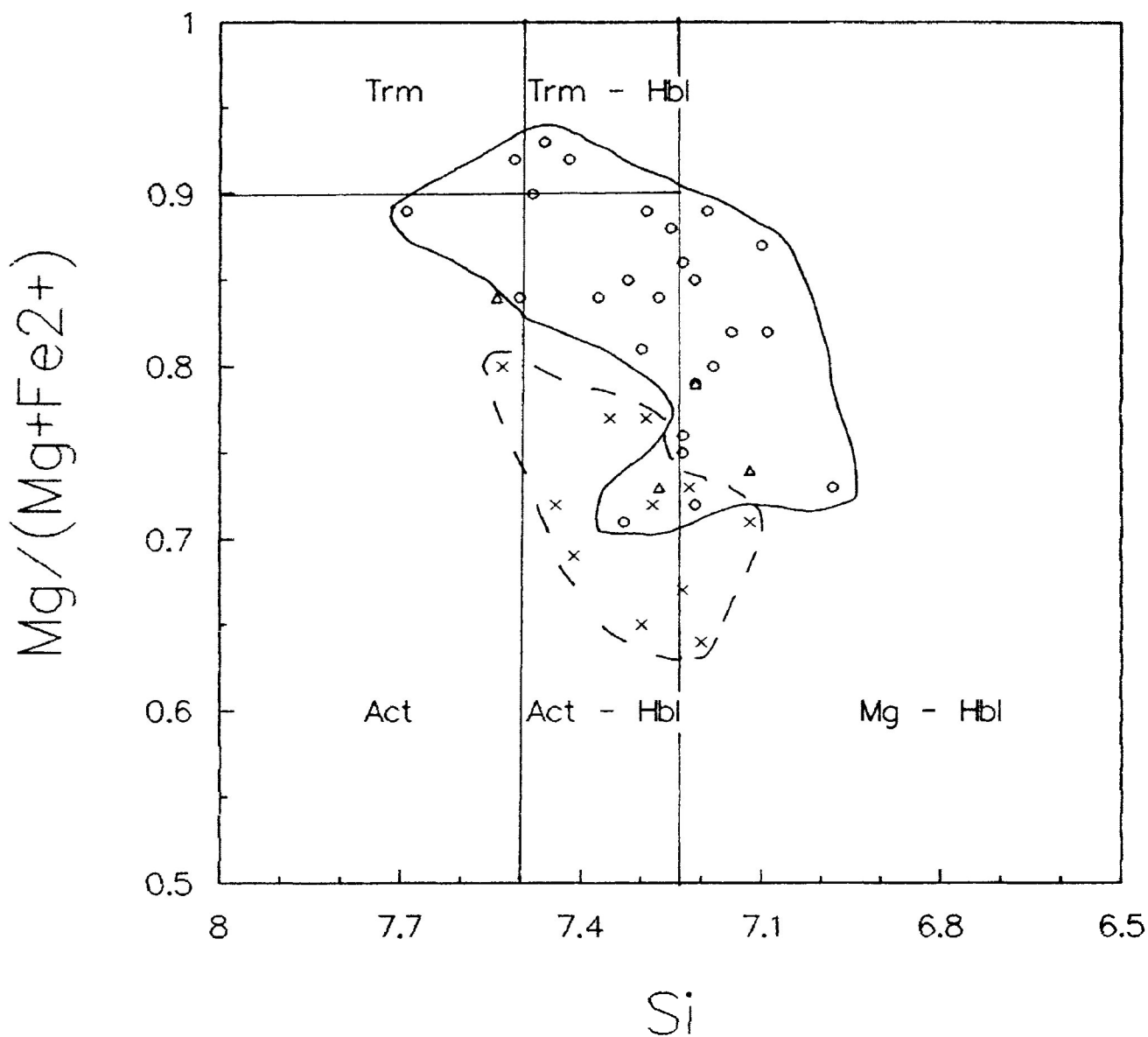


Figure 4.1 : Classification of calcic amphiboles, in which $(Na + K) < 0.50$, $Ti < 0.50$, and $Si > 6.50$.
 Trm - Tremolite, Act - Actinolite, Hbl - Hornblende
 o oikocrystic, x prismatic, Δ tonalite

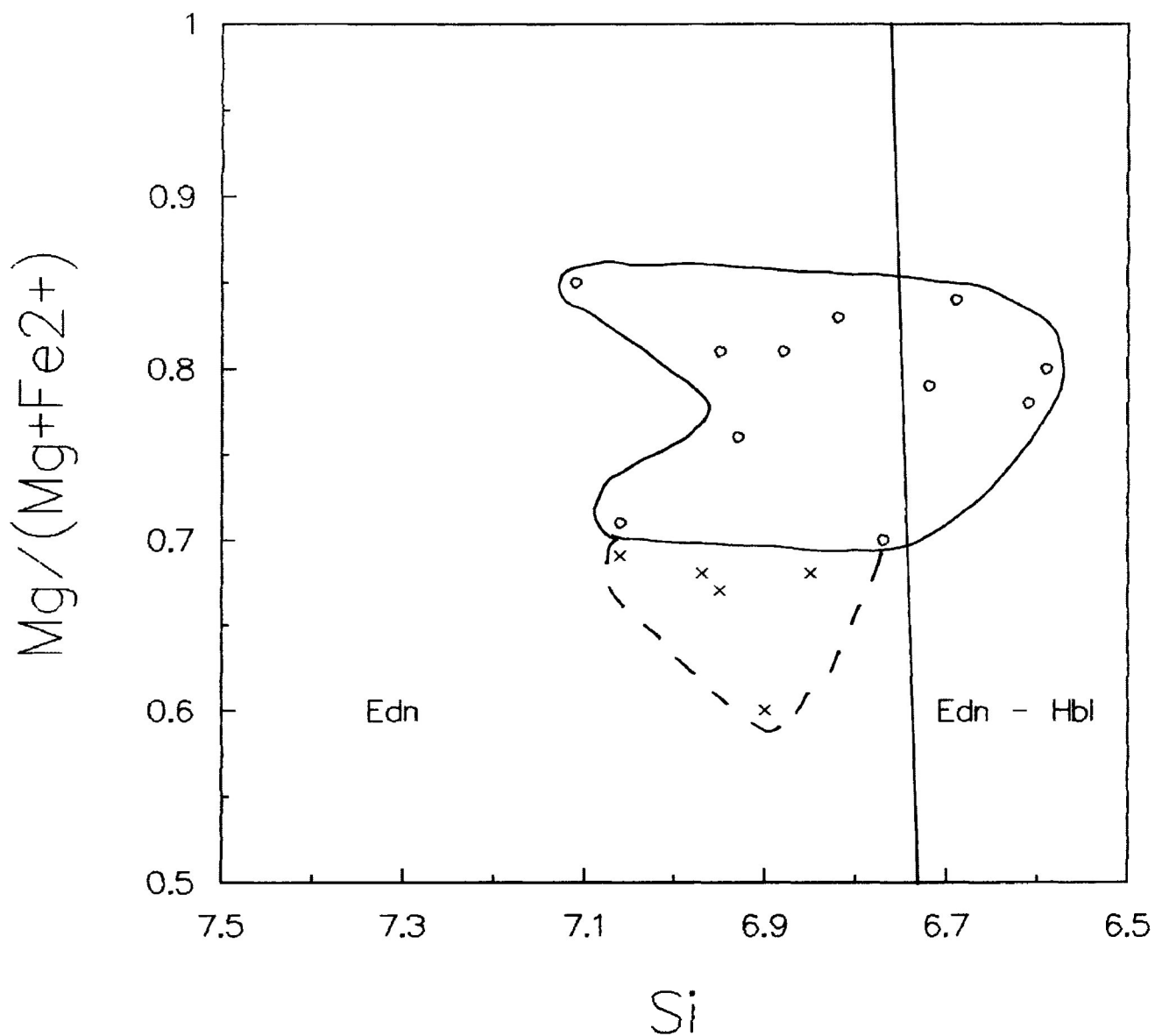


Figure 4.2 : Classification of calcic amphiboles,
in which $(Na + K) > 0.50$, $Ti < 0.50$, and $Si > 6.50$.

Edn - Edenite, Hbl - Hornblende

o oikocrystic, x prismatic

4.1, Table 4.1).

The amphiboles from the tonalite veins appear to be intermediate compositions between the oikocrystic and prismatic amphiboles (Figure 4.1). The amphiboles from the tonalite veins are magnesio - hornblende, actinolitic - hornblende, and actinolite. The amphiboles from the tonalite veins are more Ca-poor than the amphiboles from the hornblendites (Table 4.1, analyses 9, 10).

Figure 4.1 shows a trend as Si increases, Mg also increases for oikocrystic and prismatic amphiboles. This trend is also seen from core to rim in zoned oikocrystic grains. One zoned oikocrystic grain from sample AK-11A has a magnesio - hornblende core, surrounded by actinolitic - hornblende, and a actinolite rim (Table 4.1, analyses 1,2,3). The grain also shows from core to rim Si and Mg increases, and Al, Fe, and K decreases. Several oikocrystic grains are surrounded by tremolitic - hornblende halos which are also Si- and Mg-rich, and Al-, Fe-, and K-poor (Table 4.1, analysis 4).

4.3. Biotite

The biotite from the ultramafic rocks is phlogopite $[K_2(Mg, Fe^{2+})_6Si_6Al_2O_{20}(OH)_4]$, whereas biotite from the tonalite is Al-annite $[K_2(Fe^{2+}, Mg)_5Al(Si_5Al_3)O_{20}(OH)_4]$ formerly siderophyllite (Figure 4.3) (Guidotti, 1984). The benefit of using the Al(tot) - Mg - $Fe^{2+}(tot)$ ternary diagram over the $Al^{iv} - [Fe^{2+}(tot) / Fe^{2+}(tot) + Mg]$ diagram is that it avoids errors due to the $Al^{iv} - Al^{vi}$ calculation.

Table 4.2 : Representative compositions of biotite from Kawene Intrusion oxides recalculated to ideal biotite composition total (96%).

sample analysis	15-3 1	24 2	14 3
SiO ₂	39.47	39.82	37.83
TiO ₂	1.26	1.17	2.51
Al ₂ O ₃	14.09	14.49	15.75
FeO(tot)	10.73	10.53	20.24
MnO			0.49
MgO	19.11	18.69	9.23
K ₂ O	11.34	11.30	9.95
Total	96.00	96.00	96.00

Structural formulae based on 22 oxygens

Si	5.76	5.80	5.74
Ti	0.14	0.13	0.29
Al(iv)	2.24	2.20	2.26
Al(vi)	0.19	0.28	0.56
Fe ²⁺ (tot)	1.31	1.28	2.57
Mn			0.06
Mg	4.16	4.06	2.09
K	2.11	2.10	1.93
Total	15.91	15.85	15.50

1. hornblendite, 2. clinopyroxenite, 3. tonalite

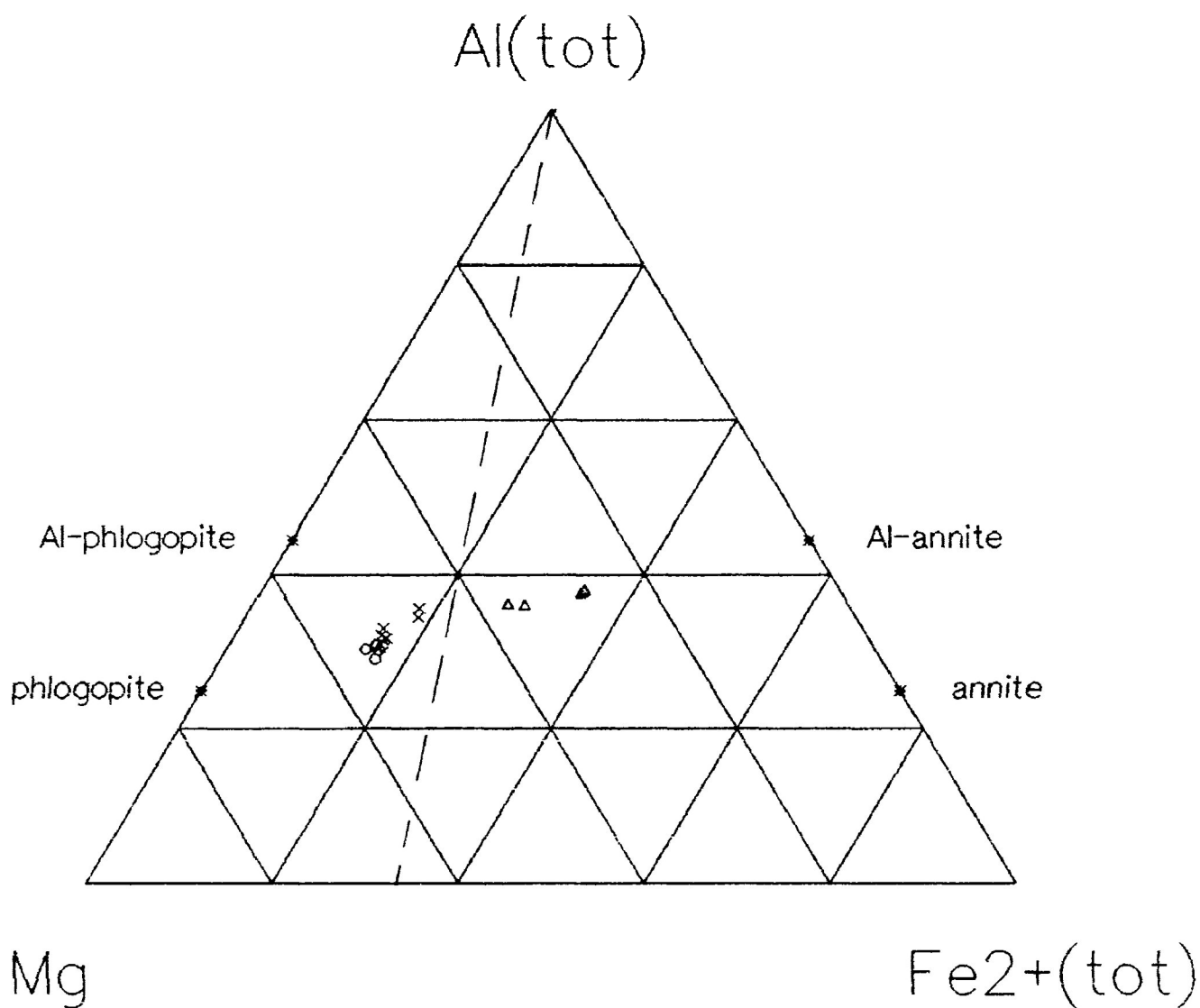


Figure 4.3 : Classification of biotites.
 o hornblende, x clinopyroxene, Δ tonalite
 -- Mg : Fe = 2 : 1

Representative compositions of biotite from the Kawene Intrusion are given in Table 4.2. The biotite compositions are close to ideal stoichiometry, since the total number of cations is ≈ 16 .

The phlogopites in the ultramafic hornblendite and clinopyroxenite cluster together with similar Fe^{2+} and $\text{Al}(\text{tot})$ values (Figure 4.3, Table 4.2, analyses 1, 2). The major difference between the biotite from the tonalite vein and the biotite from the ultramafic rocks is that the former is more Fe-rich and Mg-poor (Table 4.2, analysis 3). The Al-annite from the tonalite vein is also more Ti-, and $\text{Al}(\text{tot})$ -rich than the biotite from the ultramafic rocks.

4.4. Chlorite

Representative compositions of chlorite from the Kawene Intrusion are given in Table 4.3. The oxides were recalculated to 88% to account for the undetermined (OH). The structural formula was calculated based on 14 oxygens assuming all iron is ferrous (Laird, 1988). The structural formula approaches the ideal, since the total number of cations is ≈ 10 (Laird, 1988). These trioctahedral chlorites are ferrous clinochlore $[(\text{Mg}, \text{Fe}^{2+})_5\text{Al}](\text{Si}_3\text{Al})\text{O}_{10}(\text{OH})_8$ (Bailey, 1980). The chlorite from the hornblendites is more Fe-rich and more Mg-poor than the chlorite from the clinopyroxenite.

Chlorite is a secondary mineral in igneous rocks formed by the deuteric or hydrothermal alteration of primary ferromagnesian minerals (e.g. clinopyroxene, amphibole, and biotite) (Bailey,

Table 4.3 : Representative compositions of chlorite from Kawene Intrusion oxides recalculated to ideal chlorite composition total (88%).

sample analysis	17A-2 1	13C-1 2
SiO ₂	30.45	30.26
Al ₂ O ₃	19.40	20.07
Cr ₂ O ₃	0.17	
FeO(tot)	17.42	13.56
MnO	0.18	0.38
MgO	20.38	23.73
Total	88.00	88.00

structural formulae based on 14 oxygens

Si	3.03	2.96
Al(iv)	0.97	1.04
Al(vi)	1.31	1.28
Cr	0.01	
Fe ²⁺ (tot)	1.45	1.11
Mn	0.02	0.03
Mg	3.03	3.46
Total	9.82	9.88

1. hornblendite, 2. clinopyroxenite

1988). Chlorite is also a common accessory mineral in low - to - medium grade regional metamorphic rocks (Bailey, 1988).

4.5. Feldspar

Representative compositions of the feldspars from the Kawene Intrusion are given in Table 4.4. That from the hornblendite and hornblendite - tonalite vein is K-feldspar (Or_{99-100}), albite ($\text{Ab}_1\text{An}_{99}$), and oligoclase ($\text{Ab}_{73-84}\text{An}_{16-26}\text{Or}_{0-1}$) (Table 4.4, analyses 1 - 4). The feldspar from the tonalite vein is oligoclase and Na-rich andesine ($\text{Ab}_{72-90}\text{An}_{10-32}\text{Or}_{0-2}$) (Table 4.4, analyses 5 - 7).

4.6. Summary

The mafic silicates in the ultramafic rocks are Ca- and Mg-rich. The clinopyroxenes are diopside and augite; the most common amphiboles are magnesio - hornblende and actinolitic - hornblende; the biotites are phlogopites; and the chlorites are ferrous clinocllore. The feldspars in the ultramafic rocks are K-feldspar, albite, and oligoclase.

The amphibole and biotite in the tonalite veins are more Fe-rich than in the ultramafic rocks. The amphiboles are magnesio - hornblende and actinolitic - hornblende, and the biotites are Al-annite. The feldspars in the tonalite veins is oligoclase and Na-rich andesine. K-feldspar is rare in the tonalite veins.

Table 4.4 : Representative compositions of feldpsar from Kawene Intrusion

sample analysis	16B-1 1	15B-1 2	13E-1 3	16B-1 4	18 5	14 6	12-1 7
SiO ₂	64.11	61.97	61.10	64.74	63.45	61.05	60.61
Al ₂ O ₃	23.32	24.38	25.12	17.67	24.10	25.11	26.15
CaO	0.31	3.48	5.25	0.00	2.08	4.19	6.07
Na ₂ O	12.25	10.18	8.35	0.00	10.37	9.65	7.17
K ₂ O	0.00	0.00	0.18	17.59	0.00	0.00	0.00
Total	100.00	100.00	100.00	100.00	100.00	100.00	100.00

structural formulae based on 32 oxygens

Si	11.29	10.98	10.84	12.05	11.17	10.82	10.70
Al	4.84	5.09	5.25	3.88	5.00	5.25	5.45
Ca	0.06	0.66	1.00		0.39	0.80	1.15
Na	4.18	3.50	2.87		3.54	3.32	2.46
K			0.04	4.18			
Total	20.38	20.22	20.00	20.10	20.10	20.18	19.76

Ab	98.62	84.12	73.44		90.01	80.63	68.13
An	1.38	15.88	25.52		9.99	19.37	31.87
Or			1.04	100.00			

1. albite from hornblendite
2. oligoclase from hornblendite - tonalite vein
3. oligoclase from hornblendite - tonalite vein
4. K-feldspar from hornblendite
5. oligoclase from tonalite
6. oligoclase from tonalite
7. Na-rich andesine from tonalite

Chapter 5

Sulfide Mineralogy and Petrology

5.1. Introduction

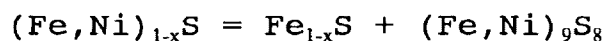
In the Kawene Intrusion, the most common sulfides in the ultramafic clinopyroxenites and hornblendites are pyrrhotite and chalcopyrite. The other sulfides found in these ultramafic rocks, in decreasing order of abundance, are ; pentlandite, galena, violarite, and sphalerite. Pyrrhotite, chalcopyrite, and pentlandite are commonly found either intergrown in veinlets which intrude the ultramafic rocks, or interstitial to euhedral silicates. Pyrrhotite and chalcopyrite contain euhedral silicate (mostly hornblende and chlorite) inclusions. Pyrrhotite, chalcopyrite, and pentlandite crystallized from a late stage, magmatic melt.

In the Kawene Intrusion, the most common sulfide in the tonalite veinlets is pyrite. The other sulfides in order of decreasing abundance are ; pyrrhotite, chalcopyrite, pentlandite, and galena. The major difference between the sulfides in the ultramafic rocks and those in the tonalite veinlets is that the ultramafic rocks do not contain pyrite. The grain size of the sulfides in the ultramafic rocks is much larger (mm scale) than the grain size in the tonalite veinlets (μm scale).

In many of the sulfide systems (e.g. Fe-S, Ni-Fe-S, Cu-Fe-S), there are extensive fields of solid solution that are reduced at lower temperatures (Craig and Vaughan, 1990). In the Fe-S system

the pyrrhotite solid solution cools to produce monoclinic pyrrhotite, hexagonal pyrrhotite, and troilite (FeS) (Craig and Vaughan, 1990; Craig and Scott, 1974).

In the Ni-Fe-S system, the monosulfide solid solution (mss) cools to produce pyrrhotite and pentlandite by a reaction such as:



(Craig and Vaughan, 1990). Pentlandite exsolves as the sulfur-poor boundary of the monosulfide solid solution retreats towards more sulfur-rich compositions (Craig and Vaughan, 1990; Kelly and Vaughan, 1983; Francis et al., 1976; Craig and Scott, 1974).

This is reflected in the common textures observed between pyrrhotite and pentlandite. For example, pentlandite crystallizes into coarse grained, chainlike veinlets, interstitial to pyrrhotite and chalcopyrite during slow cooling of the mss between 610°C and 250°C (Kelly and Vaughan, 1983; Durazzo and Taylor, 1982; Craig and Vaughan, 1981). Pentlandite blades exsolve from pyrrhotite between 250°C and 150°C (Durazzo and Taylor, 1982). Below 150°C, the diffusion rates of nickel from the mss are slow, and the exsolved pentlandite is trapped as flames (Kelly and Vaughan, 1983; Durazzo and Taylor, 1982; Craig and Vaughan, 1981). The exsolution of pentlandite flames within nickeliferous pyrrhotite, and the intergrowths of pentlandite laths or blebs have a crystallographically - controlled relationship (Craig and Vaughan, 1990; Kelly and Vaughan, 1983). In general, exsolution occurs such that pentlandite (111), (110), and (112) planes are parallel to the (001), (110), and (100) planes of the pyrrhotite (Francis et al.,

1976). The greatest degree of lattice match (or coherency) occurs for the preferred orientation (111) pentlandite parallel to (001) pyrrhotite (Francis et al., 1976).

In the Cu-Fe-S system, it is possible to remove from or add metal atoms to the crystal structure at high temperatures to produce an intermediate solid solution (iss) (Craig and Vaughan, 1990; Craig and Scott, 1974). The iss cools to produce assemblages containing chalcopyrite, talnakhite ($\text{Cu}_9\text{Fe}_8\text{S}_{16}$), mooihoekite ($\text{Cu}_9\text{Fe}_9\text{S}_{16}$), haycockite ($\text{Cu}_4\text{Fe}_5\text{S}_8$), and cubanite (CuFe_2S_3) (Craig and Vaughan, 1990; Craig and Scott, 1974; Cabri, 1973; Cabri and Hall, 1972).

5.2. Sulfides in the Ultramafic Rocks

5.2.1 Pyrrhotite

The general formula of pyrrhotite is Fe_{1-x}S , where $0 < x < 0.125$. The non-stoichiometric composition is due to the removal of Fe atoms to produce vacancies in hexagonal NiAs - structured FeS (Craig and Vaughan, 1990; Vaughan and Craig, 1978; Craig and Scott, 1974; Tokonami et al., 1972). The vacancies are disordered at high temperatures, and become ordered at low temperatures to produce monoclinic pyrrhotite (Craig and Vaughan, 1990; Vaughan and Craig, 1978; Craig and Scott, 1974; Tokonami et al., 1972). The ordering of vacancies in monoclinic pyrrhotite results in ferrimagnetism at room temperature (Craig and Vaughan, 1990; Vaughan and Craig, 1978).

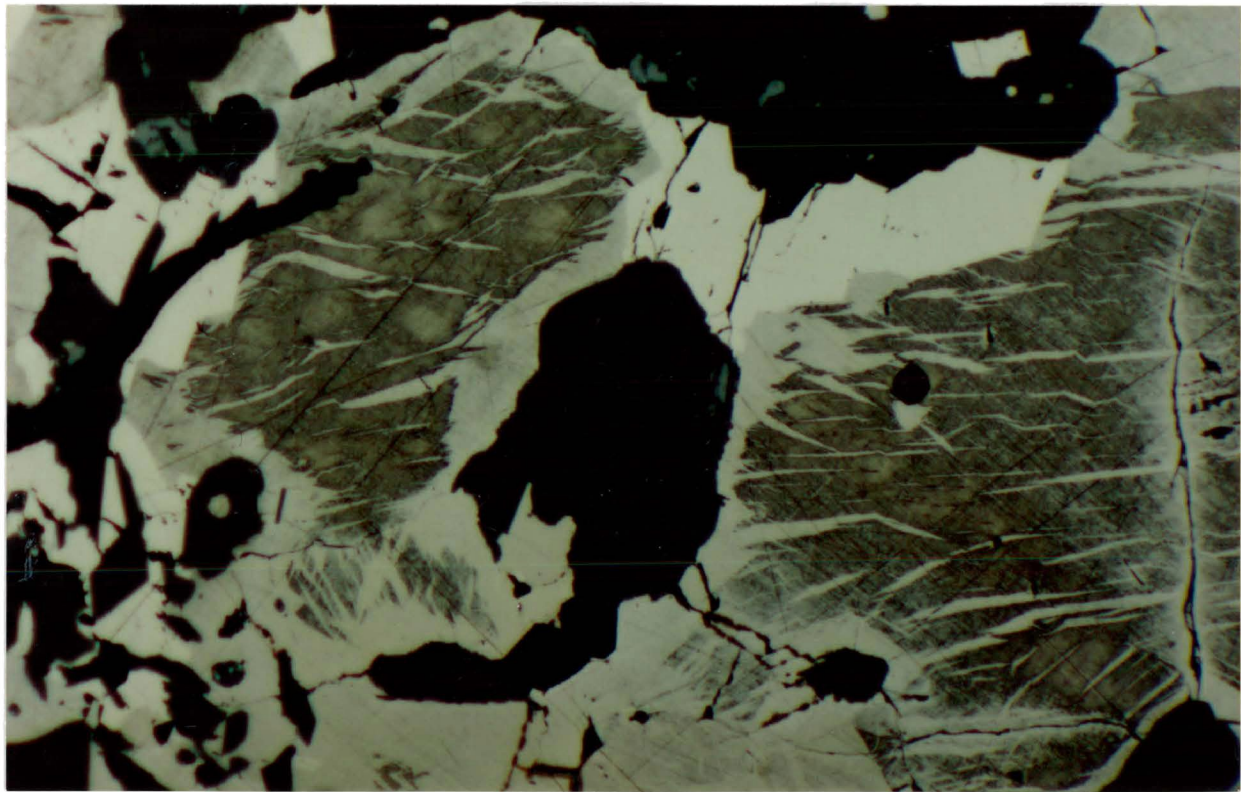
5.2.2. Pyrrhotite Paragenesis

Polished sections containing pyrrhotite veinlets from the Kawene Intrusion were cleaned using 0.3 μm alumina powder and methanol. Intergrowths of hexagonal and monoclinic pyrrhotite can be distinguished by etching a polished surface (Craig and Vaughan, 1981; Arnold, 1966). The cleaned sections were etched in hydriodic acid (HI). Excess acid was cleaned off using alumina powder and methanol. Under reflective light, hexagonal pyrrhotite tarnishes dark brown, and monoclinic pyrrhotite remains light brown.


In the Kawene Intrusion, the pyrrhotites are composed of relict hexagonal cores, and monoclinic rims (Figure 5.1, 5.2). Monoclinic pyrrhotite also occurs along fractures within the hexagonal pyrrhotite. Parallel, lenticular monoclinic pyrrhotite is enclosed in the hexagonal pyrrhotite. Hexagonal pyrrhotite may have monoclinic pyrrhotite occurring as rims, fingers, and flames along grain boundaries and internal fractures due to replacement (Craig, 1990; Craig and Vaughan, 1981). Replacement along grain boundaries commonly appears as thin laths of the replacing phase (monoclinic pyrrhotite) projecting into the host phase (hexagonal pyrrhotite) (Craig and Vaughan, 1981). Replacement may result from one or more of the following processes : dissolution and subsequent reprecipitation (hydrothermal), oxidation (weathering), and solid state diffusion (cooling of solid solution) (Craig and Vaughan, 1981). The monoclinic pyrrhotite in the Kawene Intrusion crystallized due to cooling of the monosulfide solid solution because the contacts between the hexagonal and monoclinic

Figure 5.1 : Hexagonal pyrrhotite core (dark brown) with monoclinic pyrrhotite (beige) along the rim and along cleavage planes from drill core 27C. Pentlandite (white) is enclosed in monoclinic pyrrhotite (top right).

Figure 5.2 : Hexagonal pyrrhotite cores (dark brown) with monoclinic pyrrhotite (beige) along rims and cleavage planes from drill core 27C. Pentlandite (white) and silicates are enclosed in the monoclinic pyrrhotite.



0 0.5 mm

A horizontal scale bar with vertical tick marks at each end, indicating a length of 0.5 mm.

pyrrhotite is sharp and euhedral. The monoclinic pyrrhotite did not crystallize from a hydrothermal fluid because it has euhedral grain boundaries with magmatic chalcopyrite indicating simultaneous crystallization (Figure 5.4). The monoclinic pyrrhotite did not crystallize from weathering because weathering would result in irregular, anhedral contacts.

Hexagonal and monoclinic pyrrhotite from the Kawene Intrusion are intruded by a veinlet of granular pentlandite which indicates that pyrrhotite crystallized before pentlandite (Figure 5.3).

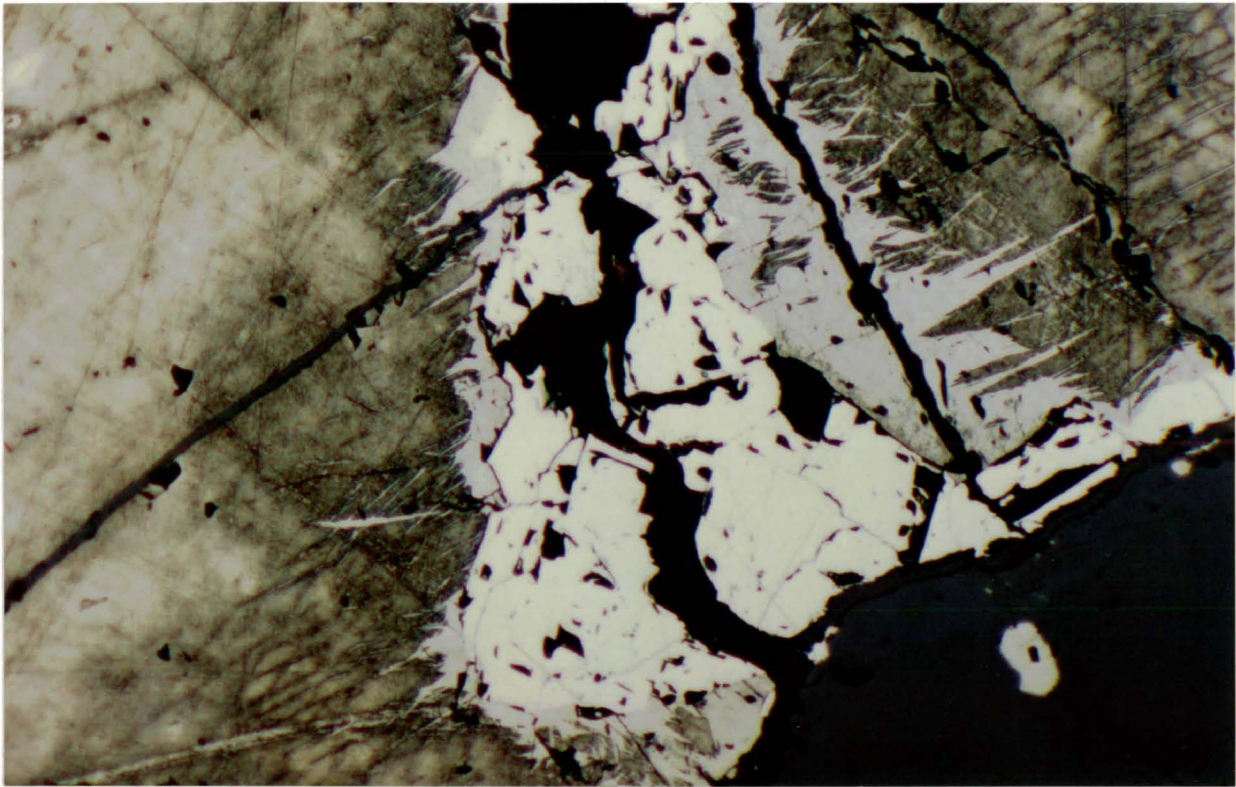
The Kawene pyrrhotite under crossed polars has a granular texture (Figure 5.4). The granular texture could have been formed by slow cooling or by recrystallization (Craig, 1990). The pyrrhotite along the boundary with chalcopyrite is monoclinic pyrrhotite.

Kawene monoclinic pyrrhotite is interstitial to the silicates which indicates that the silicates crystallized before the monoclinic pyrrhotite (Figure 5.5). Pyrrhotite, in ore deposits, occurs commonly as interstitial anhedral masses (Craig and Vaughan, 1990).

The monoclinic pyrrhotite may also be twinned (grain in the bottom right of Figure 5.5). The twinning may be a primary growth texture because the polysynthetic lamellar twins have irregular widths, are unevenly distributed, and are present only in some grains (Ramdohr, 1969). The fractures occurred after the crystallization of the monoclinic pyrrhotite and development of twinning.

Figure 5.3 : Pentlandite (white) veinlet intruding hexagonal pyrrhotite (dark brown) and monoclinic pyrrhotite (beige) from drill core 27C.

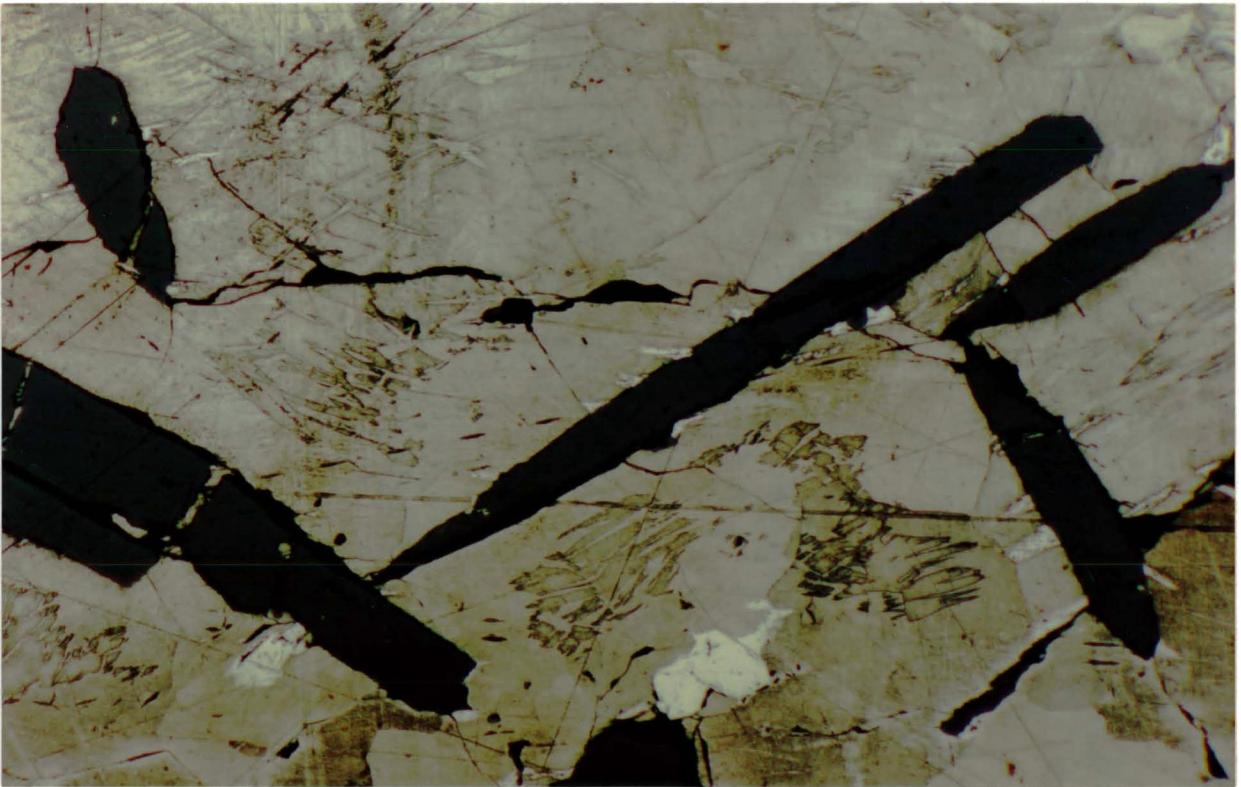
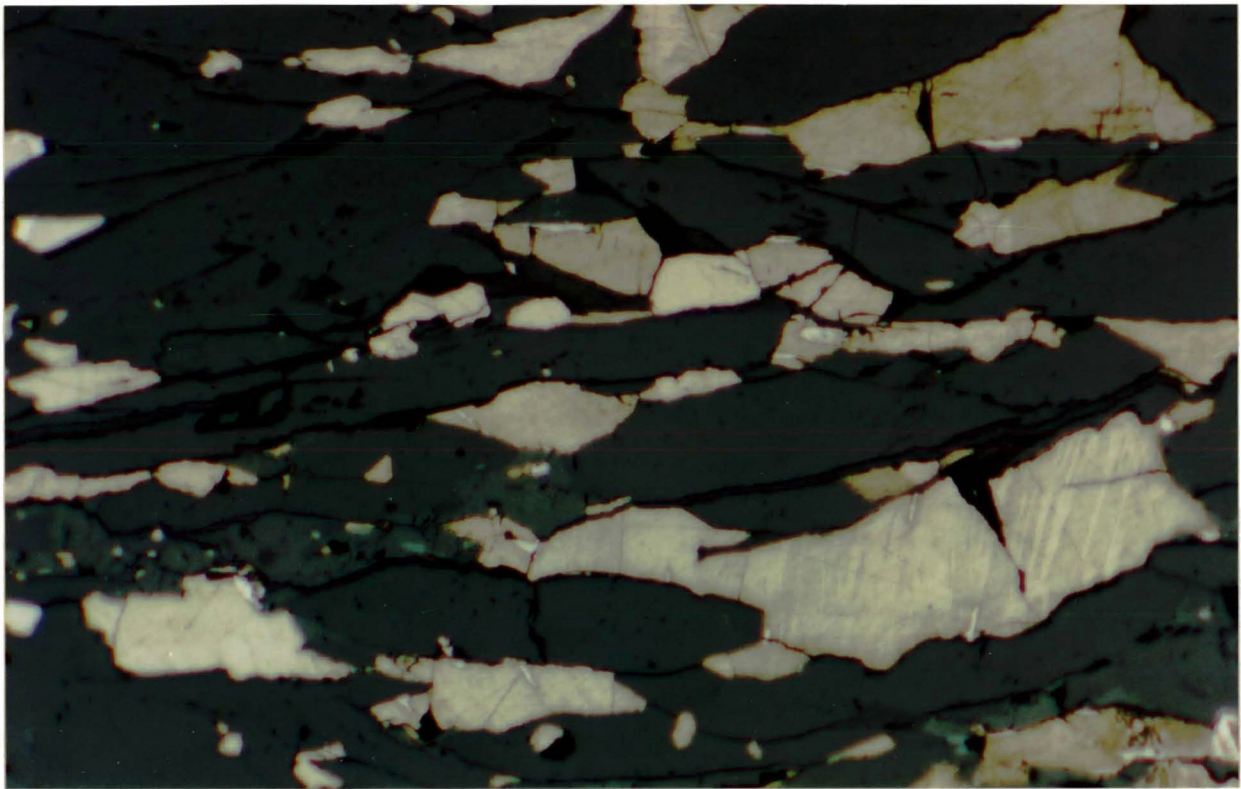
Figure 5.4 : Granular pyrrhotite (beige) with euhedral boundary to chalcopyrite (yellow) from drill core 13B. Pyrrhotite and chalcopyrite contain euhedral silicates.



0 0.5 mm

Figure 5.5 : Monoclinic pyrrhotite (beige) and pentlandite blebs and grains (white) interstitial to silicates from drill core 17D. The monoclinic pyrrhotite grain (bottom right) is twinned.

Figure 5.6 : Euhedral hornblende grains (grey), relict hexagonal pyrrhotite (dark brown), and pentlandite (white) enclosed in monoclinic pyrrhotite (beige) from drill core 17D. Pentlandite blebs occur along hornblende grains.



0 0.5 mm

A horizontal scale bar is located below the two micrographs. It consists of a solid black line with short vertical tick marks at each end. The number '0' is positioned at the left end, and '0.5 mm' is positioned at the right end.

Figure 5.6 shows euhedral hornblende grains, pentlandite, and relict hexagonal pyrrhotite enclosed in monoclinic pyrrhotite. Inclusions of hornblende needles within monoclinic pyrrhotite indicates that the amphiboles crystallized from residual water - rich fluids trapped in pore spaces with the monosulfide solid solution.

Representative compositions of pyrrhotite from the Kawene Intrusion are given in Table 5.1. Hexagonal and monoclinic pyrrhotite may contain minor amounts of Ni (< 0.39 at%). Hexagonal and monoclinic pyrrhotite typically contain < 1.0 at% Ni (Misra and Fleet, 1973). There is very little difference between the amount of Ni in the hexagonal and monoclinic pyrrhotite.

5.2.3. Chalcopyrite Paragenesis

The intermediate solid solution in the magmatic Cu-Fe-S system crystallizes four low temperature phases upon cooling : chalcopyrite, talnakhite, mooihoekite, and haycockite (Kissin and Scott, 1982; Cabri and Hall, 1972).

Aqua regia was spread over Cu-Fe-sulfide - rich polished sections from the Kawene Intrusion (drill core 13E, biotite hornblendite - tonalite veinlet, and 16B, clinopyroxene hornblendite) to tarnish the Cu-Fe-sulfides. The Cu-Fe-sulfides either did not tarnish or very weakly tarnished, which indicates either chalcopyrite or haycockite is present (Figure 5.7).

The anisotropism was examined under reflective light, and the Cu-Fe-sulfides were weakly anisotropic which indicates either

Table 5.1 : Representative compositions of sulfides from the Kawene Intrusion (atomic and weight %)

analysis	at%						wt%						probe section
	Fe	Ni	Co	Cu	Zn	S	Fe	Ni	Co	Cu	Zn	S	
1	47.45	0.39				52.16	60.99	0.52				38.49	13B-1
2	47.47					52.53	61.15					38.85	28A
3	46.45	0.27				53.28	60.07	0.37				39.56	13B-1
4	46.72					53.28	60.43					39.57	15-1
5	24.84			25.13		50.03	34.80			30.24		34.96	15B-1
6	24.91			25.26		49.83	34.48			30.73		34.80	28A
7	24.00	26.98	1.48			47.53	29.55	34.92	1.93			33.60	13B-1
8	25.14	26.09	1.82			46.95	30.87	33.67	2.36			33.10	15-3
9	17.77	24.63	1.00			56.60	23.01	33.54	1.37			42.09	15-3
10	19.55	20.73	2.50			57.21	25.44	28.36	3.45			42.75	15B-1
11	21.98	19.47	1.19			57.36	28.68	26.71	1.64			42.97	AK-10
12	6.20				44.67	49.13	7.16				60.31	32.53	16B-1
13	6.32				43.86	49.82	7.33				59.51	33.16	15B-2

1,2. hexagonal pyrrhotite

3,4. monoclinic pyrrhotite

5,6. chalcopyrite

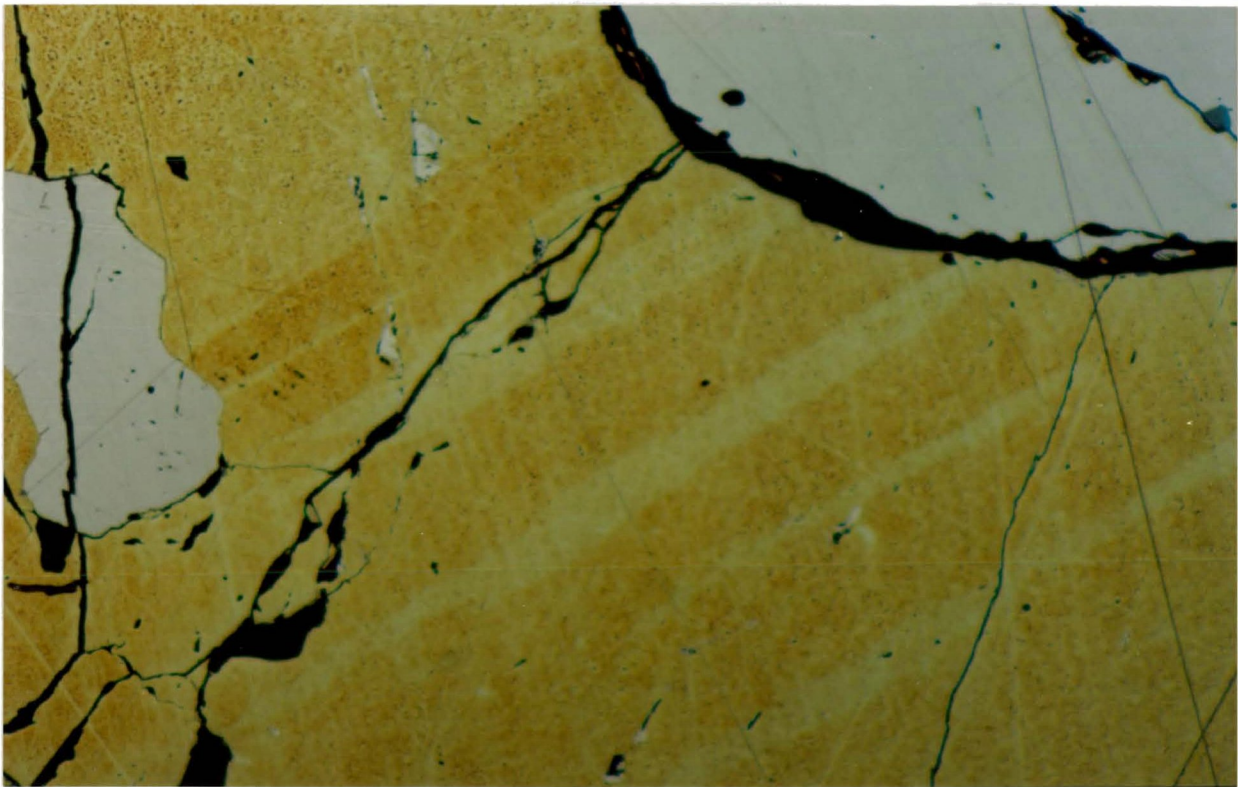
7,8. pentlandite

9,10,11. violarite

12,13. sphalerite

Figure 5.7 : Untarnished (yellow) and weakly tarnished chalcopyrite (dark yellow) with euhedral silicate inclusions from drill core 13E.

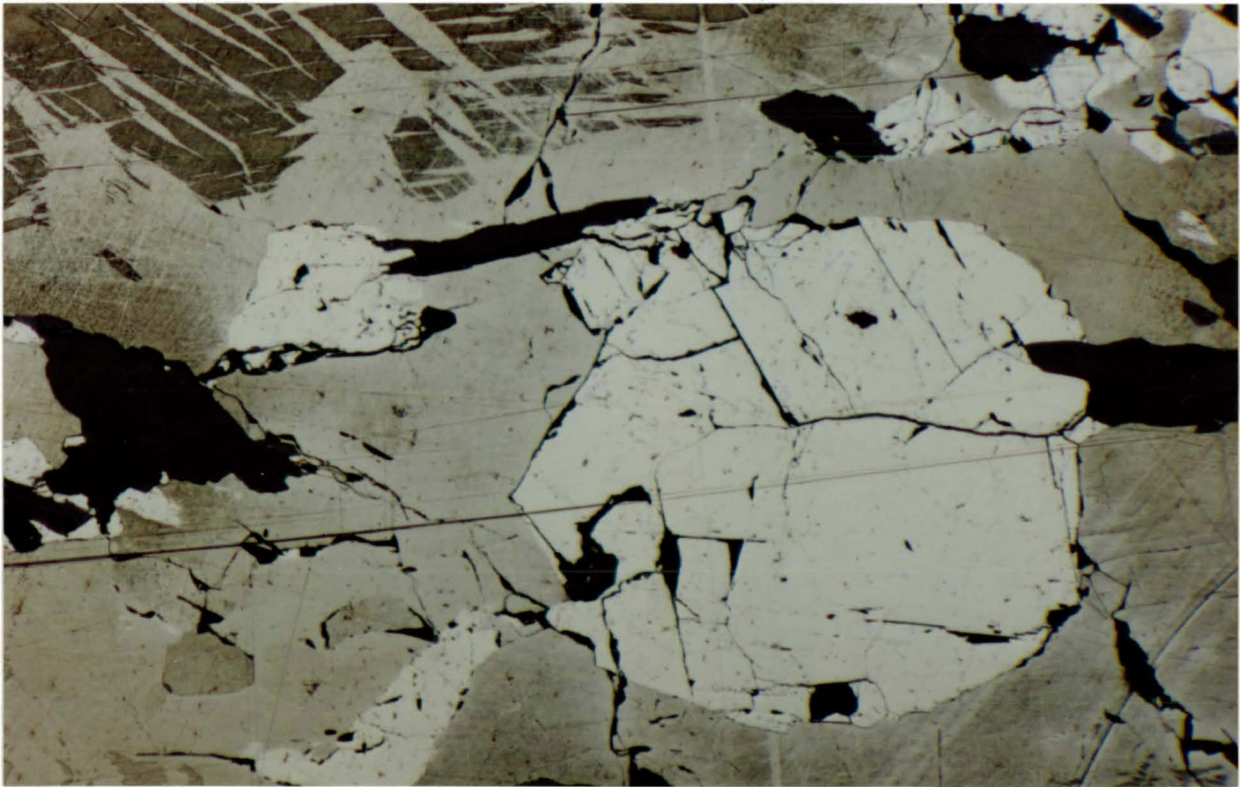
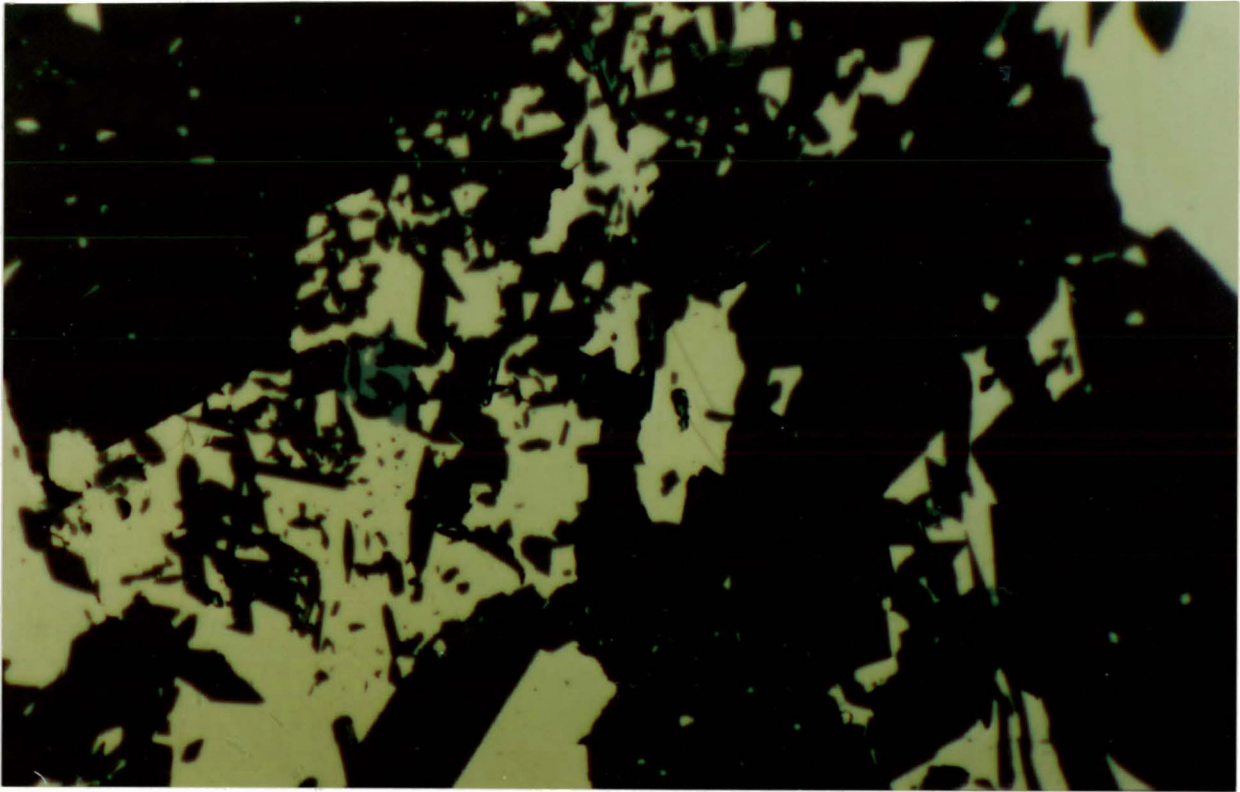
Figure 5.8 : Twinned chalcopyrite (yellow) in contact with pyrrhotite (beige) from drill core 16B.



0 0.5 mm

Figure 5.9 : Chalcopyrite (yellow) and sphalerite (light grey) interstitial to euhedral silicates (dark grey) from drill core 13B.

Figure 5.10 : Large pentlandite circular grain (white), granular pentlandite, silicates (dark grey), and relict hexagonal pyrrhotite (dark brown) enclosed in monoclinic pyrrhotite from drill core 17D.



0 0.5 mm

A horizontal scale bar with vertical tick marks at each end. The left end is labeled '0' and the right end is labeled '0.5 mm'.

chalcopyrite or mooihoekite is present.

The Cu-Fe-sulfides showed twinning in drill core 16B (Figure 5.8) which indicates either chalcopyrite or haycockite is present. The twinning is a primary growth texture because the polysynthetic twins have irregular widths, and are present only in some grains (Ramdohr, 1969).

Phase relations dictate that chalcopyrite can not coexist with haycockite and mooihoekite (Kissin and Scott, 1982). The tarnishing, anisotropism, and twinning match the characteristics of chalcopyrite for the Cu-Fe-sulfides from the Kawene Intrusion.

Chalcopyrite and pyrrhotite have an euhedral mutual boundary, and they also contain euhedral silicate inclusions (Figure 5.4).

Kawene chalcopyrite is interstitial to euhedral silicates (Figure 5.9). Chalcopyrite, in general, tends to occur as anhedral masses interstitial to other sulfides (Craig and Vaughan, 1990).

Representative compositions of chalcopyrite from the Kawene Intrusion are given in Table 5.1.

5.2.4. Pentlandite Paragenesis

Generally, at high temperatures, pentlandite exsolves from pyrrhotite as blebs along grain boundaries of pyrrhotite and as granular pentlandite (Garuti et al., 1986; Kelly and Vaughan, 1983). At lower temperatures, where rates of diffusion and exsolution are slower, pentlandite exsolves as flames (Garuti et al., 1986; Kelly and Vaughan, 1983).

Kawene pentlandite occurs as blebs at monoclinic pyrrhotite -

silicate, and at monoclinic pyrrhotite - hornblende grain boundaries (Figure 5.5, 5.6).

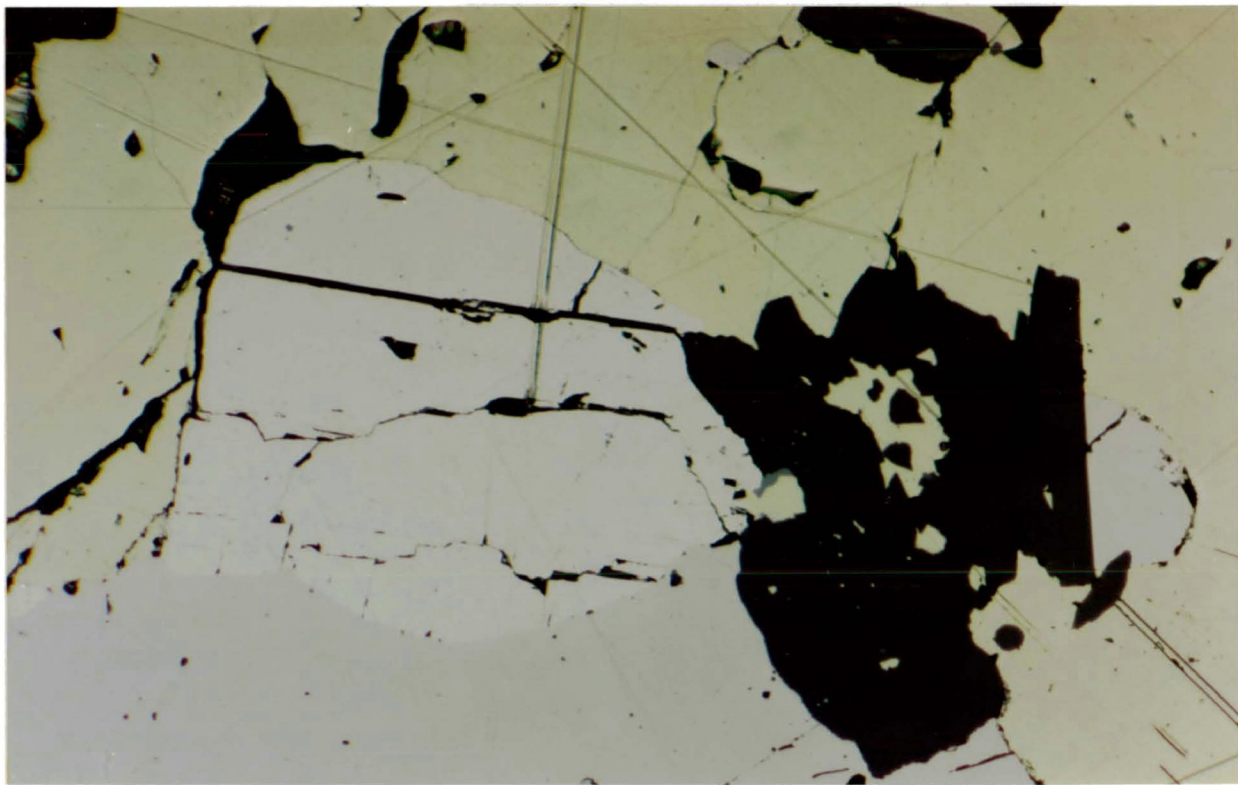
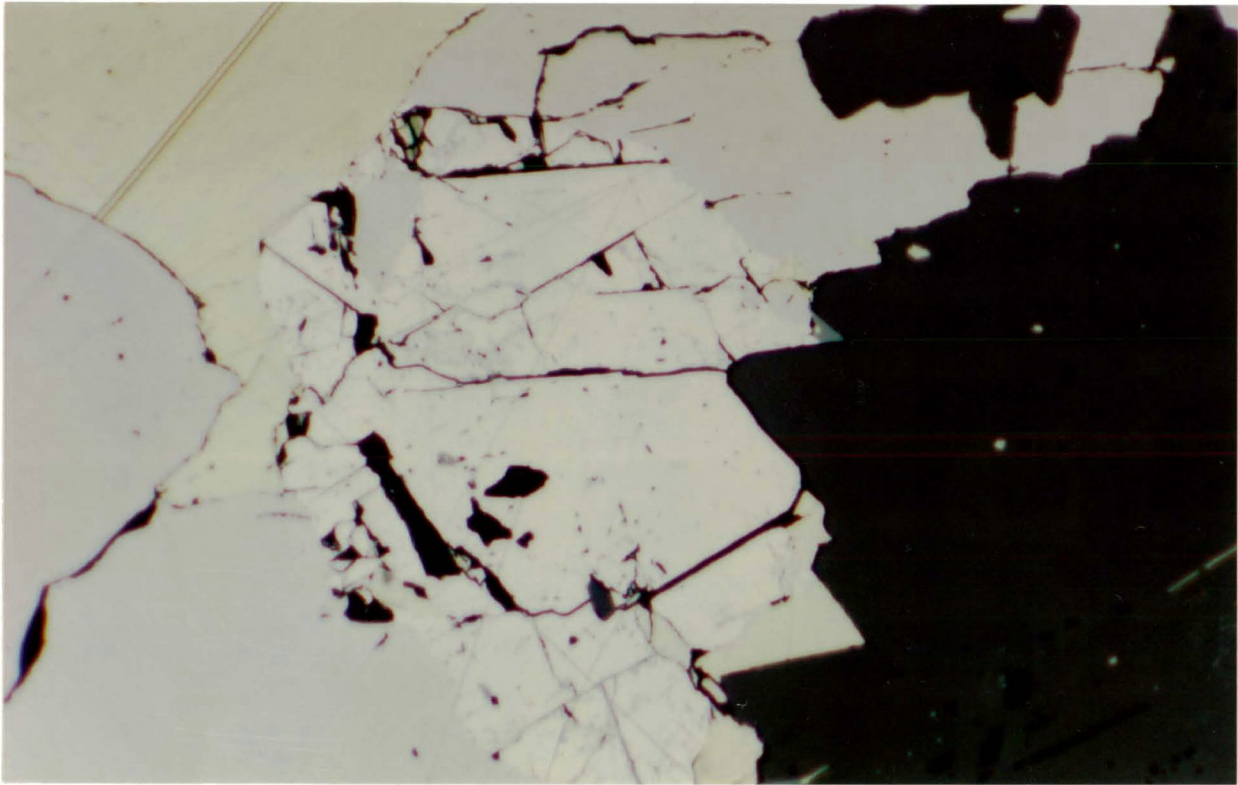
Granular pentlandite occurs between the two pyrrhotite grains (Figure 5.2). Two granular pentlandite grains also occur in contact with euhedral monoclinic pyrrhotite interstitial to the silicates (Figure 5.5).

Granular pentlandite also appears as circular "eyes" (Figure 5.10, 5.11, 5.12). The pentlandite "eyes" are fractured because pentlandite undergoes substantial volume contraction upon cooling (Craig and Vaughan, 1990). Pentlandite has a coefficient of thermal expansion 2 to 10 times greater than that of pyrrhotite and chalcopyrite (Rajamani and Prewitt, 1975). The greater shrinkage results in greater stress and subsequent fractures (Craig and Vaughan, 1990).

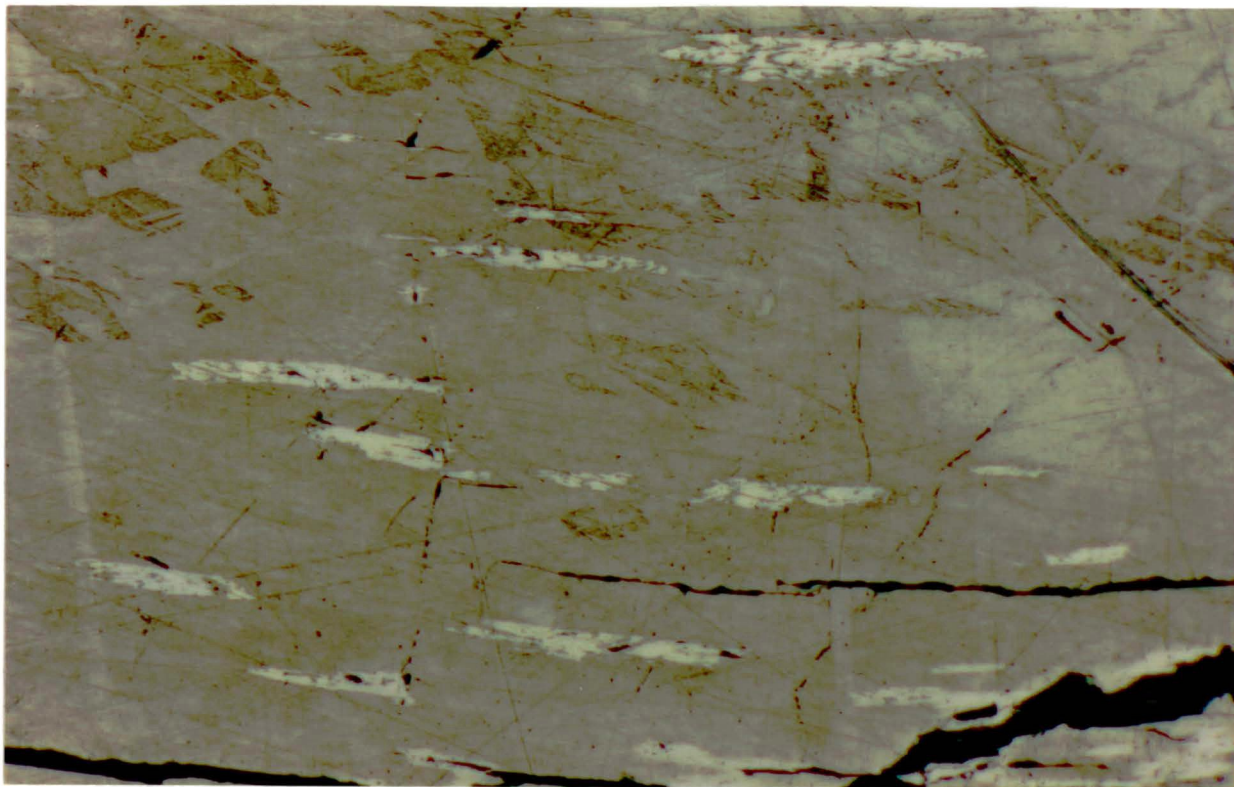
In the Kawene Intrusion, pentlandite flames exsolve from monoclinic pyrrhotite parallel to a crystallographic orientation (coherent exsolution) (Figure 5.13). Pentlandite flames consist of coarsened blebs and lamellae orientated at low angles to the direction of elongation (Kelly and Vaughan, 1983). The blebs and lamellae are coarsened perpendicular to the direction of lamellae elongation (Kelly and Vaughan, 1983). Pentlandite flames are commonly found enclosed within monoclinic pentlandite (Kelly and Vaughan, 1983).

Representative compositions of pentlandite from the Kawene Intrusion are given in Table 5.1. Pentlandite contains minor amounts of Co (< 1.82 at%), and the Fe:Ni ratio is approximately 1.

Figure 5.11, 5.12 : Pentlandite circular grain (white) in euhedral contact with chalcopyrite (yellow), pyrrhotite (beige), and sphalerite (light grey) (center) from drill core 13B.



0 0.5 mm



0 0.5 mm

Figure 5.13 : Pentlandite flames exsolved from monoclinic pyrrhotite from drill core 17D.

5.2.5. Violarite Paragenesis

Violarite $(\text{Fe,Ni})_3\text{S}_4$ is a hydrothermal alteration product of pentlandite (Anthony et al., 1990; Misra and Fleet, 1974; Nickel et al., 1974). Pentlandite alters to violarite by the selective removal of metal atoms (Misra and Fleet, 1974; Nickel et al., 1974). Thus, violarite is more S-rich than pentlandite. Violarite has the same octahedral cleavage as pentlandite, since they have the same S substructure (Misra and Fleet, 1974; Nickel et al., 1974). The alteration of pentlandite to violarite results in volume reduction, which produces shrinkage cracks in violarite (Patterson and Watkinson, 1984; Misra and Fleet, 1974; Nickel et al., 1974).

Violarite is an intermediate composition in the solid solution series between greigite (Fe_3S_4) and polydymite (Ni_3S_4) (Misra and Fleet, 1974). The maximum thermal stability of Ni-rich violarite (FeNi_2S_4) is $461 \pm 3^\circ\text{C}$ (Craig, 1971).

In the Kawene Intrusion, violarite commonly occurs along cracks and cleavage planes of pentlandite (Figure 5.14, 5.15). This is the characteristic violarite texture (Craig and Vaughan, 1981; Misra and Fleet, 1974).

Representative compositions of violarite from the Kawene Intrusion are given in Table 5.1. The Fe : Ni ratio in violarite $[(\text{Fe,Ni})_3\text{S}_4]$ is approximately 1. Violarite contains minor amounts of Co (< 2.50 at%). Violarite in other Ni deposits commonly has a Fe : Ni ratio of 1 : 2 (Anthony et al., 1990). More Fe-rich violarite is characteristic of pyrrhotite bearing assemblages

a)

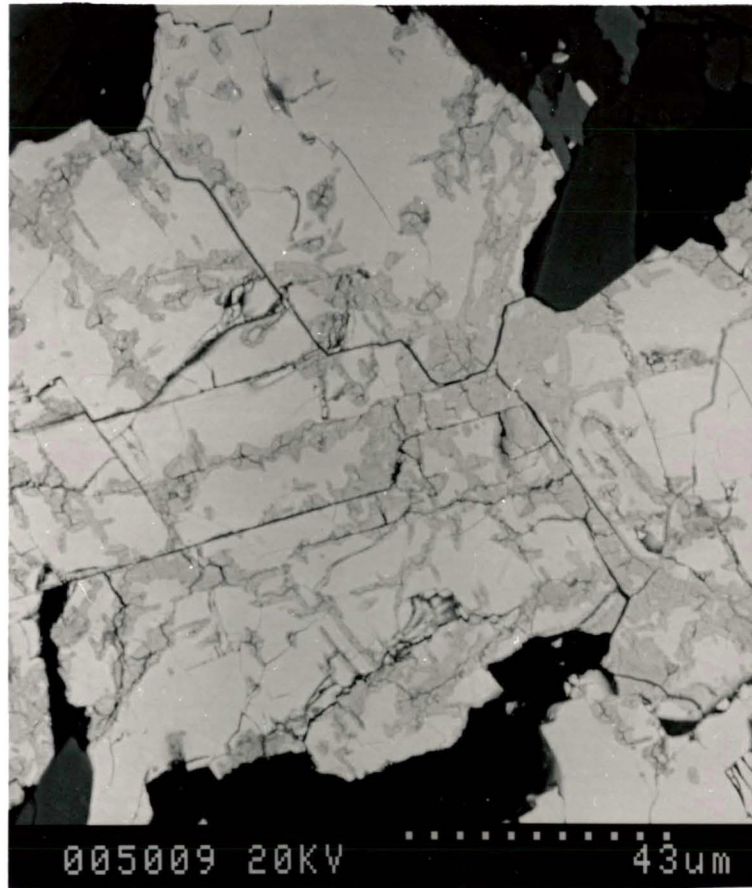


Figure 5.14a, b : SEM / BSE images of pentlandite altering to violarite along cracks from drill core 17B-2.

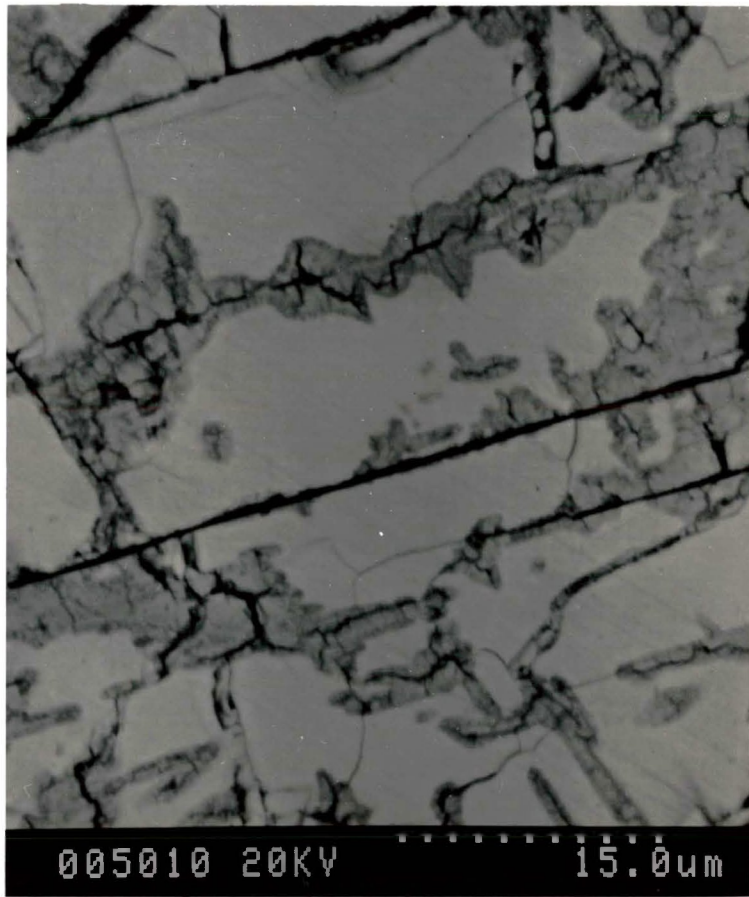


Figure 5.14 b

a)



Figure 5.15a, b : SEM / BSE images of pentlandite altering to violarite along cracks and cleavage planes from drill core 15B-1. The bright white PGM grain in b) is PdBi₃.

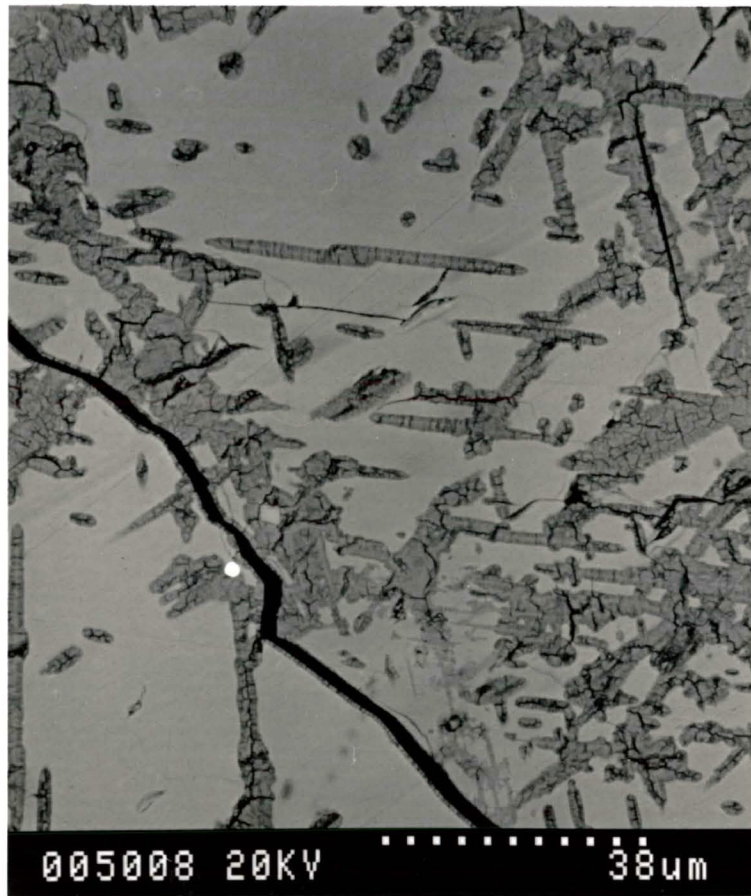


Figure 5.15 b

(Misra and Fleet, 1974). The violarite solid solution extends to more Fe-rich compositions with decreasing temperature (Misra and Fleet, 1974; Craig, 1971).

5.2.6. Galena Paragenesis

In the Kawene Intrusion, galena has the same euhedral - to - subhedral habit as the Platinum Group Minerals (PGM), and is found in the same paragenesis i.e. enclosed within sulfides, at sulfide - silicate boundaries, enclosed within silicates, and at silicate - silicate boundaries. Galena also has a similar grain size as the PGM. The largest grain of galena found is 80 μm in diameter, and most of the grains are < 30 μm .

Galena has the same hydrothermal origin as the Platinum Group Minerals. Generally, galena is found in hydrothermal veins formed under a wide range of temperatures (Anthony et al., 1990; Klein and Hurlbut, 1985). Galena from the Kawene Intrusion is intergrown with the hydrothermal minerals of the Bi - Te - Se - S compositional group (section 9.1.1).

Quantitative analyses of Kawene galena were not obtained because of the spectral peak overlap between Pb M_{α} and S K_{α} , and the lack of a Pb standard. Qualitative analyses of galena reveals that the galena from the Kawene Intrusion contains minor amounts of Se. Galena forms a solid solution series with clausthalite (PbSe) (Anthony et al., 1990). Galena and clausthalite occur in hydrothermal deposits (Anthony et al., 1990; Klein and Hurlbut, 1985).

5.2.7. Sphalerite Paragenesis

In the Kawene Intrusion, sphalerite is found enclosed in pyrrhotite and chalcopyrite, and at pyrrhotite - silicate and at chalcopyrite - silicate grain boundaries (Figure 5.11, 5.12). Sphalerite is also interstitial to euhedral silicates (Figure 5.9).

Sphalerite is a refractory mineral formed under a wide variety of hydrothermal temperatures (Anthony et al., 1990; Klein and Hurlbut, 1985).

Representative compositions of sphalerite from the Kawene Intrusion are given in Table 5.1. Sphalerite contains minor amounts of Fe (6.20 and 6.32 at%) which results in mol% FeS values of 12.2 and 12.6 respectively. These low mol% FeS values suggest that the sphalerite has reequilibrated with monoclinic pyrrhotite by outward diffusion of FeS from sphalerite during postmetamorphic cooling (Craig and Vaughan, 1981). Most greenschist assemblages indicate recrystallization temperatures on the order of 400 °C (Bryndzia et al., 1988). The presence of monoclinic pyrrhotite is indicative of an open system behaviour where S has been gained or lost, and the bulk composition of the pyrrhotite was severely affected (Bryndzia et al., 1988).

5.2.8. Paragenesis of the Sulfides in the Ultramafic Rocks

Table 5.2 : The maximum thermal stabilities of the sulfide minerals

Sulfides		
Mineral	Temp. (°C)	Reference
hexagonal pyrrhotite	1190 - 150	(Vaughan and Craig, 1978; Craig and Vaughan, 1990)
galena	1127 ±5	(Barton and Skinner, 1967)
pentlandite - granular, massive blades flames	610 - 250 250 - 150 < 150	(Durazzo and Taylor, 1982)
chalcopyrite	557	(Craig, 1982)
violarite	461	(Vaughan and Craig, 1978)
chalcopyrite + pyrrhotite	330 ±5	(Vaughan and Craig, 1978)
monoclinic pyrrhotite	254	(Kissin and Scott, 1982)

The paragenesis of the sulfides from the Kawene Intrusion was determined from their petrographic textures. Sulfide - silicate immiscibility causes the sulfide melt to separate from the silicate melt (Craig, 1990). As the sulfides occur along euhedral silicate grain boundaries, the silicate minerals (including hornblende and chlorite) crystallized before the sulfide minerals. The enclosing silicate minerals generally crystallize before the sulfide minerals (pyrrhotite, pentlandite, and chalcopyrite) (Craig, 1990; Garuti et al., 1986). The textures of the sulfides suggests that the hexagonal pyrrhotite was the first sulfide to crystallize from the

monosulfide solid solution (mss) at some high temperature. The sulfides from the Kawene Intrusion resemble those from Sudbury, and the hexagonal pyrrhotite in the Sudbury Complex crystallized at 850 - 375 °C (Craig and Vaughan, 1981).

The hexagonal pyrrhotite has jagged, irregular margins which suggests that it was replaced by the surrounding monoclinic pyrrhotite. Cooling of the mss resulted in the crystallization of monoclinic pyrrhotite and granular pentlandite. Cooling of the intermediate solid solution (iss) resulted in the crystallization of chalcopyrite. Monoclinic pyrrhotite, granular pentlandite, and chalcopyrite crystallized below 254 °C. Note that monoclinic pyrrhotite, pentlandite "eyes", and chalcopyrite have mutual euhedral boundaries, suggesting simultaneous crystallization from a late stage, magmatic melt. Upon cooling of the monoclinic pyrrhotite, pentlandite flames exsolved (< 150 °C).

Metamorphic, hydrothermal fluids intruded the ultramafic rocks, and crystallized galena and sphalerite. As galena is found intergrown with native Bi and bismuthinite, it must have crystallized below 270 °C (section 9.1.1). The hydrothermal fluids also altered the pentlandite to violarite below 461 °C.

Chapter 6

Platinum Group Mineralogy

Pd-Bi-Te-Sb Compositional Group

6.1. Introduction

Numerous Platinum Group Minerals (PGM) were found in the mineralized area of the Kawene Intrusion (Table 6.1). The most common PGM are : PdBiTe (michenerite), PdBi₂ (froodite), Pd₂Bi₃ (unnamed), PtAs₂ (sperryllite), and native Bi. The PGM range in size from 1 - 25 μm , and in habit from euhedral - to - subhedral.

Platinum Group Minerals are most commonly found enclosed within sulfides, and at sulfide - silicate boundaries. The other PGM parageneses are enclosed within silicates (usually clinopyroxenes), and at silicate - silicate boundaries. PGM are associated with the following sulfides in descending order of frequency of occurrence : chalcopyrite, pyrrhotite, pentlandite, violarite, minor galena, minor sphalerite, and rare bravoite. The most common parageneses and habit for the PGM are : euhedral PGM enclosed in sulfides, euhedral PGM at sulfide - silicate boundaries, subhedral PGM enclosed in sulfides, and subhedral PGM at sulfide - silicate boundaries. The most common habit for PGM enclosed in silicates is euhedral, and the most common habit for PGM at silicate - silicate boundaries is subhedral.

The PGM at sulfide - silicate boundaries can be :

1. partially enclosed in the sulfide (Figure 6.1);
2. partially enclosed in the silicate (Figure 6.2);
3. parallel to the grain boundaries (Figure 6.3);

Table 6.1 : Platinum - Group Minerals and Bi compounds found in the mineralized area of the Kawene Intrusion listed in decreasing order of abundance. * - unnamed mineral. ss - solid solution.

<u>Formula</u>	<u>Name</u>
PdBiTe	michenerite
PdBi ₂	froodite
Pd ₂ Bi ₅	*
(Pt, Ir) (As, S) ₂	sperrylite
Bi	native Bi
Bi ₂ S ₃	bismuthinite
(Ag, Ni) S	*
Pd ₂ Bi ₃	*
Bi ₂ Te	hedleyite - pilsenite (ss)
BiS	*
Bi ₄ (Te, Se, S) ₃	*
PdBi, PdBi(+S)	sobolevskite
PdBiTe(+Sb)	Sb-bearing michenerite
Bi ₃ Te ₂	pilsenite - hedleyite (ss)
PdBi ₃	*
Pd ₂ BiSb(+Te)	sobolevskite - stibiopalladinite (Pd ₃ Sb ₂) (ss)
Bi (S, Te, Se)	*
Ag ₂ Te	hessite
Bi ₃ S ₂	*
(Rh, Co) AsS	Co-bearing hollingworthite
Bi ₃ (Te, S, Se) ₂	*
Bi ₄ Te ₃	pilsenite
Bi ₇ Te ₃	hedleyite
Pd ₃ Bi ₂ Sb	sobolevskite - sudburyite (PdSb) (ss)
Pd ₂ Bi (Te, Sb)	sobolevskite - stibiopalladinite - michenerite (ss)
Au ₃ Ag ₂	electrum
PbTe	altaite
Bi ₃ (Te, Se) ₂	pilsenite - paraganajuaite (Bi ₂ Se ₃) (ss)
BiTe	tsumoite
Bi ₂ (S, Te, Se) ₃	tetradymite (Bi ₂ Te ₂ S) - bismuthinite (ss)
Ag ₃ Te ₂	stutzite

Table 6.2 : Platinum - Group Minerals and Bi compounds compositionally grouped and listed in decreasing order of abundance. For the names of the minerals see Table 6.1.

Pd-Bi compounds : PdBi, PdBi(+S), Pd₂Bi₃, PdBi₂, Pd₂Bi₅, PdBi₃

michenerite : PdBiTe, PdBiTe(+Sb)

Bi-S compounds : Bi₂S₃, BiS, Bi₃S₂

Bi-Te compounds : BiTe, Bi₄Te₃, Bi₃Te₂, Bi₃(Te,Se)₂, Bi₂Te, Bi₇Te₃

Bi-Te-Se-S : Bi₄(Te,Se,S)₃, Bi(S,Te,Se), Bi₃(Te,S,Se)₂, Bi₂(S,Te,Se)₃

PtAs₂, (Pt,Ir)(As,S)₂, Pt(As,S)₂, (Pt,Ir)As₂, (Pt,Ir,Rh)As₂

Native Bi

(Ag,Ni)S

Pd-Bi-Te-Sb compounds : Pd₂BiSb(+Te), Pd₃Bi₂Sb, Pd₂Bi(Te,Sb)

Ag₂Te, Ag₃Te₂

(Rh,Co)AsS

Au₃Ag₂

PbTe

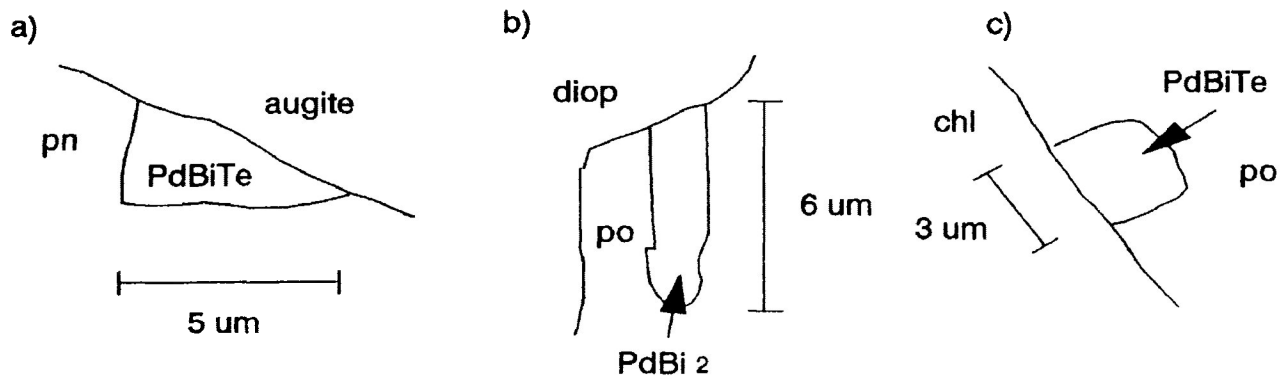


Figure 6.1 : PGM partially enclosed in sulfides

a) euhedral michenerite from drill core 13D-2

b) euhedral froodite from drill core 17A-2

c) euhedral michenerite from drill core 13.

pn - pentlandite, diop - diopside, po - pyrrhotite,

chl - chlorite

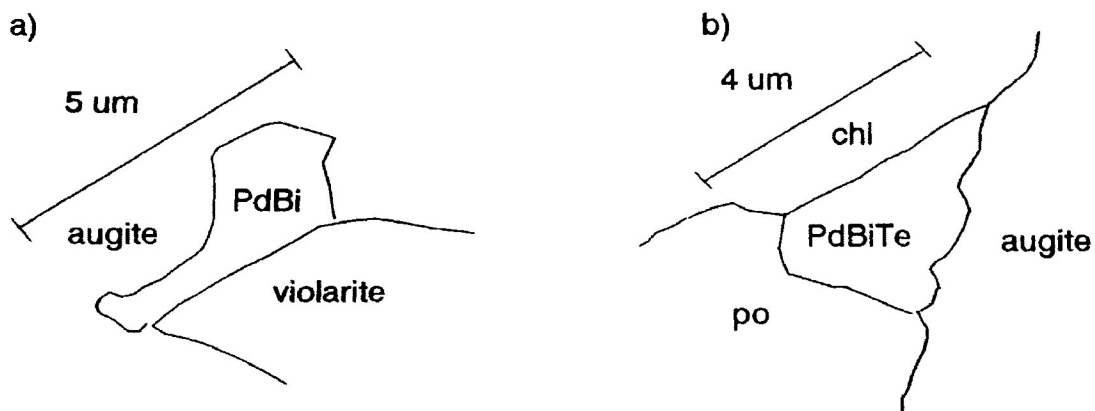


Figure 6.2 : PGM partially enclosed in silicates

a) subhedral sobolevskite from drill core 17A-2

b) subhedral michenerite from drill core 13C-2

chl - chlorite, po - pyrrhotite

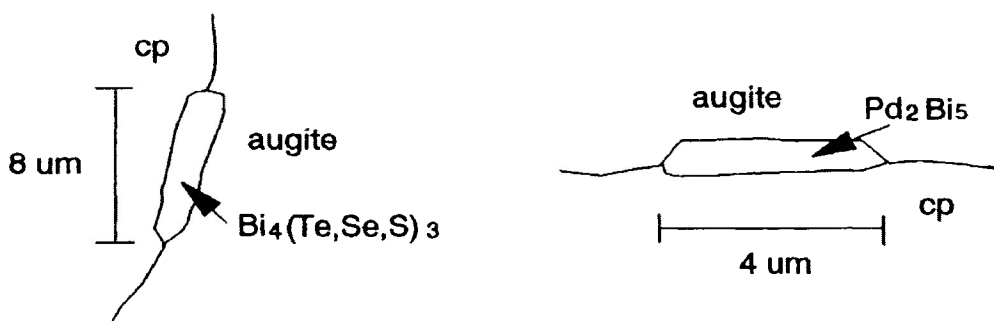


Figure 6.3 : PGM parallel to sulfide - silicate boundary
 a) subhedral $\text{Bi}_4(\text{Te,Se,S})_3$ from sample AK-3A
 b) subhedral Pd_2Bi_5 from drill core 15B-2
 cp - chalcopyrite

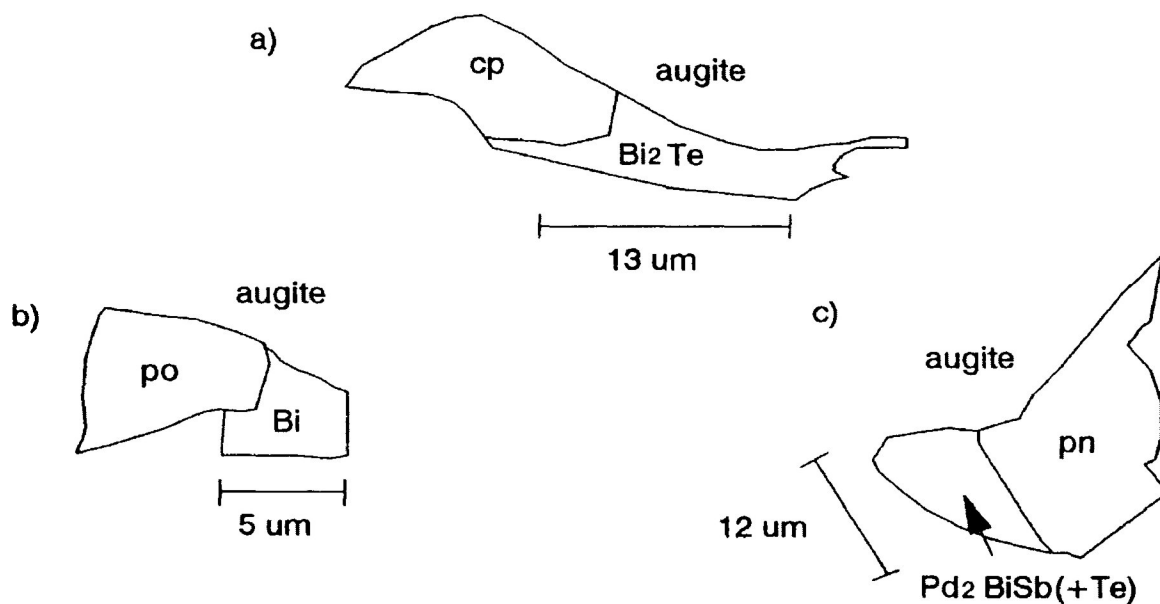


Figure 6.4 : PGM attached to fine grained sulfides enclosed in silicate.
 a) subhedral Bi_2Te from drill core 13B-1
 b) euhedral native Bi from drill core 15-1
 c) euhedral sobolevskite - stibiopalladinite (ss) from drill core 15-1
 cp - chalcopyrite, po - pyrrhotite, pn - pentlandite

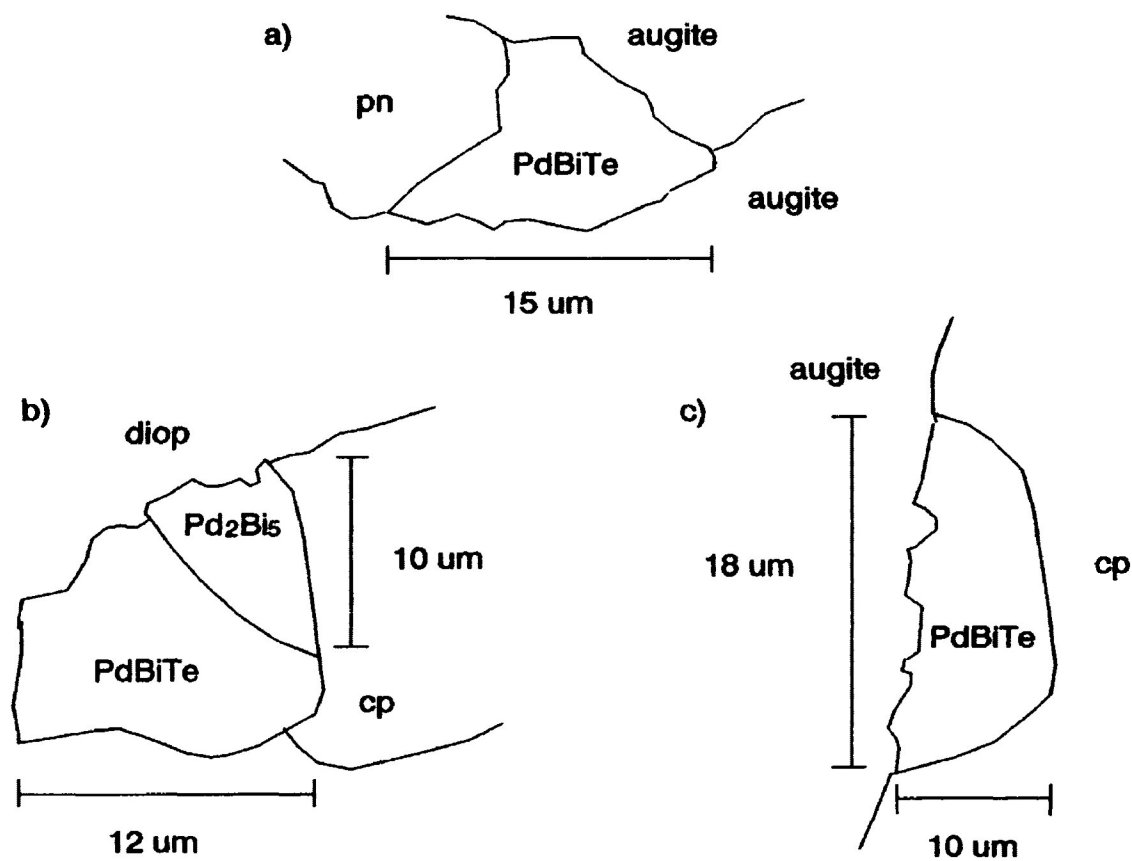


Figure 6.5 : PGM euhedral to sulfides and subhedral to silicates

a) michenerite from drill core 13C-2

b) composite grain of michenerite and Pd₂Bi₅ from drill core 17B-2

c) michenerite from drill core 13D-1.

pn - pentlandite, cp - chalcopyrite, diop - diopside.

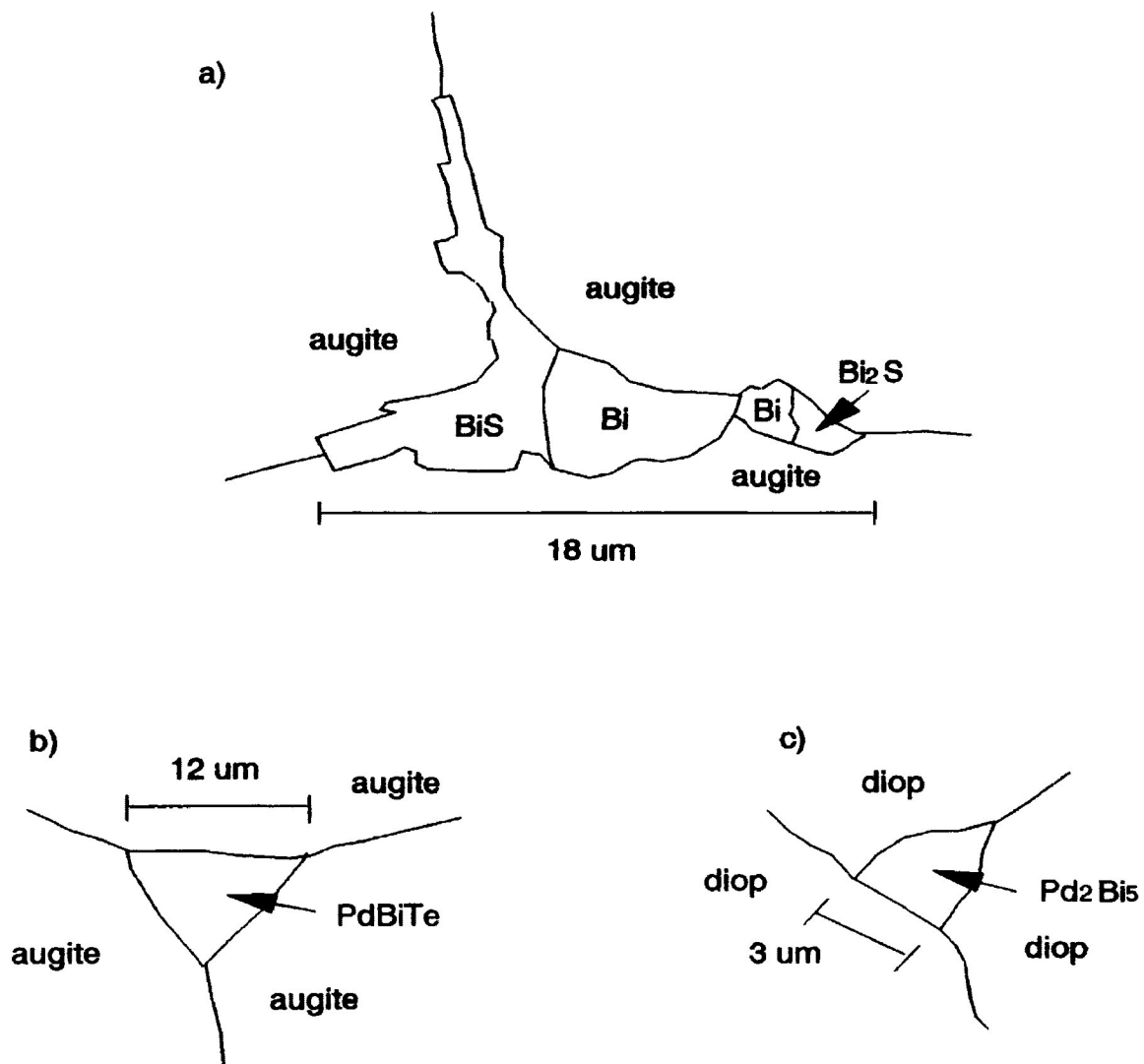


Figure 6.6 : PGM at triple junctions between silicates
 a) subhedral - to - anhedral Bi - S compounds and native Bi
 from drill core 15-5
 b) subhedral michenerite from drill core 15-2
 c) subhedral Pd₂Bi₅ from drill core 17B-2.
 diop - diopside

4. attached to a fine grained sulfide enclosed within a silicate (Figure 6.4);

5. euhedral to the sulfide, and subhedral - anhedral to the silicate (Figure 6.5).

Some of the PGM at silicate - silicate boundaries are found at triple junctions (Figure 6.6).

A total of 1078 PGM, Bi telluride and Bi sulfide grains were found in 42 polished sections. The PGM will be described as compositional groups :

1. Pd - Bi compounds, michenerite, Pd-Bi-Te-Sb compounds

2. native Bi, Bi - S compounds, Bi - Te compounds, Bi-Te-Se-S compounds

3. sperrylite, (Ag,Ni)S, hessite, Co-bearing hollingworthite, electrum, altaite

These compositional groups are individually listed in Table 6.2 in decreasing order of abundance.

6.2. Pd - Bi Compounds

Sobolevskite (PdBi) was first reported by Evstigneeva et al., (1975) from Oktyabr mine, Noril'sk area (Table 5, analysis 1,3). Sobolevskite was named for Petr Grigorevich Sobolevski (1781 - 1841), a Russian metallurgist, who studied the platinum deposits in the Ural Mountains (Anthony et al., 1990). Sobolevskite is believed to be hexagonal (Anthony et al., 1990).

Froodite was discovered by Michener (1940) after superpanning mill concentrates from Frood mine, Sudbury (Table 5, analysis 7).

Michener described froodite as PdBi_3 . It was named by Hawley and Berry (1958) after the type locality Frood mine, and redefined as PdBi_2 . Cabri et al. (1973) confirmed that froodite is monoclinic.

The Pd - Bi compounds range from PdBi (sobolevskite) to PdBi_3 (unnamed). The most common Pd - Bi compound in the Kawene Intrusion is PdBi_2 (froodite) with 141 grains found, and ranges in size from 1 to 15 μm . The other Pd - Bi compounds are :

Pd_2Bi_5 (unnamed)	115 grains found, size 1 - 14 μm ;
Pd_2Bi_3 (unnamed)	33 grains found, size 1 - 8 μm ;
PdBi_3 (unnamed)	12 grains found, size 1 - 12 μm ;
PdBi (sobolevskite)	10 grains found, size 1 - 5 μm .

The most common parageneses of the Pd - Bi compounds (for single grains and composite grains) are : enclosed within chalcopyrite, pentlandite, pyrrhotite, and augite; at chalcopyrite - pentlandite boundaries; enclosed within violarite; and at pyrrhotite - augite boundaries. They are also in contact with : diopside, chlorite, and rarely K - feldspar, calcite, sphene, biotite, hornblende, bravoite, plagioclase, and quartz. Figure 6.7 shows a froodite cluster enclosed within a calcite veinlet which intrudes pentlandite from drill core 16A. This indicates that the froodite and calcite crystallized from the same hydrothermal fluid which intruded the pentlandite.

Representative compositions of Pd - Bi compounds are given in Table 6.3. All of the Pd - Bi atomic % compositions obtained were plotted in the ternary Pd - Bi - Te diagram (Figure 6.8). An SEM / EDS spectrum of a Pd_2Bi_5 grain from drill core 13C-2 (Table 6.3,

a)

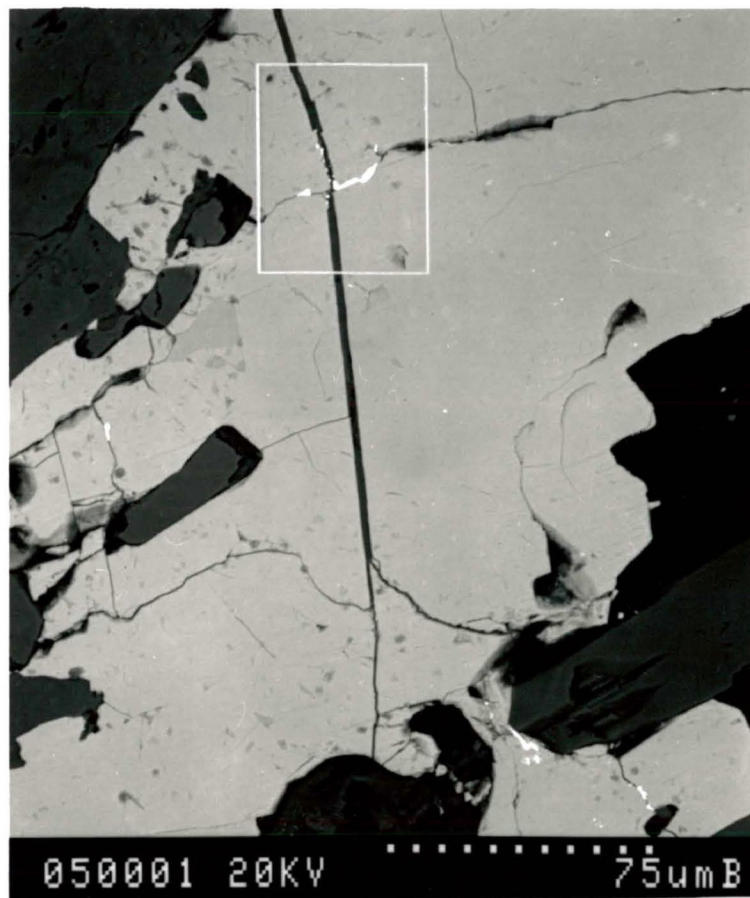


Figure 6.7a, b : SEM / BSE images of froodite grains clustered within a calcite veinlet which intrudes pentlandite from drill core 16A.



Figure 6.7 b

Table 6.3 : Representative compositions of Pd - Bi compounds from Kawene Intrusion (atomic and weight %)

analysis	at%		wt%		size	probe section	formula	
	Pd	Bi	Pd	Bi				
ideal	50.00	50.00	33.74	66.26			PdBi	
	40.00	60.00	25.34	74.66			Pd ₂ Bi ₃	
	33.33	66.66	20.29	79.71			PdBi ₂	
	28.57	71.43	16.92	83.08			Pd ₂ Bi ₅	
1	46.96	53.04	31.07	68.93	5 um	17B-2	PdBi	
2	46.31	53.69	30.51	69.49	5 um	17B-2		
3	42.49	57.51	27.33	72.67	8 um	AK-10	Pd ₂ Bi ₃	
4	40.82	59.18	25.99	74.01	8 um	AK-10		
5	39.54	60.46	24.98	75.02	8 um	AK-2		
6	38.59	61.41	24.23	75.77	8 um	AK-2		
7	37.70	62.30	23.55	76.45	8 um	AK-10		
8	33.50	66.50	20.41	79.59	8 um	AK-2		PdBi ₂
9	32.22	67.78	19.49	80.51	15 um	17B-1		
10	31.55	68.45	19.01	80.99	15 um	15-1		
11	30.23	69.77	18.07	81.93	12 um	13C-2	Pd ₂ Bi ₅	
12	27.74	72.26	16.34	83.66	10 um	17A		
13	27.00	73.00	15.84	84.16	10 um	AK-10		

Table 6.4 : Representative compositions of Te-, S-, and Au-bearing Pd - Bi compounds from Kawene Intrusion (atomic and weight %)

analysis	at%					wt%					size	probe section
	Pd	Bi	Te	S	Au	Pd	Bi	Te	S	Au		
1	30.21	68.34	1.45			18.18	80.77	1.06			9 um	15B-1
2	28.86	69.06	2.08			17.28	81.22	1.50			9 um	15B-1
3	44.68	53.72		1.48		29.64	70.02		0.29		4 um	AK-2
4	33.94	52.53		13.53		24.04	73.07		2.88		2 um	AK-2
5	26.64	69.79			3.57	15.64	80.47			3.88	3 um	AK-3A
6	24.93	70.53			4.55	14.50	80.61			4.89	3 um	AK-3A

1,2. Pd₂Bi₅(+Te)

3. PdBi(+S)

4. Pd₂Bi₃(+S)5,6. Pd₂Bi₅(+Au)

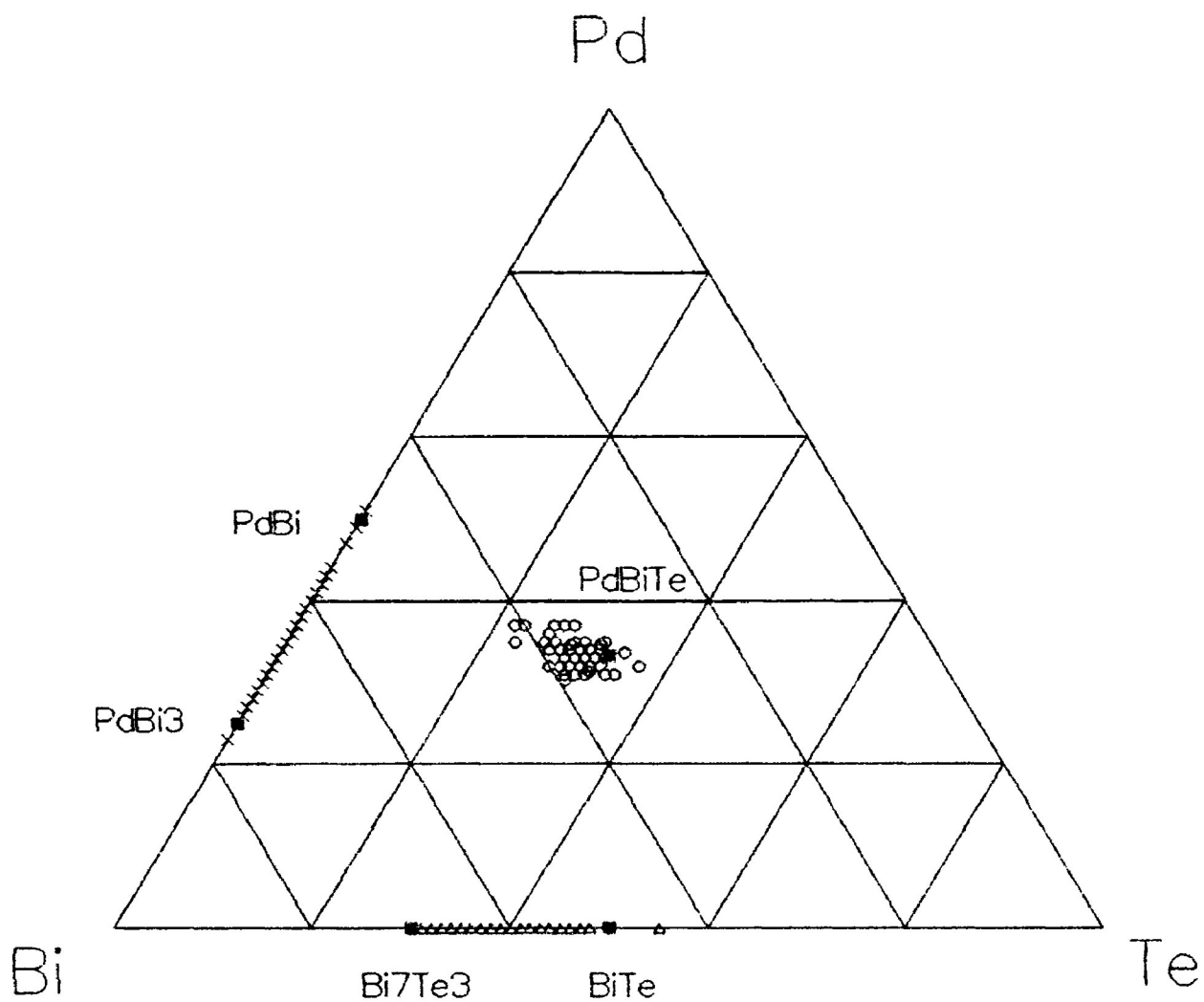


Figure 6.8 : Pd - Bi - Te ternary diagram (atomic %)

○ michenerite PdBiTe

× Pd - Bi

△ Bi - Te

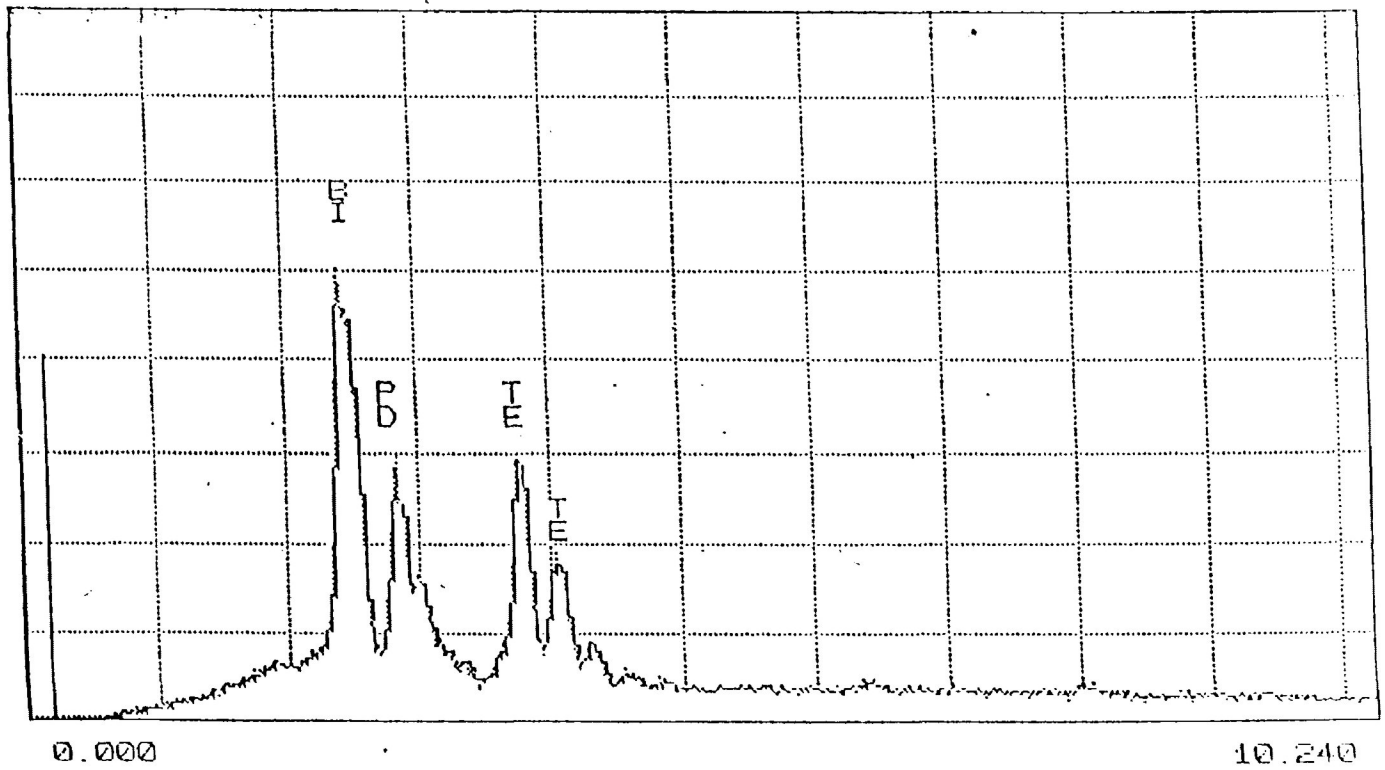
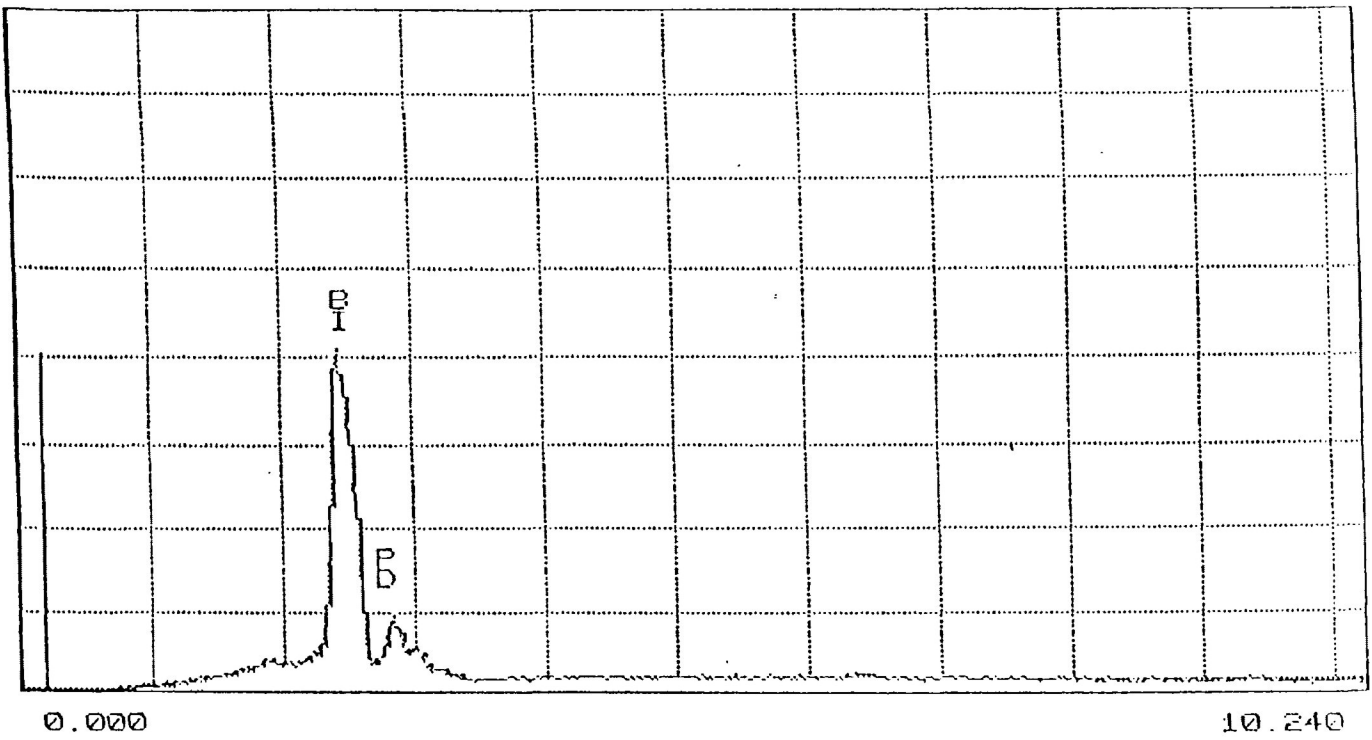


Figure 69 : SEM / EDS spectra of a) Pd₂Bi₅ grain from drill core I3C-2
b) michenerite grain from drill core I3D-I.

analysis 11) is found in figure 6.9a.

A histogram of the number of analyses vs. the Bi : Pd ratio (Figure 6.10) shows an overall approximately gaussian distribution with Bi : Pd = 2.5 (Pd_2Bi_5) as the most common Pd - Bi compound. In the Kawene samples, there are more froodite grains than Pd_2Bi_5 , but more analyses of Pd_2Bi_5 were obtained because for a period of time grains were analyzed qualitatively, and termed froodite without actually checking the exact Bi : Pd atomic ratio. Therefore, some of the "froodite" grains may actually be Pd_2Bi_5 . These qualitative analyses are not included in the histogram. The histogram also shows several smaller peaks which represent individual phases : PdBi, Pd_2Bi_3 , PdBi₂, and Pd_2Bi_5 . The standard deviation was calculated using the Bi : Pd ratios of the compositions of the michenerite standard given in table 2.3. The variation of sobolevskite and froodite compositions in literature shows that the unnamed Pd_2Bi_3 and Pd_2Bi_5 are not included in these previously published compositions.

The continuum in the histogram is not caused by analytical bias because the width of the 2σ bar is less than the width of one column in the histogram. Pd_2Bi_3 is not a result of a solid solution of sobolevskite and froodite, since sobolevskite is hexagonal and froodite is monoclinic. Previous authors have not found that the crystal symmetry for these PGM change with decreasing temperatures. Pd_2Bi_3 may be an intermediate phase produced by atomic scale layering of sobolevskite and froodite. Even though sobolevskite and native Bi have the same crystal symmetry, it seems unlikely

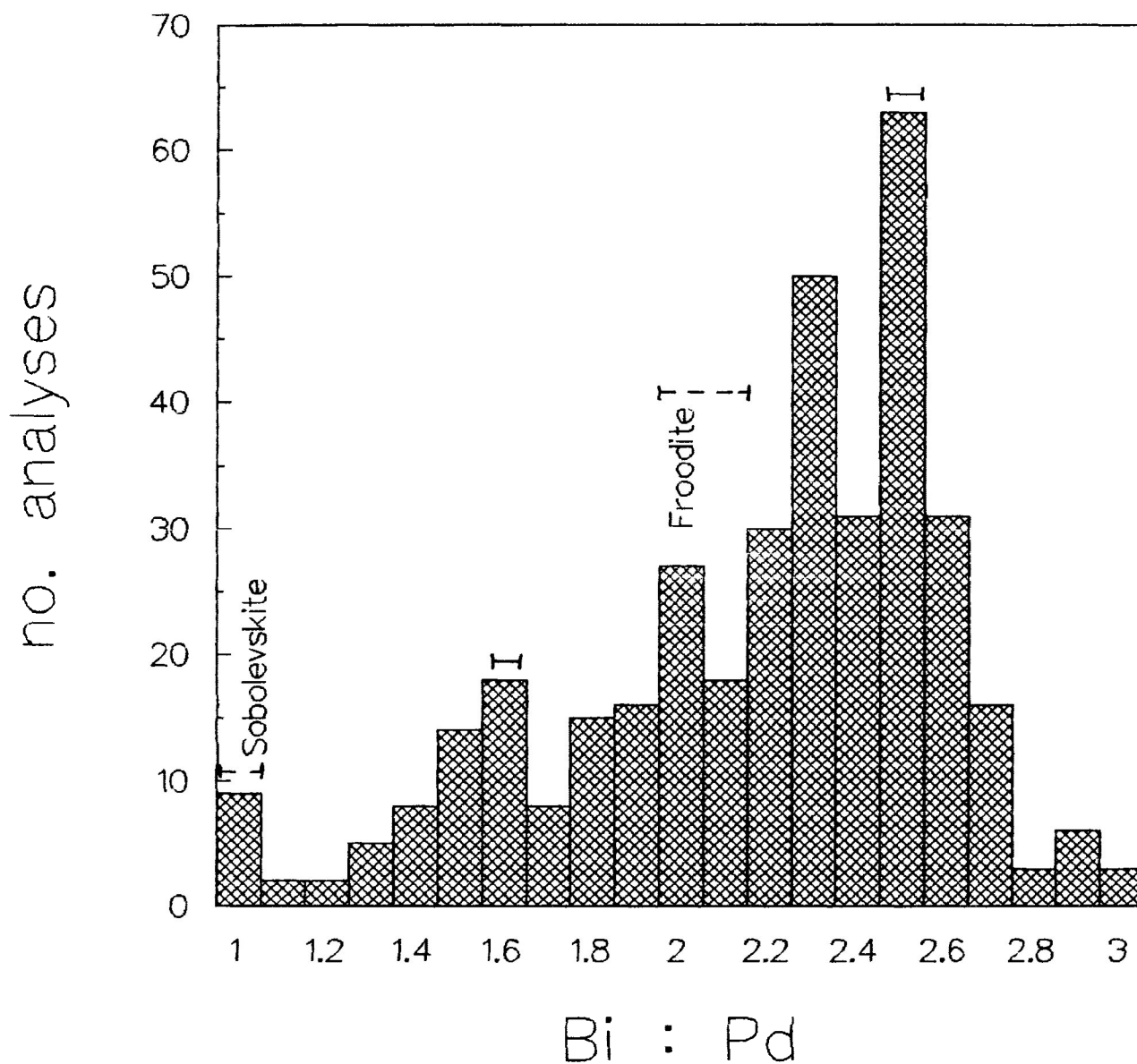


Figure 6.10 : number of analyses vs. Bi : Pd histogram (atomic %)
 Total number of analyses = 375.
 Deviation of analyzed standard (2σ) for Bi : Pd = ± 0.06 .
 Standard deviation error bar H
 Literature variation bar H--H

Table 6.5 : Comparative sobolveskite (analyses 1-4) and froodite (analyses 5-12) (weight %)

analysis	Pd	Bi	Te	Sb	Pt	Fe	Cu	Ag	S	total
1	35.5	64.0								99.5
2	34.7	63.9								98.6
3	34.4	66.2								100.6
4	32.0	65.0			0.8			0.5		98.3
5	21.58	78.55								100.12
6	20.50	79.50					0.19		0.11	100.30
7	20.30	80.00	0.16	0.10						100.56
8	20.3	79.7								100.0
9	19.97	79.68	1.45			0.18	0.06			101.34
10	19.90	79.20	0.38							99.48
11	19.40	79.40			0.51					99.31
12	19.30	81.50	0.39							101.19

1. Oktyabri mine, Noril'sk (Evstigneeva et al., 1975)
2. Strathcona deposit, Sudbury (Li and Naldrett, 1993)
3. Oktyabri mine, Noril'sk (Evstigneeva et al., 1975)
4. Lubin mine, Poland (Kucha, 1981)

5. Duluth Complex (Mogessie et al., 1991)
6. Strathcona deposit, Sudbury (Li and Naldrett, 1993)
7. Frood mine, Sudbury (Cabri and Laflamme, 1976)
8. Pipe mine, Manitoba (Laflamme, 1979) unpublished internal report
9. Upper Zone, Eastern Bushveld (Harney and Merkle, 1990)
10. Creighton mine, Sudbury (Cabri and Laflamme, 1976)
11. Coleman mine, Sudbury (Cabri and Laflamme, 1976)
12. Oktyabri mine, Noril'sk (Genkin et al., 1972)

that Pd_2Bi_5 is a solid solution of these two minerals. Pd_2Bi_5 is probably a real phase in the Pd - Bi system because it is one of the most abundant Pd - Bi compound in the Kawene Intrusion.

Pd - Bi compounds containing minor amounts of Te, S and Au were also found (Table 6.4). S and Te substitutes for Bi, and Au substitutes for Pd. Nine grains of $\text{PdBi}(\text{+S})$ ranging in size from 1 to 5 μm were found. Five grains of $\text{Pd}_2\text{Bi}_3(\text{+S})$ ranging in size from 1 to 4 μm were found. The most common paragenesis of S-bearing Pd - Bi compounds is grains enclosed in violarite. They are also found in contact with : diopside, bravoite, augite, chlorite, pyrrhotite, and chalcopyrite. Three grains of $\text{Pd}_2\text{Bi}_5(\text{+Te})$ ranging in size from 1 to 9 μm were found enclosed in chalcopyrite. Two grains of $\text{Pd}_2\text{Bi}_5(\text{+Au})$ ranging in size from 2 to 3 μm were found enclosed in augite, and at an augite - chalcopyrite boundary.

Compositions of Pd - Bi compounds from other localities are found in Table 6.5. The Kawene sobolevskite is richer in Bi than the examples from Noril'sk, Sudbury, and Poland. The composition of the froodite grains from the Kawene Intrusion is within the narrow range of froodite compositions from other localities. The composition of the $\text{Pd}_2\text{Bi}_5(\text{+Te})$ grains from the Kawene Intrusion resemble the froodite compositions from Creighton mine and Oktyabri mine.

6.3. Michenerite

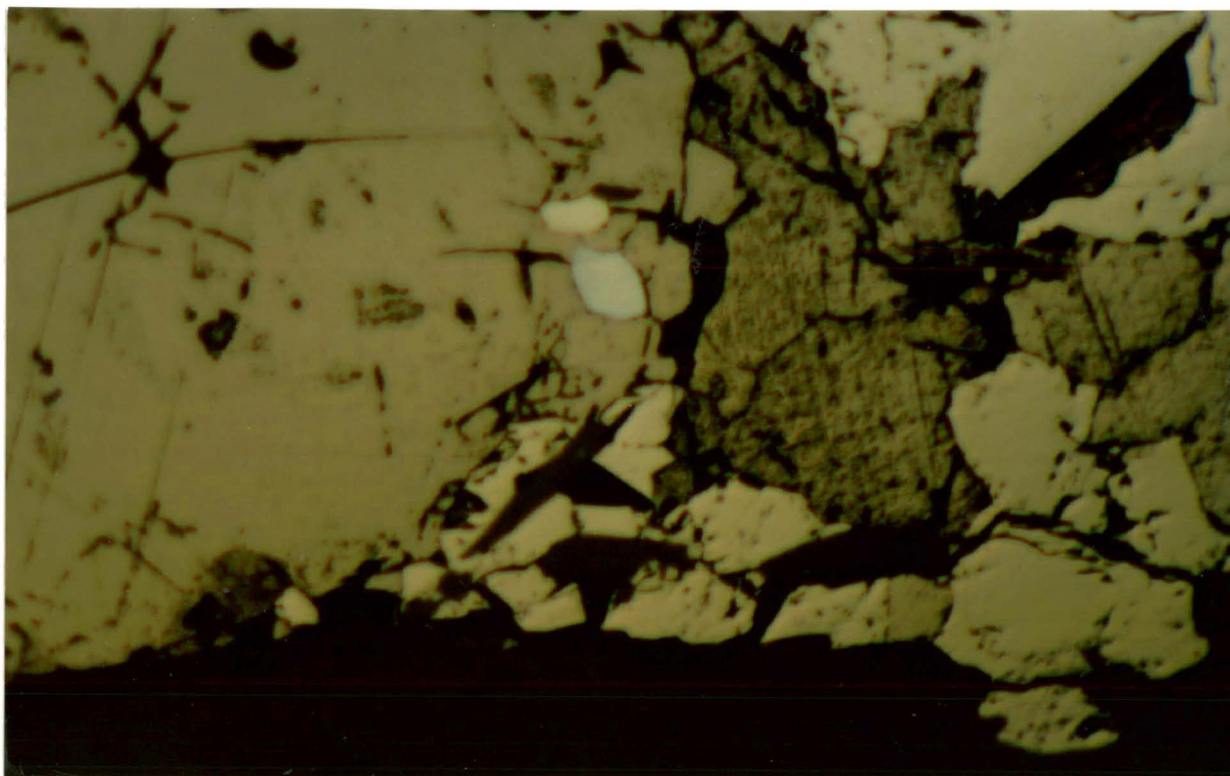
Michenerite (PdBiTe) was first reported as Pd_2Bi_3 (an unnamed mineral) from superpanning mill concentrates from the arsenic and

lead - copper rich ores of the Frood mine, Sudbury area by Michener (1940). Michenerite was named after Dr. Michener by Hawley and Berry (1958), and defined as PdBi_2 . Cabri et al. (1973) redefined michenerite as cubic PdBiTe , and reported that synthetic michenerite melts at $489 \pm 2^\circ\text{C}$ after a study of the Vermilion and Frood mine samples, Sudbury area (Table 6.8, analysis 12).

Michenerite is by far the most common PGM found in the Kawene Intrusion with a total of 195 grains found. The michenerite grains range in size from 1 to 23 μm . One euhedral ($38 \times 27 \mu\text{m}$) michenerite grain in drill core #16B-1 was found within monoclinic pyrrhotite (Figure 6.11) (Table 6.6, analysis 1).

The most common parageneses of michenerite grains are grains enclosed within chalcopyrite, augite, and pyrrhotite; at chalcopyrite - augite boundaries; and at pyrrhotite - augite boundaries. Michenerites are also found in contact with the following silicates : chlorite, diopside, sphene, and minor biotite, calcite, plagioclase, and K-feldspar. They are also associated with the following sulfides : pentlandite, violarite, minor bravoite, and minor sphalerite. A cluster of michenerite grains from drill core 13C-2 shows several different parageneses (Figure 6.12).

Representative compositions of michenerite grains are given in Table 6.6. An SEM / EDS spectrum of michenerite from 13D-1, (Table 6.6., analysis 6) is illustrated in figure 6.9b. All of the michenerite atomic % compositions obtained were plotted in the ternary Pd - Bi - Te diagram (Figure 6.8). The slightly Bi-rich



0 100 um
|-----|

Figure 6.11 : Euhedral 38 um michenerite (grey) and 25 um Pd₂BiSb(+Te) stibiopalladinite - sobolevskite solid solution (yellow) enclosed in monoclinic pyrrhotite. Right - hexagonal pyrrhotite (dark brown) and pentlandite (cream). From drill core 16B-1.

a)



Figure 6.12a, b : SEM / BSE images of michenerite grains enclosed in pyrrhotite (po), enclosed in augite, and at pyrrhotite - augite grain boundary from drill core 13C-2. The 15 μm michenerite grain is at pentlandite - augite grain boundary.

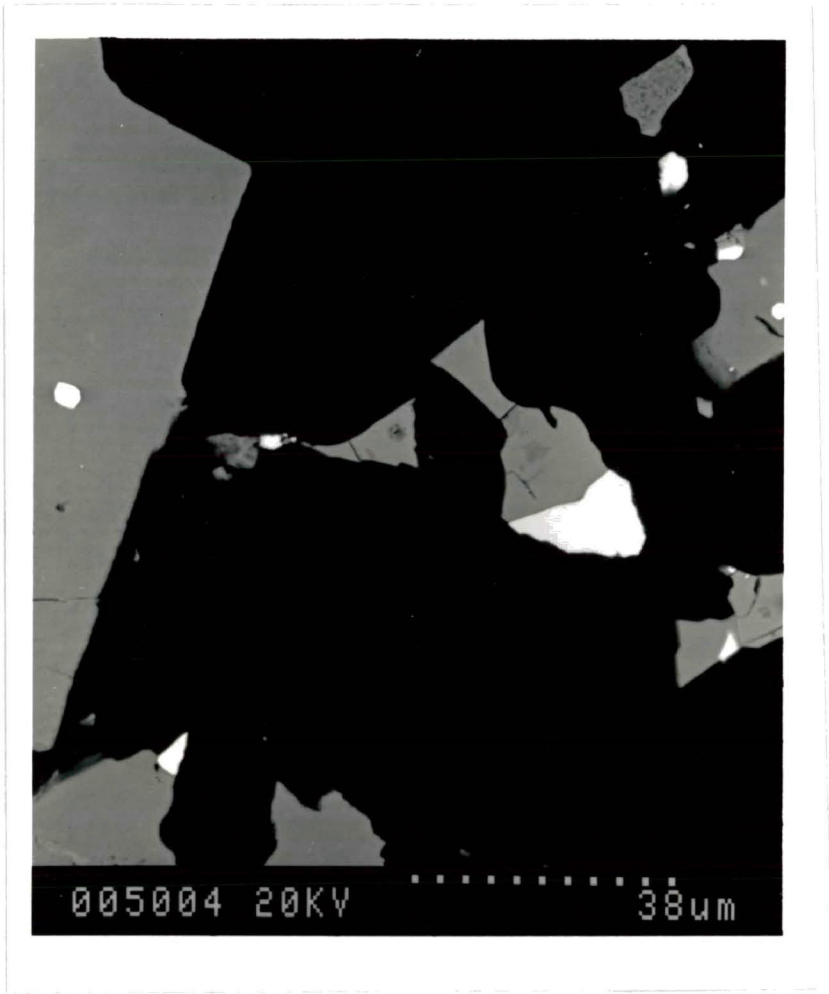


Figure 6.12 b

Table 6.6 : Representative compositions of michenerite from Kawene Intrusion (atomic and weight

analysis	at%			wt%			size	probe section
	Pd	Bi	Te	Pd	Bi	Te		
ideal	33.33	33.33	33.33	24.02	47.18	28.80		
1	29.79	39.18	31.04	20.69	53.45	25.86	38 um	16B-1
2	30.74	38.81	30.45	21.42	53.13	25.45	10 um	16B-1
3	31.25	37.87	30.88	21.90	52.14	25.96	38 um	16B-1
4	32.20	40.17	27.63	22.32	54.70	22.97	12 um	13B-1
5	32.37	34.52	33.10	23.14	48.48	28.38	12 um	15-3
6	33.78	33.67	32.55	24.31	47.60	28.09	18 um	13D-1
7	34.58	36.61	28.81	24.52	50.99	24.50	20 um	16B-2
8	34.72	33.21	32.08	25.09	47.12	27.80	12 um	15-2
9	35.18	35.79	29.03	25.07	50.11	24.82	16 um	27A
10	35.68	37.97	26.35	25.15	52.57	22.28	12 um	13B-1

Table 6.7 : Representative compositions of Sb-bearing michenerite from Kawene Intrusion (atomic and weight %)

analysis	at%				wt%				size	probe section
	Pd	Bi	Te	Sb	Pd	Bi	Te	Sb		
1	29.33	35.93	31.39	3.55	20.75	49.91	26.63	2.71	8 um	28A
2	30.51	38.11	29.14	2.24	21.35	52.40	24.46	1.79	9 um	28A
3	31.45	35.63	31.05	1.87	22.33	49.69	26.45	1.52	20 um	15B-1
4	31.77	37.71	30.00	0.53	22.30	52.01	25.26	0.42	8 um	28A

Table 6.8 : Comparative michenerite compositions (weight %)

analysis	Pd	Bi	Te	Sb	Pt	Fe	Ni	Cu	S	Ag	total
1	21.36	43.90	32.86		2.60						100.72
2	21.86	47.74	29.20		0.85						99.70
3	22.23	49.53	26.92				0.41				98.82
4	22.84	48.44	27.56	0.17			0.01		0.07		99.09
5	23.03	43.82	29.85	0.47	2.78	0.12		0.10			100.17
6	23.4	40.8	35.1	0.7	1.5						98.7
7	23.5	48.0	27.7								99.2
8	23.60	45.40	30.60	0.81			0.56				100.97
9	23.8	39.1	29.9	5.4			0.6				98.8
10	23.80	46.40	28.30	1.40		0.07	0.36				100.33
11	24.05	39.95	32.55	1.86	0.85		0.11	0.32			99.72
12	24.0	46.5	28.8	0.4							99.7
13	24.1	36.6	32.4	5.3	1.1		0.1			0.2	99.8
14	24.1	44.5	29.7	1.0			0.7				100.0
15	24.6	48.1	28.4			1.5					102.6

1. Allarechka District, Kola region, (Yakovlev et al., 1991)
2. Strathcona deposit, Sudbury (Li and Naldrett, 1993)
3. Geordie Lake Intrusion, Coldwell Complex, (Mulja and Mitchell, 1990)
4. Duluth Complex, (Mogessie et al., 1991)
5. Upper Zone, East Bushveld Complex, (Harney and Merkle, 1990)
6. Rathbun Lake, Northeastern Ontario, (Rowell and Edgar, 1986)
7. Frood mine, Sudbury, (Cabri and Laflamme, 1976)
8. Crean Hill, Sudbury, (Cabri and Laflamme, 1976)
9. Copper Cliff, Sudbury, (Cabri and Laflamme, 1976)
10. Pipe mine, Manitoba, (Laflamme, 1979) unpublished internal report
11. Blue Lake, Labrador Trough, Quebec, (Beaudoin et al., 1990)
12. Vermillion Mine, Sudbury, (Cabri et al., 1973)
13. Kambalda, Western Australia, (Hudson, 1986)
14. Hitura, Finland, (Hakli et al., 1976)
15. J-M Reef, Stillwater Complex, (Volborth et al., 1986)

michenerite analyses cluster close to the ideal composition.

Grains of michenerite containing minor amounts (0.53 - 3.55 at%) of Sb were also found. The 15 Sb-bearing michenerite grains range in size from 2 - 20 μm . Representative compositions of these minerals are found in Table 6.7. Their most common paragenesis is enclosed within chalcopyrite. They are also found in contact with augite, pentlandite, and violarite.

Compositions of michenerite from other localities are listed in Table 6.8. The Bi-rich michenerites from the Kawene Intrusion resemble the michenerites from the Coldwell, Duluth, Stillwater, and Sudbury Complexes. The Sb-bearing michenerites from the Kawene intrusion resemble the michenerites from the Duluth Complex, Crean Hill mine, Vermillion mine, and Pipe mine.

6.4. Pd - Bi - Te - Sb Compounds

Sudburyite can vary in composition from end member PdSb to Ni-bearing sudburyite (up to 8.7 wt% Ni) (Cabri and Laflamme, 1974). Sudburyite is hexagonal with a space group $P6_3/mmc$ (Anthony et al., 1990). Sudburyite was first discovered in Frood and Copper Cliff South mines in Sudbury by Cabri and Laflamme (1974). It was named for its type locality Sudbury (Anthony et al., 1990).

Stibiopalladinite from its type locality Farm Tweefontein, near Potgietersrust, South Africa is considered to have a composition between Pd_5Sb_2 and Pd_8Sb_3 (Cabri et al., 1975). Its general formula is $(\text{Pd}, \text{Cu})_{5+x}(\text{Sb}, \text{As}, \text{Sn})_{2-x}$, where $x \approx 0.05$ and $\text{Pd} \gg \text{Cu}, \text{Sb} \gg \text{As}, \text{Sn}$ (Cabri and Chen, 1976). Stibiopalladinite is

hexagonal and has a space group of $P6_3/mmc$, $P6_3mc$, or $P\bar{6}2c$ (Anthony et al., 1990; Cabri and Chen, 1976). This is similar to the space group of sudburyite. Stibiopalladinite is named for its composition (Anthony et al., 1990).

The most common Pd - Bi - Te - Sb compound in the Kawene Intrusion is $Pd_2BiSb(+Te)$ with 12 grains found ranging in size from 1 - 15 μm . One anomalous large grain from drill core 16B-1 is 25 x 15 μm in size, and is found at a monoclinic pyrrhotite - diopside boundary (Figure 6.11). An SEM / EDS spectrum of $Pd_2BiSb(+Te)$ of this grain is given in figure 6.13. The other Pd - Bi - Te - Sb compounds are :

Pd_3Bi_2Sb 6 grains found, size 2 - 7 μm ;
 $Pd_2Bi(Te,Sb)$ 6 grains found, size 2 - 8 μm ;
 $PdSb(+Bi,Te)$ 3 grains found, size 2 - 3 μm ;
 $Pd_3BiSb_2(+Te)$ 2 grains found, size 3,7 μm .

The most common parageneses of the Pd - Bi - Te - Sb compounds are : enclosed in chalcopyrite, pentlandite, pyrrhotite, and augite. They are found in contact with the following silicates : diopside, K-feldspar, apatite, chlorite. They are also found in contact with the following sulfides : violarite, bravoite, and sphalerite.

Representative compositions of Pd - Bi - Te - Sb compounds are given in Table 6.9. Pd in these compounds has a narrow range of 43.23 - 52.97 at%. Bi ranges from 14.07 - 33.73 at%, Te ranges from 0.00 - 15.76 at%, and Sb ranges from 5.87 - 35.73 at%. Compositions for $PdSb(+Bi,Te)$ are not given in the table due to the

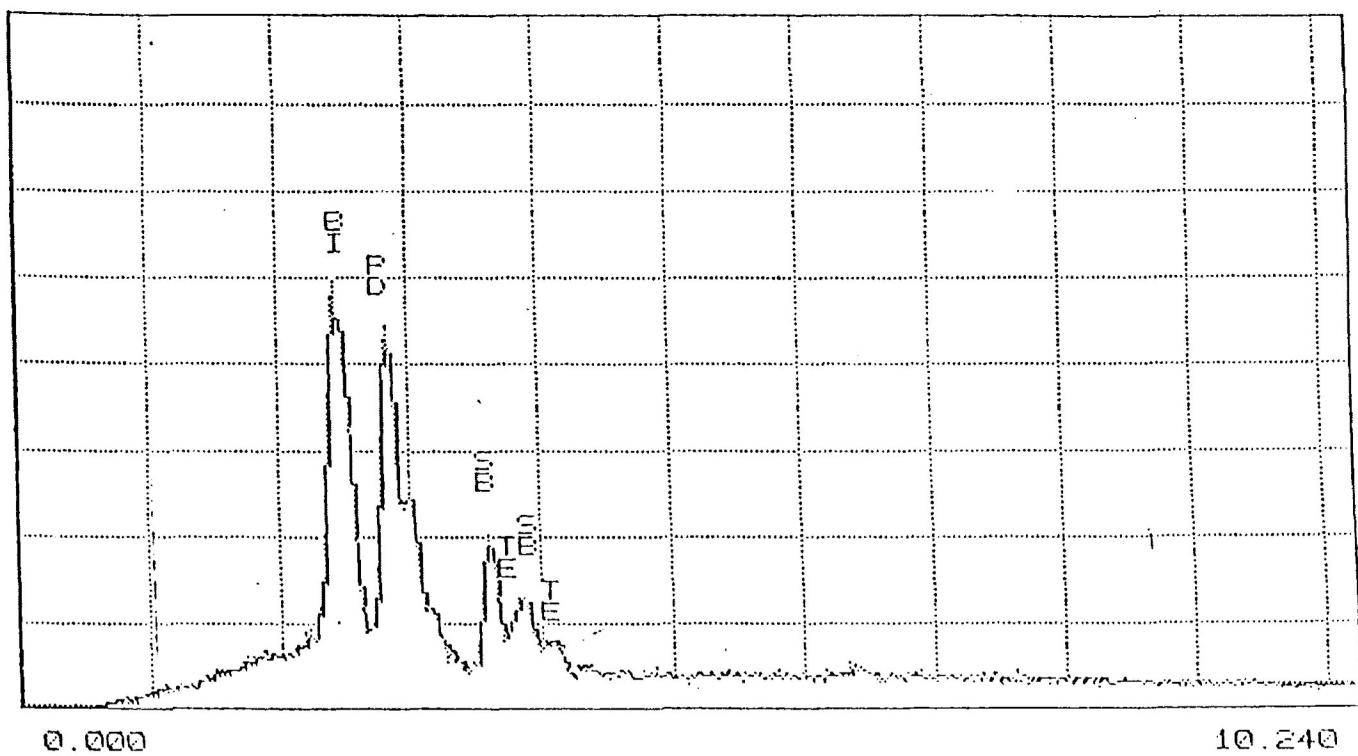


Figure 6.13 : SEM / EDS spectrum of Pd₂BiSb(+Te) from drill core I6B-I.

Table 6.9 : Representative compositions of Pd - Bi - Te - Sb compounds from Kawene Intrusion (atomic and weight %)

analysis	at%				wt%				size	probe section
	Pd	Bi	Te	Sb	Pd	Bi	Te	Sb		
ideal	50.00	50.00			33.74	66.26				PdBi
	50.00			50.00	46.64			53.36		PdSb
	71.43			28.57	68.60			31.40		Pd5Sb2
	33.33	33.33	33.33		24.02	47.18	28.80			PdBiTe
1	48.92	22.25		28.83	38.95	34.79		26.26	15 um	15B-1
2	50.32	32.07		17.61	37.71	47.20		15.09	7 um	AK-10
3	51.72	31.87		16.41	38.86	47.03		14.11	7 um	AK-10
4	52.97	31.42		15.61	39.97	46.55		13.47	7 um	AK-10
5	46.62	14.07	5.58	35.73	39.04	23.14	5.60	34.23	7 um	13
6	46.85	15.22	4.19	33.74	38.93	24.82	4.17	32.07	7 um	13
7	43.23	25.73	10.15	20.89	33.30	38.92	9.37	18.41	7 um	AK-10
8	44.16	25.92	7.91	22.01	34.04	39.24	7.31	19.41	7 um	AK-10
9	45.63	29.01	3.62	21.73	34.62	43.23	3.29	18.86	12 um	15-1
10	46.46	27.76	3.91	21.87	35.55	41.71	3.59	19.15	25 um	16B-1
11	47.18	27.39	6.36	19.07	36.18	41.25	5.84	16.73	12 um	15-1
12	44.12	34.17	15.76	5.94	32.22	49.01	13.80	4.97	8 um	16B-1
13	46.07	33.73	14.33	5.87	33.82	48.63	12.62	4.93	8 um	16B-1
14	46.53	31.02	10.04	12.42	34.80	45.57	9.01	10.63	7 um	16A
15	48.68	31.30	7.18	12.84	36.47	46.07	6.45	11.01	7 um	16A

1-4. Pd3Bi2Sb sobolevskite - sudburyite

5,6. Pd3BiSb2(+Te) stibiopalladinite (+Bi,Te)

7-11. Pd2BiSb(+Te) sobolevskite - stibiopalladinite

12-15. Pd2Bi(Te,Sb) sobolevskite - stibiopalladinite - michenerite

unreliability of analyses from small grains 2-3 μm in diameter.

The atomic % compositions of the Pd - Bi - Te - Sb compounds were plotted in the PdBi - PdSb - PdTe plane from the Pd - Bi - Te - Sb quaternary diagram to classify the compositions (Figure 6.14). The compositions of Sb-bearing michenerite were also plotted in the quaternary diagram (section 6.3). The compositions represent an almost continuous solid solution between sudburyite (PdSb), stibiopalladinite (Pd_3Sb_2), sobolevskite (PdBi), and michenerite (PdBiTe). The phases in the quaternary system from the Kawene Intrusion are :

PdSb(+Bi,Te) sudburyite - stibiopalladinite solid solution (ss);

Pd_3BiSb_2 (+Te) stibiopalladinite +Bi,Te;

Pd_2BiSb (+Te) sobolevskite - stibiopalladinite solid solution;

Pd_2Bi (Te,Sb) sobolevskite - stibiopalladinite - michenerite ss.

The Pd - Bi - Sb atomic % compositions were plotted in a Pd - Bi - Sb ternary diagram (Figure 6.15). $\text{Pd}_3\text{Bi}_2\text{Sb}$ is a solid solution of sobolevskite and sudburyite.

One 4 μm grain enclosed in chalcopyrite from sample AK-10 is an intergrowth of Sb-bearing michenerite and Pd_2Bi (Te,Sb) (Figure 6.16). The Te - Sb varies in each zone from Te > Sb in michenerite to Sb \approx Te to Sb > Te in Pd_2Bi (Te,Sb). This grain supports the existence of a sobolevskite - stibiopalladinite - michenerite solid solution.

Another 7 μm grain from drill core 13 enclosed in pentlandite is an intergrowth of stibiopalladinite (Pd_3BiSb_2 (+Te)) and PdSb(+Bi,Te). This grain is an example of the stibiopalladinite -

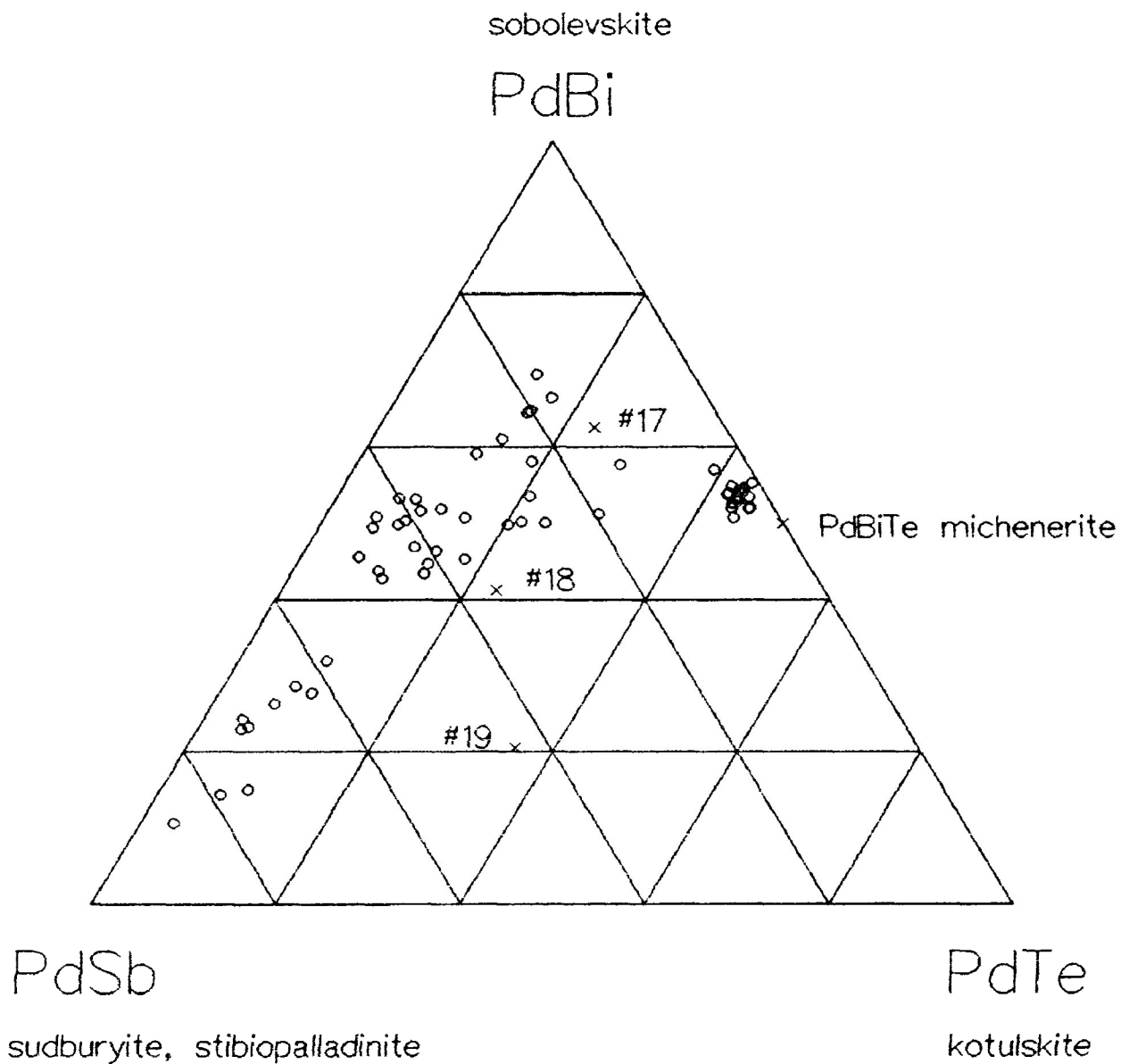


Figure 6.14 : PdBi - PdSb - PdTe ternary diagram (atomic %) #17, 18, 19 Table 6.10, UN1976-4

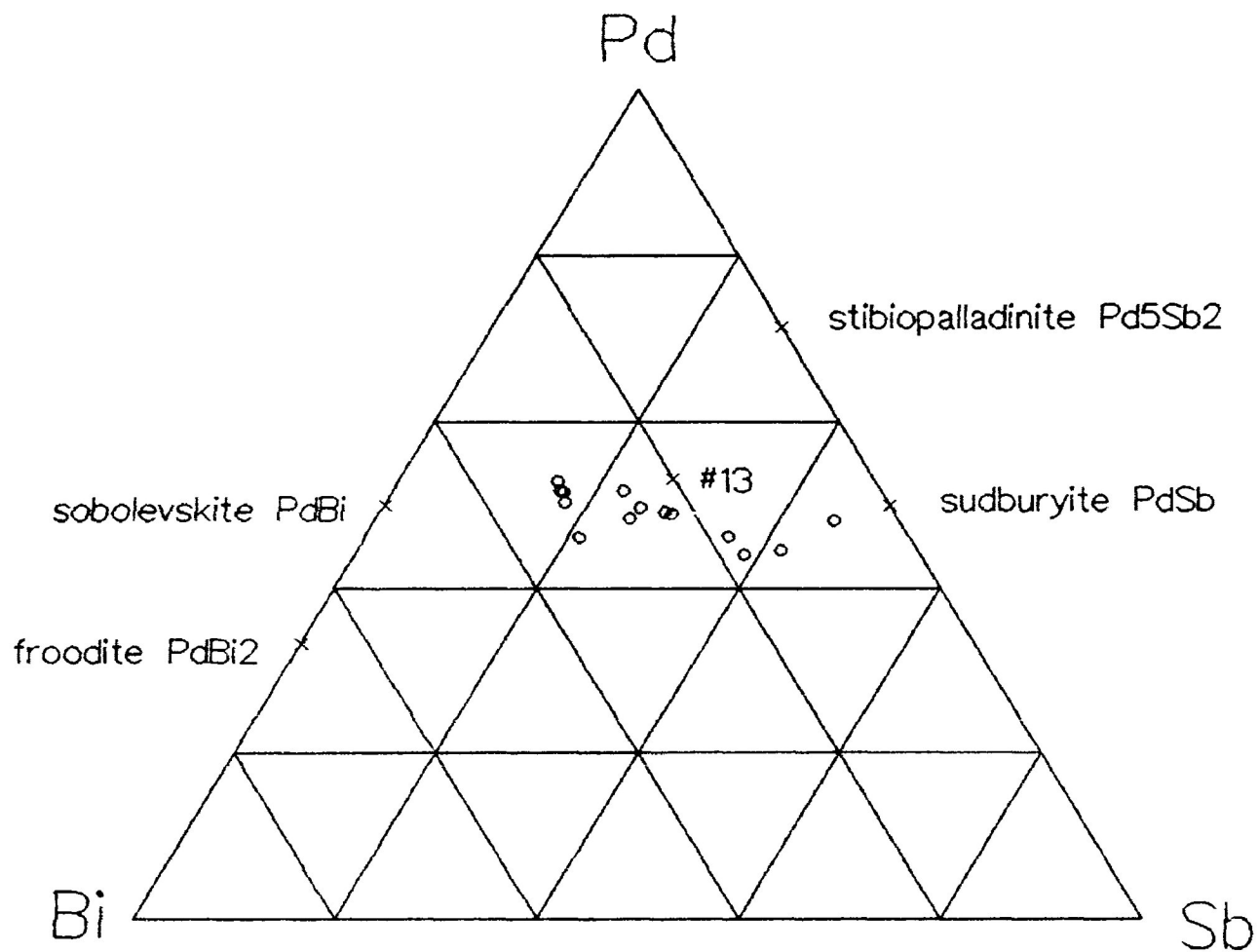


Figure 6.15 : Pd - Bi - Sb ternary diagram (atomic %)

#13 Table 6.10, UN1961-8

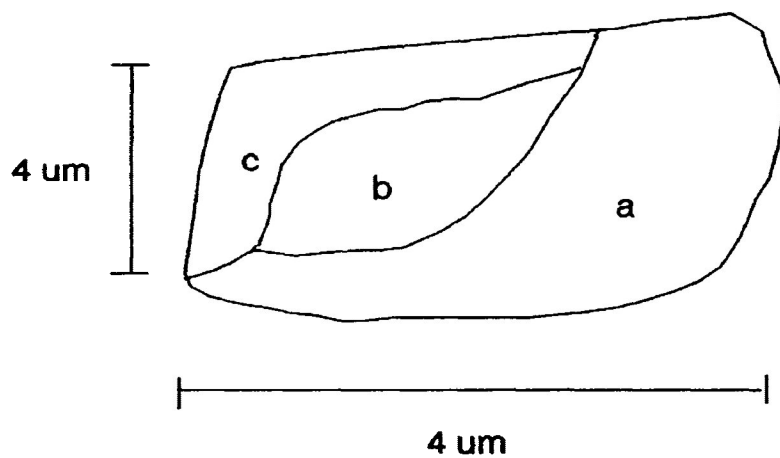


Figure 6.16 : Intergrowth of a) Sb-bearing michenerite ($Te > Sb$), b) sobolevskite - stibiopalladinite - michenerite ($Te = Sb$), and c) sobolevskite - stibiopalladinite - michenerite ($Te < Sb$) from drill core AK-10.

sudburyite solid solution. Stibiopalladinite and sudburyite are hexagonal with a space group $P6_3/mmc$ (Anthony et al., 1990). Hudson and Donaldson (1984) also found stibiopalladinite and sudburyite intergrown. Their electron microprobe analyses of sudburyite indicated that there is a wide variation in its composition due to the substitution of Te and Bi for Sb. The ratio of Te + Bi : Sb can be up to 3:1 (Hudson and Donaldson, 1984).

Beaudoin et al., (1990) studied the solid solution in the Pd - Bi - Te - Sb system by examining sobolevskite - kotulskite (PdTe) solid solution. They also plotted compositions in the PdBi - PdSb - PdTe plane. They considered that the compositions change within the Pd - Bi - Te - Sb system from PdTe to PdBiTe to PdSb with decreasing temperature.

Cabri and Laflamme (1976) also plotted their unknowns (UN1976-4) in the PdBi - PdSb - PdTe plane (Table 6.8, analyses 17, 18, and 19). They concluded that there is a wide solid solution with the hexagonal NiAs structure extending over most of the composition triangle. Sobolevskite, sudburyite, stibiopalladinite, and kotulskite are all hexagonal, but michenerite is cubic (Anthony et al., 1990).

Compositions of sudburyite, stibiopalladinite, and Pd - Bi - Te - Sb from other localities are given in Table 6.10. For examples of sobolevskite compositions see Table 6.5, and for examples of Sb-bearing michenerite see Table 6.8. Sobolevskite - sudburyite from the Kawene Intrusion (Table 6.9, analysis 1) closely matches UN1961-8 from the Driekop mine, South Africa (Table

Table 6.10 : Comparative Pd - Bi - Te - Sb compositions (weight %)

analysis	Pd	Bi	Te	Sb	Pt	Ir	Pb	Sn	Ni	Fe	Cu	As	S	total
1	39.38	0.35		54.16	0.27	0.12			2.65	1.20	0.89			99.58
2	40.80	4.50	0.12	51.30					3.20			0.52		100.44
3	41.03	0.75	0.04	54.06	0.31	0.56			2.69	0.35	0.11	0.33		100.23
4	41.89	0.89	0.04	53.57	0.43	0.47			2.14	0.72	0.18	0.13		100.46
5	41.90	5.40	0.14	49.60					2.18			0.03		99.25
6	43.9	4.8	5.7	44.6					0.7					99.7
7	44.40	3.30	3.90	45.30					0.53			1.88		99.31
8	46.0			53.3										99.3
9	46.21	0.54	0.89	51.63	0.43				0.20			0.07		99.97
10	67.7			30.7				0.1			1.7	0.2		100.4
11	68.2			30.4	1.7							1.8		103.5
12	41.94	9.42	16.06	32.39	0.26				0.17			0.16		100.40
13	43.6	32.2		25.2										101.0
14	26.8	10.0	58.0	6.5										101.3
15	35.27	15.43	16.77	21.00	0.64		2.15	2.04	2.53	3.01			0.32	99.15
16	37	5	17	41										100
17	37.4	45.9	10.4	6.1										99.8
18	40.3	32.3	11.1	16.2										99.9
19	42.3	17.8	18.8	22.0										100.9

1. Blue Lake, Labrador Trough, Quebec (Beaudoin et al., 1990) sudburyite
2. Sudbury (Cabri and Laflamme, 1974)
- 3,4. Blue Lake, Labrador Trough, Quebec (Beaudoin et al., 1990)
5. Sudbury (Cabri and Laflamme, 1974)
6. "Y" deposit, Southwest China (Cabri and Laflamme, 1981)
7. Sudbury (Cabri and Laflamme, 1974)
8. Witwatersrand Reefs, South Africa (Feather, 1976)
9. Kambalda, Western Australia (Hudson and Donaldson, 1984)

10. Farm Tweefontein, near Potguetersrust, South Africa (Cabri andstibiopalladinite)
11. Driekop mine, South Africa (Tarkian and Stumpfl, 1975)

12. Kambalda, Western Australia (Hudson and Donaldson, 1984) sudburyite(+Bi,Te)
13. UN1961-8, Driekop, Transvaal, South Africa (Stumpfl, 1961) sobolevskite - sudburyite
14. UN1974-14 Northeast China (Cabri, 1981) Pd - Bi - Te - Sb
15. unnamed PGM-1 Blue Lake, Labrador Trough, Quebec (Beaudoin et al., 1990)
16. UN1974-7 Northeast China (Cabri, 1981)
17. UN1976-4 Creighton mine, Sudbury (Cabri and Laflamme, 1976)
- 18, 19. UN1976-4 Vermilion mine, Sudbury (Cabri and Laflamme, 1976)

6.10, analysis 13). UN1976-4 from the Creighton and Vermilion mines (Table 6.10, analyses 17, 18) plots on the PdBi - PdTe - PdSb ternary diagram near the sobolevskite - stibiopalladinite - michenerite compositions from the Kawene Intrusion (Figure 6.14).

Chapter 7

Bi - Te - Se - S Compositional Group

7.1. Native Bi

Native Bi is hexagonal, rhombohedral with a space group $R\bar{3}m$ (Anthony et al., 1990). This is the same crystal symmetry as the Bi - Te compounds. Native Bi may contain minor amounts of As, Te, and S (Anthony et al., 1990; Klein and Hurlbut, 1985). The name bismuth comes from the German weisse masse, later wismuth, meaning white mass (Anthony et al., 1990). Native Bi is commonly found in hydrothermal veins with ores of Co, Ni, Ag, and Sn (Anthony et al., 1990).

Native Bi crystals range in size from 1 - 12 μm ; 39 grains were found. Native Bi is usually found along grain boundaries with the most common habit being at augite - Bi-S compound boundaries. It is found in contact with the following sulfides : galena, pyrrhotite, chalcopyrite, and pentlandite. It is found also in contact with the following silicates : diopside, K-feldspar, chlorite, biotite, plagioclase, quartz, and apatite.

7.2. Bi - S Compounds

Bismuthinite (Bi_2S_3) is orthorhombic, and is typically found in low to high temperature hydrothermal vein deposits (Anthony et al., 1990; Klein and Hurlbut, 1985). Bismuthinite was named for its composition (Anthony et al., 1990).

The Bi - S compounds in the Kawene Intrusion range in

composition from Bi_2S_3 (bismuthinite) to BiS (unnamed) to Bi_3S_2 (unnamed). Bi_2S_3 is the most common Bi - S compound in the Kawene Intrusion with 37 grains found ranging in size from 1 - 20 μm in diameter. The other Bi - S found are :

BiS 29 grains found, size 1 - 18 μm ;

Bi_3S_2 11 grains found, size 1 - 10 μm .

The Bi - S compounds are commonly found intergrown with Pd - Bi compounds, michenerite, native Bi, and minor galena. In the Duluth Complex, Bi_2S_3 is intergrown with froodite (PdBi_2) (Mogessie et al., 1991).

A few Bi - S compounds contain minor amounts of Pt which substitutes for Bi, and Se which substitutes for S (Table 7.1). These compounds are :

$(\text{Bi,Pt})\text{S}$ (unnamed) 3 grains found, size 2 - 5 μm ;

$(\text{Bi,Pt})(\text{S,Se})$ (unnamed) 2 grains found, size 5 and 12 μm ;

$\text{Bi}_2(\text{S,Se})_3$ (unnamed) 2 grains found, size 4 μm .

The most common parageneses for the Bi - S compounds are at the boundaries between augite - augite, augite - diopside, and diopside - diopside grains. Bi - S compounds are in contact with the following sulfides : pyrrhotite, chalcopyrite, pentlandite, and minor sphalerite, bravoite, and violarite. Bi - S compounds are also found in contact with the following silicates : chlorite, calcite, and minor plagioclase, K - feldspar, biotite, and hornblende. Figure 7.1 shows Bi_2S_3 grains from drill core 15 - 5 at pyrrhotite - diopside, and pentlandite - diopside boundaries, along fractures within pentlandite, and at pyrrhotite - pentlandite

Table 7.1 : Representative compositions of Bi - S compounds from Kawene Intrusion (atomic and weight %)

analysis	at%				wt%				size	probe section
	Bi	S	Pt	Se	Bi	S	Pt	Se		
ideal	40.00	60.00			81.30	18.70				Bi ₂ S ₃
	50.00	50.00			86.70	13.30				BiS
	60.00	40.00			90.72	9.28				Bi ₃ S ₂
1	39.32	60.68			80.86	19.14			9 um	15B-1
2	40.59	59.41			81.66	18.34			20 um	15-5
3	43.96	56.04			83.64	16.36			9 um	15B-1
4	52.62	47.38			87.87	12.13			18 um	15-5
5	60.93	39.07			91.04	8.96			10 um	17A-2
6	48.56	46.70	4.74		80.75	11.91	7.34		12 um	15-6
7	44.86	45.96	4.74	4.44	77.32	12.15	7.63	2.89	12 um	15-6
8	36.95	58.69		4.35	77.63	18.91		3.46	4 um	AK-2
9	40.51	54.77		4.71	79.92	16.57		3.51	4 um	AK-2

1,2,3. Bi₂S₃

4. BiS

5. Bi₃S₂

6. (Bi,Pt)S

7. (Bi,Pt)(S,Se)

8,9. Bi₂(S,Se)₃Table 7.2 : Comparative Bi₂S₃ compositions (weight %)

analysis	Bi	S	Se	Cu	Fe	Ni	Pb	Pd	Ag	Te	total
1	74.8	18.2		1.1	0.5		3.1				97.7
2	76.50	21.03		0.61			1.92				100.06
3	76.94	14.45	8.80								99.89
4	78.0	17.7		1.1	0.6		4.1				101.5
5	79.28	18.46		0.48	0.74		1.68				100.64
6	80.2	18.0								0.1	98.3
7	80.72	19.21				0.02		0.08	0.23		100.61
8	81.4	18.6		0.2			1.1				101.3

1. Inakuraishi mine, Japan (Maeda and Ito, 1989)

2. Deepwater, New South Wales, Australia (Plimer, 1977)

3. Guanajuato, Mexico (Anthony et al., 1990)

4. Inakuraishi mine, Japan (Maeda and Ito, 1989)

5. Jonquiere, Quebec (Anthony et al., 1990)

6. Borzsony, Hungary (Sztrokay and Nagy, 1982)

7. Duluth Complex (Mogessie et al., 1991)

8. Tsumo mine, Japan (Shimazaki and Ozawa, 1978)

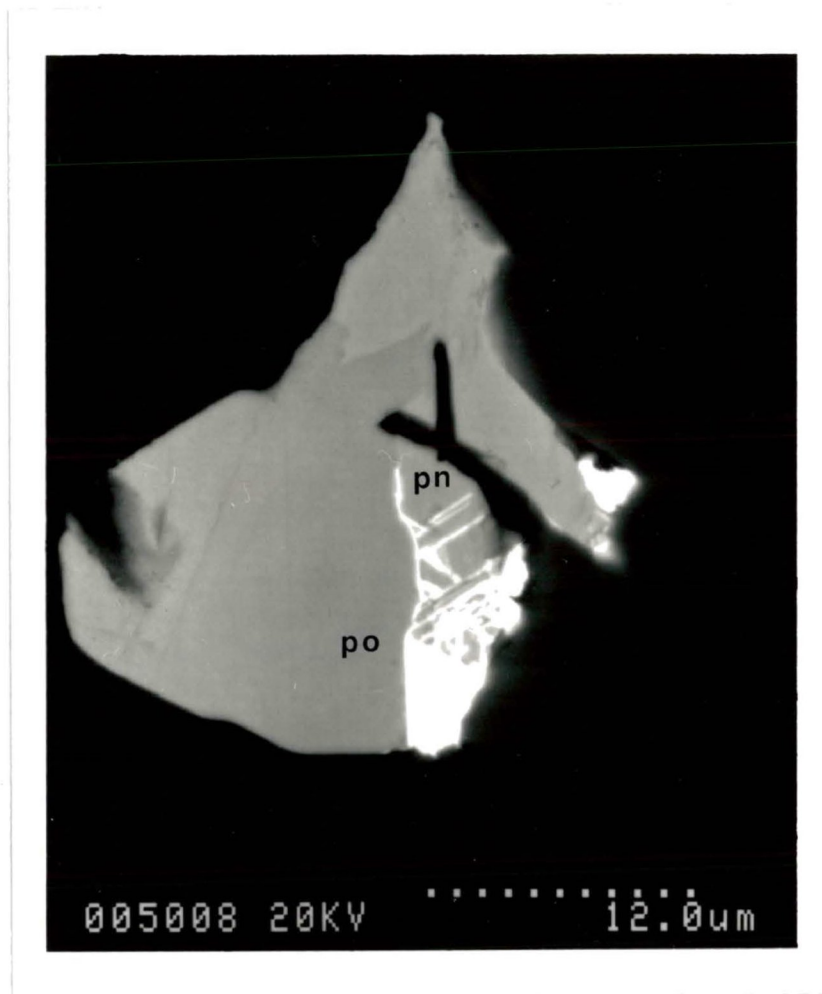


Figure 7.1 : A SEM / BSE image of bismuthinite found along fractures and at pyrrhotite (po) - pentlandite (pn) - diopside grain boundaries from drill core 15-5.

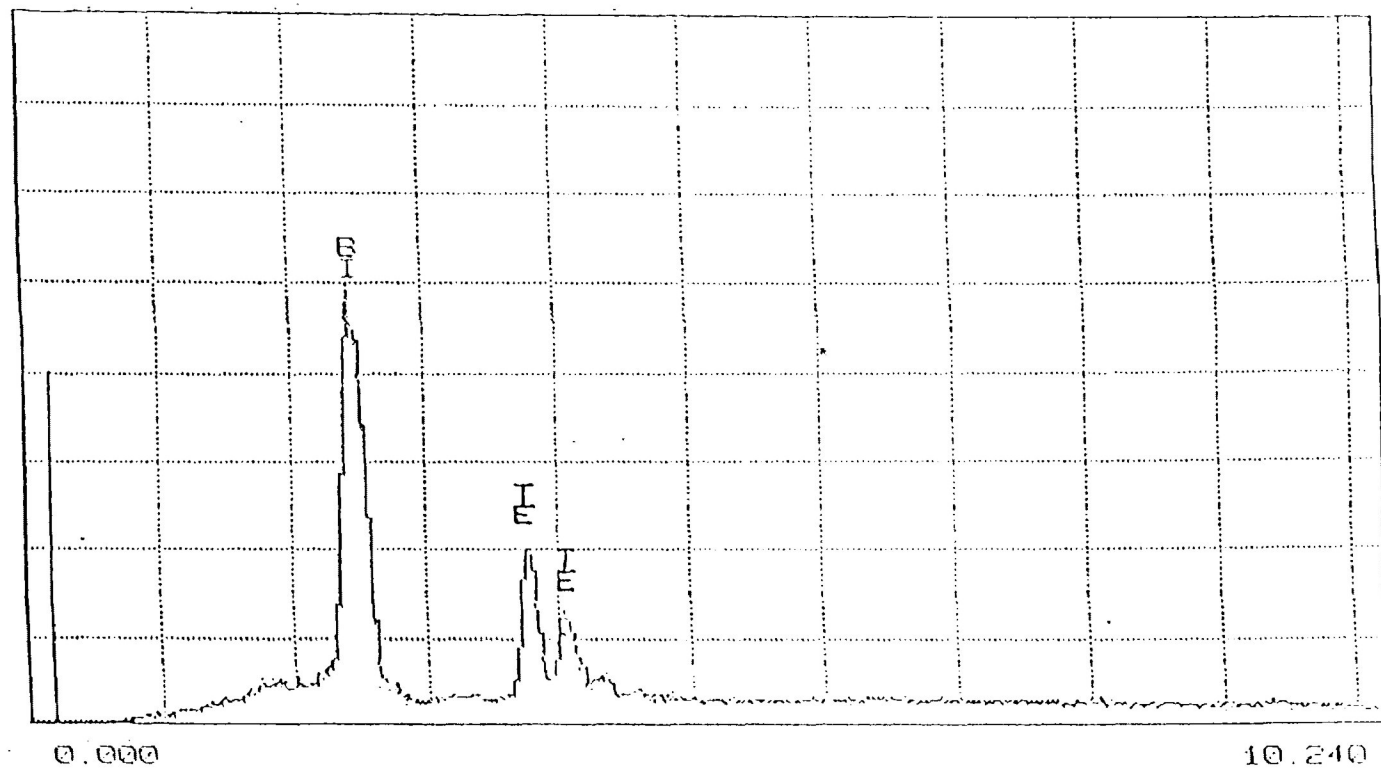
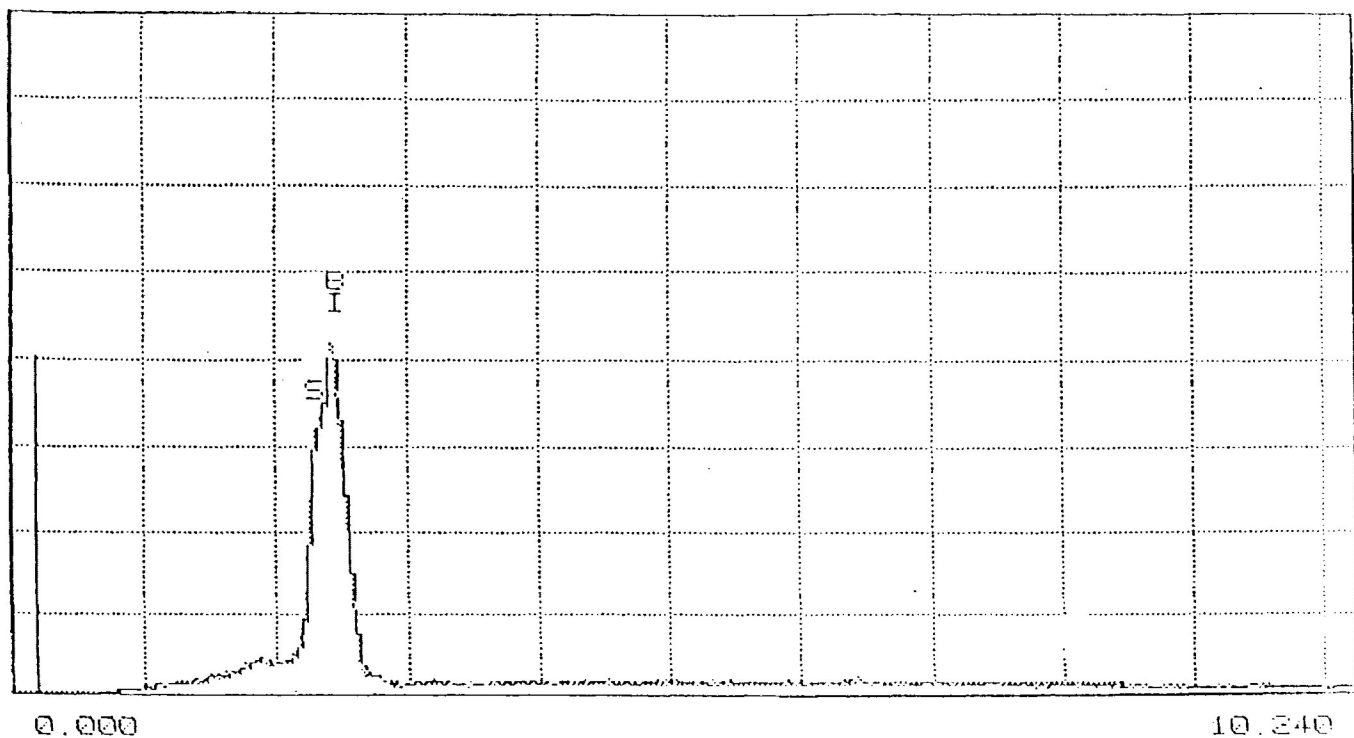


Figure 72 : SEM / EDS spectra of a) Bi₂S₃ grain from drill core I5-5
b) Bi₃Te₂ grain from drill core I5B-3.

boundaries.

Representative compositions of Bi - S compounds are given in table 7.1. The Bi_2S_3 compositions from the Kawene Intrusion resemble the ideal composition. The Bi - S compounds contain minor amounts of Pt (7.34 - 7.63 wt%) and Se (2.89 - 3.51 wt%).

There is a spectral peak overlap in SEM / EDS analyses between Bi M, S K, and Pb M elemental peaks. In order to check for the presence of Pb, each Bi - S compound was analyzed for 10 seconds over the energy range 1 - 20 KeV. This typically showed the presence of both Bi L peaks and the absence of Pb L peaks (see section 2.8). The "chi-squared" for each quantitative analysis (< 1.5) indicated absence of other peaks in spectra.

An SEM / EDS spectrum of a 20 μm Bi_2S_3 grain from drill core 15 - 5 is given in figure 7.2a (Table 7.1, analysis 2). Note that this spectrum does not show peaks due to the excitation of the surrounding biotite, chlorite, and pyrrhotite matrix.

Compositions of bismuthinite from other localities are found in Table 7.2. There are very few published microprobe analyses of Bi_2S_3 . The bismuthinite from the Kawene Intrusion resembles the bismuthinite from the Duluth Complex, U.S.A.; Borzsony, Hungary; and Tsumo mine, Japan.

7.3. Bi - Te Compounds

Tsumoite (BiTe) was named by Shimazaki and Ozawa (1978) for its type locality Tsumo mine, Japan (Table 7.5, analysis 6). Tsumoite is hexagonal, rhombohedral with space group $\text{P}\bar{3}\text{m}1$ (Anthony

et al., 1990). Since the number of layers in the unit cell is three times the number of atoms in the unit formula for phases in the Bi - Te and Bi - Se systems, and BiTe has a 12 layer structure, the formula for tsumoite should be written as Bi_2Te_2 ($3 * (2\text{Bi} + 2\text{Te}) = 12$ atoms) (Shimazaki and Ozawa, 1978).

BiTe is also known as wehrlite. Wehrlite is similar to tsumoite in that it is also rhombohedral with a space group $R\bar{3}m$ (Chizhikov and Shchastlivyi, 1970). The difference between tsumoite and wehrlite is that for tsumoite, the c-axis of the unit cell is about 24 Å with a 12 layer structure and for wehrlite, the c-axis is about 30 Å which suggests a 15 layer structure (Shimazaki and Ozawa, 1978; Cabri and Laflamme, 1976; Chizhikov and Shchastlivyi, 1970; Berry and Thompson, 1962). Wehrlite was named after Wehrle who studied this Bi - Te compound in 1831 (Ozawa and Shimazaki, 1982).

Wehrlite was discredited by Ozawa and Shimazaki (1982), since they had previously studied wehrlite (1978) from its type locality Deutsch - Pilsen, Hungary, and proved that it is a mixture of Bi_4Te_3 (pilsenite) and Ag_2Te (hessite). Huot (1841) was the first to describe wehrlite from Deutsch - Pilsen as a silver - bearing bismuth telluride. Sipoez (1886) determined the composition of the wehrlite from the type locality to be 4.37 Ag, 59.47 Bi, 35.47 wt% Te for a total of 99.31 wt%. Warren and Peacock (1945) believe that wehrlite is a bismuth - tellurium alloy with minor silver. Recent authors, such as Volborth et al. (1986) and Garuti and Rinaldi (1986), still use the name "wehrlite" rather than tsumoite.

In this thesis, BiTe will be called tsumoite because this is the name that has been approved by the Commission on New Minerals and Mineral Names IMA, and to avoid confusion with the ultramafic rock name wehrlite (an olivine clinopyroxene peridotite) which is found at the center of the Kawene Intrusion.

Pilsenite (Bi_4Te_3) and hedleyite (Bi_7Te_3) also are hexagonal, rhombohedral with a $R\bar{3}m$ space group (Anthony et al., 1990; Ozawa and Shimazaki, 1982). The c-axis for pilsenite is 41.92 Å, and for hedleyite is 119.0 Å (Anthony et al., 1990). Note that as the at% of Bi increases from tsumoite (50 at%), to pilsenite (57 at%), to hedleyite (70 at%), the length of the c-axis also increases. Pilsenite is named after its type locality Borzsony (Deutsch - Pilsen), Hungary (Table 7.5, analysis 10). Pilsenite typically has a hydrothermal origin (Anthony et al., 1990). Hedleyite was named after its type locality Good Hope Claim, Hedley, British Columbia by Warren and Peacock (1945) (Table 7.5, analysis 23, 24).

The Bi - Te compounds in the Kawene Intrusion range in composition from BiTe (tsumoite), Bi_4Te_3 (pilsenite), Bi_3Te_2 (unnamed), Bi_2Te (unnamed), and Bi_7Te_3 (hedleyite). The most common Bi - Te compound is Bi_2Te with 31 grains found, and ranges in size from 1 - 15 μm in diameter. The other Bi - Te compounds are :

BiTe 4 grains found, size 2 - 4 μm ;

Bi_4Te_3 7 grains found, size 1 - 7 μm ;

Bi_3Te_2 14 grains found, size 1 - 20 μm ;

Bi_7Te_3 6 grains found, size 1 - 15 μm .

The Se, S and Pd-bearing Bi - Te compounds also found are :

$\text{Bi}_3(\text{Te},\text{Se})_2$ 5 grains found, size 2 - 9 μm ;

$\text{Bi}_2(\text{Se},\text{Te})$ 2 grains found, size 7, 8 μm ;

$\text{Bi}_2\text{Te}(+\text{Pd})$ 2 grains found, size 6, 15 μm .

The most common paragenesis of Bi - Te compounds is at augite - augite grain boundaries. Bi - Te compounds are found in contact with the following silicates : diopside, chlorite, biotite, calcite, hornblende, plagioclase, K - feldspar, epidote, and sphene. The Bi - Te compounds are found in contact with the following sulfides : pyrrhotite, chalcopyrite, pentlandite, and minor galena, violarite, and magnetite.

Representative compositions of Bi - Te compounds are given in Table 7.3. Representative compositions are not given for tsumoite because of the unreliability of analyses of small grains (2 - 4 μm). All of the Bi - Te atomic % compositions obtained were plotted in the ternary Pd - Bi - Te diagram (Figure 6.8). An SEM / EDS spectrum of a Bi_3Te_2 grain from drill core 15B-3 is given in figure 7.2b (Table 7.3, analyses 5).

The most abundant Bi - Te compounds Bi_3Te_2 and Bi_2Te in the Kawene Intrusion are believed to be a solid solution of pilsenite, and hedleyite. Table 7.3 shows that the Bi - Te compounds cover the full range from 28.61 - 45.63 at% Te. Warren and Peacock (1945) were the first to suggest the close structural similarities between hedleyite and tsumoite, and to provide evidence for a range of solid solubility in the Bi - Te system between 30 - 60 at% Te. Brown and Lewis (1962) agreed that a wide range of solid solution

Table 7.3 : Representative compositions of Bi - Te compounds from Kawene Intrusion (atomic and weight %)

analysis	at%		wt%		size	probe section	formula
	Bi	Te	Bi	Te			
ideal	40.00	60.00	53.07	48.19			Bi ₂ Te ₃
	50.00	50.00	62.09	37.91			BiTe
	57.14	42.86	68.59	31.41			Bi ₄ Te ₃
	60.00	40.00	71.07	28.93			Bi ₃ Te ₂
	66.67	33.33	76.61	23.39			Bi ₂ Te
	70.00	30.00	79.26	20.74			Bi ₇ Te ₃
1	54.37	45.63	66.12	33.88	4 um	AK-86-9B	Bi ₄ Te ₃
2	55.08	44.92	66.76	33.24	3 um	28A	
3	56.85	43.15	68.33	31.67	7 um	13D-1	
4	57.53	42.47	68.92	31.08	6 um	13	
5	60.02	39.98	71.09	28.91	20 um	15B-3	Bi ₃ Te ₂
6	60.98	39.02	71.90	28.10	18 um	13C-1	
7	62.08	37.92	72.83	27.17	8 um	28A	
8	63.05	36.95	73.65	26.35	15 um	AK-86-9B	
9	63.97	36.03	74.41	25.59	13 um	13B-1	Bi ₂ Te
10	65.78	34.22	75.90	24.10	13 um	13B-1	
11	66.04	33.96	76.11	23.89	12 um	13B-1	
12	67.75	32.25	77.47	22.53	15 um	13B-1	
13	69.31	30.69	78.71	21.29	12 um	13B-1	Bi ₇ Te ₃
14	70.31	29.69	79.50	20.50	15 um	13B-1	
15	71.39	28.61	80.34	19.66	12 um	13B-1	

Table 7.4 : Representative compositions of Se- and Pd-bearing Bi - Te compounds from Kawene Intrusion (atomic and weight %)

analysis	at%				wt%				size	probe section
	Bi	Te	Se	Pd	Bi	Te	Se	Pd		
1	55.35	25.05	19.61		70.91	19.60	9.49		9 um	15-4
2	59.57	25.31	15.13		73.79	19.13	7.08		9 um	15-4
3	63.39	13.73	22.87		78.83	10.42	10.75		7 um	17A-2
4	66.94	15.75	17.31		80.55	7.88	11.57		8 um	15-5
5	51.10	36.60		12.31	64.10	28.03		7.87	15 um	AK-3A
6	61.88	34.87		3.25	72.96	25.10		1.94	6 um	AK-3A
7	62.37	35.57		2.06	73.26	25.51		1.23	6 um	AK-3A

1. Bi₄(Te,Se)₃
2. Bi₃(Te,Se)₂
- 3,4. Bi₂(Se,Te)
- 5,6,7. Bi₂Te(+Pd)

exists in the Bi - Te system with the lower limits of 31 - 32 at% Te. Dobbe (1993) also observed a solid solution between pilsenite and hedleyite (30 - 43 at% Te) which he called bismuthian tsumoite $\text{Bi}(\text{Te}_{0.75}\text{Bi}_{0.25})$ (Bayliss, 1991). Sztrokay and Nagy (1982) listed several similar structural and physical properties between the known Bi - Te phases : rhombohedral crystal structure, cleavage parallel to the basal plane, mechanical translation characteristics, low hardness, lamellar layered habit, and optical properties.

The representative compositions of Se and Pd-bearing Bi - Te compounds are given in Table 7.4. Note that the Bi - Te compounds can contain substantial amounts of Se (up to 11.57 wt%), in some instances the amount of Se is greater than the amount of Te. $\text{Bi}_2\text{Te}(\text{+Pd})$ may be a solid solution between Bi_2Te and PdBiTe (michenerite).

There is also a known solid solution between Bi_2S_3 - Bi_2Se_3 - Bi_2Te_3 phases in the $\text{Bi}_2(\text{S,Se,Te})_3$ system (Strokay and Nagy, 1982; Miller, 1981; Glatz, 1967). Bi_2Se_3 and tellurobismuthite (Bi_2Te_3) do not occur in the Kawene Intrusion, but bismuthinite (Bi_2S_3) does occur in association with the Bi - Te compounds. Bi_2Se_3 has dimorphic forms : guanajuatite (orthorhombic) and paraguajuatite (hexagonal) (Anthony et al., 1990). Bismuthinite and guanajuatite are orthorhombic with space groups Pbnm and Pnma respectively (Anthony et al., 1990). Paraguajuatite and tellurobismuthite are hexagonal, rhombohedral with a space group $\text{R}\bar{3}\text{m}$ which is identical to the crystal symmetry of wehrlite, pilsenite, and hedleyite

(Anthony et al., 1990). All of the end member minerals in the solid solution system $\text{Bi}_2(\text{S,Se,Te})_3$ have a hydrothermal origin (Anthony et al., 1990).

In the Kawene Intrusion, the $\text{Bi}_2(\text{S,Se})_3$ grain may be a result of the solid solution between bismuthinite and guanajuatite (Table 7.1, analyses 8,9). The $\text{Bi}_4(\text{Te,Se})_3$ and $\text{Bi}_3(\text{Te,Se})_2$ grains may be solid solutions between pilsenite and paraguanajuatite (Table 7.4, analyses 1,2). The $\text{Bi}_2(\text{Se,Te})$ grain may be a solid solution between paraguanajuatite, pilsenite, and hedleyite (Table 7.4, analyses 3,4).

Bi - Te compositions (weight %) from other localities are given in Table 7.5. These compositions show that Bi can range from 50.1 - 81.6 wt%. Although Bi_3Te_2 and Bi_2Te are unnamed, they have been previously recognized (Table 7.5, analyses 11 - 21).

Ag is found in Bi - Te compounds as they are commonly associated with hessite (Ag_2Te) (Mogessie et al., 1991; Oen and Kieft, 1984; Harris et al., 1983; Mposkos, 1983; Sztrokay and Nagy, 1982). Bi - Te compounds also contain minor amounts of Pb due to their close association with altaite (PbTe) and galena (McQueen, 1990; Garuti and Rinaldi, 1986; Mposkos, 1983; Shimazaki and Ozawa, 1978; Cabri and Laflamme, 1976). Bi - Te compounds are also associated with native Bi and bismuthinite (Bi_2S_3) (Mogessie et al., 1991; Sztrokay and Nagy, 1982; Gamyandin et al., 1982; Shimazaki and Ozawa, 1978; Lindahl, 1975). In the Kawene Intrusion, Bi - Te compounds, native Bi, bismuthinite, and galena, and rare hessite and altaite can be found in contact with or in close proximity to

Table 7.5 : Comparative Bi - Te compounds compositions (weight %)

analysis	Bi	Te	Se	S	Sb	As	Ag	Ni	Pd	Pb	Fe	Cu	total	formula
1	50.1	46.5	0.4										97.0	Bi ₂ Te ₃
2	51.08	47.27		0.11			0.13			0.45	1.93		100.97	
3	52.6	46.8	0.5				0.1						100.0	
4	59.18	36.64			0.22	0.98				1.84			98.86	BiTe
5	59.41	40.29		0.11			0.12	0.36	0.35				100.64	
6	61.1	37.6								1.0			99.7	
7	62.80	34.40			0.05					1.60			98.85	
8	63.9	37.2											101.1	
9	65.3	35.9											101.2	
10	66.0	34.0					0.3						100.3	Bi ₄ Te ₃
11	67.8	28.0					0.2			4.3			100.3	Bi ₃ Te ₂
12	68.20	28.10			0.17					1.30			97.77	
13	70.5	28.7											99.2	
14	71.19	24.93			0.82	1.16				1.53			99.63	
15	71.30	29.08											100.38	
16	72.8	26.2		0.3						0.3	0.1	0.3	100.0	
17	73.40	25.10			0.11					0.48			99.09	
18	74.6	23.8		0.2	0.3					0.5	0.3	0.1	99.8	Bi ₂ Te
19	75.1	23.1		0.1	0.8					0.6	0.1	0.2	100.0	
20	76.44	22.04											98.48	
21	76.8	22.6											99.4	
22	80.46	17.59											98.92	Bi ₇ Te ₃
23	80.60	18.52		0.12									99.24	
24	81.55	17.60		0.04									99.19	
25	81.6	17.5	0.3	0.1									99.5	

1. Tunaberg copper deposits, Central Sweden (Dobbe, 1991)
2. Dragset deposit, Norway (McQueen, 1990)
3. Glava, Sweden (Oen and Kieft, 1984)
4. Kolar gold deposit, India (Safonov et al., 1984)
5. Duluth Complex (Mogessie et al., 1991)
6. Tsumo mine, Japan (Shimazaki and Ozawa, 1978)
7. Froid mine, Sudbury (Cabri and Laflamme, 1976)
- 8, 9. Khakandya, Northeast USSR (Gamyandin et al., 1982)
10. Borzsony, Hungary (Sztrokay and Nagy, 1982)
11. Ivrea - Verbano, Western Italian Alps (Garuti and Rinaldi, 1986)
12. Levack West, Sudbury (Cabri and Laflamme, 1976)
13. Borzsony, Hungary (Sztrokay and Nagy, 1982)
14. Kolar gold deposit, India (Safonov et al., 1984)
15. Koronuda, Macedonia, Greece (Mposkos, 1983)
16. Tunaberg Pb-Zn deposit, Sweden (Dobbe, 1993)
17. Froid mine, Sudbury (Cabri and Laflamme, 1976)
- 18, 19. Tunaberg Pb-Zn deposit, Sweden (Dobbe, 1993)
- 20, 21. Ergelyakh deposit, Northeast USSR (Gamyandin et al., 1982)
22. Indre Gressdal deposit, Northern Norway (Lindahl, 1975)
- 23, 24. Good Hope Claim, Hedley, British Columbia (Warren and Peacock, 1945)
25. Millapaya, Bolivia (Anthony et al., 1990)

each other. These minerals also share the same paragenesis suggesting that they have a common hydrothermal origin.

The pilsenite and Bi_3Te_2 from the Kawene Intrusion resemble those from Borzsony, Koronuda, Tunaberg, and Froot mine (Table 7.5, analyses 10, 13, 15, 16, 17). The Bi_2Te from the Kawene Intrusion resembles the Bi_2Te from Tunaberg, Sweden and Ergelyakh deposit, Northeast, USSR (Table 7.5, analyses 18 - 21). Hedleyite from the Kawene Intrusion resembles the hedleyite from Indre Gressdal deposit, Northern Italy and from Hedley, British Columbia (Table 7.5, analyses 22, 23).

7.4. Bi - Te - Se - S Compounds

The most common Bi - Te - Se - S compound is $\text{Bi}_4(\text{Te,Se,S})_3$ with 26 grains found ranging in size from 2 - 15 μm in diameter. The other Bi - Te - Se - S compounds are :

$\text{Bi}_2(\text{S,Te,Se})_3$ 4 grains found, size 2 - 8 μm ;

$\text{Bi}(\text{S,Te,Se})$ 12 grains found, size 2 - 10 μm ;

$\text{Bi}_3(\text{Te,S,Se})_2$ 8 grains found, size 1 - 15 μm .

Some grains are intergrowths of the following pairs of phases :

$\text{Bi}_2(\text{S,Te,Se})_3$ and $\text{Bi}(\text{S,Te,Se})$;

$\text{Bi}(\text{S,Te,Se})$ and $\text{Bi}_4(\text{Te,Se,S})_3$;

$\text{Bi}_4(\text{Te,Se,S})_3$ and $\text{Bi}_3(\text{Te,S,Se})_2$.

The most common paragenesis of Bi - Te - Se - S compounds is at augite - augite boundaries. They are found in contact with the following silicates : diopside, and rare chlorite, biotite, sphene, and amphibole. They are found also in contact with chalcopyrite

and minor pyrrhotite. The majority of these compounds were found in surface samples AK-2 and AK-3A (clinopyroxene hornblendites). Only one $\text{Bi}_3(\text{S,Te,Se})_2$ grain was found in drill core 13D-1.

The largest Bi - Te - Se - S compound (a 20 μm grain) is an intergrowth of $\text{Bi}_4(\text{S,Te,Se})_3$ and $\text{Bi}_3(\text{Te,S,Se})_2$ at an augite - chalcopyrite boundary from sample AK-2 (Figure 7.3). The other grains in the cluster are also Bi - Te - Se - S compounds.

Representative compositions of the Bi - Te - Se - S compounds are given in Table 7.6. The compositions for each of the elements in these compounds can be quite variable. The Bi ranges from 41.08 - 61.41 at%, Te ranges from 13.06 - 22.35 at%, S ranges from 8.87 - 37.39 at%, and Se ranges from 4.32 - 17.56 at%.

An SEM / EDS spectrum of $\text{Bi}_4(\text{S,Te,Se})_3$ from the 20 μm grain from AK-2 is given in figure 7.4.

The Bi-poor compounds $\text{Bi}_2(\text{S,Te,Se})_3$ and $\text{Bi}(\text{S,Te,Se})$ are S-rich. The representative compositions in Table 7.6 show that S ranges from 34.18 - 37.39 at% for the $\text{Bi}_2(\text{S,Te,Se})_3$ and $\text{Bi}(\text{S,Te,Se})$, and S ranges from 6.80 - 16.53 at% for $\text{Bi}_4(\text{Te,Se,S})_3$ and $\text{Bi}_3(\text{Te,S,Se})_2$. The S vs. Bi plot shows two clusters : the S-rich and Bi-poor cluster, and the Bi-rich and S-poor cluster (Figure 7.5). The S - Te - Se ternary diagram shows a distinct S-rich cluster separate from the more Te-rich cluster (Figure 7.6). The Se vs. Bi plot also shows two clusters : Se-poor and Bi-poor cluster, and moderate Se and Bi-rich cluster (Figure 7.7).

Some of these Bi - Te - Se - S compounds are believed to be a result of solid solution in the $\text{Bi}_2(\text{Te,Se,S})_3$ system (section 7.5).



Figure 7.3 : A SEM / BSE image of a 20 μm $\text{Bi}_4(\text{S,Te,Se})_3$ - $\text{Bi}_3(\text{S,Te,Se})_2$ intergrowth found at a chalcopyrite (cp) - augite grain boundary from sample AK-2. The other bright white grains are also Bi - Te - Se - S compounds.

Table 7.6 : Representative compositions of Bi - Te - Se - S compounds from Kawene Intrusion (atomic and weight %)

analysis	at%				wt%				size	probe section
	Bi	Te	Se	S	Bi	Te	Se	S		
1	41.08	14.12	7.41	37.39	70.54	14.80	4.81	9.85	6 um	AK-2
2	42.76	18.08	4.32	34.84	70.34	18.17	2.69	8.80	4 um	AK-3A
3	44.30	15.92	6.26	33.52	72.01	15.79	3.84	8.36	8 um	AK-2
4	45.31	14.59	6.70	33.40	73.22	14.40	4.09	8.29	6 um	AK-2
5	46.04	13.23	6.25	34.49	74.53	13.08	3.82	8.57	8 um	AK-2
6	46.90	13.53	5.39	34.18	75.11	13.23	3.26	8.40	8 um	AK-2
7	50.76	20.22	15.79	13.24	71.39	17.36	8.39	2.85	4 um	AK-3A
8	53.65	19.12	16.86	10.37	73.19	15.94	8.69	2.18	7 um	AK-2
9	54.34	21.30	17.56	6.80	72.44	17.33	8.84	1.38	7 um	AK-2
10	56.77	14.79	11.90	16.53	77.94	12.40	6.18	3.48	20 um	AK-2
11	57.13	13.06	12.98	16.83	78.70	10.99	6.76	3.55	20 um	AK-2
12	58.23	22.35	8.53	10.89	75.86	17.77	4.20	2.17	8 um	AK-3A
13	59.40	13.57	12.70	14.33	79.53	11.10	6.42	2.95	20 um	AK-2
14	61.42	15.86	13.85	8.87	79.05	12.47	6.73	1.75	9 um	AK-2

1,2. Bi₂(S,Te,Se)₃

3-6. Bi(S,Te,Se)

7. Bi(Te,Se,S)

8,9. Bi₄(Te,Se,S)₃

10,11. Bi₄(S,Te,Se)₃

12. Bi₄(Te,S,Se)₃

13. Bi₃(S,Te,Se)₂

14. Bi₃(Te,Se,S)₂

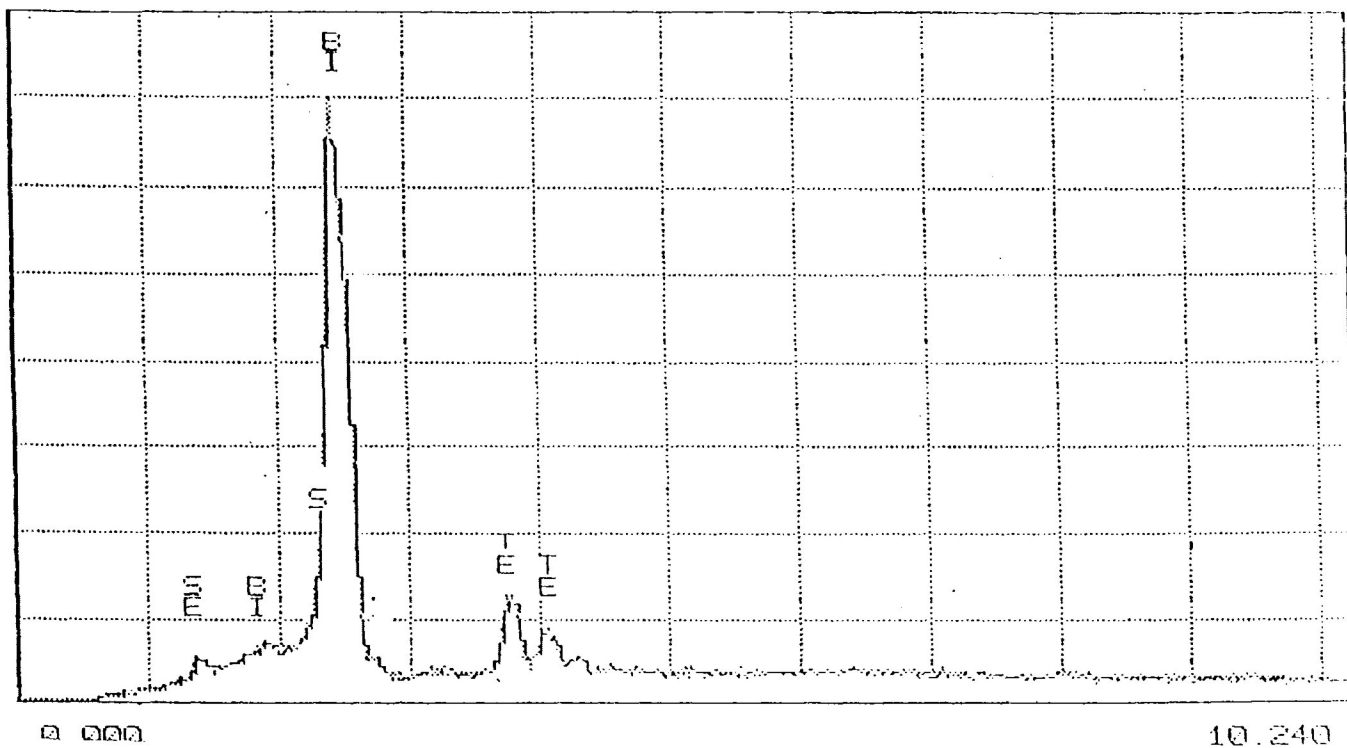


Figure 74 : SEM / EDS spectrum of $\text{Bi}_4(\text{S},\text{Te},\text{Se})_3$ from sample AK-2.

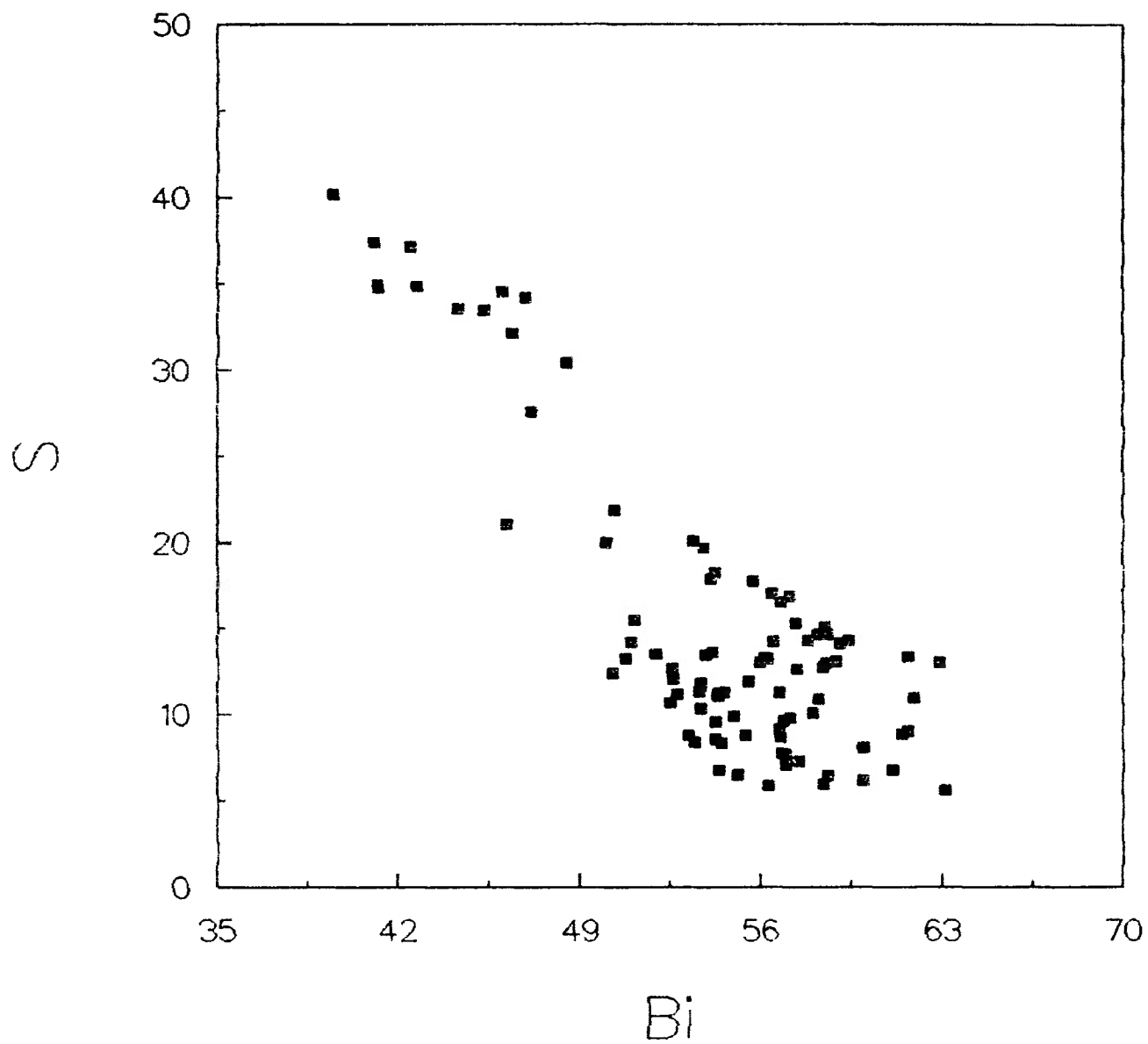


Figure 7.5 : S vs. Bi (atomicz)

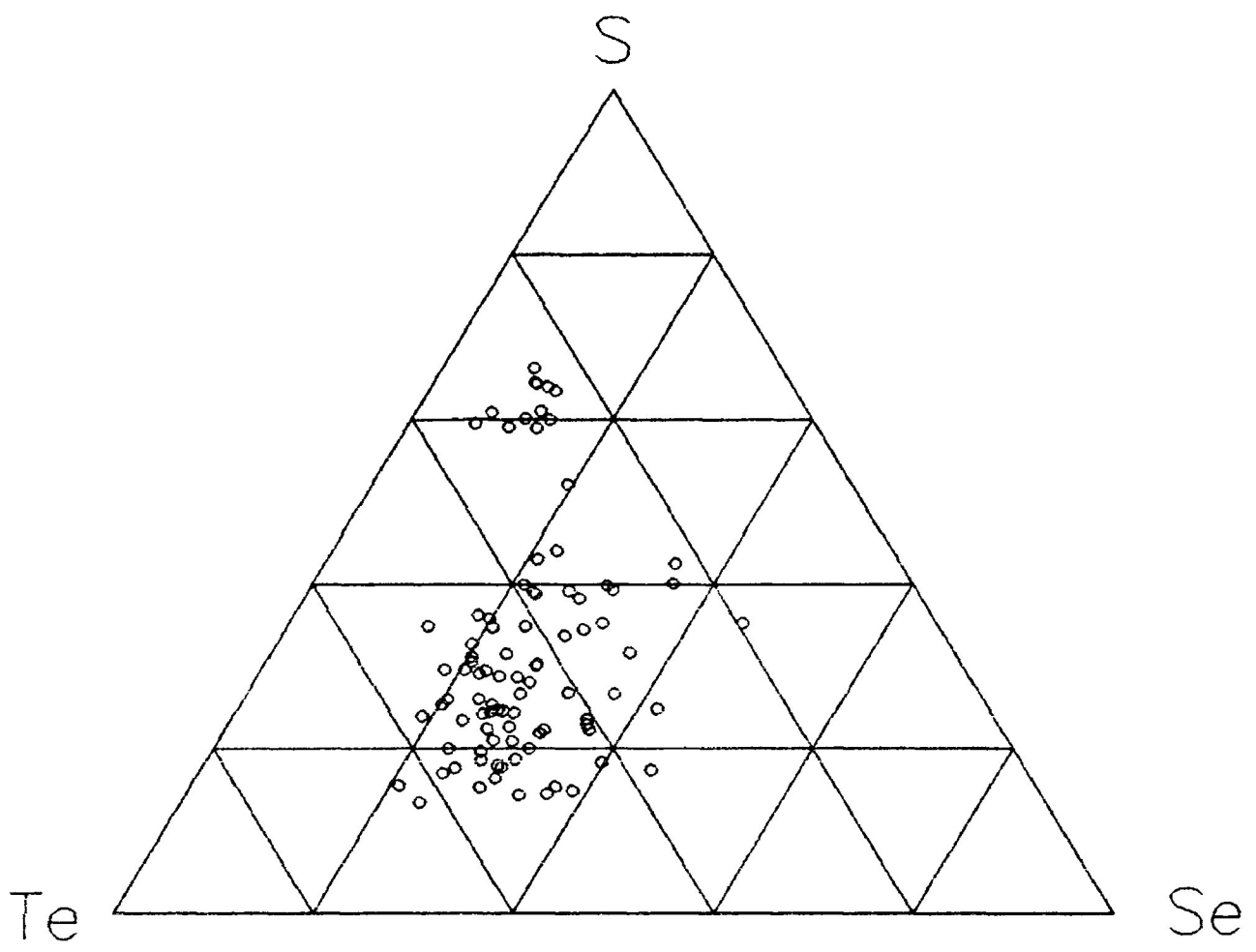


Figure 7.6 : S - Te - Se ternary diagram (atomic%)

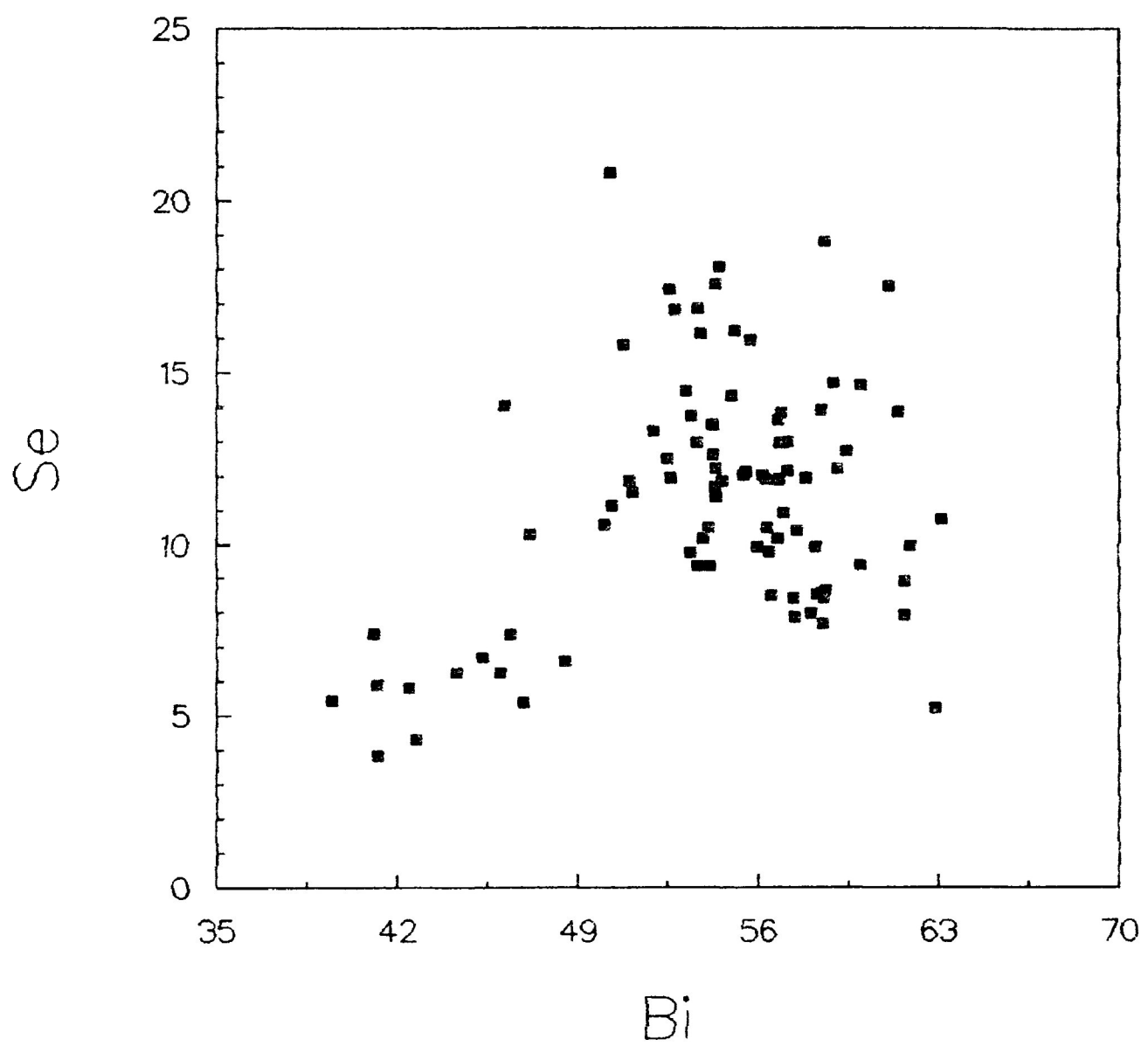


Figure 7.7 : Se vs. Bi (atomic%)

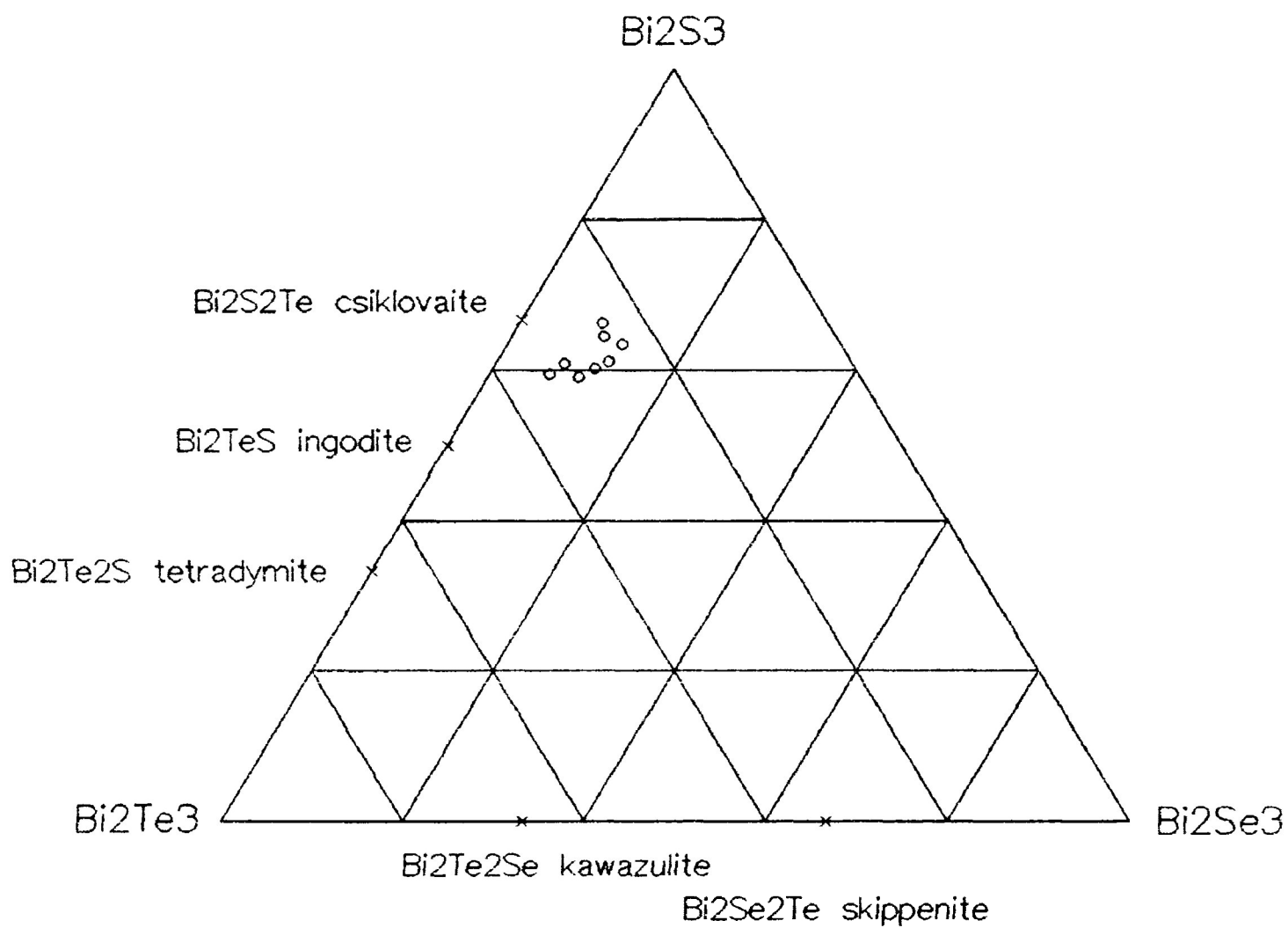


Figure 7.8 : Analyses of Bi₂(S,Te,Se)₃ minerals (atomic %)

Miller (1981) used a $\text{Bi}_2\text{S}_3 - \text{Bi}_2\text{Te}_3 - \text{Bi}_2\text{Se}_3$ ternary diagram to try to classify his unknown minerals within this system. The $\text{Bi}_2(\text{S,Te,Se})_3$ minerals from the Kawene Intrusion were plotted in the same diagram (Figure 7.8). S, Te, and Se were calculated for a total of 3 atoms. The minerals cluster near csiklovaite ($\text{Bi}_2\text{S}_2\text{Te}$) which reflects the S-rich nature of the Bi-poor minerals. The composition of the csiklovaite from Ciclova, Romania is Bi 67.76, Te 20.41, S 9.97, and Se 1.37 wt% for a total of 99.51 wt% (Anthony et al., 1990). This composition resembles the composition for $\text{Bi}_2(\text{S,Te,Se})_3$ found in table 7.6, analysis 2. Csiklovaite was discredited as a mineral by Bayliss (1991) who determined that it is a mixture of 60 wt% tetradyomite (Bi_2STe_2) and 40 wt% bismuthinite (Bi_2S_3).

Chapter 8

Miscellaneous Platinum Group Minerals

8.1. Sperrylite

Sperrylite (PtAs_2) was first described from the Vermilion deposit, Sudbury by Wells (1889) (Table 8.2, analysis 12). Sperrylite was named for Francis L. Sperry (? - 1906), a chemist in Sudbury, who first found the mineral (Anthony et al., 1990). It was later reported by Hawley (1962) and Michener (1940) to be embedded in coarse grained massive chalcopyrite within the Sudbury Complex. Isometric sperrylite commonly exhibits euhedral cubic or octahedral habits (Anthony et al., 1990).

Sperrylite is the only Pt mineral found in the Kawene Intrusion. Sperrylite in the Kawene Intrusion may contain minor amounts of Ir and Rh which substitute for Pt, and minor S which substitutes for As. The sperrylite grains are usually euhedral. A total of 50 sperrylite grains were found of which :

PtAs_2	31 grains found, size 1 - 18 μm ;
$(\text{Pt}, \text{Ir})(\text{As}, \text{S})_2$	7 grains found, size 2 - 7 μm ;
$\text{Pt}(\text{As}, \text{S})_2$	7 grains found, size 1 - 6 μm ;
$(\text{Pt}, \text{Ir})\text{As}_2$	5 grains found, size 2- 5 μm ;
$(\text{Pt}, \text{Ir}, \text{Rh})(\text{As}, \text{S})_2$	2 grains found, size 2, 7 μm .

One euhedral, anomalously large (150 μm long x 30 μm wide) sperrylite $(\text{Pt}, \text{Ir})(\text{As}, \text{S})_2$ grain was found in drill core 16B-1 (Figure 8.1). This is the largest PGM found in the Kawene Intrusion. This sperrylite grain is found enclosed within a monoclinic pyrrhotite veinlet. The monoclinic pyrrhotite veinlet

a)

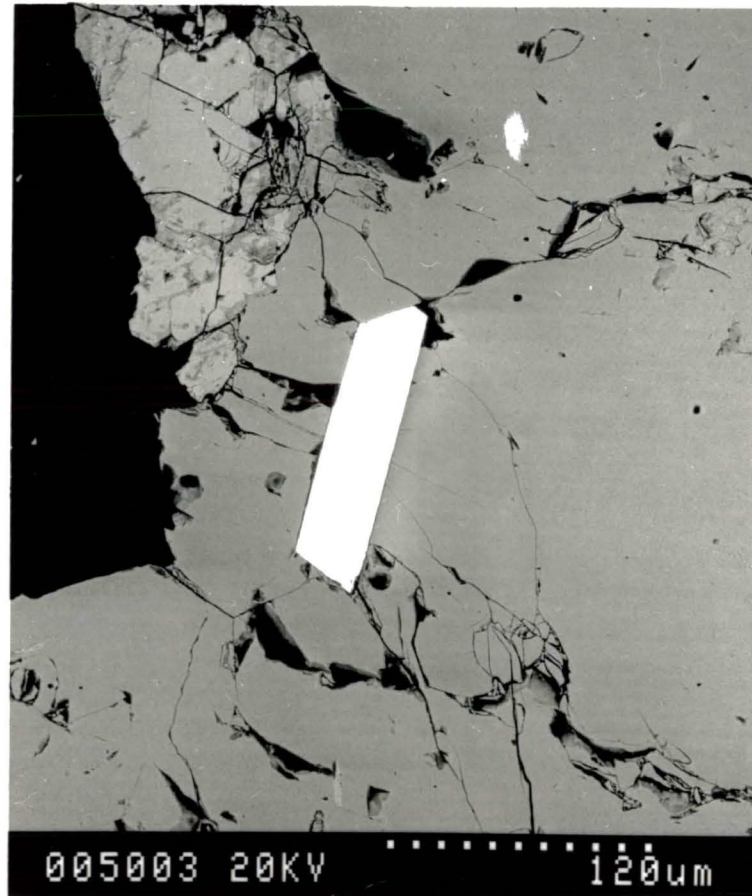


Figure 8.1 : A SEM / BSE image of an euhedral, 150 μm sperrylite grain enclosed in monoclinic pyrrhotite from drill core 16B-1. a) SEM / BSE picture b) reflective light picture. Dark brown - hexagonal pyrrhotite, cream - pentlandite altering to violarite. The silicate (left) is K-feldspar.



0 100 um

b)

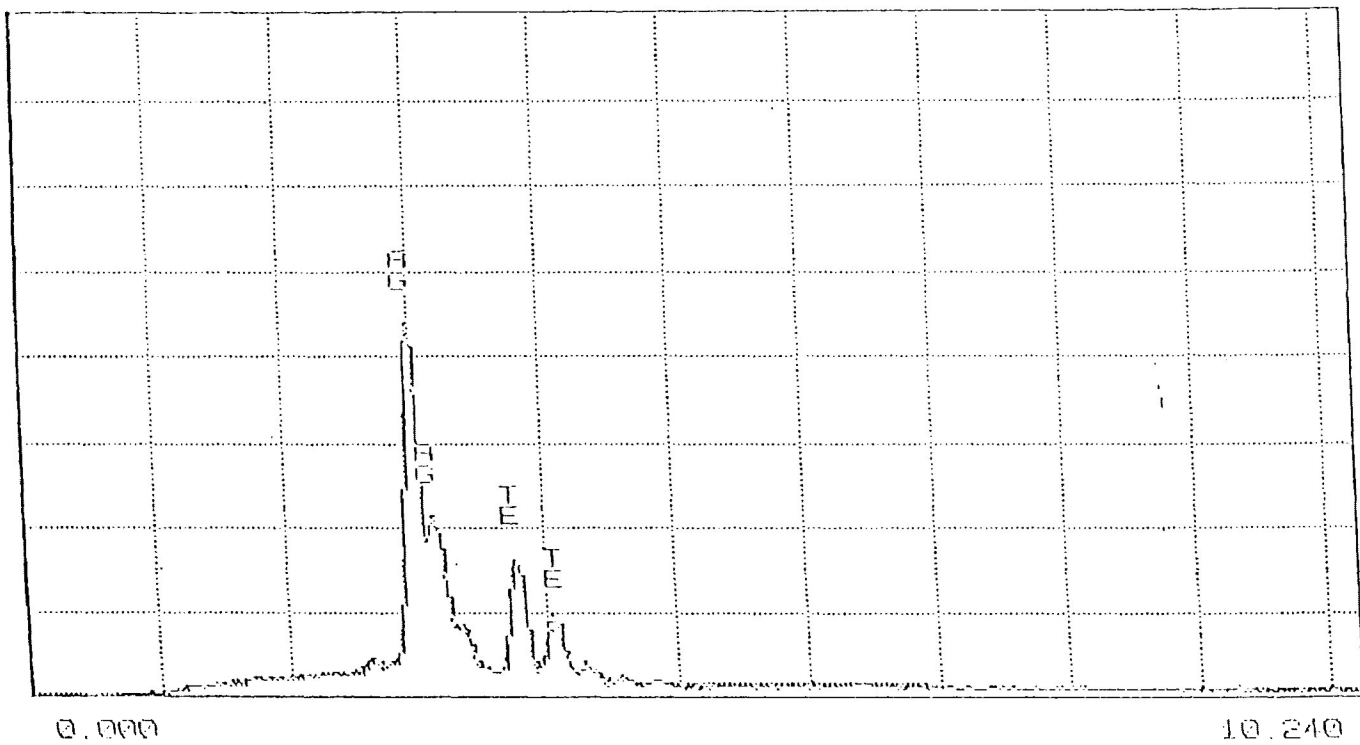
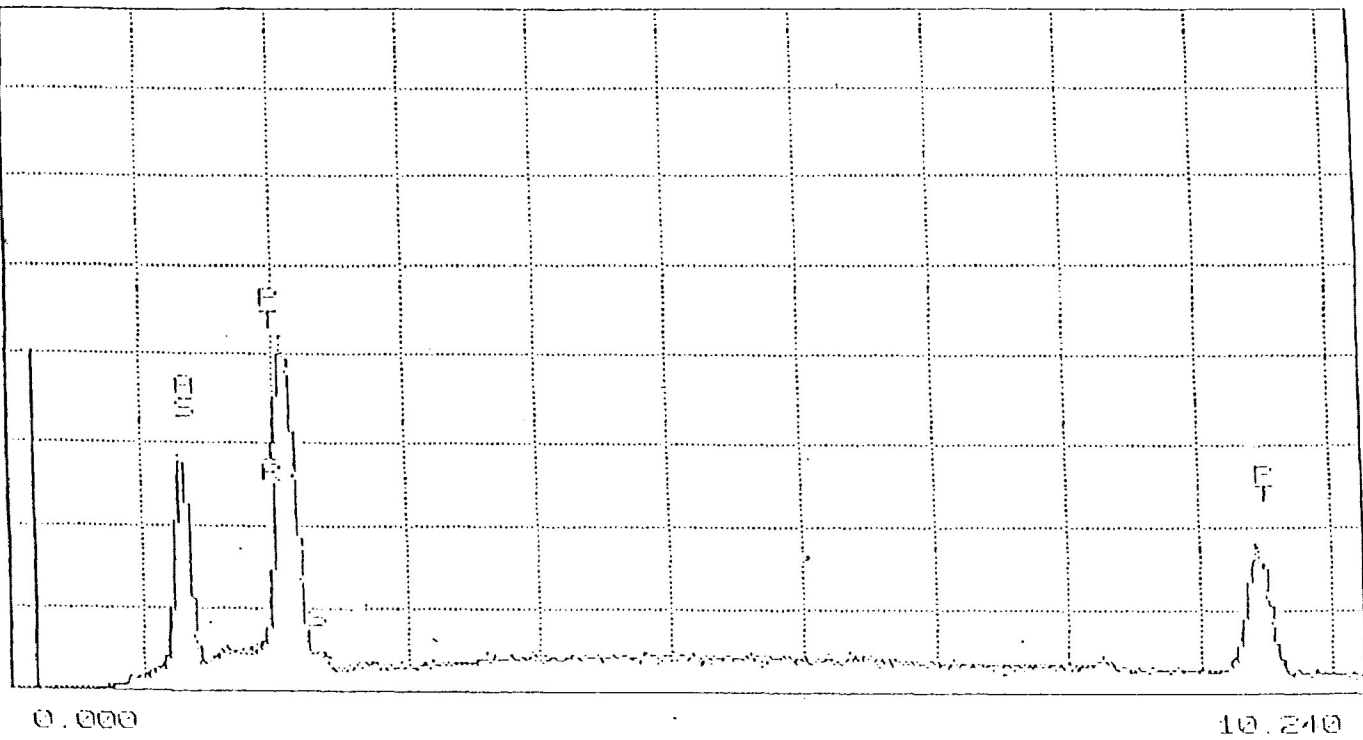


Figure 2 : SEM / EDS spectra of a) $(Pt, Ir)(As, S)_2$ grain from drill core I6B-I b) Ag_2Te grain from sample AK-9-86B.

Table 8.1 : Representative compositions of sperrylite from Kawene Intrusion (atomic and weight %)

analysis	at%					wt%					size	probe section	
	Pt	As	Ir	Rh	S	Pt	As	Ir	Rh	S			
ideal	33.33	66.66				56.56	43.44						
1	29.42	63.68	3.23		3.67	51.03	42.41	2.51		1.05		150 um	16B-1
2	29.56	66.67	1.54		2.23	51.83	44.88	2.64		0.65		150 um	16B-1
3	29.90	70.10				52.62	47.38					18 um	13D-1
4	30.14	68.22	1.64			55.05	42.00	2.95				5 um	13B-1
5	31.20	63.98	1.99	0.80	2.02	53.35	42.00	3.36	0.72	0.57		7 um	13B-1
6	30.96	61.97		0.91	6.16	55.04	42.31		0.85	1.80		7 um	13B-1
7	34.87	60.76			4.38	59.17	39.60			1.22		6 um	13B-1

Table 8.2 : Comparative sperrylite compositions (weight %)

analysis	Pt	As	Ir	Rh	Pd	Ru	Os	Cu	Fe	Ni	Sb	S	Te	total
1	53.40	41.00	0.63	1.80		0.26					2.10	0.91		100.10
2	54.40	42.20	1.80					0.08	0.14	1.10	0.16			99.88
3	54.4	45.6									0.1			100.1
4	55.04	42.95	1.42	0.30	0.06	0.03	0.03	0.04	0.28	0.05		0.07		100.27
5	55.1	37.6	1.8								1.4	0.2		100.4
6	55.5	45.5						0.9						101.9
7	55.80	41.80		0.18							0.30		1.20	99.28
8	56.3	43.1												99.4
9	56.5	42.3									1.4	0.2		100.4
10	56.62	43.28						0.13	0.28	0.01				100.10
11	56.7	42.7												99.4
12	56.80	42.80									0.08			99.68
13	56.9	43.3									0.12			100.32
14	57.00	43.20									0.09			100.29
15	57.1	42.8		1.2	0.1			0.1			0.1			101.4
16	57.11	42.29									0.57			99.97
17	57.5	42.8												100.3

1. Onverwacht, Transvaal, South Africa, (Cabri et al., 1977)
2. Pipe mine, Manitoba, (Laflamme, 1979) unpublished internal report
3. Hitura, Finland, (Hakli et al., 1976)
4. Duluth Complex, (Mogessie et al., 1991)
5. Driekop mine, South Africa, (Tarkian and Stumpfl, 1975)
6. Koillismaa Complex, Northern Finland, (Piispanen and Tarkian, 1984)
7. New Rambler mine, Wyoming (Loucks and McCallum, 1980)
8. Crean Hill, Sudbury Complex, (Cabri and Laflamme, 1976)
9. Pondoland, Northern Transkei, southern Africa, (Tischler et al., 1981)
10. Allarechka District, Kola region, USSR, (Yakovlev et al., 1991)
11. Rathbun Lake, Northeast Ontario, (Rowell and Edgar, 1986)
12. Vermilion mine, Sudbury Complex, (Cabri and Laflamme, 1976)
13. Froid mine, Sudbury Complex, (Cabri and Laflamme, 1976)
14. Creighton, Sudbury Complex, (Cabri and Laflamme, 1976)
15. Merensky Reef, Transvaal, South Africa, (Brynard et al., 1976)
16. Strathcona, Sudbury, (Li and Naldrett, 1993)
17. Stillwater, (Volborth et al., 1986)

intrudes K-feldspar, and contains minor amounts of pentlandite altering to violarite. This sperrylite grain is found in the same sample as the anomalously large michenerite grain described previously (section 6.3). An SEM / EDS spectrum of the 150 μm sperrylite is shown in Figure 8.2a. Representative compositions for this grain are given in Table 8.1, analyses 1 and 2.

The most common parageneses of sperrylite grains are : enclosed within augite and pyrrhotite; and at chalcopyrite - augite and pyrrhotite - chlorite grain boundaries. The sperrylites are found also in contact with : violarite, pentlandite, diopside, epidote, minor K-feldspar and apatite.

Representative compositions of sperrylite grains are found in Table 8.1. The analyses range in Pt from 51.02 - 59.17 wt%, and in As from 39.60 - 47.38 wt%. Deviation from ideal composition is probably due to the minor amounts of Ir, Rh, and S in the sperrylite crystals.

Compositions of sperrylite from other localities are listed in Table 8.2. These have a narrower range of Pt (53.40 - 57.5 wt%), and contain minor amounts of Pd, Ru, Os, Cu, Fe, Ni, Sb, and Te; elements which are not found in quantities detected by SEM / EDS in the sperrylites of the Kawene Intrusion. Many sperrylite grains contain Sb as a result of their solid solution with geversite (PtSb_2). The composition of the sperrylites of the Kawene Intrusion resemble the composition of the sperrylites from Hitura, Koillismaa Complex, Crean Hill, Frood mine, and Stillwater.

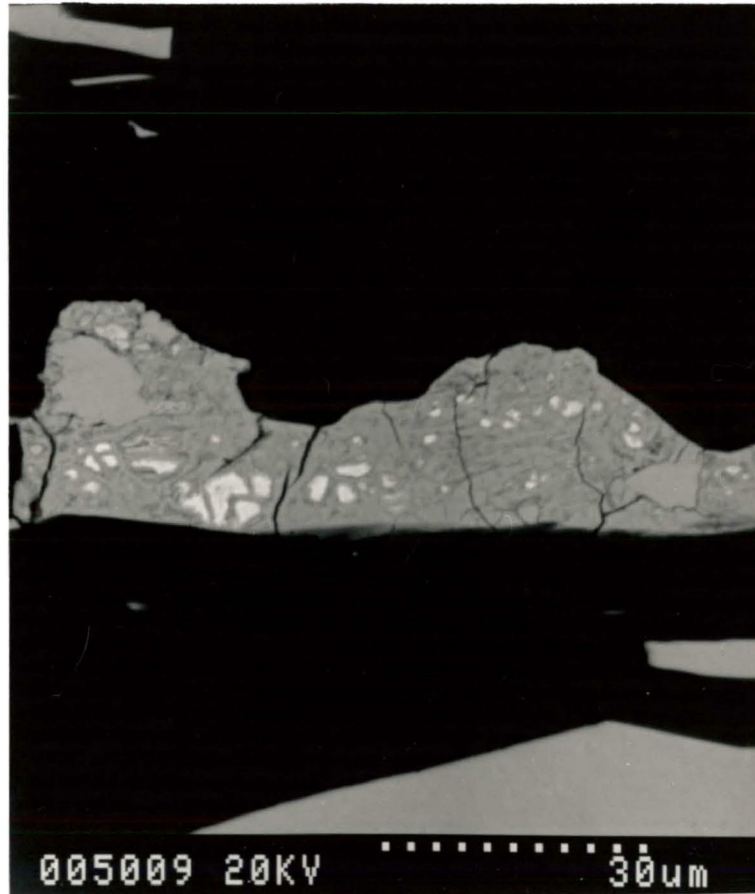


Figure 8.3 : A SEM / BSE image of numerous (Ag,Ni)S grains enclosed in violarite from sample AK-9-86B. Violarite also contains three chalcopyrite inclusions (far left and far right).

Table 8.3 : Representative compositions of (Ag,Ni)S from Kawene Intrusion (atomic and weight%)

analysis	at%			wt%			size
	Ag	Ni	S	Ag	Ni	S	
1	28.55	17.90	53.55	50.42	17.21	32.37	2 um
2	33.28	12.01	54.71	59.56	11.68	28.76	4 um
3	39.58	11.23	49.19	65.72	10.15	24.13	2 um
4	40.08	14.65	45.27	62.46	12.43	25.11	2 um

Table 8.4 : Representative compositions of Ag - Te compounds from Kawene Intrusion (atomic and weight %)

analysis	at%		wt%		size	probe section	formula
	Ag	Te	Ag	Te			
ideal	60.00	40.00	55.91	44.09			Ag ₃ Te ₂
	62.50	37.50	58.49	41.51			Ag _{5-x} Te ₃
	66.67	33.33	62.86	37.14			Ag ₂ Te
1	59.90	40.10	55.81	44.19	15 um	AK-9-86B	Ag ₃ Te ₂
2	60.89	39.11	56.83	43.17	15 um	AK-9-86B	
3	65.65	34.35	61.77	38.23	10 um	AK-9-86B	Ag ₂ Te
4	66.36	33.64	62.51	37.49	10 um	AK-9-86B	

8.2. (Ag,Ni)S

The (Ag,Ni)S (unnamed) grains are found in one violarite (Fe,Ni)₃S₄ grain in the sample AK-86-9B (hornblende clinopyroxenite) (Figure 8.3). There are 34 (Ag,Ni)S subhedral grains which range in size from 2 - 4 μm found in the cluster. The violarite has a mottled, fractured appearance and contains inclusions of chalcopyrite. Ag-rich pentlandite probably altered to form violarite and (Ag,Ni)S, while the chalcopyrite remained unaltered.

Representative compositions of the (Ag,Ni)S are given in Table 8.3. These analyses should be considered qualitative rather than quantitative because of the small size of the grains, and the violarite matrix.

8.3. Ag - Te Compounds

Hessite (α -Ag₂Te) is monoclinic below 155°C, and (β -Ag₂Te) is pseudocubic above 155°C (Anthony et al., 1990; Chizhikov and Shchastlivyi, 1970). It is commonly found in moderate and low temperature hydrothermal veins (Anthony et al., 1990). Hessite was first described by G. Rose in 1830 in samples from the Zavodinskii mine, USSR (Table 8.5, analysis 18) (Stumpfl and Rucklidge, 1968). Hessite was named after Germain Henri Hess (1802 - 1850), a Swiss - Russian chemist (Anthony et al., 1990).

Stutzite (Ag_{5-x}Te₃, where x = 0.24 - 0.36) is hexagonal (Anthony et al., 1990; Stumpfl and Rucklidge, 1968). Originally Ag_{5-x}Te₃ was called empressite until empressite was redefined as AgTe, and stutzite was redefined as Ag_{5-x}Te₃ (Stumpfl and Rucklidge, 1968;

Fleischer, 1966; Honea, 1964). It occurs as replacement masses in hydrothermal deposits associated with other tellurides and sulfides (Anthony et al., 1990). Stutzite was named after Andreas Stutz (1747 - 1806), a mineralogist from Vienna, Austria.

Ag_3Te_2 (unnamed) is formed by a peritectic reaction in the Ag - Te system (Chizhikov and Shchastlivyi, 1970).

The Ag - Te compounds in the Kawene Intrusion are dominated by Ag_2Te (hessite) with 11 grains found ranging in size from 2 - 10 μm . Ag_3Te_2 (unnamed) with 3 grains found with size 2, 3, and 15 μm . These grains were only found in 4 polished thin sections in the Kawene Intrusion : 13D-1, 13D-2, 13E-2, and AK-9-86B. All of these polished thin sections are hornblende clinopyroxenites except for 13E-2 which is a biotite hornblendite intruded by a tonalite veinlet.

The most common parageneses for the Ag - Te compounds are grains enclosed in augite, and in contact with chlorite and diopside. They are also in contact with the following sulfides : pentlandite, Ag-bearing pentlandite, violarite, and chalcopyrite. These compounds are commonly intergrown with PbTe (altaite), and Pt - Sb compounds, and rarely with Bi_2Te , Se-bearing galena, and michenerite.

Representative compositions of Ag_2Te and Ag_3Te_2 are given in Table 8.4. The Ag -Te compositions from the Kawene Intrusion are close to the ideal compositions for Ag_2Te and Ag_3Te_2 . Note that the Ag_3Te_2 composition from the Kawene Intrusion (Table 8.4, analysis 2) is similar to the composition for $\text{Ag}_{5-x}\text{Te}_3$ (Table 8.5, analysis 4,5).

Table 8.5 : Comparative Ag - Te compounds (weight %)

analysis	Ag	Te	Pd	Pt	Cu	Ni	Hg	Pb	Au	S	Bi	Sb	total	formula
1	55.61	43.53											99.14	Ag ₃ Te ₂
2	57.28	42.79											100.07	
3	56.7	42.9											99.6	Ag _{5-x} Te ₃
4	56.78	41.27			1.27		0.60						99.92	
5	56.8	39.7	0.75	0.38					1.54				99.2	
6	57.1	42.6											99.7	
7	57.6	41.2											98.8	
8	58.10	40.00	0.07		0.20		0.24			0.07		0.13	98.81	Ag ₂ Te
9	59.2	38.9									0.2		98.3	
10	59.40	39.89			0.93				0.12				100.34	
11	59.5	38.4											97.9	
12	60.23	38.36											98.59	
13	61.16	36.11						1.90					99.17	
14	61.52	37.77							1.01				100.30	
15	61.66	37.76											99.42	
16	61.66	38.26	0.03			0.06				0.02	0.58		100.61	
17	62.37	38.08											100.45	
18	62.42	36.96											99.38	
19	62.6	37.5											100.1	
20	62.90	36.80						0.18					99.88	
21	63.23	36.61											99.84	

1,2. Geordie Lake Intrusion, Coldwell Complex (Mulja and Mitchell, 1990)

3. Lindquist Lake, British Columbia (Stumpfl and Rucklidge, 1968)

4. Ashanti mine, Ghana (Bowell et al., 1990)

5. Thierry mine, Northwestern Ontario (Patterson and Watkinson, 1984)

6. Red Cloud mine, Colorado (Anthony et al., 1990)

7. Glava, Varmland, Sweden (Oen and Kieft, 1984)

8. Salt Chuck Intrusion, Alaska (Watkinson and Melling, 1992)

9. Borzsony, Hungary (Sztrokay and Nagy, 1982)

10. Ashanti mine, Ghana (Bowell et al., 1990)

11. Koillismaa Layered Igneous Complex, Finland (Piispanen and Tarkian, 1984)

12. Kolar gold deposit, India (Safonov et al., 1984)

13. San Sebastian, Mexico (Anthony et al., 1990)

14. Botes, Romania (Anthony et al., 1990)

15. Strathcona deposit, Sudbury (Li and Naldrett, 1993)

16. Duluth Complex (Mogessie et al., 1991)

17. Geordie Lake Intrusion, Coldwell Complex (Mulja and Mitchell, 1990)

18. Savodinskii mine, USSR (Anthony et al., 1990)

19. Glava, Varmland, Sweden (Oen and Kieft, 1984)

20. Ivrea - Verbano Basic Complex, Western Italian Alps (Garuti and Rinaldi, 1986)

21. Koronuda, Macedonia, Greece (Mposkos, 1983)

Ag_3Te_2 may actually be a slight variation in the $\text{Ag}_{5-x}\text{Te}_3$ composition. An SEM / EDS spectrum of hessite from drill core AK-9-86B (Table 8.4, analysis 4) is given in figure 8.2b.

Ag - Te compositions from other localities are given in table 8.5. Ag_3Te_2 from the Kawene Intrusion resembles those from Geordie Lake, Lindquist Lake, Red Cloud mine, and Glava (Table 8.5, analyses 1 - 3, 6, 7). Hessite from the Kawene Intrusion closely resemble those from Sudbury, Geordie Lake Intrusion, Duluth Complex, Savodinskii mine, Glava, and Ivrea - Verbano Basic Complex (Table 8.5, analyses 15 - 20).

8.4. Hollingworthite - Cobaltite

Hollingworthite (RhAsS) is cubic with a space group of $\text{Pa}\bar{3}$ (Anthony et al., 1990). Hollingworthite was first identified by Stumpfl and Clark (1965) from Pt concentrates from the Driekop mine, South Africa (Table 8.7, analysis 7). Complete solid solution exists between RhAsS , PtAsS (platarsite), and IrAsS (irarsite) (Ohnenstetter et al., 1991; Tarkian and Prichard, 1987; Tarkian, 1987; Stumpfl, 1972). Tarkian (1987) studied compositional data for these sulfarsenides from various locations around the world, and concluded that there are two varieties of hollingworthite : one with $\text{Ru} > \text{Ir}$ (at%) which falls in the $\text{RhAsS} - \text{RuAsS}$ (ruarsite) - PtAsS ternary system, and another with $\text{Ir} > \text{Ru}$ which falls in the $\text{RhAsS} - \text{IrAsS} - \text{PtAsS}$ ternary system. Stumpfl (1972) suggested that hydrothermal fluids generated by late - magmatic or metamorphic processes are agents of PGE-sulfarsenide

mineralization. Hollingworthite was named after Professor Sidney Ewart Hollingworth (1899 - 1966), an eminent British geologist (Anthony et al., 1990; Stumpfl and Clark, 1965).

Cobaltite (CoAsS) is interpreted as a sextuplet of orthorhombic (Pca₂) interpenetrating twin-related domains about a $\bar{3}$ twin axis [111] (Bayliss, 1989, 1982). Twinning occurs extensively in all cobaltites (Bayliss, 1969). As and S are ordered at the atomic level, and the interatomic distances are approximately equal in length ($a \approx b \approx c$) (Bayliss, 1989, 1982). Cobaltite has a pseudocubic or pseudopyrithedron crystal form (Anthony et al., 1990; Klein and Hurlbut, 1977). When orthorhombic (Pca₂) cobaltite is heated at 850°C, As and S disorders to create a cubic (Pa3) structure (Bayliss, 1989, 1982, 1969). Evidence for the orthorhombic nature of cobaltite is seen in X-ray precession photographs which show the presence of (010) and (110) reflections which are forbidden by the cubic space group Pa3 (Bayliss, 1989, 1982, 1969). There is a solid solution within the CoAsS - NiAsS - FeAsS system which is seen in the metal compositional variation ((Mogessie et al., 1991; Yakovlev et al., 1991; Piispanen and Trakian, 1984; Mposkos, 1983; Bayliss, 1982; Cabri and Laflamme, 1976). Cobaltite occurs in high temperature hydrothermal deposits as disseminations, and as veins in contact metamorphosed rocks (Anthony et al., 1990; Klein and Hurlbut, 1977). Cobaltite is also found in massive Fe-Ni-Cu-S ores from Sudbury area deposits (Cabri and Laflamme, 1976). The name cobaltite is derived from its chemical composition (Anthony et al., 1990).

Hollingworthite is the only Rh mineral found in the Kawene Intrusion. Nine grains of hollingworthite was found ranging in size from 1 - 6 μm . Two grains of hollingworthite - cobaltite solid solution [(Rh,Co)AsS] were found with grain size 1.5 and 4 μm . Two grains of cobaltite (CoAsS) was found with grain size 3 and 9 μm . The most common element which substitutes for Rh is Co. The other substituting elements are Pd, Pt, Ni, Ir, and rarely Pb.

The most common paragenesis of these sulfarsenides is as euhedral grains enclosed within pyrrhotite. They are in subhedral - to - euhedral contact with : augite, diopside, chlorite, and magnetite. They are also in euhedral contact with : pentlandite, violarite, and chalcopyrite. They may also be intergrown with sperrylite. These sulfarsenides are only found within hornblendites.

Representative compositions of sulfarsenides are given in table 8.6. The hollingworthite compositions 1, 4 and 7 are As-rich and S-poor, which may be due to As substituting for S. Ohnenstetter et al. (1991) believed that As - S substitution covers a range from $\text{MeAs}_{0.40}\text{S}_{1.60}$ to $\text{MeAs}_{1.36}\text{S}_{0.64}$ where Me is metal e.g. Rh, Pt, Ir. Mposkos (1983) found a much narrower range for the As - S substitution in cobaltite ($\text{MeAs}_{0.86-1.01}\text{S}_{0.91-1.11}$). The cobaltite composition 8 is As-rich and Co-poor.

The compositions in atomic % of the hollingworthites were plotted in the Rh - Pt - Ir and Rh - Pt - Co ternary diagrams (Figure 8.4, 5). In the Rh - Pt - Ir ternary diagram, most of the hollingworthites do not contain Ir, and have less than 10 at% Pt

Table 8.6 : Representative compositions of Rh - Co sulfarsenides from Kawene Intrusion (atomic and weight %)

analysis	at%							wt%							size
	Rh	Co	Pd	Pt	Ni	As	S	Rh	Co	Pd	Pt	Ni	As	S	
ideal	33.33					33.33	33.33	49.00					35.70	15.30	RhAsS
		33.33				33.33	33.33		35.53				45.15	19.32	CoAsS
1	29.39	3.50	1.87			38.50	26.74	42.51	2.90	2.78			40.54	11.27	6 um
2	26.99	6.17		0.41	0.73	33.00	32.71	40.95	5.36		1.15	0.63	36.44	15.46	6 um
3	26.59	5.36		0.66	0.64	33.85	32.91	40.18	4.64		1.89	0.56	37.24	15.50	6 um
4	16.76	7.82	2.17	4.65		37.31	31.29	24.30	6.49	3.26	12.77		39.39	13.79	9 um
5	16.73	10.05	2.35	1.01		35.91	32.50	26.54	9.12	3.86	3.05		41.47	15.49	9 um
6	14.36	12.91	1.95	1.77		31.92	37.09	23.19	11.93	3.26	5.44		40.54	18.65	6 um
7	10.67	17.23	1.05			38.08	32.31	17.85	16.51	1.82			46.37	16.84	9 um
8		23.69			2.79	39.53	33.99		24.88			2.91	52.78	19.42	3 um

1. 17B-1, hollingworthite

2,3. 17A, hollingworthite

4. 13E-1, hollingworthite

5. 13E-1, hollingworthite - cobaltite (ss)

6. 15-4, hollingworthite - cobaltite (ss)

7. 13E-1, hollingworthite - cobaltite (ss)

8. AK-11A, cobaltite

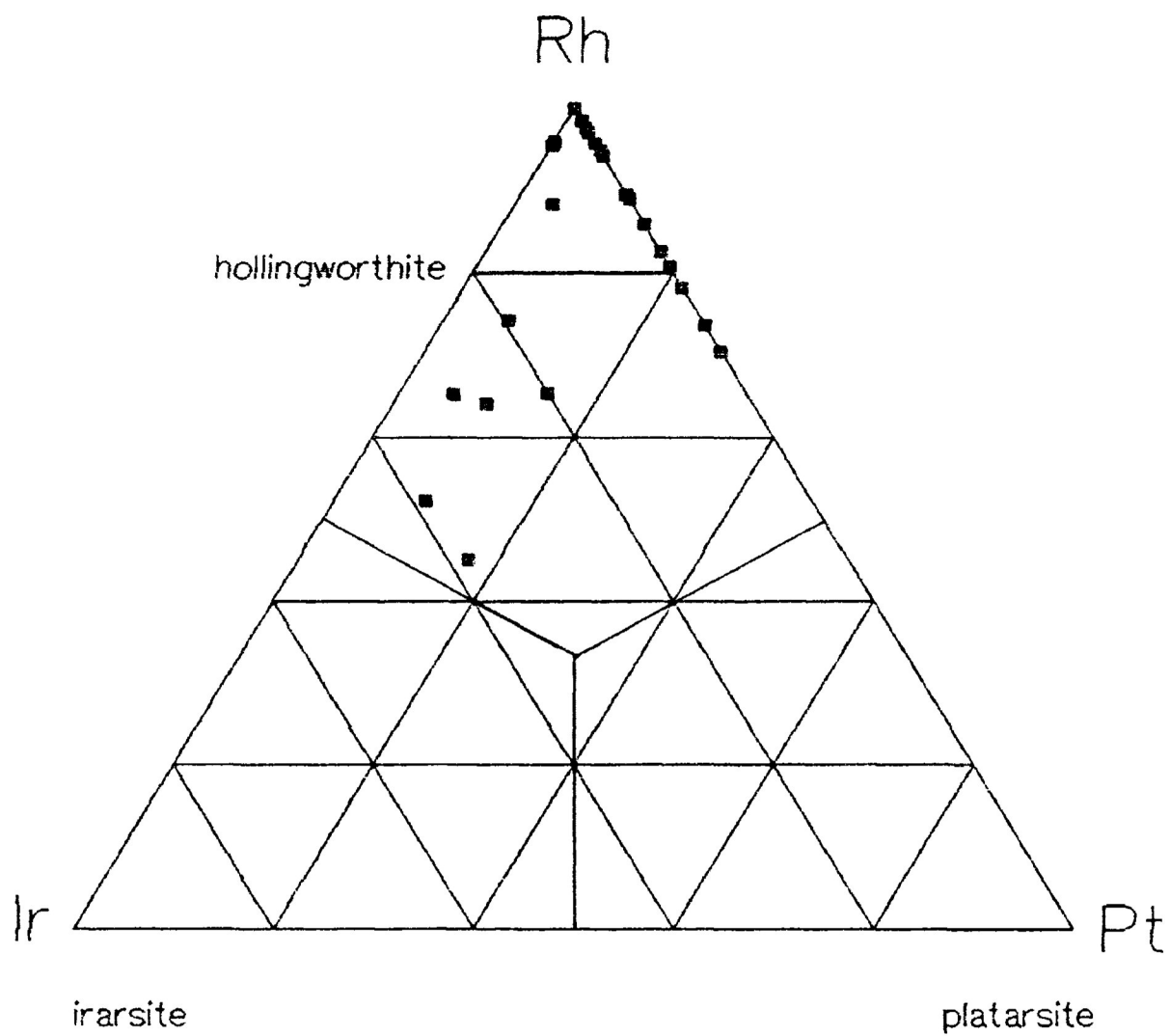


Figure 8.4 : Rh - Pt - Ir ternary diagram (atomic %)

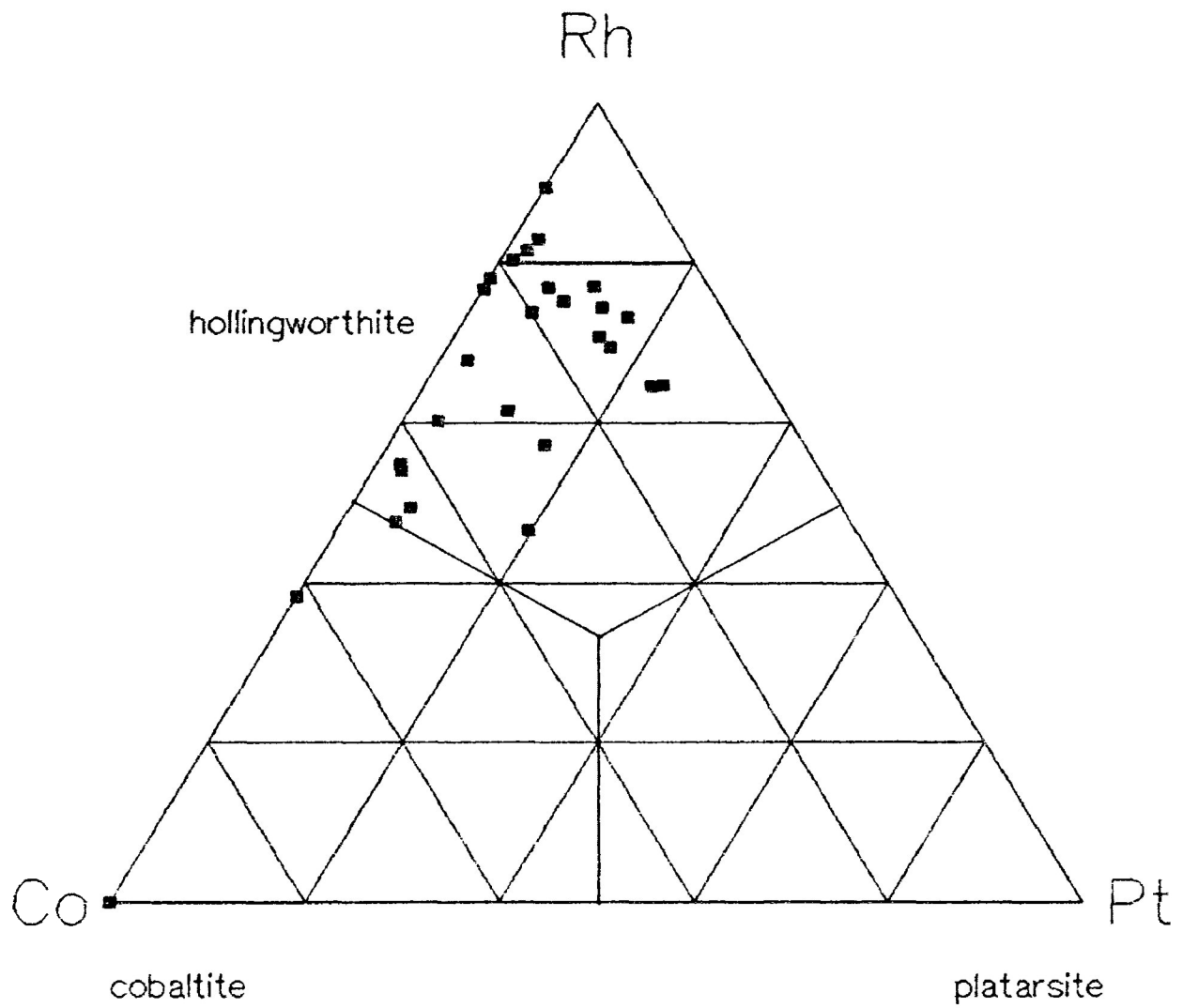


Figure 8.5 : Rh - Pt - Co ternary diagram (atomic %)

(Figure 8.4). In the Rh - Pt - Co ternary diagram, the hollingworthites appear to form a solid solution with cobaltite (Figure 8.5).

Compositions of hollingworthite and cobaltite from other localities are given in table 8.7. Very few hollingworthites contain Co, and very few cobaltites contain Rh. Hollingworthites from Werner Lake (Table 8.7, analysis 3) and Hitura (Table 8.7, analysis 4) are similar to those from the Kawene Intrusion. Many of the hollingworthites contain Pt and Ir due to the solid solution between RhAsS - PtAsS (platarsite) - IrAsS (irarsite). All of the cobaltites from other localities contain Ni and Fe due to solid solution between CoAsS - NiAsS (gersdorffite) - FeAsS (arsenopyrite).

The Kawene sulfarsenides may be a solid solution (ss) of hollingworthite and cobaltite rather than an intergrowth of two phases. On BSE images, only one phase can be seen. Hollingworthite is cubic, and cobaltite is pseudocubic. Hollingworthite always contains Co (3.50 - 17.23 at%) (Table 8.6). In figure 8.5, a continuous solid solution of hollingworthite and cobaltite can be seen rather than two distinct end member clusters. One 9 μm grain from 13E-1 shows zoning in which a hollingworthite core (Table 8.6, analysis 4) is surrounded by a (hollingworthite - cobaltite) ss inner rim (Table 8.6, analysis 5), and a (cobaltite - hollingworthite) ss outer rim (Table 8.6, analysis 7). Co increases from 7.82 at% in the core to 17.23 at% in the outer rim.

Cabri and Laflamme (1976) noted that cobaltite may contain

Table 8.7 : Comparative hollingworthite (1-7) and cobaltite (8-18) compositions (weight %)

analysis	Rh	Pd	Pt	Ir	Ru	Co	Ni	Fe	As	S	total
1	47.62							3.60	37.02	14.99	100.29
2	44.54	1.30	3.91	0.70			0.18	0.40	34.04	14.92	99.99
3	41.30	0.85	0.61	0.22	2.80	2.50	1.30		33.30	16.40	99.20
4	36.2					4.9	2.3	3.4	35.8	17.0	99.6
5	33.24	4.90	13.74						30.86	14.08	100.05
6	32.1	8.9		1.0	3.1				31.7	10.5	99.4
7	30.8	8.7	10.3	3.1					32.6	13.9	99.4
8	4.02		1.77			15.73	8.18	6.16	43.91	19.10	100.33
9	0.39	0.06	0.09			19.80	10.20	6.20	45.40	18.90	101.04
10						19.9	10.4	7.0	41.3	20.7	99.3
11						22.87	9.00	4.17	44.12	19.05	99.21
12	2.29	0.27	0.01			23.01	6.20	3.67	44.53	19.65	101.72
13						24.9	6.1	3.6	47.7	19.4	101.7
14						28.52	2.70	6.07	39.93	22.40	99.62
15						28.64	3.06	4.11	44.77	19.34	99.92
16						31.20	1.82	4.47	42.17	21.54	101.21
17						33.2	0.5	1.9	45.0	20.1	100.7
18						34.2	0.1	1.7	43.0	20.5	99.5
19						35.3	0.8	0.4	45.4	19.9	101.8

1. Shetland ophiolite complex (Tarkian and Prichard, 1987)
2. Two Duck Lake, Coldwell complex (Ohnenstetter et al., 1991)
3. Werner Lake, Ontario (Rucklidge, 1969)
4. Hitura Nickel deposit, Finland (Hakli, 1976)
5. Oulanka, Kola region, USSR (Yakovlev et al., 1991)
6. Driekop mine, South Africa (Stumpfl, 1972)
7. Driekop mine, South Africa (Stumpfl and Clark, 1965)
8. Pansky, Kola region, USSR (Yakovlev et al., 1991)
9. Crean Hill, Sudbury (Cabri and Laflamme, 1976)
10. Hitura Nickel deposit, Finland (Hakli, 1976)
11. Geordie Lake, Coldwell complex (Mulja and Mitchell, 1991)
12. Pechenga, Kola region, USSR (Yakovlev et al., 1991)
13. Koillismaa Layered Igneous Complex, Finland (Piispanen and Tarkian, 1984)
14. Duluth Complex (Mogessie et al., 1991)
15. Cobalt, Ontario (Anthony et al., 1990)
16. Koronuda, Macedonia, Greece (Mposkos, 1983)
17. Torrington New South Wales, Australia (Bayliss, 1969)
18. Bimbowrie, Australia (Bayliss, 1969)
19. Tunaberg Copper deposits, Central Sweden (Dobbe, 1991)

minor amounts of Rh, Pt, and Pd in solid solution at the Kanichee Cu - Ni deposit and in Sudbury area deposits, Ontario (Table 8.7, analysis 9). The cobaltite - gersdorffite from Crean Hill mine, Sudbury contains the highest concentration of PGE content with 1.53 wt% Rh, 0.19 wt% Pt, and 0.27 wt% Pd (Cabri and Laflamme, 1976).

Yakovlev et al. (1991) also found cobaltites from the Kola region, USSR contain minor Rh, Pt, and Pd contents (Table 8.7, analyses 8, and 12). The PGE concentration does not exceed a total of 20 at% in cobaltite (Yakovlev et al., 1991). The PGE concentration in cobaltite increases with the temperature of formation from greenschist metamorphism to amphibolite metamorphism to a magmatic origin (Yakovlev et al., 1991). The Co content in hollingworthite reaches a maximum of 6.73 at% in examples from the Karikyavr massif, Kola region (Yakovlev et al., 1991).

8.5. Electrum

Electrum (Au,Ag) is an alloy which results from the complete solid solution between isometric native gold and > 20% native silver (Anthony et al., 1990; Klein and Hurlbut, 1985). Electrum was found with two slightly different compositions :

Au₃Ag₂ with 6 grains found ranging in size 2 - 10 μm and

AuAg with 3 grains found ranging in size 0.5 - 7 μm .

An SEM / EDS spectrum of a 10 μm Au₃Ag₂ grain from drill core 13C-2 is given in figure 8.6.

Electrum is typically found enclosed in sulfides : pentlandite, chalcopyrite, pyrrhotite, and violarite. One electrum

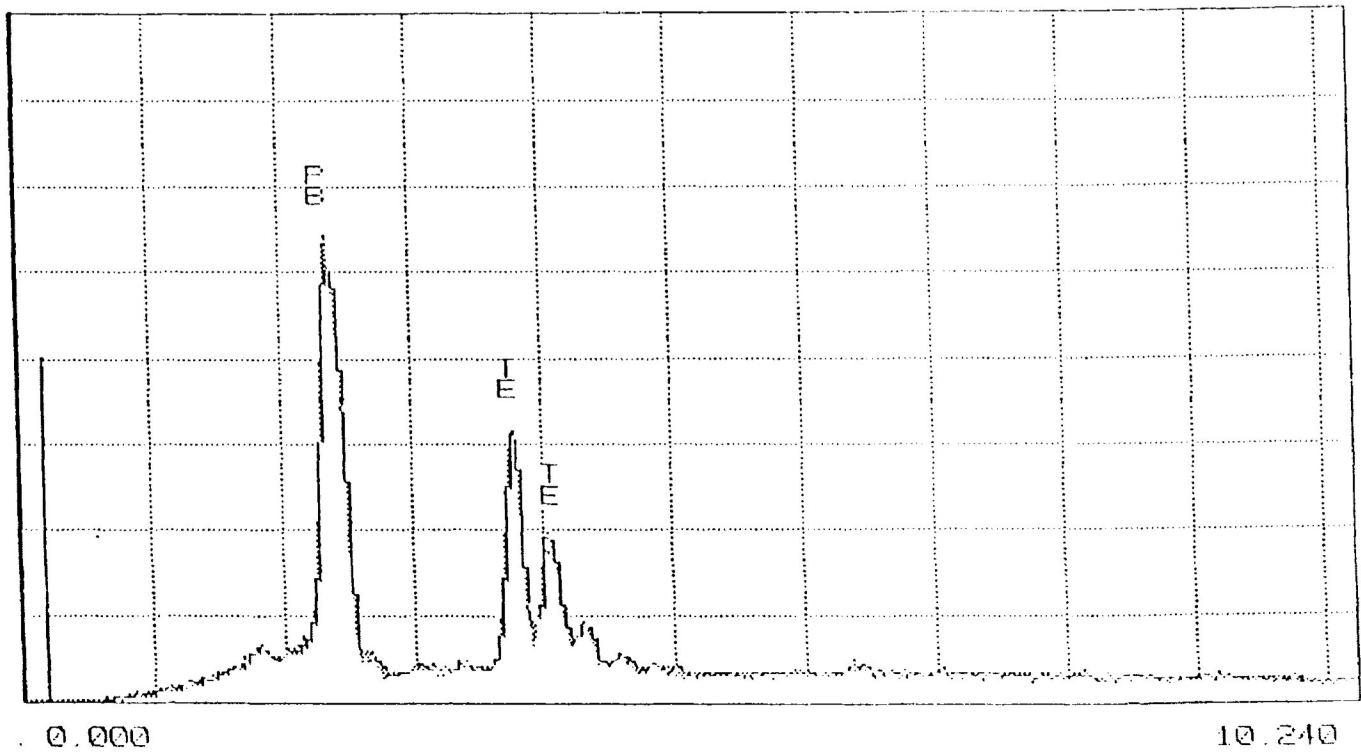
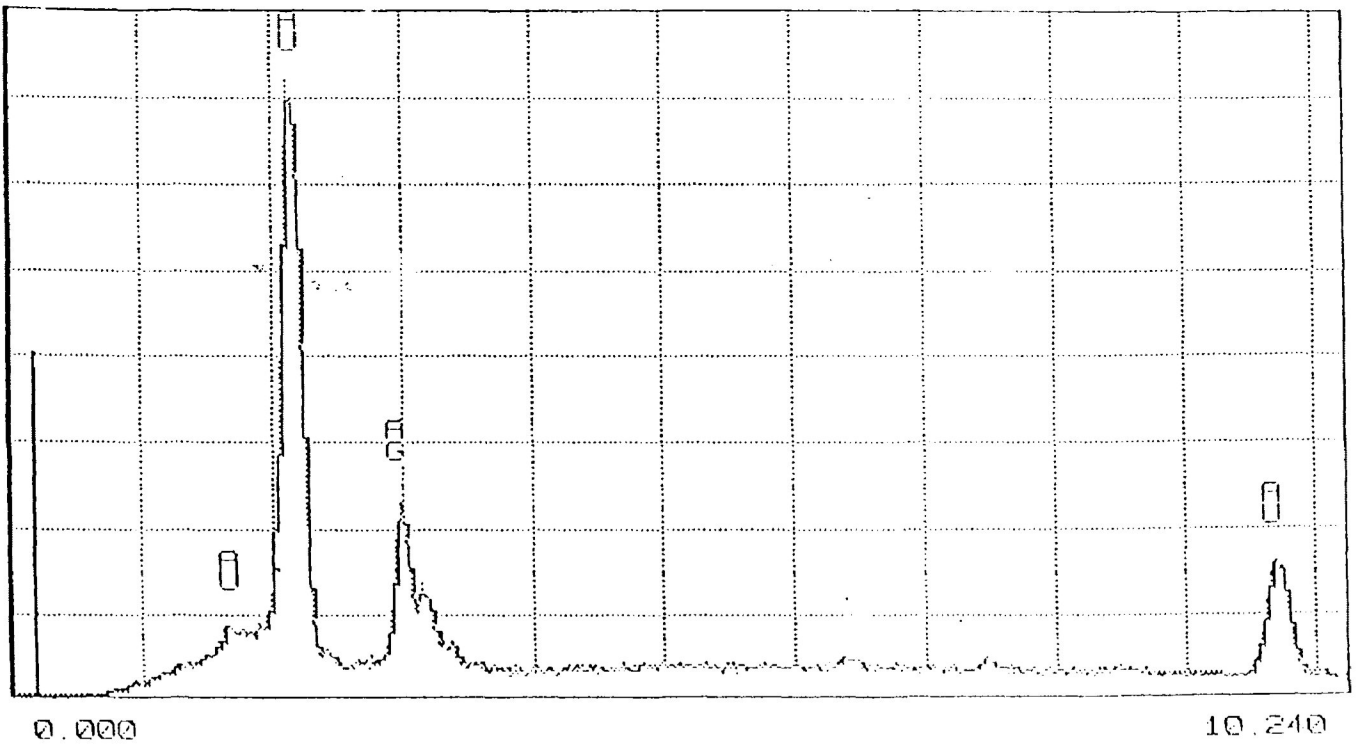


Figure 86 : SEM / EDS spectra of a) Au_3Ag_2 grain from drill core I3C-2
b) PbTe grain from I3D-1.

Table 8.8 : Representative compositions of electrum from Kawene Intrusion (atomic and weight %)

analysis	at%		wt%		size	probe section	formula
	Au	Ag	Au	Ag			
ideal	50.00	50.00	64.61	35.39			AuAg
	60.00	40.00	73.25	26.75			Au ₃ Ag ₂
1	52.80	47.20	67.14	32.86	7 um	13E-1	AuAg
2	56.79	43.21	70.59	29.41	10 um	13C-1	Au ₃ Ag ₂
3	59.44	40.56	72.80	27.20	10 um	13C-2	
4	61.48	38.52	74.45	25.55	8 um	13D-1	

Table 8.9 : Comparative electrum compositions (weight %)

analysis	Au	Ag	Te	S	Cu	Fe	total	formula
1	54.51	45.49					100.00	Au ₂ Ag ₃
2	60.68	39.20					99.88	AuAg
3	64.60	33.90					98.50	
4	67.39	30.08	0.03	0.03	0.07	0.09	97.69	
5	67.58	32.06					99.64	
6	68.5	31.5					100.0	
7	71.0	29.0					100.0	Au ₃ Ag ₂
8	71.8	28.2					100.0	
9	73.2	26.7					99.9	
10	77.96	23.91					101.87	
11	83.3	16.7					100.0	Au ₃ Ag
12	84.5	14.6					99.1	
13	86.0	11.3					97.3	

1. Boston Creek Flow, Ontario (Stone et al., 1992)
2. Jales gold mine, Portugal (Neiva and Neiva, 1990)
3. Kolar gold mine, India (Safonov et al., 1984)
4. Ratagain Intrusion, Northwest Scotland (Alderton, 1986)
5. Koronuda, Macedonia, Greece (Mposkos, 1983)
6. Ivrea - Verbano, Western Italian Alps (Garuti and Rinaldi, 1986)
7. Ilomantsi, Eastern Finland (Johanson and Kojonen, 1989)
8. New Rambler, Wyoming (McCallum et al., 1976)
9. Glava, Varmland, Sweden (Oen and Kieft, 1984)
10. Kolar gold mine, India (Safonov et al., 1984)
11. Ivrea - Verbano, Western Italian Alps (Garuti and Rinaldi, 1986)
12. Stillwater, Montana (Volborth et al., 1986)
13. Glava, Varmland, Sweden (Oen and Kieft, 1984)

grain was found at an augite - diopside - chalcopyrite grain boundary. The majority (7) of the electrum grains were found in the drill core samples 13C, 13D, and 13E. These samples are a clinopyroxenite - hornblendite contact intruded by a tonalite vein.

Representative compositions of electrum are given in table 8.8. The Au and Ag contents ranges from 67.14 - 74.45 wt%, and from 25.55 - 32.86 wt% respectively. Electrum compositions from other localities are given in table 8.9. The electrum from the Kawene Intrusion closely matches these compositions e.g. analyses 4 - 9. Electrum from all of the localities is associated with hessite, and/or Bi - Te compounds, and/or galena. Most of the hessite grains from the Kawene Intrusion are also found in the drill core sample 13D and 13E.

8.6. Altaite

Altaite (PbTe) is cubic, and is named after the type locality in the Altai Mountains, USSR (Anthony et al., 1990; Klein and Hurlbut, 1985). Altaite is commonly found in hydrothermal gold deposits e.g. Kolar, India and Ashanti, Ghana (Anthony et al., 1990; Bowell et al., 1990; Safonov et al., 1984).

In the Kawene Intrusion, 6 grains of altaite was found with a size of 4, 15, and 18 μm . All of these grains were found in clinopyroxenite from drill core 13D-1 and 13D-2. Altaite is in subhedral - to - euhedral contact with augite, chlorite, biotite, pyrrhotite, and chalcopyrite. The altaite is intergrown with hessite and Pt - Sb compounds. Altaite is associated with hessite

Table 8.10 : Representative compositions of altaite from Kawene Intrusion (atomic and weight %)

analysis	at%		wt%		size	probe section
	Pb	Te	Pb	Te		
ideal	50.00	50.00	61.91	38.09		
1	50.42	49.58	62.28	37.72	18 um	130-1
2	51.24	48.76	63.05	36.95	18 um	130-1
3	52.74	47.26	64.44	35.56	18 um	130-1
4	53.97	46.03	65.56	34.44	15 um	130-1
5	54.54	45.46	66.08	33.92	15 um	130-1
6	55.11	44.89	66.60	33.40	15 um	130-1

Table 8.11 : Comparative altaite compositions (weight %)

analysis	Pb	Te	Ag	Bi	Cu	Fe	Au	Pd	Pt	Se	Sb	S	total
1	59.8	35.8	0.4	0.5	0.9	0.1				1.1			98.6
2	59.81	37.91	0.23	0.60	0.04	1.38							100.03
3	60.13	38.64	0.60										99.54
4	60.8	35.1	0.5	0.5	1.4	0.1				1.4			99.8
5	61.33	38.43	0.43		0.01	0.13	0.02			0.08			100.43
6	61.47	36.21						0.09	0.16		0.57	0.39	98.89
7	61.50	38.39											99.89
8	61.52	38.48											100.00
9	61.53	37.35	0.03	0.16	0.04								99.05
10	61.63	38.31											99.94
11	62.30	37.30	0.32										99.88
12	62.6	35.9											98.5
13	63.0	35.5								1.1			99.6
14	63.74	37.11											100.84

1. Glava, Varmland, Sweden (Oen and Kieft, 1984)
2. Dragsest deposit, Norway (McQueen, 1990)
3. Geordie Lake Intrusion, Coldwell Complex (Mulja and Mitchell, 1990)
4. Glava, Varmland, Sweden (Oen and Kieft, 1984)
5. Kalgoorlie, Western Australia (Anthony et al., 1990)
6. Blue Lake, Labrador Trough, Quebec (Beaudoin et al., 1990)
7. Kolar, India (Safonov et al., 1984)
8. Red Cloud mine, Colorado (Anthony et al., 1990)
9. Ashanti gold mine, Ghana (Bowell et al., 1990)
10. Kolar, India (Safonov et al., 1984)
11. Ivrea - Verbano, Western Italian Alps (Garuti and Rinaldi, 1986)
12. Frood mine, Sudbury (Cabri and Laflamme, 1976)
13. Coleman mine, Sudbury (Cabri and Laflamme, 1976)
14. Geordie Lake, Coldwell Complex (Mulja and Mitchell, 1990)

in other localities (Bowell et al., 1990; Mulja and Mitchell, 1990; Garuti and Rinaldi, 1986; Oen and Kieft, 1984; Safonov et al., 1984; Cabri and Laflamme, 1976). An EDS / SEM spectrum of a 15 μm altaite from 13D-1 is given in figure 8.6b (Table 8.10, analysis 4).

Representative compositions of altaite are given in table 8.10. The altaite from the Kawene Intrusion is rich in Pb (50.42 - 55.11 at%). Compositions of altaite from other localities is given in table 8.11. The altaite from the Kawene Intrusion resembles the altaite from Ivrea - Verbano, Sudbury, and Geordie Lake (Table 8.11, analyses 11 - 14).

Chapter 9

Platinum - Group Minerals Intergrowths and Clusters

9.1. Intergrowths

9.1.1. Intergrowths

In the Kawene Intrusion, 98 grains (9%) of the 1078 total PGM grains are intergrowths of two or more platinum - group minerals, Bi - S compounds, or Bi - Te compounds. In the Kola mafic - ultramafic massifs, intergrowths of 2 - 3 PGM are rare, and mostly occur in layered intrusions (Yakovlev et al., 1991). In the Sudbury complex, the polymineralic association of either a single PGM or 2 PGM (up to 5 PGM in some deposits) with hessite, altaite, tsumoite, and native Bi is common (Cabri and Laflamme, 1976). In the Tunaberg Pb - Zn deposit, Sweden, native Bi, Bi - Te compounds, and galena are found intergrown (Dobbe, 1993). In the Kawene Intrusion, the most common intergrowths occur between :

1. Pd - Bi and Bi - S compounds, 17 grains;
2. Pd - Bi compounds, 11 grains;
3. native Bi and Bi - S compounds, 9 grains;
4. Pd - Bi compounds and michenerite, 8 grains; and
5. Pd - Bi, Bi - S compounds, and michenerite, 4 grains.

These intergrowths reflect the relatively high abundance of Pd - Bi compounds, michenerite, Bi - S compounds, and native Bi.

Some examples of intergrowths within the Pd - Bi - Te - Sb compositional group are :

6. michenerite and Sb-bearing michenerite, 20 μm , drill core 15B-1

(Figure 9.1d); and

7. Pd_2Bi_5 , michenerite, Sb-bearing michenerite, $\text{Pd}_2\text{BiSb(+Te)}$ sobolevskite - stibiopalladinite (ss), 15 μm , sample AK-10 (Figure 9.1e).

Some examples of intergrowths within the Bi - Te - Se - S compositional group are :

8. Bi_3S_2 , BiS, native Bi, and Se-bearing galena, 20 μm , drill core 17A-2 (Figure 9.4c);

9. Se-bearing galena, $\text{Bi}_2(\text{Se,Te})$, native Bi, and bismuthinite, 18 μm , drill core 15-5 (Figure 9.4d); and

10. $\text{Bi}_4(\text{S,Te,Se})_3$ and $\text{Bi}_3(\text{S,Te,Se})_2$, 20 μm , sample AK-2 (Figure 9.4e, section 7.4, Figure 7.3).

These intergrowths are either distinct on the back-scattered electron (BSE) image, or if the average atomic number of the intergrown PGM are too close to be distinct on the BSE image, then the intergrown PGM are distinguished by analyzing numerous spots within the grain.

9.1.2. Intergrowths within the Pd - Bi - Te Compositional Group

The intergrowths between Pd - Bi compounds include : Pd_2Bi_5 , PdBi_2 , Pd_2Bi_3 , and PdBi. The largest example of this type of intergrowth is a 14 μm composite grain of Pd_2Bi_5 , PdBi_2 , and PdBi from sample AK-2 (Figure 9.1a). A 5 μm zoned grain from AK-2 shows a Pd_2Bi_5 core, PdBi_2 intermediate zone, and PdBi rim. Another 5 μm zoned grain from drill core 17B-1 shows a Pd_2Bi_5 core, PdBi_2 intermediate zone, and Pd_2Bi_3 rim.

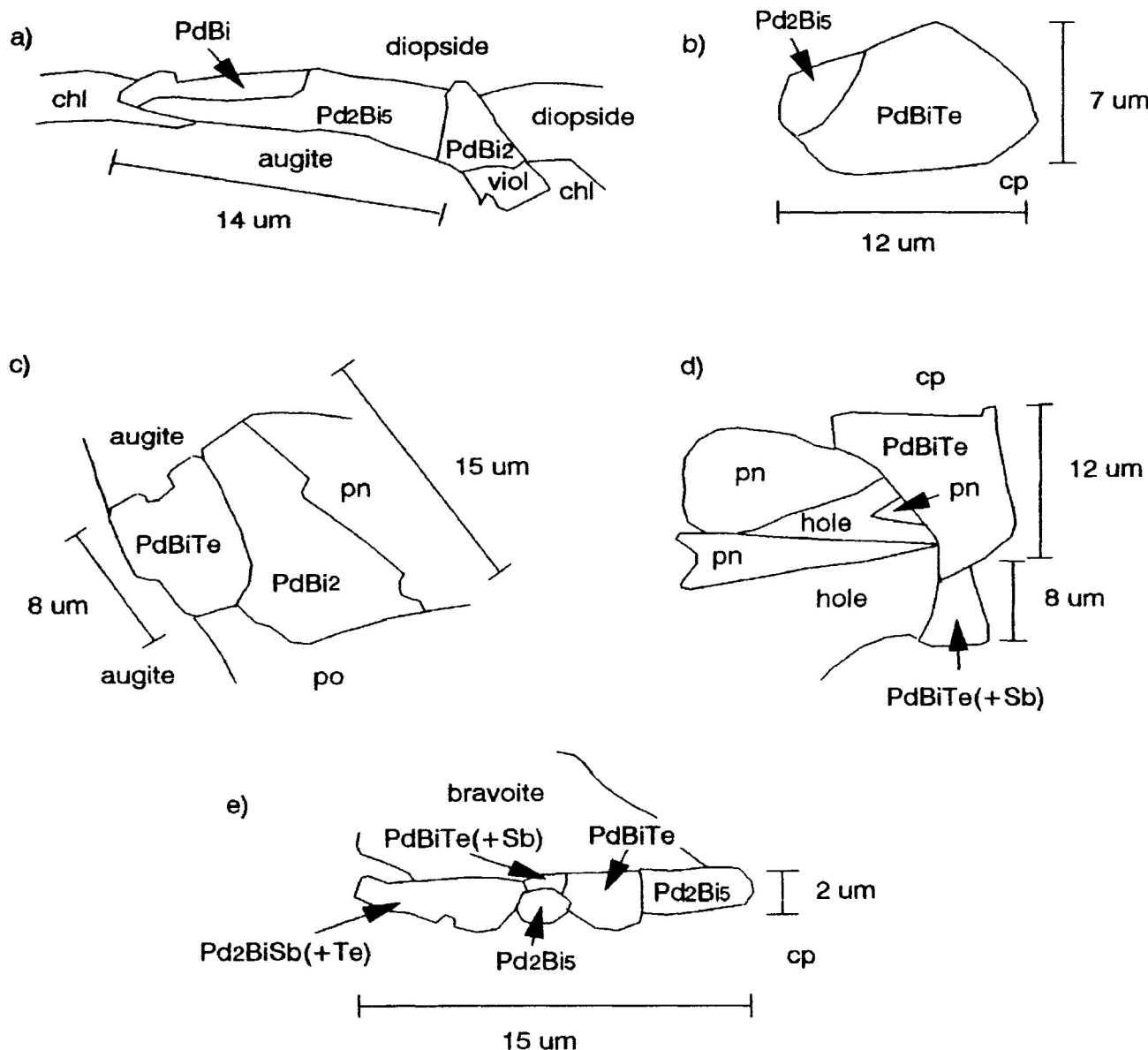


Figure 9.1 : Intergrowths within the Pd - Bi - Te - Sb compositional group

a) Intergrowth of sobolevskite, Pd₂Bi₅, and froodite from sample AK-2

b) Intergrowth of Pd₂Bi₅ and michenerite from drill core 16B-1

c) Intergrowth of michenerite and froodite from drill core 17B-1

d) Intergrowth of michenerite and Sb-bearing michenerite from drill core 15B-1

e) Intergrowth of sobolevskite - stibiopalladinite (ss), Pd₂Bi₅, Sb-bearing michenerite, and michenerite from sample AK-10.

chl - chlorite, viol - violarite, cp - chalcopyrite, pn - pentlandite, po - pyrrhotite

The intergrowths between Pd - Bi compounds and michenerite, include Pd_2Bi_5 , PdBi_2 , and Pd_2Bi_3 . Five of the intergrown grains range in size from 10 - 15 μm . The most common intergrowth with PdBiTe is Pd_2Bi_5 (5 grains). Two examples of this intergrowth are 12 μm grains of Pd_2Bi_5 and michenerite from drill core 16B-1 (Figure 9.1b) and from drill core 17B-2 (section 6.1, Figure 6.5). Another example is a 15 μm grain of michenerite and froodite from drill core 17B-1 (Figure 9.1c).

9.1.3. Intergrowths between Pd - Bi - Te and Bi - S Compositional Groups

The intergrowths between Pd - Bi and Bi - S compounds include all of the varieties of these two compounds mentioned in section 6.2 and 7.2. The largest example of this intergrowth is a 14 μm grain of Pd_2Bi_5 and Bi_3S_2 from drill core 15B-4 (Figure 9.2a).

The intergrowths between Pd - Bi, Bi - S, and michenerite include Pd_2Bi_5 , PdBi_2 , BiS , and Bi_2S_3 . An example of this intergrowth is a 7 μm grain of Pd_2Bi_5 , bismuthinite, and michenerite from sample AK-3A (Figure 9.2b).

One 10 μm grain is an intergrowth of sobolevskite, BiS , and Au. The grain was so complexly zoned that x-ray maps were required to determine the spatial relationships between the minerals. By superimposing Pd and Au x-ray maps, the Au grain is easily recognized (Figure 9.3). The Pd x-ray map represents sobolevskite, and the area with no Pd and Au is BiS .

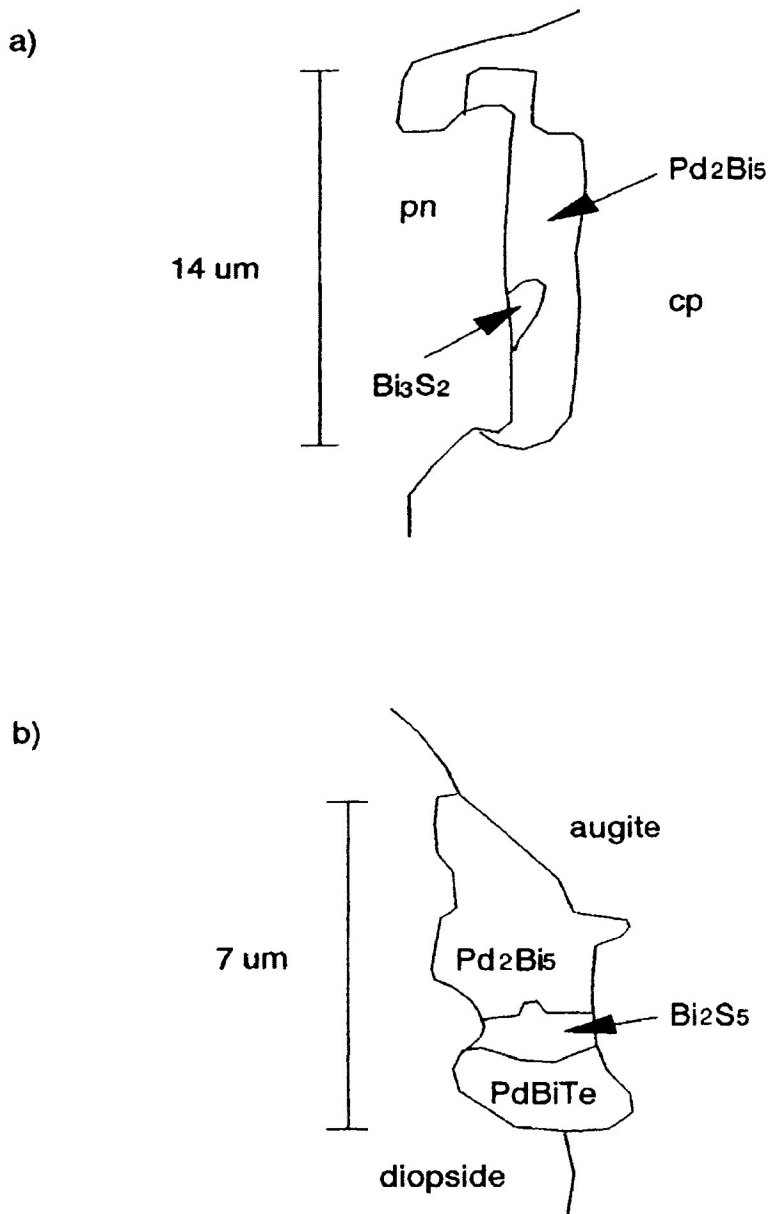


Figure 9.2 : a) Intergrowth of Pd_2Bi_5 and Bi_3S_2 from drill core 15B-4.

b) Intergrowth of Pd_2Bi_5 , bismuthinite, and michenerite from drill core AK-3A.

pn - pentlandite, cp - chalcopyrite

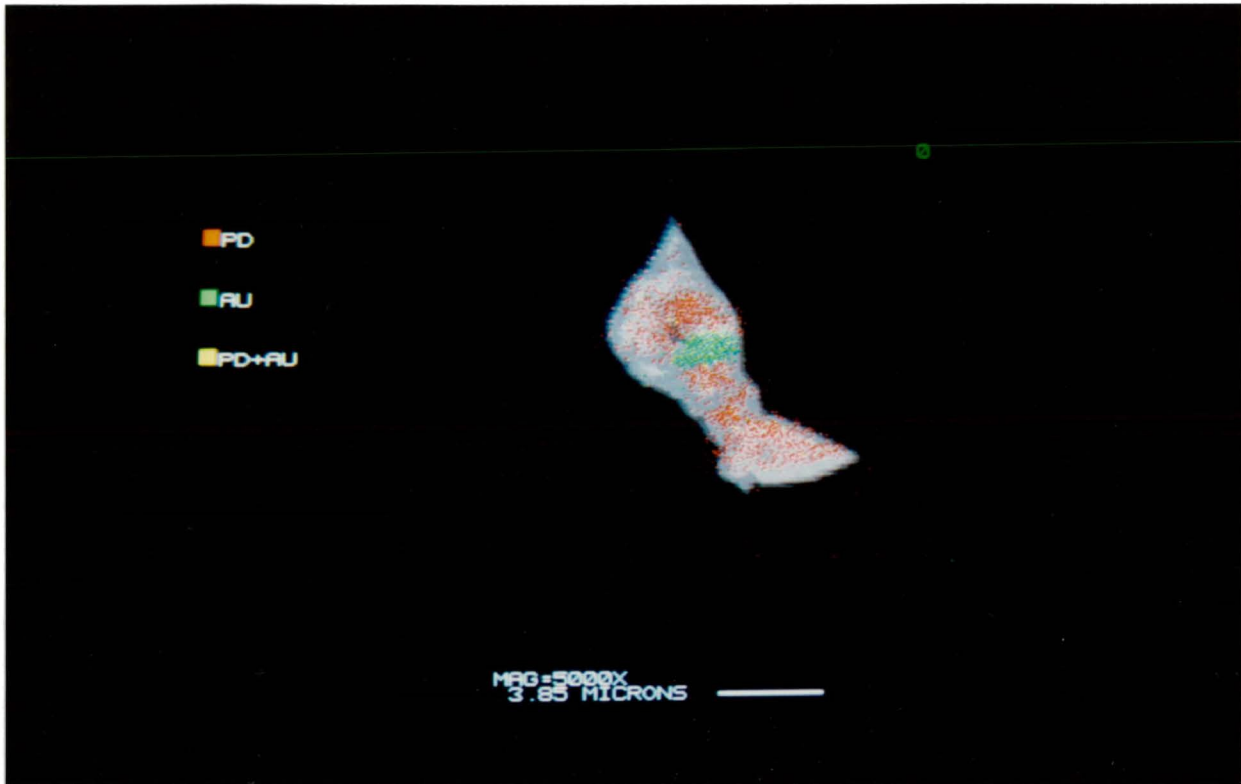


Figure 9.3 : Superimposed Pd and Au x-ray maps of a 10 μm intergrowth from drill core 15-3. Pd (orange) represents sobolevskite. Au (green) is found in the core, and BiS (grey) is found on the rim.

9.1.4. Intergrowths between Native Bi and Bi - S Compounds

The intergrowths between native Bi and Bi - S compounds include all of the varieties of Bi - S compounds mentioned in section 7.2. The largest example of this intergrowth is a 20 μm grain of native Bi enclosed in bismuthinite from drill core 15-5 (Figure 9.4a). Another example is a 18 μm grain of Bi_2S_3 , native Bi, and BiS also from 15-5 (section 6.1, Figure 6.6). One 6 μm grain from drill core 15B-2 has a native Bi core and a bismuthinite rim which indicates that native Bi crystallized before bismuthinite or was replaced by bismuthinite (Figure 9.4b).

9.1.5. Intergrowths with Sperrylite

Several PGM are intergrown with sperrylite :

1. michenerite, 10 μm , drill core 28A (Figure 9.5a);
2. Bi_3Te_2 , 25 μm , drill core 15B-3 (Figure 9.5b);
3. Co-bearing hollingworthite, 10 μm , drill core 17B-1 (Figure 9.5c); and
4. Co-bearing hollingworthite, $\text{Bi}_3(\text{Te},\text{Se})_2$, 15 μm , drill core 15-4 (Figure 9.5d, 6a).

9.1.6. Intergrowths with Stutzite and Hessite

A 12 μm grain is an intergrowth of michenerite and stutzite from drill core 13D-2 (Figure 9.7a).

Several minerals are intergrown with hessite :

1. altaite, 15 μm , drill core 13D-1 (Figure 9.7b); and
2. altaite, Bi_3Te_2 , pilsenite, Se-bearing galena, 12 μm , sample AK-

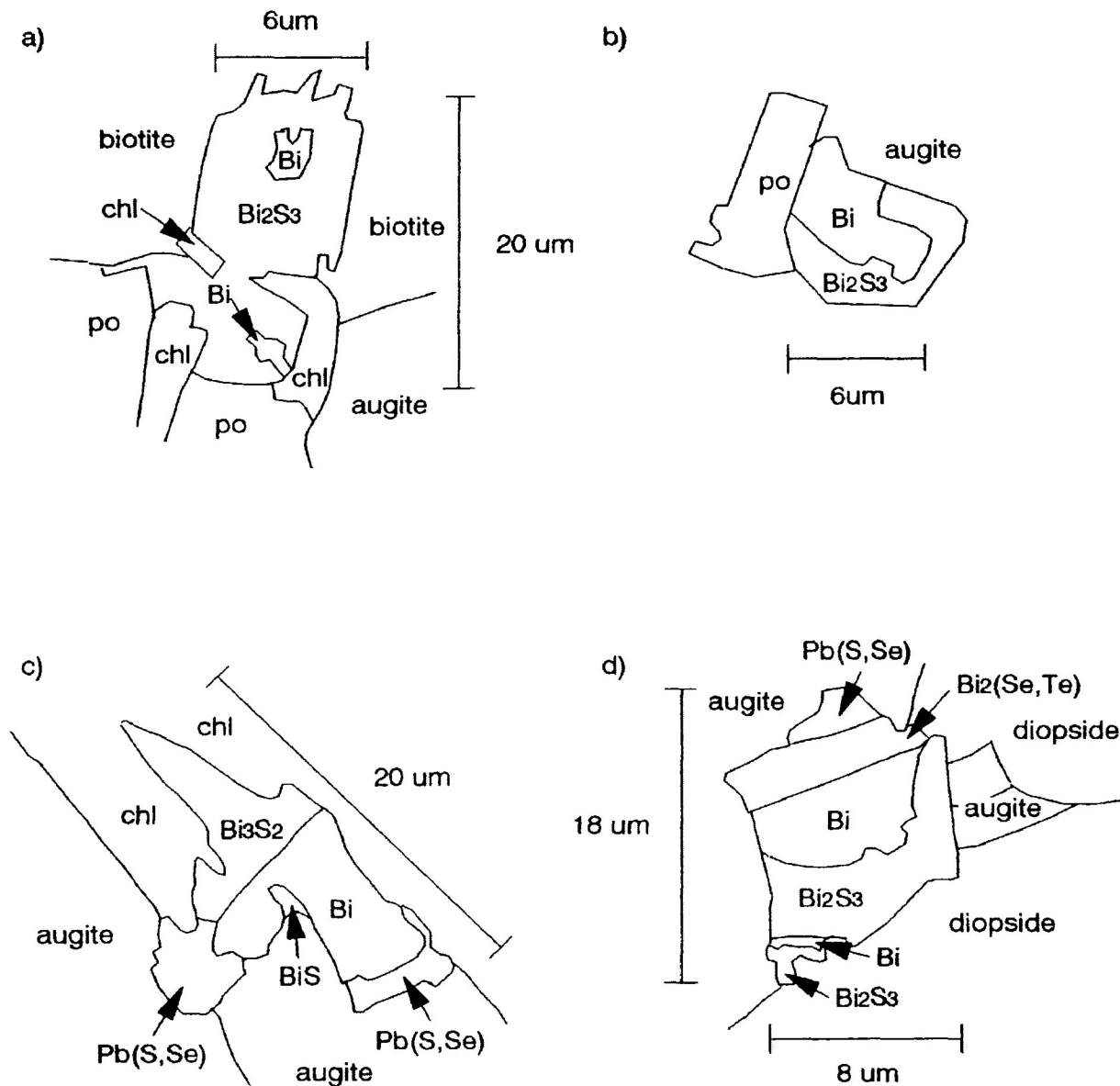


Figure 9.4 : Intergrowths within the Bi - Te - Se - S compositional group.

a) Intergrowth between native Bi and bismuthinite from drill core 15-5.

b) Intergrowth between native Bi and bismuthinite from drill core 15B-2

c) Intergrowth between Bi_3S_2 , native Bi, BiS, and Se - bearing galena from drill core 17A-2.

d) Intergrowth between Se - bearing galena, $\text{Bi}_2(\text{Se,Te})$, native Bi, and bismuthinite from drill core 15-5. chl - chlorite, po - pyrrhotite

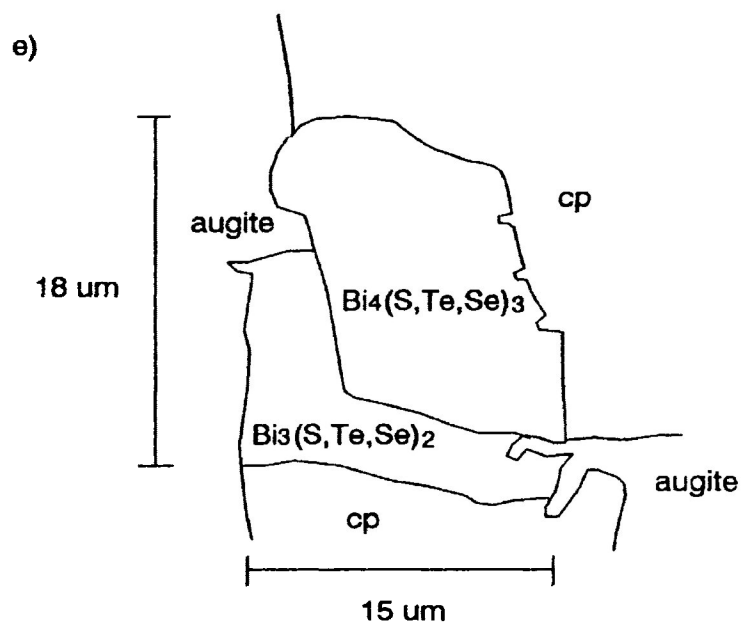


Figure 9.4e : Intergrowth between $\text{Bi}_4(\text{S,Te,Se})_3$ and $\text{Bi}_3(\text{S,Te,Se})_2$ from AK-2. cp - chalcopyrite.

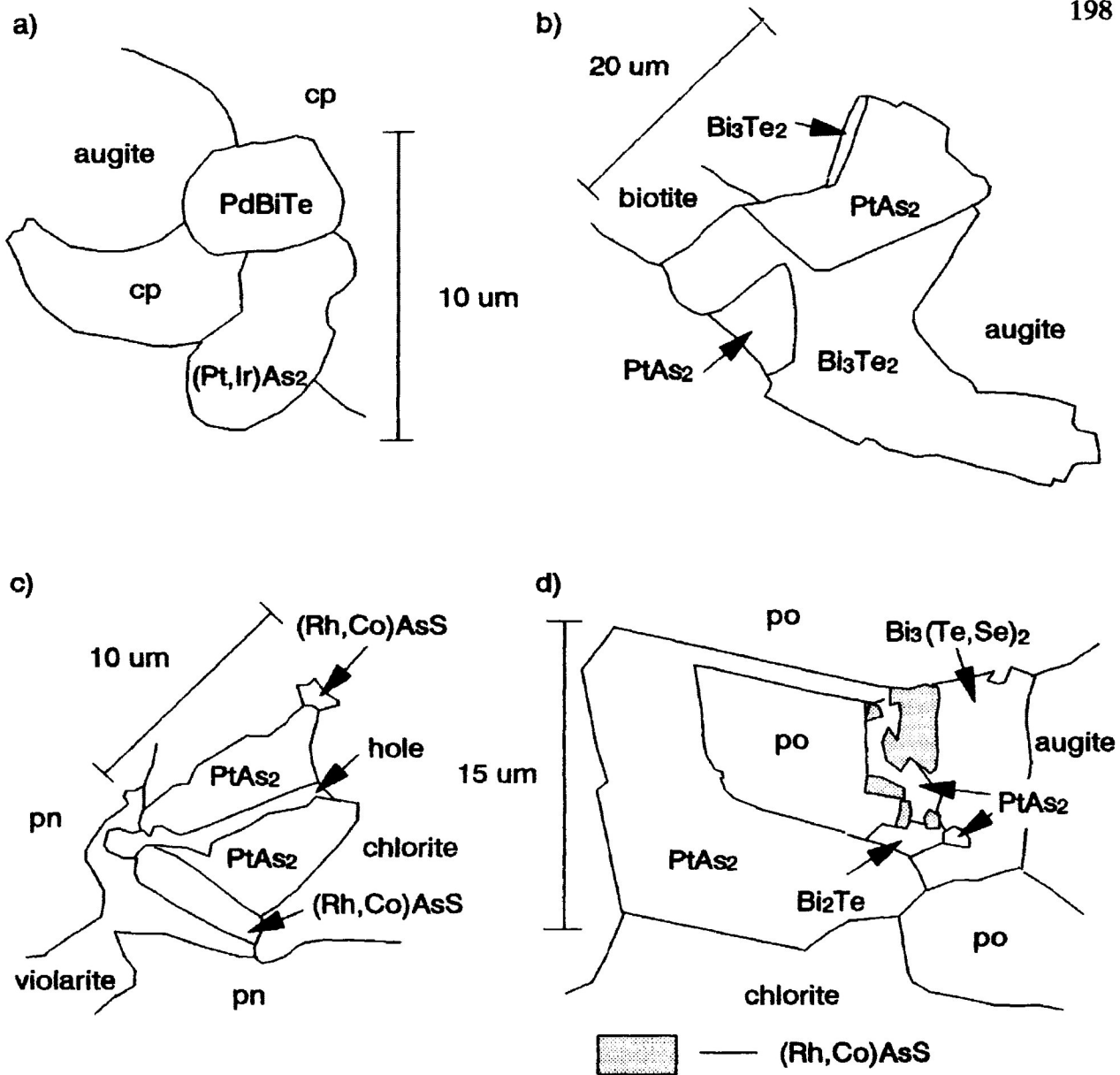


Figure 9.5 : Intergrowths with sperrylite.

a) Intergrowth between michenerite and sperrylite from drill core 28A.

b) Intergrowth between Bi₃Te₂ and sperrylite from drill core 15B-3.

c) Intergrowth between Co-bearing hollingworthite from drill core 17B-1.

d) Intergrowth between Co-bearing hollingworthite, Bi₂Te, Bi₃(Te,Se)₂ and sperrylite from drill core 15-4. cp - chalcopyrite, pn - pentlandite, po - pyrrhotite.

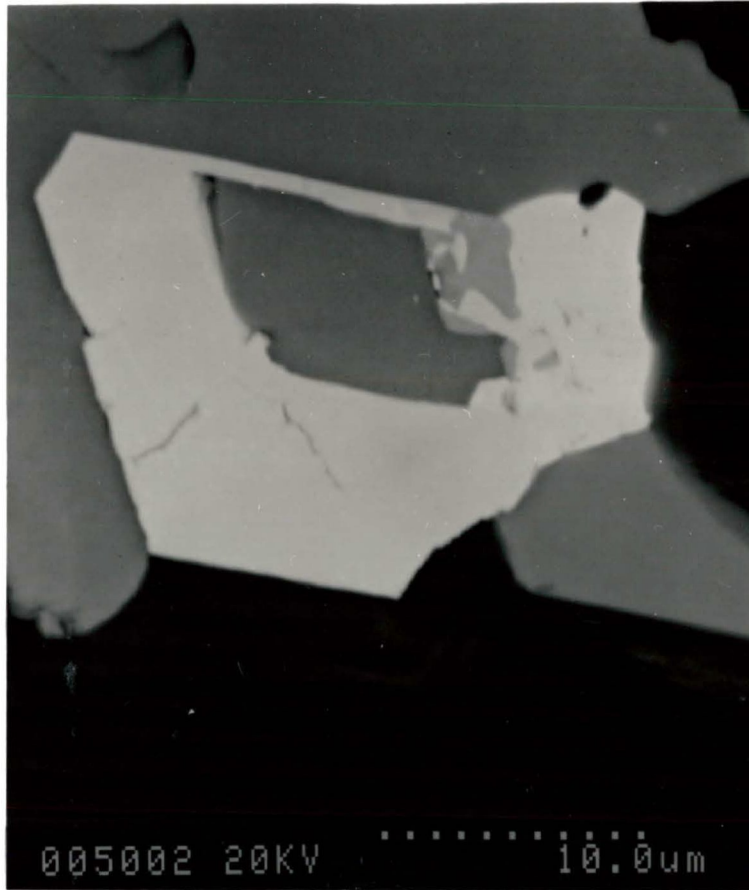


Figure 9.6a : A SEM / BSE image of a sperrylite, Co-bearing hollingworthite, and pilsenite - paraganajuaite (ss) intergrowth from drill core 15-4.

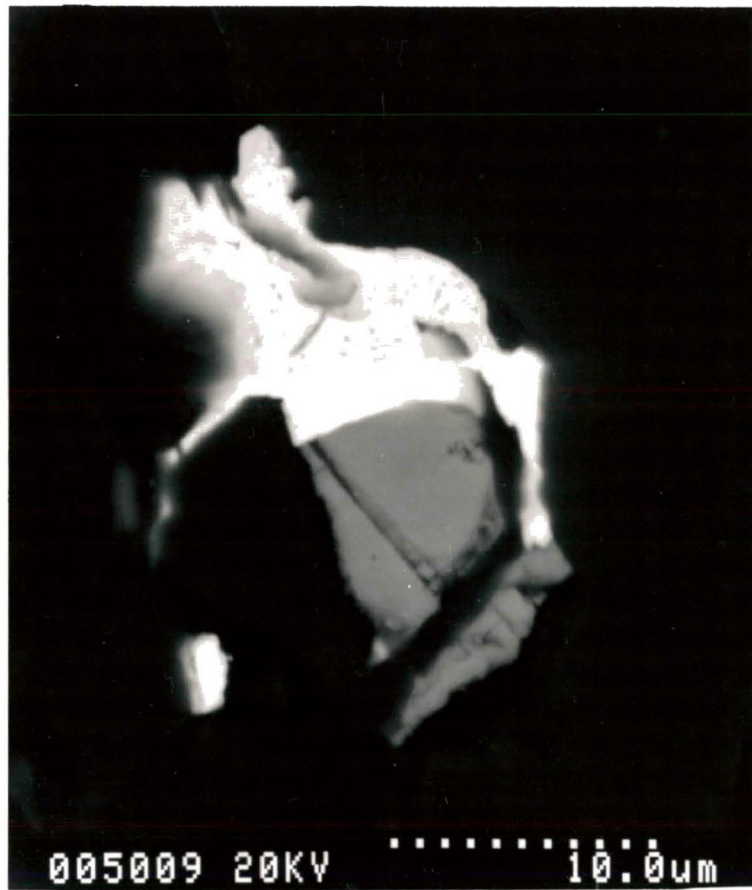


Figure 9.6b : A SEM / BSE image of a hessite, altaite, pilsenite - hedleyite (ss), pilsenite, and Se-bearing galena intergrowth from sample AK-9-86B.

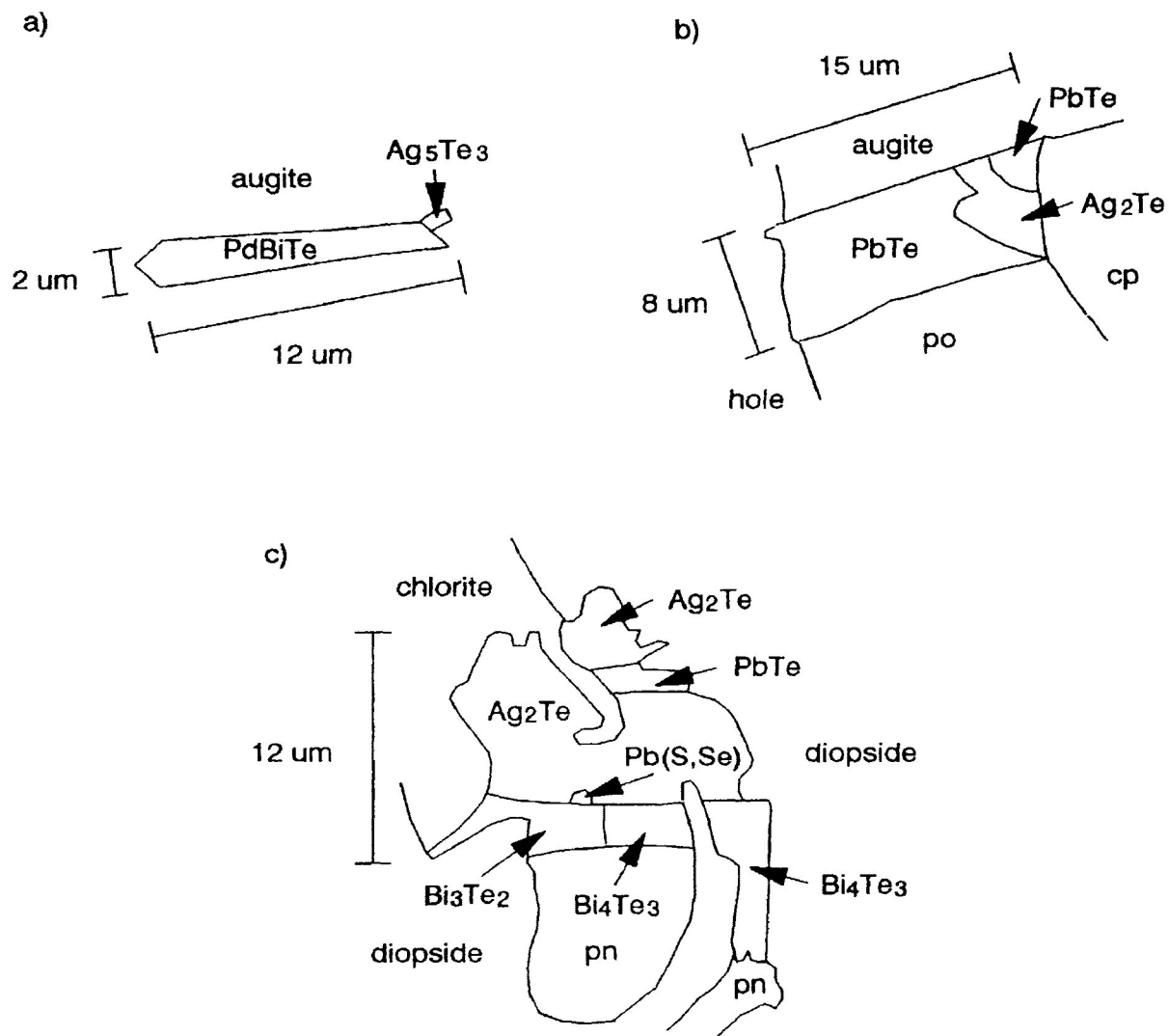


Figure 9.7 : Intergrowths with hessite and stutzite.

a) Intergrowth between michenerite and stutzite from drill core 13D-2.

b) Intergrowth between altaite and hessite from drill core 13D-1.

c) Intergrowth between altaite, hessite, Bi₃Te₂, pilsenite, and Se-bearing galena from sample AK-9-86B. cp - chalcopyrite, po - pyrrhotite, pn - pentlandite

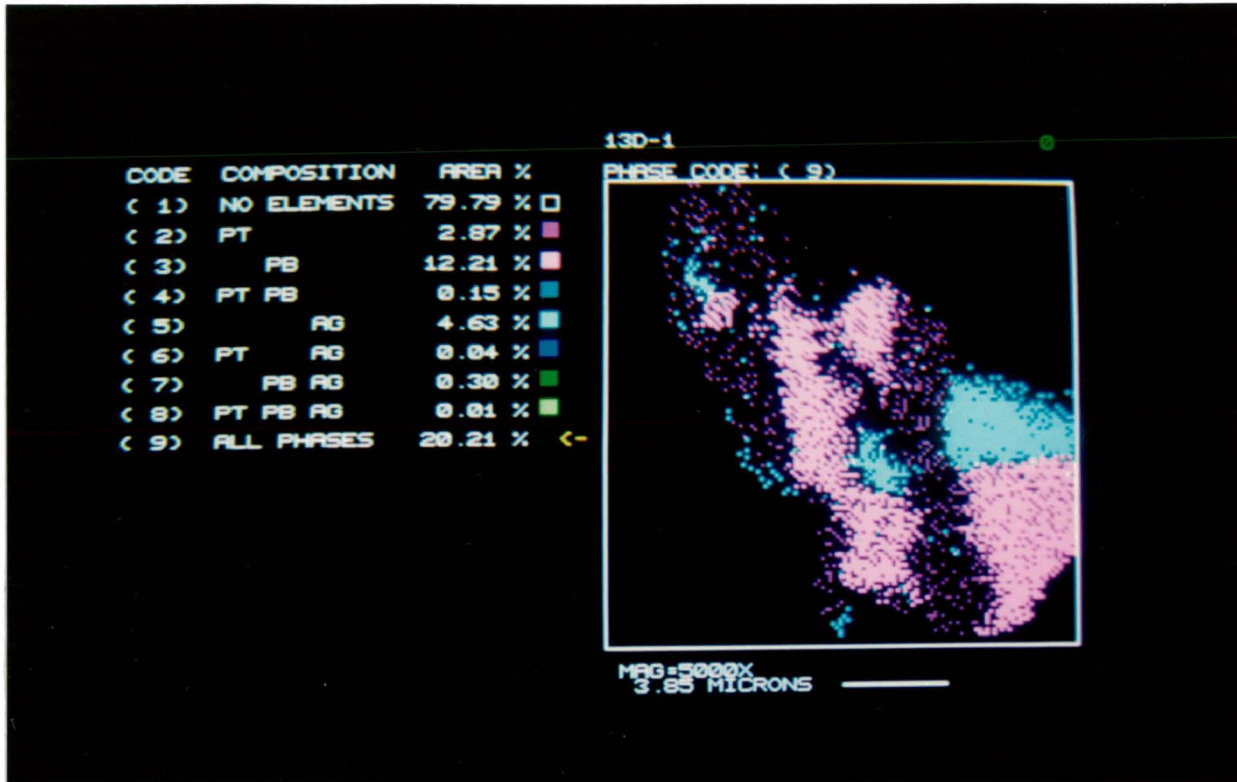


Figure 9.8 : Superimposed Pt, Pb, and Ag x-ray maps of a 18 μm intergrowth from drill core 13D-1. Pt (purple) represents a Pt - Sb compound, Pb (pink) represents altaite, and Ag (blue) represents hessite and stutzite.

9-86B (Figure 9.7c, 6b).

One 18 μm grain is a complex intergrowth of hessite, stutzite, altaite, and a Pt - Sb compound. When the Pt, Pb, and Ag x-ray maps are superimposed, the purple represents the Pt - Sb compound, the pink represents altaite, and the blue represents hessite and stutzite (Figure 9.8). Quantitative analyses could not be obtained for the Pt - Sb compound because of matrix influence due to the small size of the mineral's spatial extent.

9.2. Platinum - Group Mineral Assemblage

For the majority of PGM intergrowths found in the Kawene Intrusion, the contact between the intergrown minerals is euhedral to subhedral. These mineral intergrowths indicate simultaneous crystallization (Dobbe, 1993; Cabri and Laflamme, 1976). Exsolution textures are not known for the PGM found in the Kawene Intrusion. Native Bi may be replaced by bismuthinite, since subhedral native Bi is found either enclosed or partially enclosed within bismuthinite (Figure 9.4a,b).

In the Kawene Intrusion, the Pd - Bi - Te - Sb compositional group, Bi - Te - Se - S compositional group, electrum, Se-bearing galena, sperrylite, and Co-bearing hollingworthite crystallized at the same time (assemblage 1). Hessite, stutzite, altaite, Se-bearing galena, Bi_3Te_2 , pilsenite, and Pt - Sb compounds crystallized at the same time (assemblage 2), but not at the same time as the minerals in assemblage 1. The minerals in assemblage 2 are only found in drill core 13D-1, 13D-2, and AK-9-86B, whereas

the rest of the PGM are found throughout the mineralized area.

9.3. Platinum - Group Mineral Clusters

The distribution of the Platinum - Group Minerals, Bi - S compounds, and Bi - Te compounds in the Kawene Intrusion is heterogeneous. A polished thin section from hornblendite sample AK-2 contains the anomalous amount of 171 PGM grains. The number of PGM grains found in one polished thin section ranges from 83 (from hornblendite - tonalite drill core 15B-1) to none (from clinopyroxenite drill core 27C-2). The average number of PGM grains found in one polished thin section is 29 grains.

The Platinum - Group Minerals, Bi - S compounds, and Bi - Te compounds, may cluster together. In the Kawene Intrusion, 36 clusters were found containing 382 (35%) of the total 1078 PGM grains. The average number of PGM grains found in one cluster is 11. The most common PGM found in clusters are Pd - Bi compounds, michenerite, Bi - S compounds, and Bi - Te compounds which reflects their abundance in the intrusion.

The cluster with the most PGM by far has 73 grains in an area of 0.18 mm² from hornblendite - tonalite veinlet drill core 15B-1 (Figure 9.9a, b, c). The PGM are enclosed in chalcopyrite, and at chalcopyrite - pentlandite grain boundaries. The pentlandite is altering to violarite. The PGM either belong to the Pd - Bi - Te - Sb compositional group, or are Bi - S compounds. The PGM found in this cluster, in decreasing order of abundance, are : Pd₂Bi₅, michenerite, Sb-bearing michenerite, froodite, Pd₂BiSb(+Te)

a)

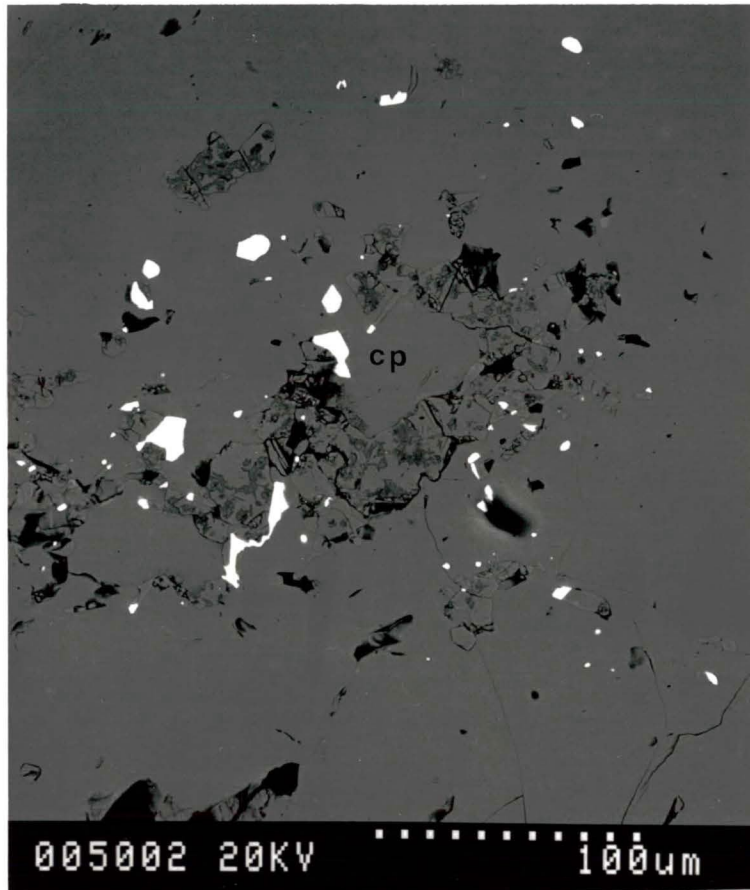


Figure 9.9a, b, c : SEM / BSE images of a PGM cluster from drill core 15B-1. The background, main sulfide, chalcopyrite (cp), contains PGM and pentlandite (pn) altering to violarite (vl) inclusions. Note that the PGM commonly occur at chalcopyrite - pentlandite grain boundaries.

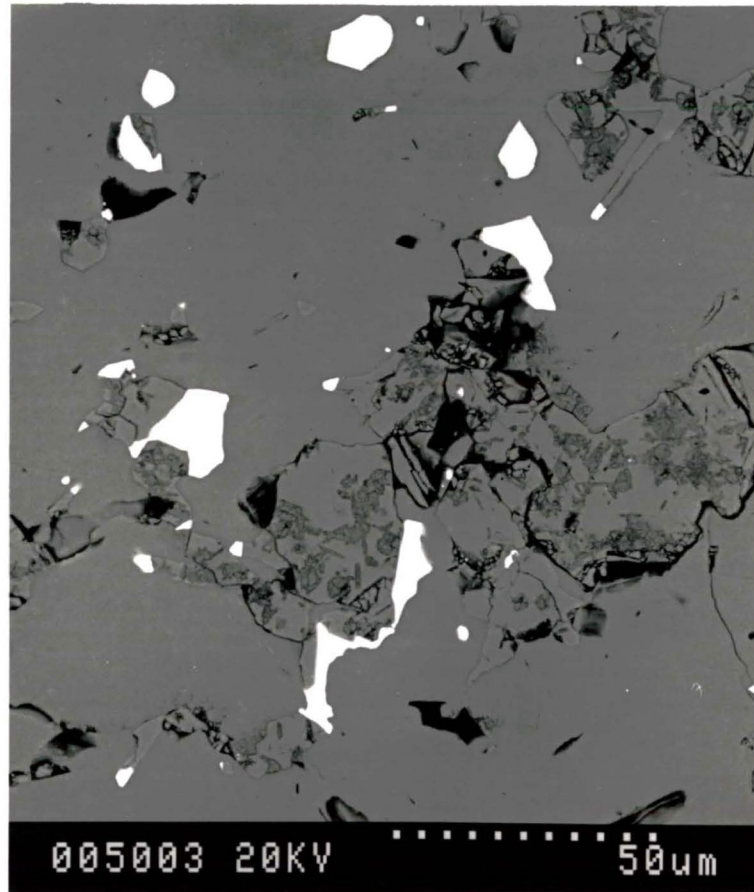


Figure 9.9 b



Figure 9.9 c

sobolevskite - stibiopalladinite (ss), BiS, Pd₂Bi₅(+Te), Te-bearing froodite, and Bi₃S₂. The largest PGM grains are Sb-bearing michenerite (20, 12, 10 μm), michenerite (14, 12, 11 μm), and Pd₂BiSb(+Te) sobolevskite - stibiopalladinite (ss) (15 μm) (Figure 9.9b).

Another cluster consists of 34 (Ag,Ni)S grains enclosed in violarite from clinopyroxenite sample AK-9-86B (section 8.2, Figure 8.3).

A cluster containing 22 PGM grains in an area of 0.01 mm² was found in hornblendite sample AK-3A. Most of the PGM are enclosed in augite. The remainder are found at augite - chlorite - pyrrhotite, at augite - chalcopyrite, and at pyrrhotite - pentlandite grain boundaries, and enclosed in pyrrhotite. The PGM belong to the Bi - Te - Se - S compositional group, Pd - Bi - Te compositional group, or are Bi - S compounds. The PGM found, in order of decreasing abundance, are : Bi₄(Te,S,Se)₃, Pd₂Bi₅, PdBi₃, Bi₂Te, michenerite, Bi₃Te₂, froodite, bismuthinite, and Bi₃S₂. The largest PGM grains are : Bi₃Te₂ (15 μm), Bi₄(Te,S,Se)₃ (8, 8 μm), and froodite (8 μm).

A cluster containing 20 PGM in an area of 0.005 mm² was found in hornblendite sample AK-10. The PGM are enclosed in chalcopyrite, at chalcopyrite - violarite grain boundary, enclosed in pyrrhotite, and at pyrrhotite - sphalerite grain boundary. The PGM belong to the Pd - Bi - Te - Sb compositional group and coexist with one grain of native Bi. The PGM found in the cluster, in decreasing order of abundance, are : Pd₂Bi₅, michenerite,

$\text{Pd}_2\text{BiSb(+Te)}$ sobolevskite - stibiopalladinite (ss), Sb-bearing michenerite, sobolevskite, PdBi_3 , Pd_2Bi_3 , $\text{Pd}_3\text{Bi}_2\text{Sb}$ sobolevskite - sudburyite (ss), and native Bi. The largest PGM grains are : PdBi_3 (12 μm), Pd_2Bi_3 (10 μm), michenerite (10 μm), and $\text{Pd}_2\text{BiSb(+Te)}$ (7 μm).

Chapter 10

Discussion

10.1. Temperature of Formation of Platinum - Group Minerals

Intergrowths of Platinum - Group Minerals crystallize at the same time (Chapter 9). The interpretation of intergrowth textures suggests that there is two PGM assemblages in the Kawene Intrusion. Assemblage 1 consists of the Pd - Bi - Te - Sb compositional group, Bi - Te - Se - S compositional group, sperrylite, Co-bearing hollingworthite, electrum, and Se-bearing galena (see section 9.2.). Assemblage 2 consists of hessite, stutzite, altaite, pilsenite, Bi_3Te_2 , and Se-bearing galena (section 9.2.). The temperature range over which each assemblage crystallized was estimated using the intergrowth textures in conjunction with the maximum thermal stability temperatures of the minerals (Table 10.1).

Assemblage 1 is considered to have crystallized between 489 - 254 °C. Sb-bearing michenerite is found intergrown with Sb-free michenerite which crystallizes below 489 °C (Figure 9.1d). Electrum is found intergrown with froodite which crystallizes below 485 °C. The temperatures of telluride deposition are generally below 354 °C, and typically below 250 °C (Afifi et al., 1988b). Sperrylite is intergrown with Bi_2Te which crystallizes below 312 °C (Figure 9.5d). Hollingworthite and cobaltite, which crystallize below 300 °C, form a solid solution series (section 8.4). Se-bearing galena is intergrown with native Bi and bismuthinite which

Table 10.1 : The maximum thermal stabilities of Platinum - Group Minerals found in the Kawene Intrusion.

Platinum - Group Minerals		
Mineral	Temp. (°C)	Reference
sperrylite	> 1400	(Vaughan and Craig, 1978)
galena	1127 ±5	(Vaughan and Craig, 1978)
electrum (53 - 62 at% Au)	1042 - 1034	(Elliot, 1965)
β-hessite	959	(Chizhikov and Shchastlivyi, 1970; Cabri and Laflamme, 1976)
α-hessite	145	(Johanson and Kojonen, 1989; Oen and Kieft, 1984)
altaite	924	(Vaughan and Craig, 1978; Afifi et al., 1988a)
altaite + galena	805	(Afifi et al., 1988a)
bismuthinite	760 ±5	(Vaughan and Craig, 1978)
Bi - Te compounds (50 - 45 at% Te) (45 - 36.5 at% Te) (36.5 - 29 at% Te)	540 420 312	(Afifi et al., 1988a; Vaughan and Craig, 1978; Elliot, 1965) BiTe Bi ₄ Te ₃ , Bi ₃ Te ₂ , Bi ₂ Te Bi ₇ Te ₃
michenerite	489 ±3	(Hoffman and MacLean, 1976; Cabri et al., 1973)
Pd - Bi compounds (47 - 33 at% Pd)	485	(Cabri and Laflamme, 1976; Elliot, 1965) PdBi, Pd ₂ Bi ₃ , PdBi ₂
cobaltite (<10 at% Fe, <10 at% Ni)	300	(Mposkos, 1983; Klemm, 1965)
native Bi	271.5	(Barton and Skinner, 1967)
native Bi + bismuthinite	270	(Barton and Skinner, 1967)
native Bi + hedleyite	266	(Afifi et al., 1988a; Barton and Skinner, 1967)
α-hessite + stutzite	120 ±15	(Afifi et al., 1988a; Kracek et al., 1966)

crystallize below 270 °C (Figure 9.4c, 4d). Relatively large (150, 38, 25 μm), euhedral sperrylite, michenerite, and stibiopalladinite - sobolevskite (ss) grains are found enclosed within monoclinic pyrrhotite (section 6.3, 6.4, 8.1). These PGM must have crystallized within the monosulfide solid solution (mss) which filled interstitial pore spaces. Therefore, the PGM in assemblage 1 must have crystallized before the monoclinic pyrrhotite at temperatures > 254 °C.

Assemblage 2 is considered to have crystallized between 145 - 120 °C. An intergrowth of hessite, altaite, Se-bearing galena, Bi_3Te_2 , and pilsenite crystallized below 145 °C (Figure 9.6b, 7b, 7c). An intergrowth of hessite, stutzite, and altaite crystallized below 120 °C (Figure 9.8). Assemblage 2 either crystallized late from the hydrothermal fluid or crystallized from a distinct low - temperature hydrothermal fluid.

As the temperature decreases, the melt is interpreted to become more Bi-rich. For example, as the crystallization temperature decreases from 540 to 420 to 312 °C, the Bi - Te compounds become more Bi-rich (Table 10.1). Hedleyite crystallizes at 312 °C, and native Bi plus hedleyite crystallize at 266 °C (Table 10.1). Native Bi crystallizes at 271.5 °C (Table 10.1).

10.2. Te_2 , S_2 , and O_2 Fugacities

The Te_2 , S_2 , and O_2 fugacity (f) stability fields during deposition were determined using the isothermal $f\text{Te}_2 - f\text{S}_2$ and $f\text{Te}_2 - f\text{O}_2$ diagrams given by Afifi et al. (1988a, 1988b). The general

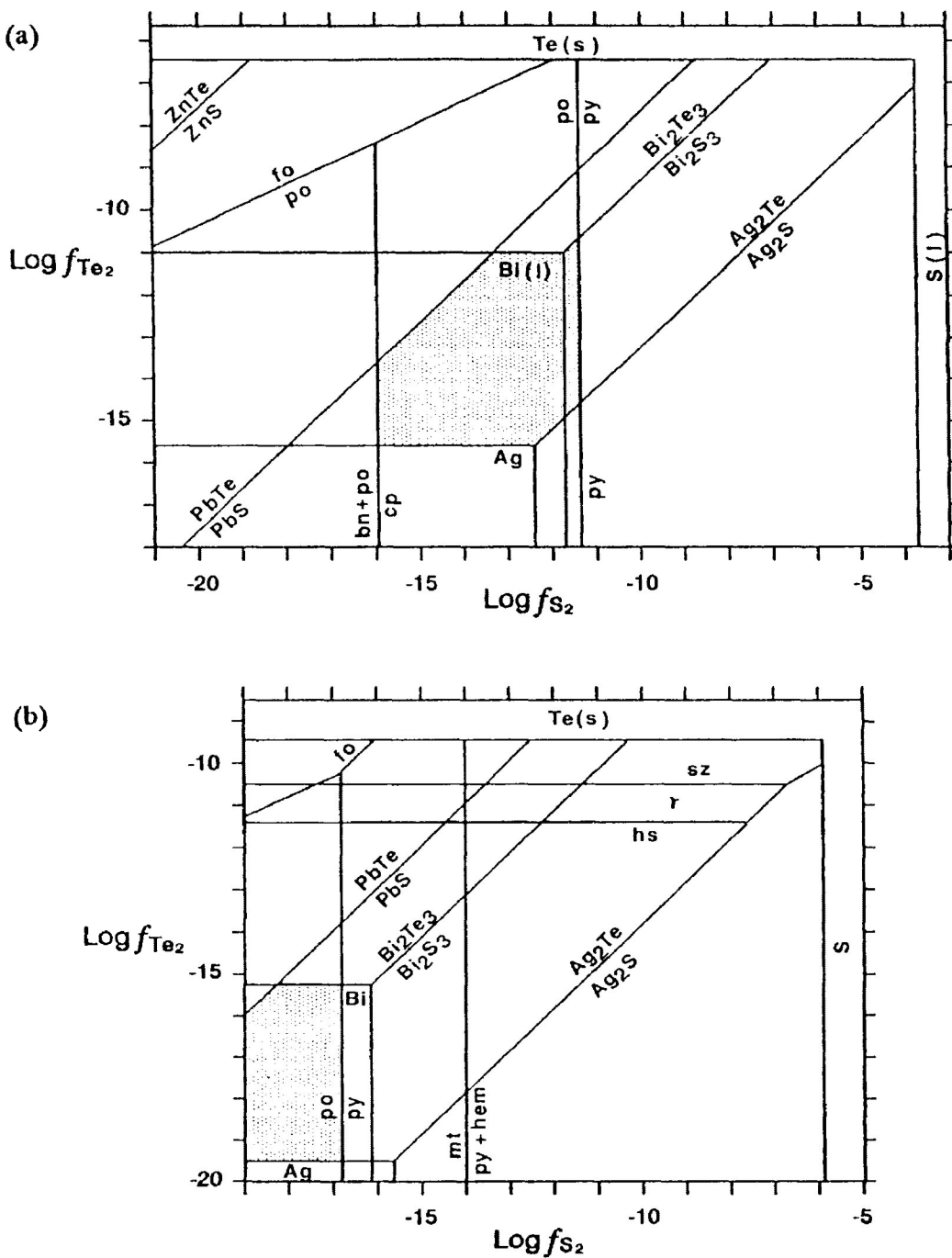


Figure 10.1 : $\text{Log } f_{\text{Te}_2}$ vs. $\text{Log } f_{\text{S}_2}$. a) at 300°C (after Afifi et al., 1988a) b) at 200°C (after Afifi et al., 1988b). Shaded region is the range in f_{Te_2} and f_{S_2} for the Kawene Intrusion. fo - frobergite (FeTe_2), po - pyrrhotite, py - pyrite, bn - bornite, cp - chalcopyrite, sz - stutzite, hs - hessite, mt - magnetite, hem - hematite.

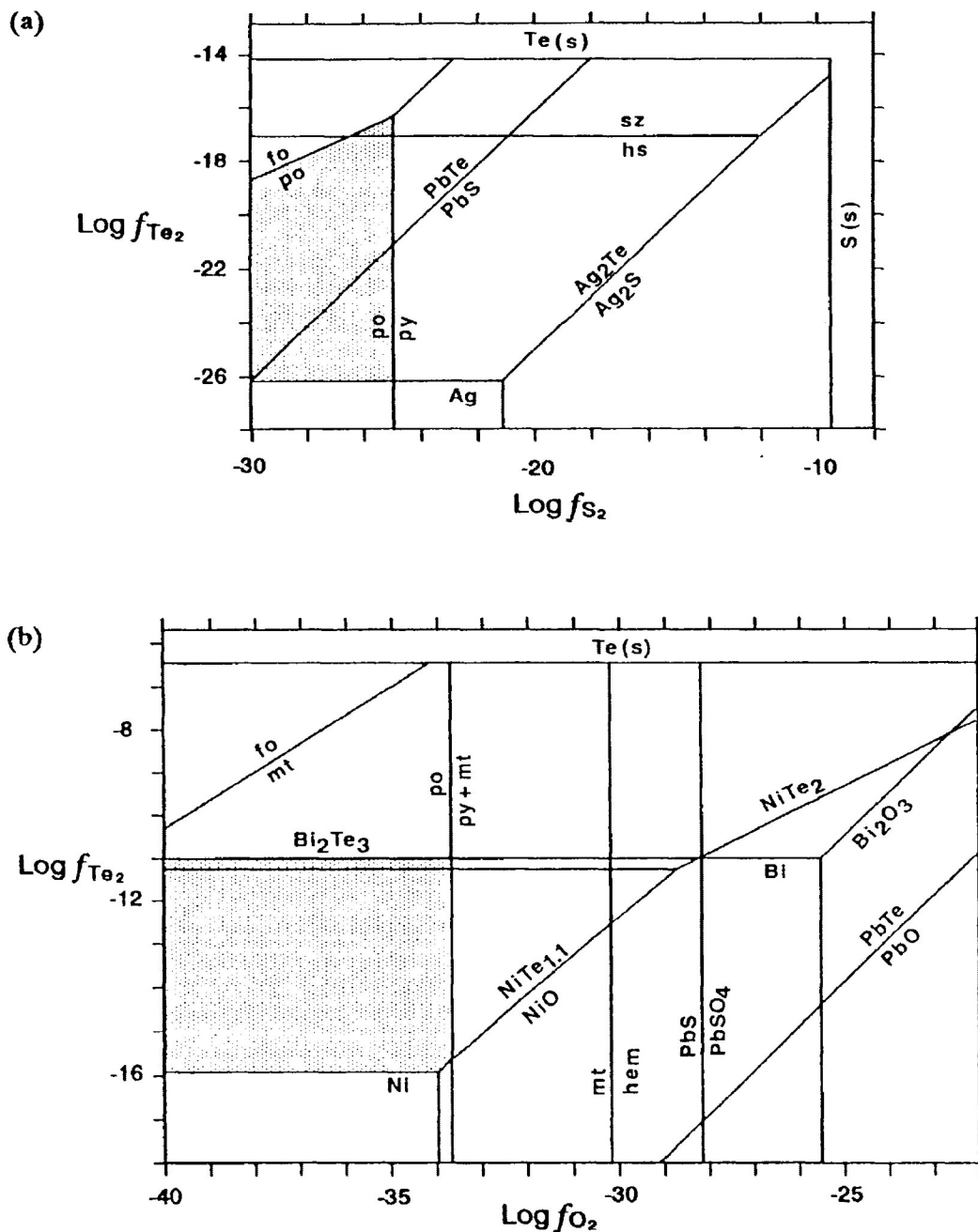


Figure 10.2 : a) $\text{Log } f_{\text{Te}_2}$ vs. f_{S_2} at 100°C (after Afifi et al., 1988a). b) $\text{Log } f_{\text{Te}_2}$ vs. f_{O_2} at 300°C (after Afifi et al., 1988a). Shaded region is the range in f_{Te_2} , f_{S_2} , and f_{O_2} for the Kawene Intrusion. fo - frobergite, po - pyrrhotite, py - pyrite, sz - stutzite, hs - hessite, mt - magnetite, hem - hematite.

trend for the deposition of the PGM is as the temperature decreases, the $f\text{Te}_2/f\text{S}_2$ increases. In assemblage 1 at 300 °C, the Te fugacity is approximately equal to the S fugacity (Figure 10.1a). The $f\text{Te}_2$ ranges from 10^{-11} to $10^{-15.5}$ bars, and the $f\text{S}_2$ ranges from 10^{-11} to 10^{-16} bars. In assemblage 1 at 200 °C, the $f\text{Te}_2$ is greater than the $f\text{S}_2$ (Figure 10.1b). The $f\text{Te}_2$ ranges from $10^{-15.2}$ to $10^{-19.5}$ bars, and $f\text{S}_2$ is $< 10^{-16.9}$ bars. In assemblage 2 at 100 °C, the $f\text{Te}_2$ is greater than the $f\text{S}_2$ (Figure 10.2a). The $f\text{Te}_2$ ranges from 10^{-16} to 10^{-26} bars, and $f\text{S}_2$ is $< 10^{-25}$ bars.

The mineral assemblages reflect the general trend in the Te and S fugacities (Afifi et al., 1988a). The presence of primary pyrrhotite and the absence of pyrite indicates a low S fugacity during the crystallization of the sulfides. In the majority of hydrothermal deposits, the crystallization of the tellurides after the sulfides represents an increase in the $f\text{Te}_2/f\text{S}_2$ ratio (Afifi et al., 1998b).

In assemblage 1 below 489 °C, Pd - Bi compounds and michenerite are common, and kotulskite (PdTe) and vysotskite (PdS) are absent which indicates low $f\text{Te}_2$ and low $f\text{S}_2$. Kotulskite is common in hydrothermal PGE deposits (e.g. Kola region, Blue Lake, and New Rambler) (Yakovlev et al., 1991; Beaudoin et al., 1990; Nyman et al., 1990). In assemblage 1, Bi occurs in native Bi, Bi - S compounds, Bi_2Te , and $\text{Bi}_4(\text{Te},\text{S},\text{Se})_3$. The presence of $\text{Bi}_4(\text{Te},\text{S},\text{Se})_3$ indicates $f\text{Te}_2 \approx f\text{S}_2$ (Afifi et al., 1988a). In assemblage 2, Bi only occurs in the more Te-rich Bi_3Te_2 and pilsenite which indicates $f\text{Te}_2 > f\text{S}_2$. In assemblage 1, Pb occurs in galena, and in assemblage

2, Pb occurs as galena and altaite. In assemblage 1, Ag occurs only in electrum, and argentite (Ag_2S) is absent. In assemblage 2, Ag occurs in hessite and stutzite. Therefore, assemblage 1 has $f\text{Te}_2 \approx f\text{S}_2$, and assemblage 2 has $f\text{Te}_2 > f\text{S}_2$.

The O_2 fugacity is low during the deposition of the PGM, as the $f\text{O}_2$ is less than $10^{-33.5}$ bars at 300 °C (Figure 10.2b). The presence of abundant pyrrhotite and rare magnetite is further evidence of a reducing environment (McQueen, 1990). Most metal oxides, except those of Fe, are not in equilibrium with sulfides and tellurides, which is consistent with the absence of all oxides except magnetite from hydrothermal telluride deposits (Afifi et al., 1988a).

10.3. Hydrothermal Origin of Platinum - Group Minerals

Many Platinum - Group Elements (PGE) deposits are believed to have a hydrothermal origin. Some of the PGE deposits recently interpreted to be hydrothermal are : Deep Copper Zone, Sudbury (Li and Naldrett, 1993; Farrow and Watkinson, 1992), in mafic - ultramafic massifs, Kola Peninsula, USSR (Yakovlev et al., 1991), Blue Lake, Labrador Trough (Beaudoin et al., 1990), Cu - Ni sulfide ore zone in the basal troctolites, Duluth Complex (Mogessie et al., 1991; Ripley, 1990), New Rambler (Nyman et al., 1990), Geordie Lake Intrusion, Coldwell Complex (Mulja and Mitchell, 1991, 1990), Salt Chuck Intrusion, Alaska (Watkinson and Melling, 1992), Boston Creek Flow, Northeastern Ontario (Stone et al., 1992), and upper zone of the Eastern Bushveld Complex (Harney and Merkle, 1990).

The Kawene Intrusion has many features in common with the

above. The characteristics that suggest that the Kawene Intrusion is a hydrothermal Platinum - Group Element deposit are :

1. The alteration of clinopyroxene and hornblende to actinolite, and the uralitization of clinopyroxene is common in the mineralized zone of the Kawene Intrusion. Clinopyroxene and hornblende also alter to chlorite, biotite, and calcite. Calcite is found at grain boundaries between sulfides and silicates.

In the Deep Copper Zone of the Sudbury Complex, the Cu-rich veins, stringers, and disseminations are commonly rimmed by alteration selvages that may include amphibole, chlorite, K-feldspar, albite, and calcite (Farrow and Watkinson, 1992). The calcite is concentrated along the edge of and enclosed within sulfide veinlets (Farrow and Watkinson, 1992). In the Duluth Complex, the pyroxene is replaced by amphibole (Ripley, 1990). In the Salt Chuck Intrusion, alteration and metamorphism has produced an alteration assemblage of actinolite, chlorite, titanite, and calcite (Watkinson and Melling, 1992). In addition, some of the sulfides in this intrusion are found within calcite-rich veinlets, or rimmed by calcite (Watkinson and Melling, 1992). In the Boston Creek Flow, during the cooling of the flow and later greenschist - facies metamorphism, clinopyroxene altered to amphibole, and the groundmass altered to amphibole and chlorite (Stone et al., 1992). In the upper zone of the Eastern Bushveld Complex, the pyroxene has altered to amphibole, chlorite, and calcite (Harney and Merkle, 1990).

2. The Kawene Intrusion contains pentlandite altering to

violarite, Se-bearing galena intergrown with Bi - Te - Se - S compounds, and sphalerite which are a known hydrothermal minerals. Primary pyrrhotite and chalcopyrite contain inclusions of euhedral, prismatic amphibole and chlorite grains.

At Blue Lake and in the Duluth Complex, the pentlandite has also altered to violarite (Beaudoin et al., 1990; Mogessie et al., 1991). The upper zone of the Eastern Bushveld Complex contains pentlandite altering to violarite, and minor amounts of sphalerite and galena (Harney and Merkle, 1990). The presence of sphalerite in the Boston Creek Flow and in the upper zone of the Eastern Bushveld Complex is evidence of hydrothermal processes, since sphalerite is unlikely to crystallize from a sulfide liquid (Stone et al., 1992; Harney and Merkle, 1990). Minor amounts of sphalerite and galena are found in the Deep Copper Zone, New Rambler, and Geordie Lake Intrusion (Li and Naldrett, 1993; Nyman et al., 1990; Mulja and Mitchell, 1990). In the Salt Chuck Intrusion, there is a close spatial relationship between PGM and minor galena (Watkinson and Melling, 1992).

In the Deep Copper Zone, needle - like and prismatic amphiboles are enclosed within sulfides (Farrow and Watkinson, 1992). In the Duluth Complex, the sulfides are intergrown with hydrous silicates (i.e. biotite) (Mogessie, 1991; Ripley, 1990). In the Salt Chuck Intrusion, the sulfides are intimately intergrown with hydrous silicates (i.e. amphibole) (Watkinson and Melling, 1992).

3. The most common PGE found in the Kawene Intrusion is Pd

followed by Pt. The C1-chondrite normalized PGE + Au plot for the Kawene Intrusion has a positively - sloped profile with Pd > Au > Pt > Rh >> Ir > Ru > Os (see MacTavish, 1992, Figure 5.13). Pd and Pt are the most soluble PGE in sulfide melts. Pd-bearing minerals dominate the Kawene Intrusion and all of the above hydrothermal PGE deposits, followed by the Pt-bearing mineral sperrylite, and minor amounts of the Rh-bearing mineral hollingworthite. The C1-chondrite normalized PGE + Au plot for the Kawene Intrusion resembles the plot for the hydrothermal deposit at Rathbun Lake (see MacTavish, 1992, Figure 5.13, 5.14). In the Geordie Lake Intrusion, the predominance of Pd over Pt-bearing minerals is attributed to the relatively evolved nature of the magma (Mulja and Mitchell, 1990).

4. Michenerite and Pd - Bi compounds dominate the Kawene Intrusion. Pd-bismuthotelluride minerals are considered to be of low temperature origin (Edgar et al., 1989). Other known low temperature hydrothermal minerals found in the Kawene Intrusion are : native Bi, bismuthinite, pilsenite, hessite, stutzite, cobaltite, and electrum. These minerals are also found in other hydrothermal PGE deposits (see chapter 6, 7, 8).

5. In the Kawene Intrusion, the paragenesis of the PGM, in descending order of abundance, are : enclosed within sulfides, at sulfide - silicate boundaries, enclosed within silicates, and at silicate - silicate boundaries. All of the PGM occur in all of the parageneses. Generally, magmatic PGM occur enclosed within sulfides, and are not found enclosed within silicates. The PGM

from the Kawene Intrusion range in habit from subhedral - to - euhedral. Their subhedral - euhedral morphology may reflect the greater force of crystallization by the PGM (Edgar et al., 1989).

In the Deep Copper Zone, Sudbury the PGM occur at the margins of sulfides, in microfractures of sulfides, and at sulfide - chlorite boundaries which suggests that the PGM crystallized after the sulfide minerals (Li and Naldrett, 1993). In the Kola region, USSR, the PGM occur within sulfides, at sulfide - silicate boundaries, and within silicates (Yakovlev et al., 1991). At Blue Lake, sudburyite occurs at sulfide - silicate boundaries in dynamically metamorphosed rocks which indicates that it precipitated directly from hydrothermal fluids (Beaudoin et al., 1990). In the Duluth Complex, the PGM are mainly located at sulfide - silicate boundaries or enclosed within altered plagioclase and olivine which suggests that the PGM were transported and deposited during a late magmatic, hydrothermal event related to the introduction of volatiles from the metasedimentary rocks (Mogessie et al., 1991). In the Salt Chuck Intrusion, the PGM are found enclosed within silicates (mostly epidote), enclosed within sulfides (mostly bornite and chalcopyrite), and at silicate - sulfide grain boundaries (Watkinson and Melling, 1992). In the Boston Creek Flow, PGM occur in fractures in pyrite, enclosed within secondary silicates, and at silicate grain boundaries (Stone et al., 1992). In the upper zone of the Eastern Bushveld Complex, most of the PGM are enclosed in silicates, and the remaining PGM are at silicate - sulfide

Table 10.2 : Temperature of formation of other hydrothermal deposits. Only minerals that are also found in the Kawene Intrusion are mentioned.

Geordie Lake Intrusion - 550 - 400 °C

- michenerite, sperrylite, electrum, hessite, altaite,
- cobaltite, galena (Mulja and Mitchell, 1990, 1991)

Jales, Northern Portugal - < 550 °C

- electrum, bismuthinite, native Bi, cobaltite, galena
- (Neiva and Neiva, 1990)

Upper Zone of the Eastern Bushveld - 490 - 400 °C

- michenerite, froodite, sperrylite, Bi-Te compounds,
- Ag-Te compounds, cobaltite, galena (Harney and Merkle, 1990)

Tunaberg, Central Sweden - 475 - 228 °C

- electrum, native Bi, bismuthinite, hessite, cobaltite,
- Se-bearing galena (Dobbe, 1991)

New Rambler, Wyoming - 475 - 300 °C

- michenerite, sperrylite, electrum, galena
- (Nyman et al., 1990; McCallum et al., 1976)

Glava, Sweden - 400 - 145 °C

- electrum, hessite, stutzite, altaite, cobaltite
- (Oen and Kieft, 1984)

Deep Copper, Sudbury - < 300 °C

- michenerite, froodite, sobolevskite, sperrylite, native Bi,
- bismuthinite, hessite, altaite, galena
- (Li and Naldrett, 1993; Farrow and Watkinson, 1992)

Ashanti, Ghana - 220 - 165 °C

- hessite, stutzite, altaite, galena (Bowell et al., 1990)

boundaries and enclosed within sulfides (Harney and Merkle, 1990).

6. Some of the PGM are found in clusters. One polished thin section may have as many as 171 PGM grains or as little as no PGM grains. Clustering of PGM grains is characteristic of the hydrothermal PGE deposit at Rathbun Lake, Ontario (Edgar et al., 1989).

7. There is no difference in the PGM assemblage, and the sulfides in the clinopyroxenites and hornblendites. Therefore, the PGM are not associated with one ultramafic rock type. The PGM are not found in the tonalite veins.

8. The temperature of formation of PGM assemblage 1 is estimated to be from 489 - 254 °C, and of PGM assemblage 2 from 145 - 120 °C (section 10.1). Table 10.2 lists the temperature of formation of some other hydrothermal PGM deposits. The Tunaberg, New Rambler, Glava, Deep Copper, and Ashanti deposits are considered to have similar temperatures of formation as the Kawene Intrusion (Table 10.2). The minerals in the Upper Zone of the Eastern Bushveld and Deep Copper deposits resemble assemblage 1, and the minerals in the Ashanti deposit resembles assemblage 2 of the Kawene Intrusion (Table 10.2).

10.4. Hydrothermal Genesis

The immiscible sulfide melt separated from the silicate melt, and the sulfide melt remained as a liquid until the silicate host rocks had cooled to subsolidus temperatures (Mulja and Mitchell, 1991). The sulfide melt and residual water - rich fluids were

trapped together within pore spaces (Mulja and Mitchell, 1991). Hydrous silicates (amphibole and chlorite) and calcite crystallized from the Ca- and volatile-rich residual fluid. This was followed by the crystallization of hexagonal pyrrhotite.

A late - stage, hydrothermal fluid remobilized the Pd and Pt from the hexagonal pyrrhotite and within the immiscible sulfide melt (Watkinson and Melling, 1992; Stone et al., 1992; Yakovlev et al., 1991). The PGE were then transported, concentrated, and finally precipitated as PGM by the volatile-rich, hydrothermal fluid (Farrow and Watkinson, 1992; Yakovlev et al., 1991; Beaudoin et al., 1990). PGM assemblage 1 and Se - bearing galena crystallized at 489 - 254 °C. Crystallization of the PGM assemblage 1 was followed by crystallization of monoclinic pyrrhotite, chalcopyrite, and pentlandite. Large, euhedral grains of sperrylite, michenerite, and stibiopalladinite - sobolevskite (ss) are found enclosed in monoclinic pyrrhotite. Monoclinic pyrrhotite, chalcopyrite, and pentlandite have euhedral boundaries to each other suggesting simultaneous crystallization. PGM assemblage 2 crystallized at 145 - 120 °C from the same, yet more evolved, hydrothermal fluid. Assemblage 2 did not crystallize as a result of metamorphism of the sulfides and PGM assemblage 1, as assemblage 2 is only found in samples 13D-1, 13D-2, and AK-9-86B, and all of the Kawene Intrusion has been metamorphosed.

Metamorphism of the ultramafic rocks had little affect on the PGM and sulfides, but further altered the silicates. Metamorphic, hydrothermal fluid altered pentlandite to violarite, and

precipitated sphalerite. The metamorphic, hydrothermal fluid also altered the silicates to amphibole, chlorite, and calcite (Watkinson and Melling, 1992).

Chapter 11

Conclusions

11.1. General Statement

The Kawene Intrusion is an ultramafic, layered, metamorphosed Cu- Ni- PGE- bearing intrusion located 29 km east of Atikokan within the Quetico Subprovince of northwestern Ontario. The Kawene Intrusion is emplaced primarily in metasedimentary turbiditic wacke. Metasedimentary migmatite is found along its northern margin. The intrusion is composed of hornblende wehrlite in the center, with hornblende clinopyroxenite, clinopyroxene hornblendite, and hornblende melagabbro at the margin (Figure 1.1). The intrusion is modally layered with gradational contacts between the alternating clinopyroxenite and hornblendite layers. The intrusion has been metamorphosed to upper greenschist - to - lower amphibolite metamorphic grade (Pirie and Mackasey, 1978). This indicates P-T conditions of 2.5 - 3.2 Kb and 450 - 525 °C (MacTavish, 1992). MacTavish (1992) believed that the Quetico intrusions resemble appinite suite bodies rather than Alaskan - type complexes.

The mineralized area of the Kawene Intrusion, located along the northeastern margin, is 90 m long, 30 m wide, and 17 m thick (Figure 1.2). The mineralized area is composed of alternating layers of hornblende clinopyroxenite and clinopyroxene hornblendite intruded by tonalite veins, and sulfide veinlets. The sulfide veinlets and the disseminated sulfides consist mainly of chalcopyrite, pyrrhotite, and pentlandite. The Platinum - Group

Minerals (PGM) are spatially associated with the sulfides.

11.2. Silicate Petrology

The mineralogy and petrology of the clinopyroxenites and hornblendites are identical except for variable amounts of clinopyroxene, hornblende, and biotite. The mafic silicates in the ultramafic rocks are Ca- and Mg-rich. The primary minerals in these ultramafic rocks are : augite, diopside, magnesio - hornblende, actinolitic - hornblende, phlogopite, calcite, and sulfides. The accessory minerals are : apatite, K-feldspar, albite, oligoclase, rutile, and rare zircon, and sphene. Alteration of clinopyroxene and hornblende to actinolite is common in these rocks. Clinopyroxene and hornblende also alter to secondary biotite, secondary calcite, and chlorite (ferrous clinochlore). Feldspar alters to saussurite, sericite, secondary calcite, and rare epidote.

The mineralized zone is cut by tonalite veins containing the primary minerals : 20 - 50 vol% quartz, 15 - 48 vol% oligoclase and Na-andesine, 1 - 40 vol% magnesio - hornblende and actinolitic - hornblende, and 2 - 25 vol% biotite (Al-annite). The hornblendes and biotites in the tonalite veins are more Fe-rich than in the ultramafic rocks. The accessory minerals are apatite, sphene, sulfides, and rare microcline. The plagioclase alters to saussurite, sericite, secondary calcite, epidote, and minor muscovite.

11.3. Sulfide Petrology

In the Kawene Intrusion, the most common sulfides in the ultramafic clinopyroxenites and hornblendites are pyrrhotite (hexagonal and monoclinic) and chalcopyrite. The other sulfides found in these ultramafic rocks in decreasing order of abundance are ; pentlandite, galena, violarite, and sphalerite. Pyrrhotite, chalcopyrite, and pentlandite are commonly found either intergrown in veinlets which intrude the ultramafic rocks, or are interstitial to euhedral silicates. Pyrrhotite and chalcopyrite contain euhedral silicate (mostly hornblende and chlorite) inclusions.

The most common sulfide in the tonalite veinlets is pyrite. The other sulfides in order of decreasing abundance are ; pyrrhotite, chalcopyrite, pentlandite, and galena. The major difference between the sulfides in the ultramafic rocks and those in the tonalite veinlets is that the ultramafic rocks do not contain pyrite. The grain size of the sulfides in the ultramafic rocks is much larger (mm scale) than the grain size in the tonalite veinlets (μm scale).

11.4. Platinum - Group Minerals

A total of 1078 Platinum Group Minerals (PGM), Bi telluride and Bi sulfide grains were found in 42 polished thin sections from the mineralized area of the Kawene Intrusion (Table 6.1). The most common PGM are : PdBiTe (michenerite), PdBi₂ (floodite), Pd₂Bi₅ (unnamed), PtAs₂ (sperryllite), and native Bi. The compositional groups of the PGM in descending order of abundance are :

1. Pd - Bi compounds, michenerite, Pd-Bi-Te-Sb compounds
2. native Bi, Bi - S compounds, Bi - Te compounds, Bi-Te-Se-S compounds
3. sperrylite, (Ag,Ni)S, hessite, stutzite, Co-bearing hollingworthite, electrum, altaite.

The PGM range in size from 1 - 25 μm , and in habit from euhedral - to - subhedral.

The most abundant Platinum Group Minerals parageneses are enclosed within sulfides, and at sulfide - silicate boundaries. The other PGM parageneses are enclosed within silicates (usually clinopyroxenes), and at silicate - silicate boundaries. PGM are associated with the following sulfides in descending order of frequency of occurrence : chalcopyrite, pyrrhotite, pentlandite, violarite, minor galena, and minor sphalerite.

In the Kawene Intrusion, 98 grains (9% of the total PGM grains) are intergrowths of two or more platinum - group minerals, Bi - S compounds, or Bi - Te compounds. In the Kawene Intrusion, the most common intergrowths occur between :

- | | |
|--|---------------|
| 1. Pd - Bi and Bi - S compounds, | 17 grains; |
| 2. Pd - Bi compounds, | 11 grains; |
| 3. native Bi and Bi - S compounds, | 9 grains; |
| 4. Pd - Bi compounds and michenerite, | 8 grains; and |
| 5. Pd - Bi, Bi - S compounds, and michenerite, | 4 grains. |

These intergrowths reflect the relatively high abundance of Pd - Bi compounds, michenerite, Bi - S compounds, and native Bi.

The PGM intergrowths from the Kawene Intrusion indicate

simultaneous crystallization. In the Kawene Intrusion, the Pd - Bi - Te - Sb compositional group, Bi - Te - Se - S compositional group, electrum, Se-bearing galena, sperrylite, and Co-bearing hollingworthite crystallized at the same time (assemblage 1). Hessite, stutzite, altaite, Se-bearing galena, Bi_3Te_2 , pilsenite, and Pt - Sb compounds crystallized at the same time (assemblage 2), but not at the same time as the minerals in assemblage 1. The minerals in assemblage 2 are only found in samples 13D-1, 13D-2, and AK-9-86B, whereas the rest of the PGM are found throughout the mineralized area.

The temperature range over which each PGM assemblage crystallized was estimated using the intergrowth textures in conjunction with the maximum thermal stability temperatures of the minerals (Table 10.1). Assemblage 1 crystallized between 489 - 254 °C, and assemblage 2 between 145 - 120 °C.

The Platinum Group Minerals, Bi - S compounds, and Bi - Te compounds may cluster together. In the Kawene Intrusion, 36 clusters were found containing 382 grains (35% of the total PGM grains). The maximum number of PGM grains found in one cluster is 73, and the average is 11. The most common PGM found in clusters are Pd - Bi compounds, michenerite, Bi - S compounds, and Bi - Te compounds which reflects their abundance in the intrusion.

The Te_2 , S_2 , and O_2 fugacity (f) stability fields during PGM deposition were determined using the isothermal f_{Te_2} - f_{S_2} and f_{Te_2} - f_{O_2} diagrams given by Afifi et al. (1988a, 1988b). The general trend for the deposition of the PGM is, as the temperature

decreases, the $f\text{Te}_2/f\text{S}_2$ increases. In assemblage 1 at 300 °C, the Te fugacity is approximately equal to the S fugacity (Figure 10.1a). The $f\text{Te}_2$ ranges from 10^{-11} to $10^{-15.5}$ bars, and the $f\text{S}_2$ ranges from 10^{-11} to 10^{-16} bars. In assemblage 1 at 200 °C, the $f\text{Te}_2$ is greater than the $f\text{S}_2$ (Figure 10.1b). The $f\text{Te}_2$ ranges from 10^{-15} to $10^{-19.5}$ bars, and $f\text{S}_2$ is $< 10^{-16.9}$ bars. In assemblage 2 at 100 °C, the $f\text{Te}_2$ is greater than the $f\text{S}_2$ (Figure 10.2a). The $f\text{Te}_2$ ranges from 10^{-16} to 10^{-26} bars, and $f\text{S}_2$ is $< 10^{-25}$ bars. Therefore, assemblage 1 has $f\text{Te}_2 \approx f\text{S}_2$, and assemblage 2 has $f\text{Te}_2 > f\text{S}_2$.

The O_2 fugacity is low during the deposition of the PGM, as the $f\text{O}_2$ is less than $10^{-33.5}$ bars at 300 °C (Figure 10.2b). The presence of abundant pyrrhotite and rare magnetite is further evidence of a reducing environment (McQueen, 1990).

11.5. Hydrothermal Origin

The characteristics that suggest that PGE mineralization in the mineralized zone of the Kawene Intrusion is hydrothermal in origin are :

1. The alteration of clinopyroxene and hornblende to actinolite, and the uranalitization of clinopyroxene is common in the mineralized zone of the Kawene Intrusion. Clinopyroxene and hornblende also alter to chlorite, biotite, and calcite. Calcite is found at grain boundaries between sulfides and silicates.

2. The Kawene Intrusion contains pentlandite altering to violarite, Se-bearing galena intergrown with Bi - Te - Se - S compounds, and sphalerite which are a known hydrothermal minerals.

3. Michenerite and Pd - Bi compounds dominate the Kawene Intrusion. Other known low temperature hydrothermal minerals found in the Kawene Intrusion are : native Bi, bismuthinite, pilsenite, hessite, stutzite, cobaltite, and electrum.

4. In the Kawene Intrusion, the paragenesis of the PGM, in descending order of abundance, are : enclosed within sulfides, at sulfide - silicate boundaries, enclosed within silicates, and at silicate - silicate boundaries.

5. Some 35% of the PGM are found in clusters possibly due to the dissolution of PGE-rich sulfides by late fluids.

6. There is no difference in the PGM assemblage, and the sulfides in the clinopyroxenites and hornblendites. Therefore, the PGM are not associated with one ultramafic rock type. The PGM are not found in the tonalite veins.

7. The temperature of formation of PGM assemblage 1 is estimated to be from 489 - 254 °C, and of PGM assemblage 2 from 145 - 120 °C (section 10.1). These temperatures are similar to those found for other hydrothermal deposits (Table 10.2).

11.6. Petrogenesis of the Mineralized Area of the Kawene Intrusion

The Quetico intrusions crystallized from a sub-alkaline, possibly calc-alkaline, olivine basalt liquid at relatively high P_{H_2O} (MacTavish, 1992). The intrusions must have crystallized under relatively high P_{H_2O} in order for hornblende to be stable over such a wide range of magmatic conditions (MacTavish, 1992).

The immiscible sulfide melt separated from the silicate melt,

and the sulfide melt remained as a liquid until the silicate host rocks had cooled to subsolidus temperatures (Mulja and Mitchell, 1991). The primary minerals of the clinopyroxenites and hornblendites (apatite, clinopyroxene, sphene, prismatic hornblende, biotite, columnar hornblende, feldspar, and oikocrystic actinolite) crystallized first. The sulfides are interstitial to euhedral silicates. The enclosing silicate minerals generally crystallize before the sulfide minerals (pyrrhotite, pentlandite, and chalcopyrite) (Craig, 1990; Garuti et al., 1986).

The sulfide melt and residual water - rich fluids were trapped together within pore spaces between the primary silicates (Mulja and Mitchell, 1991). At the same time, pre-existing primary, anhydrous silicates altered to secondary, hydrous silicates (actinolite, chlorite, bioite, calcite, and epidote), and the clinopyroxene was uralitized. Since sulfides and secondary minerals crystallize at similar low temperatures, these minerals may have formed at approximately the same time. This would explain why euhedral chlorite can be found enclosed in sulfides. Interstitial calcite crystallized from the Ca- and volatile-rich residual fluid.

A late - stage, hydrothermal fluid remobilized the Pd and Pt from the hexagonal pyrrhotite and within the immiscible sulfide melt (Watkinson and Melling, 1992; Stone et al., 1992; Yakovlev et al., 1991). The PGE were then transported, concentrated, and finally precipitated as PGM by the volatile-rich, hydrothermal fluid (Farrow and Watkinson, 1992; Yakovlev et al., 1991; Beaudoin

et al., 1990). PGM assemblage 1 and Se - bearing galena crystallized at 489 - 254 °C.

Crystallization of the PGM assemblage 1 was followed by crystallization of monoclinic pyrrhotite, chalcopyrite, and pentlandite below 254 °C. The hexagonal pyrrhotite has jagged, irregular margins which suggests that it was replaced by the surrounding monoclinic pyrrhotite. Large, euhedral grains of sperrylite, michenerite, and stibiopalladinite - sobolevskite (ss) are found enclosed in monoclinic pyrrhotite. Monoclinic pyrrhotite, chalcopyrite, and granular pentlandite have mutual euhedral boundaries to each other suggesting simultaneous crystallization. Upon cooling of the monoclinic pyrrhotite, pentlandite flames exsolved (< 150 °C).

PGM assemblage 2 crystallized at 145 - 120 °C from the same, yet more evolved, hydrothermal fluid. Assemblage 2 did not crystallize as a result of metamorphism of the sulfides and PGM assemblage 1, as assemblage 2 is only found in sample 13D-1, 13D-2, and AK-9-86B, and all of the Kawene Intrusion has been metamorphosed. This narrow area of rock may be a late shear zone.

Tonalite veins intruded the clinopyroxenites and hornblendites. The tonalite veins are not cut by sulfide veinlets. Hornblende and biotite in the intruded ultramafic rocks are aligned parallel to the tonalite veins, but not to the sulfide veinlets. Therefore, the tonalite veins intruded the ultramafic rocks after the sulfide veinlets.

As both the ultramafic rocks and the tonalite veins have been

affected by metamorphism, the metamorphic event must have occurred after the cooling of the ultramafic rocks and the tonalite veins. Metamorphism of the ultramafic rocks to upper greenschist - to - lower amphibolite metamorphic grade had little affect on the PGM and sulfides, but further altered the silicates (Pirie and Mackasey, 1978). Metamorphic, hydrothermal fluid precipitated sphalerite and altered pentlandite to violarite below 461 °C. The violarite could not have crystallized from the same hydrothermal fluid that deposited the PGM because pentlandite crystallized after PGM assemblage 1, and PGM assemblage 2 only occurs in a small portion of the mineralized zone, whereas violarite occurs throughout the entire mineralized zone. The metamorphic, hydrothermal fluid also further altered the silicates to amphibole, chlorite, and calcite (Watkinson and Melling, 1992).

References

- Afifi A.M., Kelly W.C., and Essene E.J. (1988a), Phase relations among Tellurides, Sulfides, and Oxides : I. Thermochemical data and calculated equilibria, **83**, 377 - 394.
- Afifi A.M., Kelly W.C., and Essene E.J. (1988b), Phase relations among Tellurides, Sulfides, and Oxides : II. Applications to telluride-bearing ore deposits, **83**, 395 - 404.
- Alderton D.H.M. (1986), Hessite and electrum from the Ratagain intrusion, north-west Scotland. *Mineralogical Magazine*, **50**, 179.
- Anthony J.W., Bideaux R.A., Bladh K.W., and Nichols M.C. (1990), *Handbook of Mineralogy, Volume 1 Elements, Sulfides, Sulfosalts*. Mineral Data Publishing, Tucson, Arizona.
- Augustithis S.S. (1990), *Atlas of Metamorphic - Metasomatic Textures and Processes..* Elsevier, New York.
- Arnold R.G. (1966), Mixtures of hexagonal and monoclinic pyrrhotite and the measurement of the metal content of pyrrhotite by x-ray diffraction. *American Mineralogist*, **51**, 1221 - 1227.
- Bailey S.W. (1980), Summary of recommendations of AIPEA nomenclature committee on clay minerals. *American Mineralogist*, **65**, 1 - 7.
- Bailey S.W. (1988), Chlorites : Structures and Crystal Chemistry, in (ed.), *Hydrous Phyllosilicates (exclusive of micas)*, *Reviews in Mineralogy*, volume 19, Mineralogical Society of

American, chapter 10.

- Barton P. B. and Skinner B.J. (1967), *Geochemistry Of Hydrothermal Ore Deposits*, Holt, Rinehart, and Winston, New York, 236 - 333.
- Bayliss P. (1969), X-ray data, optical anisotropism, and thermal stability of cobaltite, gersdorffite, and ullmannite. *Mineralogical Magazine*, **37**, 26 - 33.
- Bayliss P. (1982), A further crystal structure refinement of cobaltite. *American Mineralogist*, **67**, 1048 - 1057.
- Bayliss P. (1989), Crystal chemistry and crystallography of some minerals within the pyrite group. *American Mineralogist*, **74**, 1168 - 1176.
- Bayliss P. (1991), Crystal chemistry and crystallography of some minerals in the tetradymite group. *American Mineralogist*, **76**, 257 - 265.
- Beaudoin G., Laurent R., and Ohnenstetter D. (1990), First report of Platinum - Group Minerals at Blue Lake, Labrador Trough, Quebec. *Canadian Mineralogist*, **28**, 409 - 418.
- Berry L.G. and Thompson R.M. (1962), X-ray powder data for Ore Minerals : the Peacock Atlas. *Geol. Soc. Am. Mem.* 85.
- Best M.G. (1982), *Igneous and Metamorphic Petrology*. W.H. Freeman and Company, San Francisco.
- Bowell R.J., Foster R.P., and Stanley C.J. (1990), Telluride mineralization at Ashanti gold mine, Ghana. *Mineralogical Magazine*, **54**, 617 - 627.
- Brown A. and Lewis B. (1962), The systems Bismuth - Tellurium and

Antimony - Tellurium and the synthesis of the minerals hedleyite and wehrlite. *J. Phys. Chem. Solids*, **23**, 1597 - 1604.

Brynard H.J., De Villiers J.P.R., and Viljoen E.A. (1976), A mineralogical investigation of the Merensky Reef at the Western Platinum mine, near Marikana, South Africa. *Economic Geology*, **71**, 1299 - 1307.

Bryndzia L.T., Scott S.D., and Spry P.G. (1988), Sphalerite and hexagonal pyrrhotite geobarometer : experimental calibration and application to the metamorphosed sulfide ores of Broken Hill, Australia. *Economic Geology*, **83**, 1193 - 1204.

Cabri L.J. (1973), New data on phases relations in the Cu-Fe-S system. *Economic Geology*, **68**, 443 - 454.

Cabri L.J. (1981), Unnamed Platinum - Group Minerals, in Cabri L.J. (editor), *Platinum - Group Elements : mineralogy, geology, recovery*, Canadian Institute of Mining and Metallurgy, Montreal. p 175 - 195.

Cabri L.J. and Chen T.T. (1976), Stibiopalladinite from the type locality. *American Mineralogist*, **61**, 1249 - 1254.

Cabri L.J. and Hall S.R. (1972), Mooihoekite and haycockite, two new copper-iron sulfides and their relationship to chalcopyrite and talnakhite. *American Mineralogist*, **57**, 689 - 708.

Cabri L.J., Harris D.C., and Gait R.I. (1973), Michenerite (PdBiTe) and froodite (PdBi₂) confirmed from Sudbury area. *Canadian*

Mineralogist, **11**, 903 - 912.

Cabri L.J. and Laflamme J.H.G. (1974), Sudburyite, a new Palladium - Antimony mineral from Sudbury, Ontario. Canadian Mineralogist, **12**, 275 - 279.

Cabri L.J. and Laflamme J.H.G. (1976), The mineralogy of the Platinum - Group Elements from some Copper - Nickel deposits of the Sudbury area, Ontario. Economic Geology, **71**, 1159 - 1195.

Cabri L.J. and Laflamme J.H.G. (1981), Analyses of minerals containing Platinum - Group Elements, in Cabri L.J. (editor), Platinum - Group Elements : mineralogy, geology, and recovery, Canadian Institute of mining and metallurgy, Montreal. p. 151 - 173.

Cabri L.J., Laflamme J.H.G., and Stewart J.M. (1977), Platinum -group minerals from Onverwacht. II. Plarasite, a new sulfarsenide of platinum. Canadian Mineralogist, **15**, 385 - 388.

Card K.D. (1990), A review of the Superior Province of the Canadian Shield, a product of Archean accretion. Precambrian Research, **48**, 99 - 156.

Chizhikov D.M. and Shchastlivyi V.P. (1970), Tellurium and Tellurides. Collet's (Publishers) Ltd., London. 152 - 229.

Craig J.R. (1971), Violarite stability relations. American Mineralogist, **56**, 1303 - 1311.

Craig J.R. (1982), The system Cu - Fe - S. Rev. Mineralogy, **1**, 64 - 76.

- Craig J.R. (1990), Textures of the ore minerals, in Jambor J.L. and Vaughan D.J. (editors), Advanced microscopic studies of ore minerals, Mineralogical Association of Canada short course, volume 17, Ottawa. p. 213 - 261.
- Craig J.R. and Scott S.D. (1974), Sulfide phase equilibria, in Ribbe P.H. (editor), Mineralogical Society of America Short Course Notes, Volume 1, chapter 5.
- Craig J.R. and Vaughan D.J. (1981), Ore Microscopy and ore petrology. John Wiley and Sons, Toronto.
- Craig J.R. and Vaughan D.J. (1990), Compositional and textural variations of the major iron and base - metal sulphide minerals, in Gray P.M.J., Bowyer G.J., Castle J.F., Vaughan D.J., and Warner N.A. (editors), Sulphide deposits - their origin and processing, Institution of Mining and Metallurgy, London, England, 1 - 16.
- Deer W.A., Howie R.A., and Zussman J. (1992), An Introduction to the Rock Forming Minerals, second edition. John Wiley and Sons, Inc., New York.
- Dobbe R.T.M. (1991), Tellurides, Selenides and associated minerals in the Tunaberg Copper Deposits, SE Bergslagen, Central Sweden. Mineralogy and Petrology, **44**, 89 - 106.
- Dobbe R. (1993), Bismuth tellurides (joseite-B, bismuthian tsumoite) in a Pb - Zn deposit from Tunaberg, Sweden. European Journal of Mineralogy, **5**, 165 - 170.
- Durazzo A., and Taylor L.A. (1982), Exsolution in the Mss -

Pentlandite system: textural and genetic implications for Ni-sulfide ores. *Mineral. Deposita*, **17**, 313 - 332.

Edgar A.D., Charbonneau H.E., and McHardy D.C. (1989), Pd - bismuthotelluride minerals at Rathbun Lake, Ontario : significance to post-magmatic evolution of PGE deposits. *N. Jb. Miner. Mh.*, **10**, 461 - 475.

Elliot R.P. (1965), *Constitution of Binary Alloys*, first supplement. Mc-Graw - Hill Book Co., New York.

Evstigneeva T.L., Genkin A.D., and Kovalenker V.A. (1975), Sobolevskite, a new bismuthide of palladium, and the nomenclature of minerals of the system PdBi - PdTe - PdSb. *Zap. Vses. Mineral. Obshch.*, **104**, 568 - 579. (translation in *International Geology Review*, 1976, **18(7)**, 856 - 866).

Farrow C.E.G. and Watkinson D.H. (1992), Alteration and the role of fluids in Ni, Cu and Platinum - Group Element deposition, Sudbury Igneous Complex contact, Onaping - Levack area, Ontario. *Mineralogy and Petrology*, **46**, 67 - 83.

Feather C.E. (1976), Mineralogy of Platinum-group minerals in the Witwatersrand, South Africa. *Economic Geology*, **71**, 1399 - 1428.

Fitzgerald R. (1973), *Electron Microprobe Instrumentation*, in Andersen C.A. (editor), *Microprobe Analysis*, John Wiley and Sons, Inc. New York.

Fleischer M. (1966), *Index of new mineral names, discredited*

minerals, and changes of mineralogical nomenclature in Volumes 1 - 50 of the American Mineralogist. American Mineralogist, **51**, 1247 - 1357.

Francis C.A., Fleet M.E., Misra K.C., and Craig J.R. (1976), Orientation of exsolved pentlandite in natural and synthetic nickeliferous pyrrhotite. American Mineralogist, **61**, 913 - 920.

Gamyarin G.N., Leskova N.V., Vyal'sov L.N., and Laputina I.P. (1982), Bismuth tellurides - Bi_2Te and BiTe - in deposits of Northeast USSR. International Geology Review, **24(4)**, 451 - 457.

Garuti G., Fiandri P., and Rossi A. (1986), Sulfide composition and phase relations in the Fe-Ni-Cu ore deposits of the Ivrea - Verbano basic complex (western Alps, Italy). Mineral. Deposita, **22**, 22 - 34.

Garuti G. and Rinaldi R. (1986), Mineralogy of Melonite - group and other Tellurides from the Ivrea - Verbano basic complex, Western Italian Alps. Economic Geology, **81**, 1213 - 1217.

Genkin A.D., Vyal'sov L.N., Evstigneeva T.L., and Marchukova I.D. (1972), Moncheite and michenerite from the copper - nickel ores of the Oktyabrskoe ore deposit. Zap. Vses. Mineral. Obshch., **101**, 112 - 118 (in Russian).

Glatz A.C. (1967), The Bi_2Te_3 - Bi_2S_3 system and the synthesis of the mineral tetradymite. American Mineralogist, **52**, 161 - 170.

Goldstein J.I., Newbury D.E., Echlin P., Joy D.C., Fiori C., and

- Lifshin E. (1981), Scanning Electron Microscopy and X-ray Microanalysis. Plenum Press, New York.
- Guidotti C.V. (1984), Micas in Metamorphic Rocks, in Bailey S.W. (ed.) Micas, Reviews in Mineralogy, volume 13, Mineralogical Society of America, chapter 10.
- Hakli T.A., Hanninen E., Vuorelainen Y., and Papunen H. (1976), Platinum - Group minerals in the Hitura Nickel deposit, Finland. Economic Geology, **71**, 1206 - 1213.
- Harney D.M.W. and Merkle R.K.W. (1990), Pt - Pd minerals from the upper zone of the eastern Bushveld Complex, South Africa. Canadian Mineralogist, **28**, 619 - 628.
- Harris D.C., Sinclair W.D., and Thorpe R.I. (1983), Telluride minerals from the Ashley deposit, Bannockburn Township, Ontario. Canadian Mineralogist, **21**, 137 - 143.
- Hawley J.E. (1962), The Sudbury ores : their mineralogy and origin. Canadian Mineralogist, **6**, 200 - 209.
- Hawley J.E. and Berry L.G. (1958), Michenerite and froodite, palladium bismuth minerals. Canadian Mineralogist, **6**, 200 - 209.
- Hoffman E. and MacLean W.H. (1976), Phase relations of Michenerite and Merenskyite in the Pd - Bi - Te system, **71**, 1461 - 1468.
- Honea R. (1964), Empressite and stuetzite redefined. American Mineralogist, **49**, 325 - 338.
- Hudson D.R. (1986), Platinum - Group minerals from the Kambalda Nickel Deposits, Western Australia. Economic Geology, **81**,

1218 - 1225.

Hudson D.R. and Donaldson M.J. (1984), Mineralogy of platinum group elements in the Kambalda nickel deposits, Western Australia, in D.L. Buchanan and M.J. Jones (editor), Sulphide deposits in mafic and ultramafic rocks, Institution of Mining and Metallurgy. p 55 - 61.

Huot J.J. (1841), Manual de Mineralogie, Paris, 1, 188. as found in (Ozawa and Shimazaki, 1982).

Johanson B. and Kojonen K. (1988), Ore mineralogy of gold occurrences in the Hattu schist belt, Ilomantsi, Eastern Finland. Geological Survey of Finland, 10, 49 - 52.

Kelly D.P. and Vaughan D.J. (1983), Pyrrhotite - pentlandite ore textures : a mechanistic approach. Mineralogical Magazine, 47, 453 - 463.

Kissin S.A. and Scott S.D. (1982), Phase relations involving pyrrhotite below 350°C. Economic Geology, 77, 1739 - 1754.

Klein C. and Hurlbut C.S. Jr. (1985), Manual of Mineralogy, 20th edition. John Wiley and Sons, Toronto.

Klemm D.D. (1965) N. Jb. Miner. Abh., 103, 205 - 255.

Kracek F.C., Ksanda C.J., and Cabri L.J. (1966), Phase relations in the system silver - tellurium. American Mineralogist, 51, 14 - 28.

Kucha H. (1981), Precious metal alloys and organic matter in the

Zechstein copper deposits, Poland. *Tschermaks Mineral. Petrog. Mitt.*, **28**, 1 - 16.

Laird J. (1988), Chlorites : Metamorphic Petrology, in Bailey S.W. (ed.) *Hydrous Silicates (exclusive of micas)*, Reviews in Mineralogy, volume 19, Mineralogical Society of America, chapter 11.

Leake B.E. (1978), Nomenclature of Amphiboles. *Canadian Mineralogist*, **16**, 501 - 520.

Li C. and Naldrett A.J. (1993), Platinum-group minerals from the Deep Copper zone of the Strathcona deposit, Sudbury, Ontario. *Canadian Mineralogist*, **31**, 31 - 44.

Lindahl I. (1975), Hedleyite ($\text{Bi}_{14}\text{Te}_6$) from the Vaddasrieppe area, North Troms, Northern Norway. *Norsk Geologisk Tidsskrift*, **55**, 283 - 290.

Loucks R.R. and McCallum M.E. (1980), Platinum-group minerals in the New Rambler copper-nickel deposit, Wyoming : preliminary report. *Proc. XIth I.M.A. Meeting, Novosibirsk*, **1**, 200 - 218.

MacKenzie W.S., Donaldson C.H., and Guilford C. (1982), *Atlas of igneous rocks and their textures*. John Wiley and Sons, Inc., New York.

MacTavish, A. (1992), *The Geology, Petrology, Geochemistry, Sulfide and Platinum-Group Element Mineralization of the Quetico Intrusions, Northwestern Ontario*. Unpublished M.Sc. thesis, Lakehead University, Thunder Bay, Ontario.

- Maeda H. and Ito Y. (1989), Bismuth-bearing minerals from the Inakuraishi ore deposits, Southwestern Hokkaido, Japan. *Mining Geology*, **39(3)**, 223 - 229.
- McCallum M.E., Loucks R.R., Carlson R.R., Cooley E.F., and Doerge T.A. (1976), Platinum metals associated with hydrothermal copper ores of the New Rambler Mine, Medicine Bow Mountains, Wyoming. *Economic Geology*, **71**, 1429 - 1450.
- McMillan, D.J., Baughman, G.D., and Schamber (1985) Experience with multiple least squares fitting with derivatives, in *Microbeam Analysis* (Armstrong, J.T., ed.) San Francisco Press, 137 - 140.
- McQueen K.G. (1990), Tellurides in metamorphosed stringer ore from the Dragset deposit, South Trondelag, Norway. *N. Jb. Miner. Mh.*, **5**, 205 - 216.
- Michener C.E. (1940), Minerals associated with large sulfide bodies of the Sudbury type : Unpublished Ph.D. thesis, University of Toronto, Toronto, Canada.
- Miller R. (1981) Kawazulite $\text{Bi}_2\text{Te}_2\text{Se}$, related Bismuth minerals and selenian covellite from the Northwest Territories. *Canadian Mineralogist*, **19**, 341 - 348.
- Misra K.C. and Fleet M.E. (1973), The chemical compositions of synthetic and natural pentlandite assemblages. *Economic Geologist*, **68**, 518 - 539.
- Misra K.C. and Fleet M.E. (1974), Chemical composition and stability of violarite. *Economic Geology*, **69**, 391 - 403.

- Mogessie A., Stumpfl E.F., and Weiblen P.W. (1991), The role of fluids in the formation of Platinum - Group Minerals, Duluth Complex, Minnesota : Mineralogic, textural, and chemical evidence. *Economic Geology*, **86**, 1506 - 1518.
- Morgan, A.J. (1985), X-ray microanalysis in electron microscopy for biologists, *Royal Microscopical Society Microscopy Handbooks*. Oxford Press, New York.
- Morimoto, N. (1989) Nomenclature of Pyroxenes; Sub-committee on Pyroxenes, Nobuo Morimoto, Chairman. *Canadian Mineralogist*, **27**, 143 - 156.
- Mposkos E. (1983), A mineralogical study of the Au-Ag-Bi-Te-Cu-Co-Ni-As-S ore mineralization in Macedonia, Greece. *Chem. Erde*, **42**, 281 - 296.
- Mulja, T. (1989) : Petrology, Geochemistry, Sulfide and Platinum-Group Element Mineralization of the Geordie Lake Intrusion, Coldwell Complex, Ontario. M.Sc. thesis, Lakehead University, Thunder Bay, Ontario.
- Mulja T. and Mitchell R.H. (1990), Platinum - Group Minerals and Tellurides from the Geordie Lake Intrusion, Coldwell Complex, Northwestern Ontario. *Canadian Mineralogist*, **28**, 489 - 501.
- Mulja T. and Mitchell R.H. (1991), The Geordie Lake Intrusion, Coldwell complex, Ontario : A Palladium- and Tellurium-rich disseminated sulfide occurrence derived from an evolved tholeiitic magma. *Economic Geology*, **86**, 1050 - 1069.
- Neiva J.M.C. and Neiva A.M.R. (1990), The gold area of Jales

- (northern Portugal). *Terra Nova*, **2**, 245 - 256.
- Nickel E.H., Ross J.R., and Thornber M.R. (1974), The supergene alteration of pyrrhotite - pentlandite ore at Kambalda, Western Australia. *Economic Geology*, **69**, 93 - 107.
- Nyman M.W., Sheets R.W., and Bodnar R.J. (1990), Fluid - inclusion evidence for the physical and chemical conditions associated with intermediate - temperature PGE mineralization at the New Rambler deposit, Southeastern Wyoming. *Canadian Mineralogist*, **28**, 629 - 638.
- Oen I.S. and Kieft C. (1984), Paragenetic relations of Bi-, Ag- Au -, and other tellurides in bornite veins at Glava, Varmland, Sweden. *Neues Jahrbuch Miner. Abh.*, **149**, 245 - 266.
- Ohnenstetter D., Watkinson D.H., and Dahl R. (1991), Zoned hollingworthite from the Two Duck Lake intrusion, Coldwell complex, Ontario. *American Mineralogist*, **76**, 1694 - 1700.
- Ozawa T. and Shimazaki H. (1982), Pilsenite Re-defined and Wehrlite discredited. *Japan Academy Proceedings, Series B*, **58**, 291 - 194.
- Patterson G.C. and Watkinson D.H. (1984), Metamorphism and supergene alteration of Cu-Ni sulfides, Thierry mine, northwestern Ontario. *Canadian Mineralogist*, **22**, 13 - 21.
- Percival J.A. (1989), A regional perspective of the Quetico metasedimentary belt, Superior Province, Canada. *Can. J. Earth Sci.*, **26**, 677 - 693.

- Piisanen R. and Tarkian M. (1984), Cu-Ni-PGE mineralization at Rometolvas, Koillismaa Layered Igneous Complex, Finland. *Mineralium Deposita*, **19**, 105 - 111.
- Pirie J. (1978), Geology of the Crooked Pine Lake Area, District of Rainy River. Ontario Geological Survey Report 179.
- Pirie J. and Mackasey W.O. (1978), Preliminary Examination of Regional Metamorphism in Parts of Quetico Metasedimentary Belt, Superior Province, Ontario, in *Metamorphism in the Canadian Shield*, ed. J.A. Fraser and W.W. Heywood, Geological Survey of Canada, Paper 78 - 10, p. 37 - 48.
- Plimer I.R. (1977), Bismuth minerals from quartz pipes in Eastern Australia. *Australian Mineralogist*, **10**, 41 - 43.
- Potts P.J., and Tindle A.G. (1991), Evaluation of spectrum overlap correction in energy-dispersive x-ray spectrometry using the digital filter deconvolution procedure : application to selected interferences encountered in the microprobe analysis of minerals. *X-ray Spectrometry*, **20**, 119 - 129.
- Rajamani V. and Prewitt C.T. (1975), Thermal expansion of the pentlandite structure. *American Mineralogist*, **60**, 39 - 48.
- Ramdohr P. (1969), *The ore minerals and their intergrowths*. Pergamon, New York.
- Ripley E.M. (1990), Platinum - Group Element geochemistry of Cu - Ni mineralization in the Basal zone of the Babbitt deposit, Duluth Complex, Minnesota. *Economic Geology*, **85**, 830 - 841.
- Rowell W.F. and Edgar A.D. (1986), *Platinum - Group Element*

mineralization in a hydrothermal Cu-Ni sulfide occurrence, Rathbun Lake, Northeastern Ontario. *Economic Geology*, **81**, 1272 - 1277.

Rucklidge J. (1969), Electron microprobe investigations of Platinum metal minerals from Ontario. *Canadian Mineralogist*, **9**, 617 - 628.

Safonov Y.G., Genkin A.D., Vasudev V.N., Krishna Rao B., and Anantha Iyer G.V. (1984), Genetic features of gold ore deposit at Kolar, Dharwar craton, India. *Journal Geological Society of India*, **25(3)**, 145 - 154.

Shimazaki H. and Ozawa T. (1978), Tsumoite, BiTe, a new mineral from the Tsumo mine, Japan. *American Mineralogist*, **63**, 1162 - 1165.

Sipoez L. (1886), *Z. Kristallogr.*, **11**, 209 - 219. as found in (Ozawa and Shimazaki, 1982).

Stone W.E., Fleet M.E., Crocket J.H., and Kingston D.M. (1992), Platinum - Group Minerals in pyroxenite from the Boston Creek Flow basaltic komatiite, Abitibi Greenstone Belt, Ontario. *Canadian Mineralogist*, **30**, 109 - 119.

Stumpfl E.F. (1961), Some new platinoid-rich minerals, identified with the electron microanalyzer. *Mineral. Mag.*, **32**, 833 - 847.

Stumpfl E.F. (1972), Compositional variations in the hollingworthite - irarsite group. *N. Jb. Miner. Mh.*, **9**, 406

- 415.

Stumpfl E.F. and Clark A.M. (1965), Hollingworthite, a new Rhodium mineral, identified by electron probe microanalysis. *American Mineralogist*, **50**, 1068 - 1074.

Stumpfl E.F. and Rucklidge J. (1968), New data on natural phases in the system Ag - Te. *American Mineralogist*, **53**, 1513 -1522.

Sztrokay K.I. and Nagy B. (1982), Bismuth - Tellurium associations : new minerals of the Wehrlite - Pilsenite assemblage from Hungary, in Amstutz G.C., El Goresy A., Frenzel G., Kluth C., Moh G., Wauschkuhn A., and Zimmerman P.A. (editors), *Ore genesis, the state of the art*. Springer - Verlag, Berlin.

Tarkian M. (1987), Compositional variations and reflectance of the common Platinum - Group Minerals. *Mineralogy and Petrology*, **36**, 169 - 190.

Tarkian M. and Prichard H.M. (1987), Irarsite - hollingworthite solid - solution series and other associated Ru-, Os-, Ir-, and Rh-bearing PGM's from the Shetland ophiolite complex. *Mineral. Deposita*, **22**, 178 - 184.

Tarkian M. and Stumpfl E.F. (1975), Platinum mineralogy of the Driekop mine, South Africa. *Mineralium Deposita*, **10**, 71 - 85.

Thurston P.C. (1991), Archean Geology of Ontario : Introduction, in *Geology of Ontario*, Ontario Geological Survey, Special Volume 4, Part I, 73 - 78.

Tischler S.E., Cawthorn R.G., Kingston G.A., and Maske S. (1981), Magmatic Cu-Ni-PGE mineralization at Waterfall Gorge, Insizwa,

- Pondoland, Transkei. *Canadian Mineralogist*, **19**, 607 - 618.
- Tokonami M., Nishiguchi K., and Morimoto N. (1972), Crystal Structure of a monoclinic pyrrhotite (Fe_7S_8). *American Mineralogist*, **57**, 1066 - 1080.
- Vaughan D.J. and Craig J.R. (1978), *Mineral Chemistry of metal sulfides*. Cambridge University Press, New York.
- Volborth A., Tarkian M., Stumpfl E.F., and Housley R.M. (1986), A survey of the Pd - Pt mineralization along the 35-Km strike of the J-M Reef, Stillwater Complex, Montana. *Canadian Mineralogist*, **24**, 329 - 346.
- Warren H.V. and Peacock M.A. (1945), Hedleyite, a new bismuth telluride from British Columbia, with notes on wehrlite and some bismuth - tellurium alloys. *University of Toronto Studies, Geol. Ser.*, **49**, 55 - 69.
- Watkinson D.H. and Dahl R. (1987), Platinum - Group Mineral precipitation from fluids in pegmatitic gabbro : Two Duck Lake Intrusion, Coldwell Complex, Ontario, Canada in *Geo-Platinum '87*, 237.
- Watkinson D.H., and Irvine T.N. (1964), Peridotitic Intrusions near Quetico and Shebandowan, Northwestern Ontario : A Contribution to the Petrology and Geochemistry of Ultramafic Rocks. *Canadian Journal of earth Sciences*, **1**, 63 - 98.
- Watkinson D.H. and Melling D.R. (1992), Hydrothermal origin of Platinum - Group mineralization in low temperature Copper

Sulfide-rich assemblages, Salt Chuck Intrusion, Alaska.

Economic Geology, **87**, 175 - 184.

Wells H.L. (1889), Sperrylite, a new mineral. American Journal of Science, **37**, 67 - 70.

Wells O. (1974), Scanning Electron Microscopy. McGraw Book Company, New York.

Williams H.R. (1991), Quetico Subprovince, in Geology of Ontario, Ontario Geological Survey, Special Volume 4, Part I, 383 - 403.

Yakovlev Y.N., Distler V.V., Mitrofanov F.P., Razhev S.A., Grokhovskaya T.L., and Veselovsky N.N. (1991), Mineralogy of PGE in the Mafic-Ultramafic Massifs of the Kola Region. Mineralogy and Petrology, **43**, 181 - 192.

Appendix 1

Each Platinum - Group Mineral and Bi compound from the mineralized area of the Kawene Intrusion was found in the following polished thin sections. A total of 42 polished thin sections were examined.

Michenerite (PdBiTe) - 13, 13B-1, 13C-1, 13C-2, 13D-1, 13D-2,

13E-2, 15-1, 15-2, 15-3, 15-4, 15B-1, 15B-3, 15B-4, 16A,

16B-1, 16B-2, 16A, 16B-1, 16B-2, 17A, 17B-1, 17B-2, 17C-1,

17D-1, 17D-2, 27A, 27B-2, 28A, AK-2, AK-3A, AK-9-86B, AK-10

Froodite (PdBi₂) - 13B-1, 13E-2, 15-1, 15-2, 15-3, 15-5, 15-6,

15B-1, 16A, 17A, 17A-2, 17B-1, 17B-2, 27A, AK-2, AK-3A,

AK-9-86B, AK-10, AK-11A

Pd₂Bi₅- 13B-1, 13B-2, 13C-1, 13C-2, 15-3, 15-4, 15-5, 15-6, 15B-1,

15B-2, 15B-3, 15B-4, 16A, 16B-1, 16B-2, 17A, 17B-1, 17B-2,

17C-1, 27B-2, AK-2, AK-3A, AK-9-86B, AK-10

Sperrylite (Pt,Ir)(As,S)₂ - 13, 13B-1, 13C-2, 13D-1, 15-1, 15-4,

15B-1, 15B-2, 15B-3, 16A, 16B-1, 16B-2, 17A, 17A-2, 17B-1,

17C-1, 28A, AK-2, AK-3A, AK-5, AK-10, AK-11A

Native Bi - 13C-2, 13E-1, 13E-2, 15-1, 15-4, 15-5, 15B-1, 15B-2,

15B-4, 17A, 17A-2, 27A, AK-10

Bismuthinite (Bi₂S₃)- 13E-1, 15-4, 15-5, 15-6, 15B-1, 15B-2,

15B-3, 17A-2, 17B-2, AK-2, AK-3A

(Ag,Ni)S - AK-9-86B

Pd₂Bi₃- 13E-1, 15-1, 15-3, 17A-2, 17B-1, AK-2, AK-10, AK-11A

Hedleyite - pilsenite (ss) Bi₂Te - 13B-1, 13B-2, 13C-1, 13E-2,

15-4, 28A, AK-3A, AK-9-86B, AK-11A

BiS - 13B-1, 13E-1, 15-3, 15-4, 15-5, 15B-1, 15B-3, 15B-4, 17A-2,
17B-2, 27B-2, AK-2, AK-3A

Bi₄(Te,Se,S)₃- AK-2, AK-3A, AK-10

Sobolevskite (PdBi) - 15-3, 16A, 17A-2, 17B-2, AK-2, AK-9-86B,
AK-10

Sb-bearing michenerite (PdBiTe+Sb) - 15B-1, 28A, AK-10

Pilsenite - hedleyite (ss) (Bi₃Te₂)- 13, 13B-1, 13C-1, 13D-1,
13D-2, 13E-1, 13E-2, 15B-3, 28A, AK-9-86B

PdBi₃ - 15-1, 15-3, 15-4, 15-5, 15B-1, 17A, AK-3A, AK-10

Sobolevskite - stibiopalladinite (Pd₂BiSb+Te) - 15-1, 15B-1, 16B-1,
28A, AK-10

Bi(S,Te,Se) - AK-2, AK-3A

Hessite (Ag₂Te) - 13D-1, 13D-2, 13E-2, AK-9-86B

Bi₃S₂- 15-4, 15B-1, 15B-4, 17A-2, AK-3A

Co-bearing hollingworthite [(Rh,Co)AsS] - 13E-1, 15-2, 15-3, 15-4,
17A, 17B-1, AK-2, AK-10

Bi₃(Te,S,Se)₂- AK-2, AK-3A, AK-11A, 27B-2

Pilsenite (Bi₄Te₃)- 13, 13D-1, 28A, AK-9-86B

Hedleyite (Bi₇Te₃)- 13B-1

Sobolevskite - sudburyite (Pd₃Bi₂Sb)- 13B-1, AK-10

Sobolevskite - stibiopalladinite - michenerite [Pd₂Bi(Te,Sb)] -
13B-1, 16A, 16B-1

Electrum (Au₃Ag₂)- 13, 13C-1, 13C-2, 13D-1, AK-5

Altaite (PbTe) - 13D-1, 13D-2

Pilsenite - paraganajuaite [Bi₃(Te,Se)₂]- 13C-1, 15-4, 17A-2,
AK-11A

Tsumoite (BiTe) - 15B-3, 28A, AK-9-86B

Tetradymite - bismuthinite [Bi₂(S,Te,Se)₃]- AK-2, AK-3A

Stutzite (Ag₃Te₂)- 13D-2, AK-9-86B

Appendix 2 : Compositions of Platinum - Group Minerals which are $\geq 5 \mu\text{m}$ in diameter
(atomic and weight %)

Pd - Bi compounds

formula	at%		wt%		size	probe section
	Pd	Bi	Pd	Bi		
Pd ₂ Bi ₃	44.10	55.90	28.66	71.34	7 μm	AK-10
	40.01	59.99	25.35	74.65	7 μm	AK-10
	38.54	61.46	24.20	75.80	7 μm	AK-10
	38.24	61.76	23.97	76.03	5 μm	15-1
	37.82	62.18	23.65	76.35	7 μm	AK-10
	37.11	62.89	23.10	76.90	5 μm	AK-2
PdBi ₂	34.05	65.95	20.82	79.18	5 μm	AK-2
	33.50	66.50	20.41	79.59	8 μm	AK-2
	32.70	67.30	19.83	80.17	7 μm	AK-2
	32.53	67.47	19.72	80.28	5 μm	15-3
	32.37	67.63	19.59	80.41	5 μm	AK-2
	31.85	68.15	19.23	80.77	5 μm	AK-2
	31.76	68.24	19.15	80.85	10 μm	AK-2
	31.54	68.46	18.99	81.01	6 μm	AK-10
	31.38	68.62	18.89	81.11	8 μm	AK-3A
	31.29	68.71	18.82	81.18	6 μm	AK-9-86B
	31.17	68.83	18.74	81.26	9 μm	17A-2
	31.05	68.95	18.65	81.35	6 μm	AK-10
	31.03	68.97	18.64	81.36	5 μm	15-3
Pd ₂ Bi ₅	30.84	69.16	18.50	81.50	10 μm	27B-2
	30.79	69.21	18.47	81.53	8 μm	AK-2
	30.69	69.31	18.40	81.60	12 μm	AK-10
	30.36	69.64	18.16	81.84	9 μm	17A-2
	30.23	69.77	18.08	81.92	5 μm	AK-2
	30.21	69.79	18.06	81.94	10 μm	17B-2
	30.04	69.96	17.94	82.06	5 μm	AK-3A
	29.98	70.02	17.90	82.10	10 μm	AK-2
	29.86	70.14	17.81	82.19	7 μm	AK-10
	29.60	70.40	17.63	82.37	5 μm	AK-3A
	29.31	70.69	17.42	82.58	5 μm	AK-2
	29.25	70.75	17.39	82.61	8 μm	13B-1
	29.24	70.76	17.38	82.61	7 μm	AK-10
	29.20	70.80	17.35	82.65	5 μm	AK-10
	29.19	70.81	17.34	82.66	10 μm	AK-2
	29.08	70.92	17.27	82.73	8 μm	13B-1
	29.02	70.98	17.23	82.77	8 μm	13B-1
28.87	71.13	17.13	82.87	10 μm	27B-2	
28.76	71.24	17.05	82.95	6 μm	AK-9-86B	
28.70	71.30	17.01	82.99	5 μm	AK-2	
28.64	71.36	16.96	83.04	7 μm	AK-2	

formula	at%		wt%		size	probe section
	Pd	Bi	Pd	Bi		
Pd ₂ Bi ₅	28.57	71.43	16.92	83.08	8 um	13B-1
	28.56	71.44	16.91	83.09	8 um	13B-1
	28.50	71.50	16.87	83.13	6 um	AK-10
	28.31	71.69	16.74	83.26	8 um	13B-1
	28.27	71.73	16.71	83.29	8 um	13B-1
	28.26	71.74	16.71	83.29	8 um	13B-1
	28.22	71.78	16.68	83.32	5 um	AK-2
	27.98	72.02	16.51	83.49	8 um	13B-1
	27.97	72.03	16.50	83.50	8 um	13B-1
	27.93	72.07	16.49	83.51	5 um	AK-2
	27.77	72.23	16.37	83.63	8 um	13B-1
	27.72	72.28	16.34	83.66	7 um	AK-10
	27.71	72.29	16.33	83.67	10 um	27B-2
	27.17	72.83	15.97	84.03	12 um	AK-10
	27.16	72.84	15.96	84.04	7 um	15-3
	26.92	73.08	15.79	84.21	5 um	AK-3A
	26.79	73.21	15.70	84.30	8 um	13B-1
PdBi ₃	25.68	74.32	14.96	85.04	7 um	15-3

Michenerite

at%			wt%			size	probe section
Pd	Bi	Te	Pd	Bi	Te		
25.65	47.13	27.22	17.01	61.36	21.64	10 um	15-1
27.08	47.88	25.04	17.92	62.22	19.86	10 um	15-1
30.38	39.24	30.38	21.12	53.56	25.32	12 um	16B-1
31.53	35.52	32.96	22.39	49.53	28.07	12 um	15-3
31.54	38.41	30.06	22.05	52.74	25.21	38 um	16B-1
31.74	36.21	32.05	22.46	50.33	27.21	12 um	15-2
32.00	37.14	30.86	22.54	51.39	26.07	8 um	15-3
32.18	37.26	30.56	22.66	51.53	25.81	14 um	15B-1
32.19	35.78	32.03	22.85	49.88	27.27	8 um	27B-2
32.25	34.59	33.16	23.04	48.54	28.41	8 um	15-3
32.26	37.62	30.11	22.68	51.94	25.38	18 um	13C-1
32.35	37.33	30.32	22.78	51.62	25.60	9 um	17B-1
32.60	37.42	29.99	22.95	51.73	25.32	11 um	15B-1
32.70	35.49	31.81	23.26	49.59	27.14	12 um	15-3
32.77	37.33	29.89	23.09	51.66	25.25	5 um	15B-1
32.81	37.18	30.01	23.13	51.49	25.38	15 um	13C-2
32.89	37.76	29.35	23.12	52.13	24.74	10 um	AK-10
32.97	37.04	29.99	23.27	51.34	25.39	12 um	17B-2
33.16	36.80	30.04	23.44	51.10	25.46	7 um	15B-1
33.21	37.50	29.29	23.38	51.88	24.74	12 um	15B-1
33.28	37.31	29.41	23.46	51.67	24.87	14 um	15B-1
33.34	35.65	31.01	23.73	49.82	26.46	8 um	15-3
33.38	35.62	30.99	23.76	49.79	26.45	5 um	13B-1
33.42	35.08	31.50	23.86	49.18	26.96	12 um	15-3
33.58	36.59	29.83	23.78	50.89	25.33	5 um	13B-1
33.62	36.87	29.51	23.77	51.20	25.03	8 um	17B-1
33.68	38.03	28.29	23.67	52.49	23.84	5 um	13B-1
33.70	37.16	29.14	23.79	51.53	24.68	8 um	16B-2
33.87	37.37	28.76	23.89	51.78	24.33	12 um	AK-10
33.89	34.70	31.41	24.26	48.79	26.96	12 um	15-2
33.93	37.67	28.40	23.90	52.11	23.99	23 um	13B-1
34.12	39.27	26.61	23.82	53.88	22.30	12 um	13B-1
34.13	33.87	32.00	24.55	47.85	27.61	8 um	15-3
34.24	35.94	29.82	24.35	50.20	25.44	6 um	AK-2
34.45	38.91	26.65	24.12	53.50	22.38	23 um	13B-1
34.58	36.61	28.81	24.52	50.99	24.50	20 um	16B-2
34.89	38.94	26.17	25.34	55.56	19.10	23 um	13B-1
34.80	36.43	28.77	24.70	50.80	24.49	23 um	13B-1
34.27	36.95	28.77	24.25	51.34	24.41	9 um	13B-1
35.19	37.61	27.20	24.84	52.14	23.03	23 um	13B-1
35.03	41.98	22.99	24.15	56.84	19.01	9 um	13B-1
36.97	39.62	23.41	25.87	54.47	19.65	9 um	13B-1
37.06	36.54	26.40	26.38	51.09	22.53	8 um	15-1
37.43	40.55	22.02	26.09	55.51	18.40	9 um	13B-1
43.94	38.13	17.93	31.31	53.37	15.32	8 um	15-1

Sb - bearing michenerite

at%				wt%				size	probe section
Pd	Bi	Te	Sb	Pd	Bi	Te	Sb		
29.38	38.10	30.76	1.76	20.54	52.28	25.78	1.40	7 um	28A
29.91	37.70	29.50	2.89	20.97	51.91	24.80	2.32	10 um	15B-1
29.97	38.06	30.41	1.56	20.96	52.28	25.51	1.25	7 um	28A
30.04	37.72	29.48	2.76	21.06	51.94	24.79	2.21	10 um	15B-1
30.50	36.79	30.34	2.38	21.50	50.94	25.65	1.91	12 um	15B-1
30.07	36.29	31.72	1.91	21.25	50.35	26.86	1.54	5 um	15B-1
30.69	36.52	29.95	2.84	21.67	50.66	25.37	2.30	20 um	15B-1
31.03	35.85	31.30	1.82	22.00	49.91	26.61	1.48	8 um	15B-1
31.03	37.48	29.93	1.55	21.79	51.72	25.23	1.23	9 um	28A
31.19	37.27	29.66	1.89	21.95	51.50	25.03	1.52	12 um	15B-1
32.14	37.02	29.46	1.38	22.68	51.29	24.92	1.11	5 um	15B-1

Bismuthinite

at%		wt%		size	probe section
Bi	S	Bi	S		
39.53	60.47	80.99	19.01	5 um	17A-2
41.40	58.60	82.16	17.84	10 um	15-5
42.10	57.90	82.57	17.43	6 um	15-5
42.31	57.69	82.70	17.30	20 um	15-5
43.13	56.87	83.17	16.83	6 um	15-5

Bi - Te Compounds

formula	at%		wt%		size	probe section
	Bi	Te	Bi	Te		
Bi ₄ Te ₃	56.58	43.42	68.09	31.91	8 um	AK-9
	56.70	43.30	68.20	31.80	6 um	13D-1
	57.36	42.64	68.78	31.22	6 um	13D-1
Bi ₃ Te ₂	58.94	41.06	70.16	29.84	5 um	15B-3
	60.22	39.78	71.26	28.74	8 um	AK-9
	61.08	38.92	71.99	28.01	20 um	15B-3
	63.01	36.99	73.61	26.39	5 um	13E-2
	63.26	36.74	73.83	26.17	15 um	AK-9
Bi ₂ Te	63.51	36.49	74.02	25.98	15 um	AK-9
	63.68	36.32	74.17	25.83	15 um	AK-9
	64.25	35.75	74.64	25.36	8 um	28A
	66.71	33.29	76.65	23.35	5 um	13B-1
	66.74	33.26	76.67	23.33	7 um	13B-1
	66.96	33.04	76.85	23.15	7 um	13B-1
	67.04	32.96	76.91	23.09	7 um	13B-1
	67.16	32.84	77.01	22.99	9 um	13C-1
	68.30	31.70	77.93	22.07	7 um	13B-1
Bi ₇ Te ₃	68.79	31.21	78.31	21.69	8 um	13B-1
	68.89	31.11	78.38	21.62	8 um	13B-1
	70.54	29.46	79.69	20.31	12 um	13B-1

Bi - Te - Se - S Compounds

formula	at%				wt%				size	probe section
	Bi	Te	Se	S	Bi	Te	Se	S		
Bi(S,Te,Se)	46.42	14.11	7.36	32.11	74.53	13.08	3.82	8.57	8 um	AK-2
Bi(Te,Se,S)	51.94	21.24	13.30	13.52	72.14	18.00	6.97	2.88	6 um	AK-2
	52.47	24.36	12.48	10.69	71.20	20.18	6.39	2.23	6 um	AK-2
	52.75	19.25	16.82	11.18	72.67	16.20	8.76	2.37	6 um	AK-2
	53.42	24.42	13.74	8.42	71.40	19.93	6.94	1.73	5 um	AK-2
Bi ₄ (Te,Se,S) ₃	53.66	25.17	9.37	11.80	72.14	20.67	4.76	2.44	6 um	AK-2
	53.85	22.50	10.19	13.47	73.26	18.69	5.23	2.81	5 um	AK-3A
	54.11	22.87	9.37	13.65	73.42	18.94	4.80	2.84	5 um	AK-3A
	54.33	22.78	11.68	11.21	73.05	18.71	5.93	2.31	9 um	AK-3A
	54.36	23.21	11.37	11.06	72.94	19.02	5.76	2.27	6 um	AK-2
	54.92	20.85	14.33	9.89	73.63	17.07	7.26	2.03	6 um	AK-2
	56.51	20.75	8.50	14.24	75.78	16.98	4.31	2.93	9 um	AK-3A
	56.71	21.82	10.18	11.29	75.00	17.62	5.09	2.29	8 um	AK-3A
	56.80	22.48	12.97	7.74	74.13	17.92	6.40	1.55	6 um	AK-2
	57.10	20.94	12.17	9.78	75.15	16.83	6.05	1.97	8 um	AK-3A
	57.39	22.08	7.87	12.66	75.72	17.80	3.92	2.57	8 um	AK-3A
	57.48	24.85	10.40	7.27	73.98	19.53	5.06	1.43	5 um	AK-2
	57.82	15.97	11.93	14.28	77.86	13.13	6.06	2.95	20 um	AK-2
	58.02	23.92	7.99	10.08	75.17	18.91	3.91	2.00	6 um	AK-2
	58.48	18.79	7.67	15.06	77.80	15.27	3.86	3.07	8 um	AK-3A
58.50	20.10	8.44	12.96	77.03	16.16	4.19	2.62	8 um	AK-3A	
Bi ₃ (Te,Se,S) ₂	58.91	13.33	14.69	13.06	78.97	10.91	7.44	2.68	9 um	AK-2
	59.04	14.62	12.20	14.13	78.97	11.95	6.17	2.90	20 um	AK-2
	59.94	19.23	14.63	6.19	76.69	15.03	7.07	1.21	9 um	AK-3A
	61.65	20.41	8.94	9.00	78.17	15.80	4.28	1.75	5 um	27B-2

Sperrylite

at%				wt%				size	probe section
Pt	Ir	As	S	Pt	Ir	As	S		
29.92	9.06	61.02		48.04	14.33	37.63		5 um	28A
30.04		66.26	3.70	53.55		45.37	1.08	150 um	16B-1
30.67	3.01	62.86	3.46	52.57	5.08	41.38	0.98	5 um	13B-1
30.71		69.29		53.57		46.43		5 um	AK-2
31.34		68.66		54.31		45.69		15 um	15B-3
31.42	2.03	66.55		53.26	3.40	43.34		5 um	28A
31.46		68.54		54.45		45.55		5 um	15B-3
31.71		68.29		54.74		45.26		5 um	AK-5
31.72		68.28		54.75		45.25		5 um	AK-2
31.79		68.21		54.83		45.17		18 um	13D-1
31.88		68.12		54.93		45.07		18 um	13D-1
32.07		67.93		55.14		44.86		18 um	13C-2
32.23		67.77		55.32		44.68		12 um	13
32.38	1.72	65.91		54.52	2.85	42.63		5 um	13B-1
32.62	2.18	61.96	3.25	55.20	3.62	40.27	0.90	5 um	13B-1
32.69		67.31		55.85		44.15		5 um	AK-5
32.73		67.27		55.89		44.11		5 um	AK-2
32.89		62.97	4.15	56.95		41.87	1.18	6 um	13B-1
33.11		66.89		56.31		43.69		5 um	13B-1

Hessite

at%		wt%		size	probe section
Ag	Te	Ag	Te		
64.95	35.05	61.04	38.96	5 um	13D-1
65.49	34.51	61.60	38.40	6 um	13D-1
65.63	34.37	61.75	38.25	6 um	13D-1
65.71	34.29	61.83	38.17	5 um	13D-1
66.92	33.08	63.10	36.90	6 um	13D-1
67.16	32.84	63.36	36.64	6 um	13D-1